Improving Chemical Mechanisms for Ozone and Secondary Organic Carbon

REPORT TO THE

California Air Resources Board Research Division

Project # 12-312

Prepared by:

Dr. Christopher D. Cappa[1]
Dr. Michael J. Kleeman[1]
Dr. Anthony Wexler[1,2]

Dr. John H. Seinfeld[3]

Dr. Shantanu Jathar[4]

[1]Department of Civil and Environmental Engineering
[2]Air Quality Research Center
University of California, Davis
One Shields Avenue, Davis, CA, 95616

[3]Department of Chemical Engineering
California Institute of Technology
Pasadena, CA, 91125

[4]Department of Mechanical Engineering,
Colorado State University
Fort Collins, CO 80523-1301

March 31, 2017

DISCLAIMER

The statements and conclusions in this report are those of the contractor and not necessarily those of the California Air Resources Board. The mention of commercial products, their source, or their use in connection with material reported herein is not to be construed as actual or implied endorsement of such products.

ACKNOWLEDGEMENTS

TABLE OF CONTENTS

LIST OF TABLES

LIST OF FIGURES

LIST OF ACRONYMS

AGLY – aerosol glyoxal products contributing to SOA
AMGLY – aerosol methyl glyoxal products contributing to SOA
AMS – Aerosol Mass Spectrometer
BCs - boundary conditions
BVOC - biogenic volatile organic compounds
CARB - California Air Resources Board
CI - confidence interval
CIT - California Institute of Technology
CMAQ - Community Multiscale Air Quality model from USEPA
EC - elemental carbon
HOA – Hydrocarbon-like Organic Aerosol
ICs - initial conditions
IR – Incremental Reactivity
NH_4^+ / N(-III) - ammonium
NO_3^- / N(V) - nitrate
NOx - oxides of nitrogen
O_3 - ozone
OC - organic carbon
OM – Organic Matter
OH - hydroxyl radical
OOA – Oxygenated Organic Aerosol
MIR – Maximum Incremental Reactivity
MOIR – Maximum Ozone Incremental Reactivity
PM_{10} - Airborne particle mass with aerodynamic diameter less than 10.0 μm.
$PM_{2.5}$ - Airborne particle mass with aerodynamic diameter less than 2.5 μm.
PM - Airborne particulate matter
PN - particulate nitrate
POA – primary organic aerosol
RMSE - Root Mean Square Error
RN - reactive nitrogen
SCAQMD - South Coast Air Quality Management District
SCAQS - Southern California Air Quality Study
SJV - San Joaquin Valley Air Basin
SOA – secondary organic aerosol
SO_4^{2-} / S(VI) - sulfate
SoCAB - South Coast Air Basin
SOM – Statistical Oxidation Model
SOP - Standard Operating Procedure
SV - Sacramento Valley Air Basin
UCD - University of California at Davis
USEPA - United States Environmental Protection Agency
UV - Ultraviolet radiation
VOC - volatile organic compounds

ABSTRACT

This report explores multiple strategies to improve the accuracy of predictions for secondary organic aerosol (SOA), nitrate, and ozone formation potential within regional chemical transport models.

A statistical oxidation model (SOM) was used to explore the role of multigenerational oxidation chemistry and vapor wall loss corrections on predicted SOA concentrations. The SOM framework was incorporated into the UCD/CIT air quality model and tested for the conditions in Southern California with 8km resolution from July 20 to August 2, 2005, and in the eastern half of the US with 36 km resolution from August 20th to September 2nd, 2006. Results show that SOA concentrations predicted by the UCD/CIT-SOM model are very similar to those predicted by the standard two-product model used in CMAQ4.7 when both models use parameters that are derived from the same chamber data. Since the two-product model does not explicitly resolve multi-generational oxidation reactions, this finding suggests that the chamber data used to parameterize the models captures the majority of the SOA mass formation from multi-generational oxidation under the conditions tested. It was further observed that the use of low and high NOx yields perturbs SOA concentrations by a factor of two. This issue is probably a much stronger determinant of SOA concentrations in 3-D models than multi-generational oxidation.

SOM calculations were also performed to quantify the effects of vapor wall losses that were not accounted for previously in chamber studies. Revised SOM fits were derived for chamber data under "low" and "high" vapor wall-loss rates to bound the range of possible values and compare with the results using the base case "no" vapor wall loss parameterization. Accounting for vapor wall losses substantially increased the simulated SOA concentrations in both the Southern California and East Coast domains, with predicted increases ranging from a factor of 2-10. Lower concentrations experienced the greatest increase. In Southern California, the predicted SOA fraction of total OA increases from ~0.2 (no) to ~0.5 (low) and to ~0.7 (high), with the high vapor wall loss simulations providing best general agreement with observations. The predicted absolute values and diurnal variability in the O:C and H:C atomic ratios also agreed better with observations for the high vapor wall loss simulations. In the eastern US, the SOA fraction is large in all cases but increases further when vapor wall losses are accounted for.

Explicit reactions between biogenic VOCs and NOx were added to the base SAPRC11 mechanism to determine how they influence the predicted formation of secondary organic aerosol (including organic nitrates). These simulations used the CMAQ4.7 base two product model framework to predict SOA formation resulting from the additional gas-phase reactions. Simulations at 24/4 km resolution were conducted for conditions in Southern California during May 19-June 14, 2010 during the CALNEX field campaign and during Jan 16 – Feb 10, 2013 during the DISCOVER-AQ field campaign. The simulation results show that reactions between NOx and biogenic VOCs produce negligible SOA during winter conditions but may produce up to ~1 $\mu g\ m^{-3}$ during summer conditions. The majority of the SOA produced through these pathways is monoterpene nitrates and glyoxal / methylglyoxal. First order estimates for the efficiency of control strategies suggest that a 25% reduction in NOx emissions would produce a

~0.13 µg m^{-3} reduction in PM2.5 SOA concentrations using this modified SAPRC11 mechanism combined with the base two product model.

Finally, the ozone formation potential of individual VOC precursors was calculated for 39 cities across the US using updated conditions for meteorology, emissions, concentration of initial conditions, concentration of background species, and composition of VOC profiles. Calculations show that the actual ozone formation potential in each city increased by 17.3% when conditions were updated from 1988 to 2010, primarily due to changes in meteorology stemming from shifting seasons for peak ozone events and / or improved predictions for boundary layer heights. The MIR ozone formation potential under artificial high NOx conditions decreased by approximately 41.1% when conditions were updated from 1988 to 2010. Changes to the meteorlogy, emissions, initial conditions, background concentrations and composition profiles all contributed to the decrease in MIR. The relative ranking of the VOCs according to their reactivity did not change strongly due to the updated conditions.

EXECUTIVE SUMMARY

Background: Photochemical air quality models are the primary tool for determining the limiting precursors for various secondary pollutants in California air sheds. Chemical mechanisms are an integral part of these photochemical air quality models and must represent the state-of– the-science understanding of how ozone and other secondary pollutants are formed and their relationships to the primary pollutants emitted from different sources. The SAPRC07 chemical mechanism commonly used in California was originally developed for accurate simulation of ozone concentrations but has subsequently also been used extensively to predict precursors for secondary organic aerosol formation and nitrate formation. Both SOA and nitrate concentrations are typically under-predicted in current California air pollution episodes, motivating an examination of new approaches to improve performance.

The SAPRC chemical mechanism is also used to calculate the ozone formation potential of VOCs in order to determine which compounds should be regulated in regions where ambient ozone concentrations exceed the health-based standards. The current reactivity assessment for VOCs is based on conditions in 1988 when the methods were first developed. A re-examination of VOC reactivity using more modern conditions is required to update our understanding of VOCs that should be controlled.

The current project is divided into three major tasks to improve air quality models: (1) addition of multi-generational aging into a regional chemical transport model, (2) addition of explicit reactions to represent NOx and biogenic VOC interactions, and (3) updating of the air pollution episodes used to calculate ozone formation potential (incremental reactivity) for VOCs.

Methods:
Task 1: The statistical oxidation model (SOM) was added to SAPRC-11 to simulate the multi-generational oxidation and gas/particle partitioning of SOA in the regional UCD/CIT air quality model. In SOM, evolution of organic vapors by reaction with the hydroxyl radical is defined by (1) the number of oxygen atoms added per reaction, (2) the decrease in volatility upon addition of an oxygen atom and (3) the probability that a given reaction leads to fragmentation of the organic molecule. These SOM parameter values were fit to laboratory "smog chamber" data for each precursor/compound class.

Figure 1 shows a schematic of the carbon-oxygen grid and illustrates the oxidation of a typical SOA precursor and the movement of the product species in the SOM grid. For example, a saturated alkane with 8 carbon atoms (ALK_C08 or $C_8H_{18}O_0$ or *n*-octane; orange cell) reacts with OH to directly form 1 of 4 functionalized products with 1 to 4 oxygen atoms attached to the carbon backbone (yellow cells). In parallel, an oxygenated species (e.g. $C_8H_{15}O_3$) reacts to form directly functionalized products ($C_8H_{15}O_{4-7}$) and two fragment species.

Air quality episodes were simulated with both UCD/CIT-base and UCD/CIT-SOM in the South Coast Air Basin of California and the eastern United States.
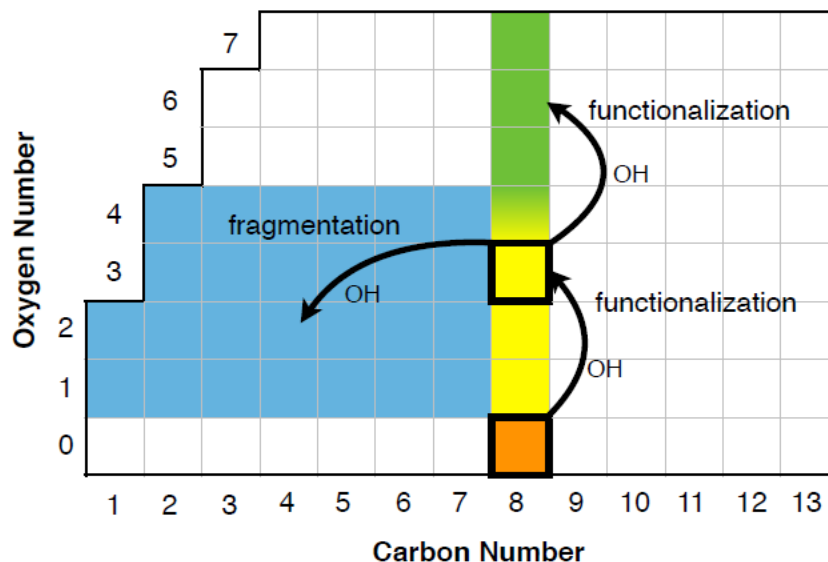
Figure 1: Schematic that demonstrates how the carbon-oxygen grid of the SOM captures the OH-driven multigenerational oxidation of gas-phase organics.

Task 2: Explicit reactions between biogenic VOCs and NOx were added to the SAPRC-11 photochemical mechanism. A total of 271 reactions were modified and / or added to the mechanism to recently discovered chemical pathways that produce organic nitrates and other forms of secondary organic aerosol. Simulations were conducted for Southern California between June – July 2010 during the CALNEX field campaign and for the San Joaquin Valley between Jan-Feb 2013 during the DISCOVER-AQ field campaign.

Task 3: Periods with maximum measured ozone concentrations were identified in the year 2010 for 39 cities across the United States. Meteorological conditions during each ozone episode were simulated using the Weather Research and Forecast (WRF) model. Emissions during each ozone episode were predicted using SMOKE operating with the National Emissions Inventory for 2011. Wildfire emissions were represented using FINN and biogenic emissions were represented using MEGAN. Full 3D model simulations were conducted for each city using the UCD/CIT air quality model. Average background VOC concentrations over each city were extracted and prepared as inputs to box model calculations for ozone reactivity. Likewise, meteorological conditions and emissions were averaged for each city as inputs to the simplified box model calculations.

Results:
Task 1: SOM simulations representing multi-generational chemistry do not predict higher SOA concentrations than the previous two-product model when both models are fit to consistent chamber data. This finding suggests that the parameters used in two-product models at least approximately account for the multi-generational chemistry that occurs during chamber experiments, and that the chamber experiments selected in the current study have the same amount of multi-generational chemistry as the atmosphere in Los Angeles and the Eastern US during the simulated episodes. However, the SOA composition predicted by SOM differs slightly from that predicted by the two-product model. Thus, explicit inclusion of multi-generational chemistry may allow for more accurate assessment of source contributions to SOA.
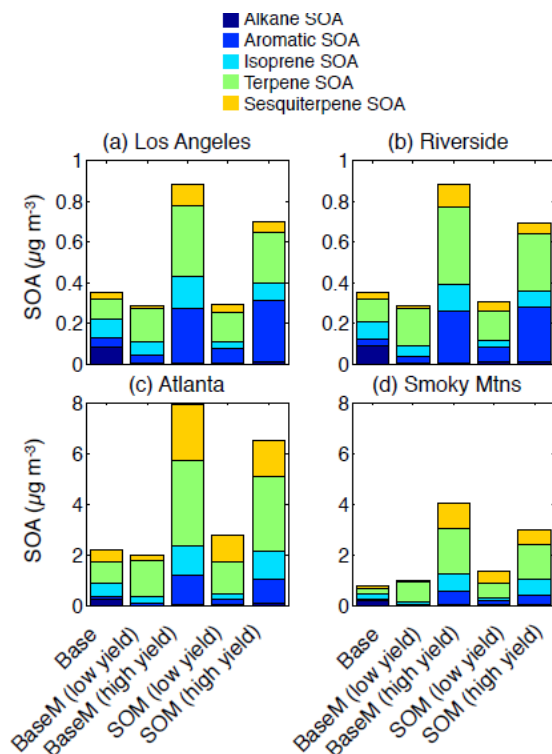
Figure 2: 14-day averaged SOA concentrations at Los Angeles (a), Riverside (b), Atlanta (c) and Smoky Mountains (d) for the Base, BaseM, and SOM simulations resolved by the precursor/ pathway.

Figure 2 compares the 14-day averaged, precursor-resolved SOA concentrations at two sites in the SoCAB (Los Angeles: urban, Riverside: urban outflow) and at two sites in the eastern US (Atlanta: urban, Smoky Mountains: remote) from Base (original CMAQ4.7 two product model), BaseM (CMAQ4.7 two product model refit to new chamber data), and the SOM. It was noted that the choice of high-NOx vs. low-NOx regimes had a large effect on predicted SOA concentrations in all simulations. The CMAQ model developed by the US EPA interpolates between these regimes based on the ratio of NO to HO_2 in each grid cell, but it is noteworthy that different chemical mechanisms predict significantly different oxidant concentrations (including HO_2). This complicates the use of NO_x-dependent SOA parameterizations as it is unclear the extent to which the simulated oxidant environment at a given NO_x matches the original experimental conditions. The choice of high-NOx vs. low-NOx regimes is therefore highly uncertain. The binary consideration of high- and low-NO_x base case and SOM parameterizations indicate that uncertainties in the NO_x regime can introduce a factor of ~2 or more uncertainty into SOA predictions. Further improvements in the representation of SOA NO_x dependence are needed.

Figure 3 shows that accounting for vapor wall losses in the SOM fits to smog chamber experiments increased ambient SOA predictions in both Los Angeles and the Eastern US. The range of wall-loss correction is uncertain but the higher estimates yield predictions for the diurnal profile of SOA concentrations that better match measurements in Southern California. While improved, the "high" vapor wall loss simulations still generally under-predict the

observed dilution-corrected SOA, which could indicate contributions from un-considered SOA precursors (e.g. semi- and intermediate-volatility organic compounds) or less well constrained oxidation pathways (e.g. nocturnal oxidation by NO_3 radicals).
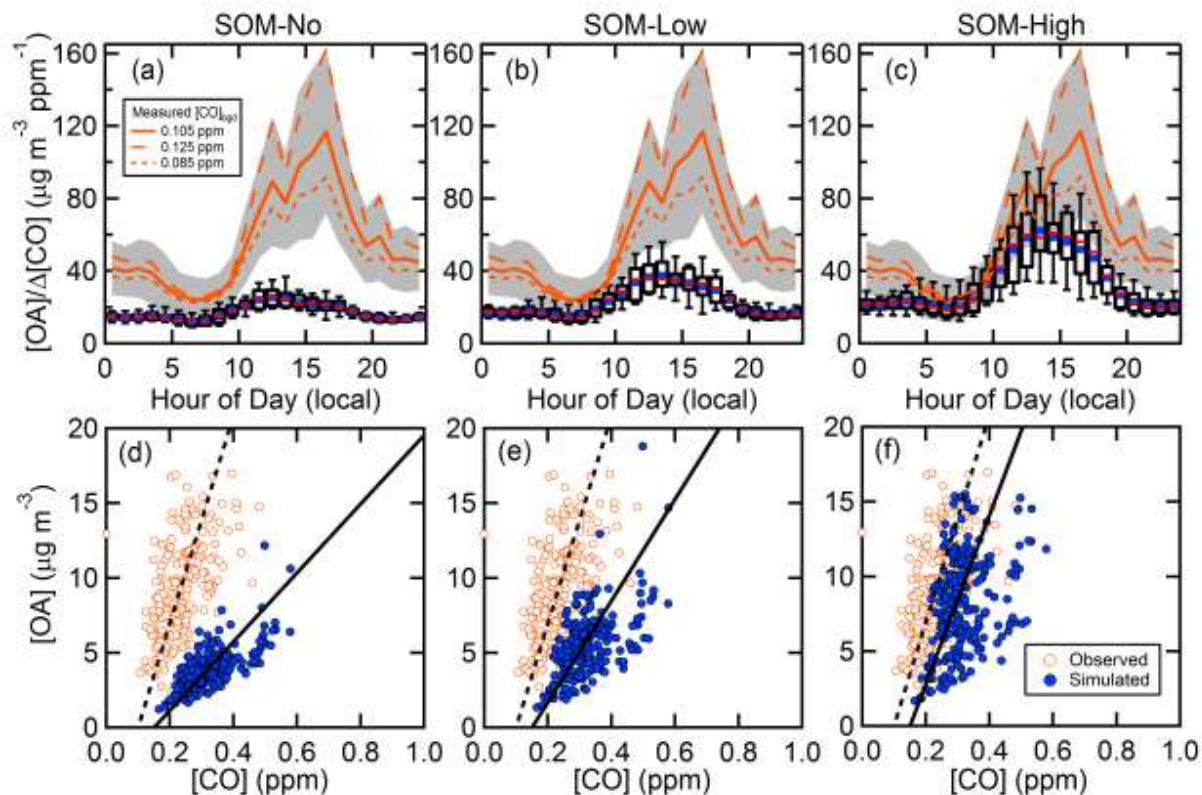
Figure 3: Simulated and observed diurnal profiles for the OA/ΔCO ratio (top panels) at Riverside, CA during the SOAR-2005 campaign for (a) SOM-no, (b) SOM-low and (c) SOM-high simulations, which refer to the vapor wall loss condition.

Task 2: Figure 4 shows that adding explicit reactions between biogenic VOCs and NOx to the SAPRC11 had little effect in the winter but increased predicted SOA concentrations by 0.9-1.0 µg m^{-3} in a summer analysis period. The majority of the additional SOA was composed of monoterpene nitrates and glyoxal / methyl glyoxal. Total nitrate concentrations did not change significantly in response to the added reactions.

(a) Ozone	(b) Organic Aerosol	(c) Nitrate
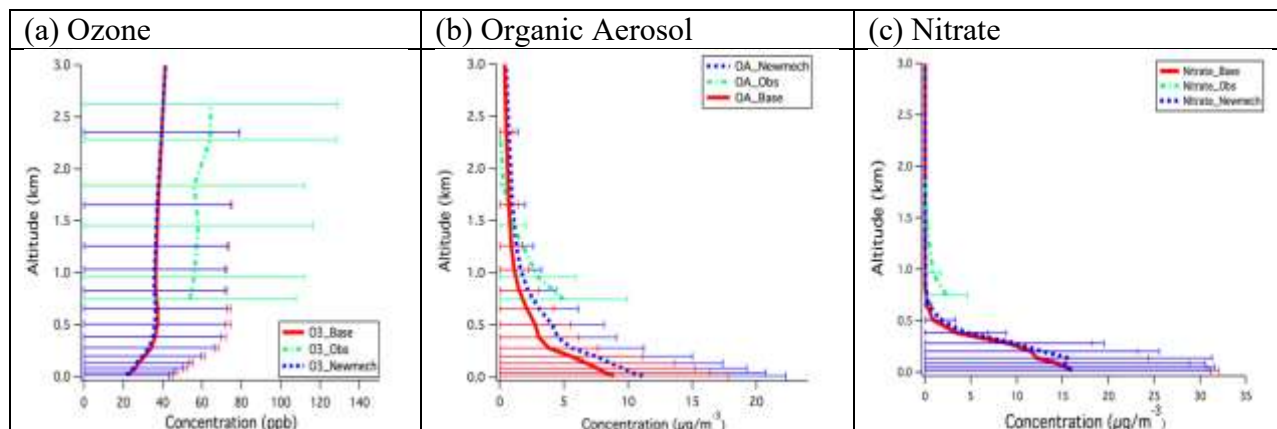
Figure 4: Change in predicted concentration caused by adding explicit reactions between biogenic VOCs and NOx in the SAPRC11 mechanism. Red line is base model, blue line is expanded model, and green line is measured concentration. Results are for June 3, 2010 above Pasadena.

Task 3: Figure 5 shows that the calculated ozone formation potential (g O3/g VOC) increased by approximately 17.3% between 1988 and 2010 for most VOCs under the actual conditions experienced in 39 cities across the US. The Maximum Incremental Reactivity (MIR) (g O3 /g VOC) decreased by ~41.1% between 1988 and 2010 for most VOCs under the artificially high NOx conditions that produce MIR values. The relative ranking of VOCs based on their ozone formation potential did not change significantly between 1988 and 2010.
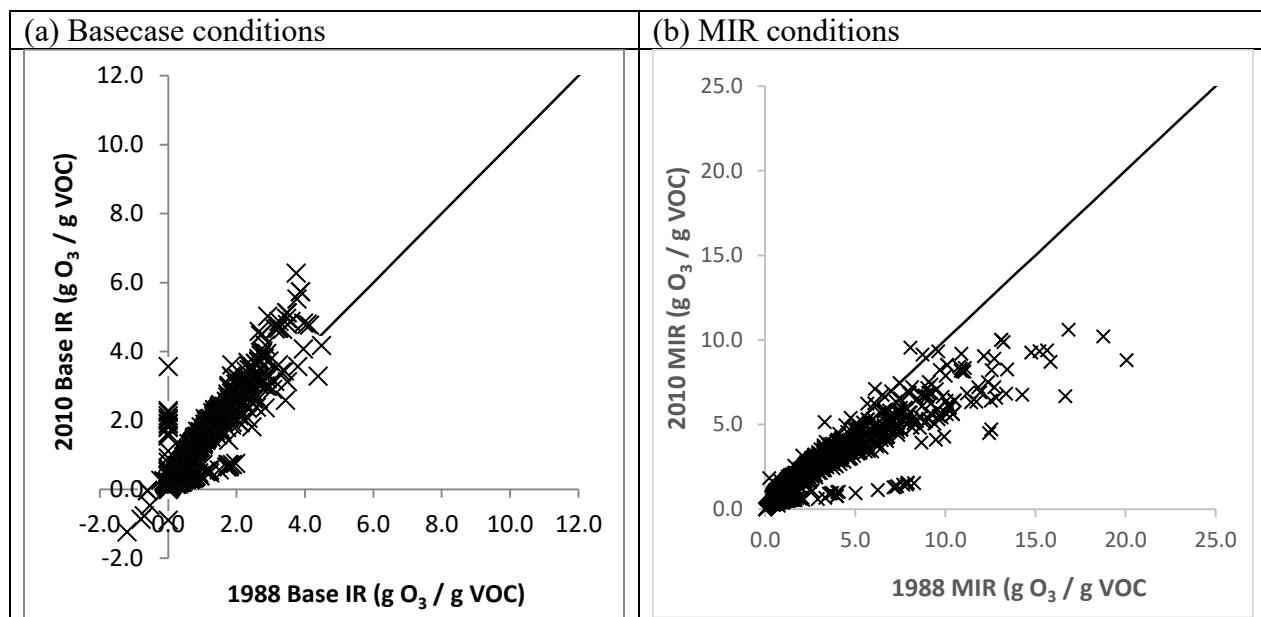
Figure 5: Ozone formation potential (g O3/g VOC) for 1192 different VOCs in 39 US cities using conditions from 1988 (x-axis) and 2010 (y-axis). Panel (a) illustrates results under the basecase conditions experienced in the 39 cities. Panel (b) illustrates results under the artificial MIR conditions.

Conclusions:
Task 1: Multi-generational aging of VOCs can be tracked explicitly in models such as SOM but the effects of aging are also approximately captured in two-product models for SOA that are fit to relevant chamber experiments. The amount of SOA predicted using an explicit representation of multi-generational aging in the SOM model is similar but slightly lower than the amount of SOA predicted by the corresponding two-product model. The correction of vapor wall losses in the SOM model increases the predicted amount of ambient SOA in simulations for both Los Angeles and the Eastern US under low-NOx conditions, but this enhancement is reduced under high-NOx conditions. Future studies should verify existing parameterizations of NOx dependence on SOA yields within regional chemical transport models.

Task 2: Explicit reactions describing the interactions between biogenic VOCs and NOx have little effect in winter but yield modest increases of ~1 μg m^{-3} in SOA concentrations during summer conditions. Emissions control programs that reduce ambient NOx concentrations will likely also reduce PM2.5 biogenic SOA concentrations by a small amount due to reduced formation of glyoxal / methyl glyoxal and monoterpene nitrates.

Task 3: The reactivity of VOCs as measured by the amount of O3 produced per unit of VOC reacted has increased between 1988 and 2010 due to changes in meteorological conditions, background VOC concentration/speciation, and emissions rates/speciation. Meteorological effects were primarily attributed to shifting seasons for peak ozone events and / or improved predictions for boundary layer heights. These results suggest that further emissions limits may be required for VOCs in regions that seek to continue lowering ambient ozone concentrations.

Future Work: The combined results from Tasks 1-3 address important questions related to air quality modeling in California and suggest logical paths for future work.

Task 1: The latest information about multi-generational oxidation, vapor wall losses, POA volatility, and S/IVOC emissions should be combined in a comprehensive model evaluation to determine the net effect on predicted organic aerosol concentrations in California. The algorithms used to select between high-NOx vs. low-NOx parameterizations in regional air quality models should be reviewed given the significant impact that this choice has on predicted SOA concentrations.

Task 2: Longer simulations should be conducted with the expanded SAPRC11 chemical mechanism to determine SOA yields from NOx reactions with biogenic hydrocarbons and the potential to reduce biogenic SOA concentrations through NOx control programs.

The cause of significant under-predictions for isoprene concentrations in California should be identified and corrected.

The resolution of model calculations should be increased to scales finer than 4km to properly represent nighttime reactions when the atmosphere is not well mixed.

Task 3: The limits applied to emissions of individual VOCs should be reviewed in the context of updated rankings based on contemporary conditions.

1   INTRODUCTION

1.1   Motivation

Photochemical air quality models are the primary tool for determining the limiting precursors for various secondary pollutants in California air sheds. Chemical mechanisms are an integral part of these photochemical air quality models and must represent the state-of– the-science understanding of how ozone and other secondary pollutants are formed and their relationships to the primary pollutants emitted from different sources. Photochemical air quality models are also routinely used in California to assess the effectiveness of air pollution control strategies to achieve the National Ambient Air Quality Standards (NAAQS) for both ozone and particulate matter (PM). Therefore, it is critical that SAPRC chemical mechanisms used in ARB's photochemical air quality models are based on the best science and updated periodically.

SAPRC chemical mechanisms have been developed or updated under ARB's sponsorship for the past 3 decades. The current widely used version of the SAPRC mechanisms is SAPRC-07, which represents the state of the science as of 2007. An updated SAPRC16 version of the aromatics mechanism was recently developed for ARB and is currently under peer review so that it can be incorporated into the modeling community and used to update the reactivity scales for VOCs.

SAPRC16 continues the SAPRC tradition of using lumped model species to represent groups of similar molecules in an effort to mechanistically represent atmospheric chemistry without incurring the massive costs associated with fully explicit chemical mechanisms such as the master chemical mechanism (MCM) [1, 2].   The SAPRC16 mechanism improves the representation of reactions that form SOA precursors from aromatic compounds, but a full mechanistic description of SOA formation from anthropogenic VOCs is still several generations away.

Over the past decade, several groups have proposed using approximate SOA calculations that fit parameters within conceptual models for SOA formation to chamber experiments and then extend the calculations to atmospheric simulations [3].   These models describe compounds spanning a range of volatility and include schemes to age the compounds across multiple generations leading to more material at decreased volatility that ultimately produce SOA [3]. This latest generation of SOA calculations is generally viewed as an improvement over the previous generation of "2 product models" [4] that have widely known deficiencies [5].   These models have not yet been rigorously tested in California.

Engineering models such as those described above are necessary in the short term, but a more mechanistic understanding of SOA development is preferable in the longer term.   Multiple studies have recently elucidated reaction pathways for the formation of SOA through the reactions between NOx and biogenic VOCs [6, 7].   The importance of these mechanisms in California has not yet been evaluated.

ARB's regulatory photochemical air quality modeling program, which provides the technical basis for both ozone and PM State Implementation Plans (SIP), routinely uses the state-of-the-

science models that contain the latest SAPRC chemical mechanism. Further improvements to this chemical mechanism will allow ARB's regulatory efforts to be based on the most credible emissions control strategies.

1.2   Research Objectives

The primary objective of this project is to further update and comprehensively evaluate detailed and condensed SAPRC mechanisms for use in photochemical air quality models that predict both gas phase and particle phase criteria pollutant concentrations. Although a recently completed mechanism project represents significant progress in the process of adapting gas-phase mechanisms to predict SOA formation from aromatics in the atmosphere [8], compounds other than aromatics should be included in modeling SOA formation.

1.3   Project Tasks

The following major tasks were identified:

Task 1: SAPRC Secondary Organic Aerosol Development.

Currently SAPRC predicts the rate of production of secondary inorganic aerosol compounds, such as nitric acid, that are partitioned between the gas and particle phase by an aerosol operator that runs in parallel with the SAPRC photochemical operator. Also, SAPRC currently focuses on predicting the concentration of gas-phase criteria pollutants and so tracks the photochemical degradation of primary volatile organic compounds for only the few generations necessary for these predictions. Accurate prediction of secondary organic aerosol compounds requires tracking the photochemical degradation of these primary VOCs for many more generations since each generation has the potential to substantially lower the vapor pressure of the reaction products. Due to the branching of the reaction pathways, the number of reactions to track grows rapidly as the number of reaction generations increases making the prediction of SOA computationally intractable [9-12] and difficult to parameterize.

Investigators at UC Davis and Lawrence Berkeley National Laboratory recently published a Statistical Oxidation Model (SOM) [13] that provides a computationally-tractable framework for predicting the formation of low volatility organic compounds that result from many-generation oxidation. In brief, the SOM allows for multi-generational, multi-phase (gas + particle) oxidation of species within an oxygen:carbon (O:C) grid. The properties of species within a given O:C grid cell and the rules for moving between O:C grid cells are fit to smog chamber data to allow for efficient, accurate and general simulation of SOA formation.

The SOM model requires parameters that must be fit to results from smog chamber experiments. Under funding from the National Science Foundation and the Department of Energy, investigators at Caltech have run numerous smog chamber experiments to characterize the secondary organic aerosol yield from various precursor gas phase organic compounds and their photochemical reactants, under a range of seed aerosol, temperature and humidity conditions

(e.g.[14-28]). Investigators at other universities, such as UC Riverside, have also performed numerous similar experiments that may provide suitable data for fitting of SOM parameters.

During Task 1 of the current project,

(1) SAPRC and SOM were combined into one photochemical modeling framework (SAPRC14) such that;
    (a) SAPRC14 continued to predict criteria pollutant and secondary inorganic aerosol concentrations as accurately as SAPRC does currently;
    (b) SAPRC14 also predicted the concentrations and vapor pressures of secondary organic aerosol compounds that have been characterized in smog chamber experiments by Caltech and other investigators worldwide; and
    (c) In the future, SAPRC14 can accommodate new data and reaction pathways that lead to gas-phase and particle-phase criteria pollutants.
    (d) Additional smog chamber experiments were performed at Caltech to fill the most important data gaps in the reaction pathways of biogenic and anthropogenic VOCs that lead to SOA.

Task 2. Update the modeling scenarios used in reactivity assessment.

One important application of the SAPRC chemical mechanism is to estimate ozone-forming potential of individual VOCs (reactivity) using a computationally efficient box model calculation. A basecase ozone formation system is defined and the additional ozone that forms per unit of individual VOC addition is predicted. Key inputs for this calculation include realistic VOC surrogate concentrations, emissions data, and meteorological scenarios that define the basecase for typical urban locations. The original VOC surrogate concentrations, emissions data, and meteorological scenarios were compiled based on 1980's data from 39 urban cities across the US. VOC surrogate concentrations were recently updated [29] for Los Angeles.

During Task 2 of the current project

(2) The conditions used to evaluate VOC reactivity were updated to the year 2010.
    (a) New meteorological scenarios were developed to represent modern conditions in 39 urban regions across the US.
    (b) New emissions scenarios were developed based on conditions in the target cities.
    (c) Background VOC concentrations were developed using full model simulations over the target cities.
    (d) Updated meteorological scenarios were combined with updated emissions and background VOC concentrations to assess VOC reactivity in 39 urban regions across the US.

Task 3. Evaluate organic nitrate and N2O5 chemical mechanisms and assess their impact on secondary aerosol formation.

Atmospheric nitrogen plays a critical role in ozone production and it contributes to particulate nitrate formation. Calculations consistently show that chemical pathways passing through N2O5

contribute strongly to particulate nitrate in the San Joaquin Valley and the South Coast Air Basin, especially during cooler fall and winter months when daytime oxidant concentrations are reduced. A recent comprehensive review of N2O5 summarizes heterogeneous atmospheric chemistry, ambient measurement, and model simulations, and entails additional research needs [30].

During Task 3 of the current project:

> (3) The SAPRC11 chemical mechanism was updated to represent explicit reactions between biogenic VOCs and NOx that may influence predicted concentrations of secondary organic aerosol and nitrate.
>> (a) The new chemical mechanism was used to simulate the CALNEX field campaign in the South Coast Air Basin in July 2010. Comparisons were made to all available ground-level and aircraft measurements.
>> (b) The new chemical mechanism was used to simulate the DISCOVER-AQ field campaign in the San Joaquin Valley in January 2013. Comparisons were made to all available ground-level and aircraft measurements.

1.4 Report Structure

This report is comprised of 7 chapters, including introduction (Chapter 1) and conclusions (Chapter 7).

Chapter 2 describes the integration of the Statistical Oxidation Model with the SAPRC11 chemical mechanism and the creation of a set of FORTRAN subroutines suitable for integration with reactive chemical transport models.

Authors note: The work in chapter 2 has been published in the journal Geophysical Model Development and may be cited in any future studies as "S.H. Jathar, C.D. Cappa, A.S. Wexler, J.H. Seinfeld, and M.J. Kleeman. Multi-generational Oxidation Model to Simulate Secondary Organic Aerosol in a 3D Air Quality Model. Geophysical Model Development, 8, pp2553-2567, 2015."

Chapter 3 investigates how incorporation of multigenerational chemistry within a secondary organic aerosol model influences predicted concentrations in California and the Eastern United States.

Authors note: The work in chapter 3 has been published in the journal Atmospheric Chemistry and Physics and may be cited in any future studies as "S.H. Jathar, C.D. Cappa, A.S. Wexler, and M.J. Kleeman. Simulating secondary organic aerosol in a regional air quality model using the statistical oxidation model – Part 1: Assessing the influence of constrained multi-generational ageing. Atmospheric Chemistry and Physics, 16, 2309-2322, 2016."

Chapter 4 expands on the investigation in Chapter 3 by also considering the effects of vapor losses to chamber walls in the experiments used to calibrate the secondary organic aerosol model.

Authors note: The work in chapter 4 has been published in the journal Atmospheric Chemistry and Physics and may be cited in future studies as "Source: C.D. Cappa, S.H. Jathar, M.J. Kleeman, K.S. Docherty, J.L. Jimenez, J.H. Seinfeld, and A.S. Wexler. Simulating secondary organic aerosol in a regional air quality model using the statistical oxidation model – Part 2: Assessing the influence of vapor wall losses. Atmospheric Chemistry and Physics, 16, 3041-3059, 2016."

Chapter 5 summarizes the re-evaluation of the ozone formation potential of volatile organic compounds (VOCs) under modern conditions for meteorology, emissions, and background VOC concentrations.

Authors note: The work of chapter 5 is still under development and will be submitted for publication at a future date.

Chapter 6 evaluates how detailed reactions between biogenic VOCs and oxides of nitrogen influence predicted concentrations of secondary organic aerosol and nitrate in California.

Authors note: The work of chapter 6 is still under development and will be submitted for publication at a future date.

1.5 Published Manuscripts

The following manuscripts have been published under full or partial support from the current project.

S.H. Jathar, C.D. Cappa, A.S. Wexler, J.H. Seinfeld, and M.J. Kleeman. Multi-generational Oxidation Model to Simulate Secondary Organic Aerosol in a 3D Air Quality Model. Geophysical Model Development, 8, pp2553-2567, 2015

S.H. Jathar, C.D. Cappa, A.S. Wexler, and M.J. Kleeman. Simulating secondary organic aerosol in a regional air quality model using the statistical oxidation model – Part 1: Assessing the influence of constrained multi-generational ageing. Atmospheric Chemistry and Physics, 16, 2309-2322, 2016

C.D. Cappa, S.H. Jathar, M.J. Kleeman, K.S. Docherty, J.L. Jimenez, J.H. Seinfeld, and A.S. Wexler. Simulating secondary organic aerosol in a regional air quality model using the statistical oxidation model – Part 2: Assessing the influence of vapor wall losses. Atmospheric Chemistry and Physics, 16, 3041-3059, 2016.

Additional manuscripts describing results from studies on ozone reactivity and NOx/VOC reactions in California will be submitted for publication at a future date.

2   MULTI-GENERATIONAL OXIDATION MODEL TO SIMULATE SECONDARY ORGANIC AEROSOL IN A 3D AIR QUALITY MODEL

Online link: S.H. Jathar, C.D. Cappa, A.S. Wexler, J.H. Seinfeld, and M.J. Kleeman. Multi-generational Oxidation Model to Simulate Secondary Organic Aerosol in a 3D Air Quality Model. Geophysical Model Development, 8, pp2553-2567, 2015

2.1   Introduction

Fine-mode organic particulate matter or organic aerosol (OA) accounts for roughly half of the dry ambient aerosol mass yet it remains one of its least understood constituents [31]. Ambient OA exists as a complex mixture of thousands of compounds with very different physical and chemical properties that arise from a host of sources and reaction pathways [32]. This OA and the organic vapors in equilibrium with it together form a dynamic system in which their mass, chemical composition and environmental properties are constantly evolving as a result of gas-, surface- and particle-phase reactions coupled to condensation and evaporation. The complexity and dynamic behavior have made it difficult to identify and model the dominant pathways that control the atmospheric burden of OA, which limits our ability to quantify its climate- and health-relevant properties.

OA is either directly emitted as primary organic aerosol (POA) or formed in the atmosphere from the oxidation of volatile organic compounds (VOC) as secondary organic aerosol (SOA). Most box (0D) and large-scale (3D) models represent SOA production from the gas-phase oxidation of certain VOCs (large alkanes, aromatics and terpenes) to yield 2 to 4 low-volatility products that partition into the particle phase [33-35]. Laboratory chamber data provide the basic information on which these SOA formation models are built. It is widely recognized that gas-phase VOC oxidation products (or more generically organic vapors) can undergo multi-generational oxidation, given sufficient time in the atmosphere, which may substantially alter the mass and properties of SOA. For example, chamber studies using surrogate molecules – aldehydes to represent gas-phase oxidation products of alkanes [36] and biogenic VOCs [37] and phenols to represent those from aromatics [38] – have highlighted the potential of VOC oxidation products to undergo multi-generational oxidation to form SOA. In chamber experiments conducted at four different facilities, Donahue et al. (2012) showed that semi-volatile organic vapors, formed from the ozonolysis of alpha-pinene, subsequently reacted with the hydroxyl radical (OH) to enhance SOA mass concentrations. While it is likely that virtually all oxidation products from SOA precursors subsequently react, what is less clear is the relevance of multi-generational oxidation of different classes of SOA precursors to the concentrations and properties of ambient OA under typical atmospheric conditions.

Laboratory chamber studies, on account of their reaction times and typical oxidant levels, are dominated by products from the first few generations of VOC oxidation; a typical chamber experiment captures from one-half to one day of atmospheric oxidation and does not fully replicate the typical atmospheric lifetime of reactive organic compounds. However, since 2nd and later-generation products are often likely to have lower vapor pressures, and thus greater SOA formation potential, SOA formation may be influenced by later generation products even at short

oxidation lifetimes. A few simple schemes have attempted to account for this multi-generational oxidation within air quality models. Most often, multi-generational oxidation has been implemented by allowing for the parameterized surrogate semi-volatile product species to undergo further "ageing" reactions. For example, Robinson et al. (2007) assumed that primary organic vapors (semi-volatile and intermediate volatility organic compounds; SVOC and IVOC) sequentially react with the OH to form products that are an order of magnitude lower in volatility than their precursor. Pye and Seinfeld (2010) represented the same pathway through a single-step reaction that reduced the volatility of the vapors by two orders of magnitude. Lane et al. (2008) and Baek et al. (2011) modeled ageing of semi-volatile SOA vapors by assuming that each reaction with the OH radical resulted in progressively lower volatility products. While such schemes have the potential to improve model-measurement comparisons, they have at least three major drawbacks. First, they do not consider the role of fragmentation, which has been shown to be quite important for oxygenated SOA precursors [42] and can lead to decreases in SOA concentrations. Second, they assume that the oxidation reactions proceed similarly for products from different classes of SOA precursors, i.e., multi-generational oxidation of alkane, aromatic, or biogenic SOA is the same. Finally, current schemes have not been tested against or constrained by measurements of multi-generational products (or classes of products) under realistic ambient conditions.

Multi-generational VOC oxidation, in theory, can be explicitly modeled using detailed gas-phase chemical mechanisms such as the MCM (Master Chemical Mechanism [1, 2]) or GECKO-A (Generator of Explicit Chemistry and Kinetics of Organics in the Atmosphere [9, 43]) and have been put to use to develop a better understanding of the reaction chemistry leading to SOA formation [11, 12, 28]. However, these mechanisms track thousands to millions of chemical species and are computationally impractical for modeling multi-generational oxidation in 3D models. Recently, there has been the development of two frameworks of intermediate complexity that allow for the treatment of multi-generational oxidation (and other aerosol processes) during SOA formation: the two-dimensional volatility basis set (2D-VBS) that uses vapor pressure and O:C (oxygen to carbon) ratio as the independent variables [44, 45] and the statistical oxidation model (SOM) that uses the number of carbon atoms and oxygen atoms per molecule as independent variables [46]. Both have provisions to treat fragmentation of the reactants as a function of their oxygen content and can be parameterized from chamber measurements [47, 48]. Both frameworks require tracking on the order of hundreds of model species, which is more computationally expensive than models with less detail, but still sufficiently modest to be realistically implemented in 3D models today.

This work describes the first implementation of the SOM model of Cappa and Wilson (2012) in a 3D air quality model. Details are provided regarding: (a) the SOM parameterization using recent low and high NO_x chamber data for six different classes of SOA precursors; (b) the integration of SOM with the gas-phase chemical mechanism SAPRC-11; and (c) the coupling of SOM with the UCD/CIT model to make air quality predictions over 2-week periods in the South Coast Air Basin (SoCAB) of California and the eastern United States (US). General results from the simulations are discussed and briefly compared with results from a current generation SOA model.

2.2 Model Description

2.2.1 Air Quality Model

The UCD/CIT air quality model is a regional chemical transport model (CTM) [49] that has been extensively used for predicting regional aerosol concentrations, including SOA [50, 51]. The UCD/CIT model simulates the emissions, transport, gas-phase chemistry, aerosol physics and chemistry (dynamic gas/particle partitioning, coagulation, thermodynamics and deposition) in the lower troposphere. The UCD/CIT model employs the condensed form of the SAPRC-11 gas-phase chemical mechanism to simulate gas-phase chemistry [52] and ISORROPIA to model inorganic aerosol thermodynamics [53]. Aerosols are represented using an 8 bin moving sectional approach to encompass a size range of 10 nm to 10 µm.

The model simulated air quality in two domains: (1) the state of California at a grid resolution of 24 km x 24 km followed by a nested simulation over SoCAB at a grid resolution of 8 km x 8 km and (2) the eastern half of the US, roughly east of the great continental divide, at a grid resolution of 36 km x 36 km. Vertically, the model domain extends up to 5 km, which is divided into 16 layers. The UCD/CIT model was run for California from July 20 to August 2, 2005 and run for the eastern US from August 20 to September 2, 2006.

2.2.2 Emissions

Anthropogenic VOC and primary particulate emissions for California are based on the California Regional PM10/PM2.5 Air Quality Study (CRPAQS) inventory of 2000 but scaled to 2005 by adjusting emissions in 2000 by fuel consumption activity [55]; emissions for area sources, point sources, and off-road sources are not changed from their year 2000 levels. FINN (Fire Inventory for National Center for Atmospheric Research) [56] and MEGAN (Model of Emissions of Gases and Aerosols from Nature) [57] are used to calculate wildfire and biogenic emissions, respectively, in California. Anthropogenic and wildfire VOC and primary particulate emissions for the eastern US are based on the 2005 National Emissions Inventory (NEI) and biogenic emissions are estimated using BEIS (Biogenic Emissions Inventory System) version 3. More details pertaining to the emissions can be found in Jathar et al. (submitted) .

The chemical mechanism SAPRC-11 is used to represent the gas-phase chemistry, from which the following model species are considered to form SOA: ALK5 (long alkanes), BENZENE (benzene), ARO1 and ARO2 (other aromatics), ISOPRENE (isoprene), TRP1 (monoterpenes) and SQT (sesquiterpenes). Except for alkanes, emissions of these model species are directly used by the SOM.

The carbon number and structure of an alkane influences its SOA mass yield; for the same structure the SOA potential increases with carbon number [59, 60], while for the same carbon number cyclic alkanes form the most SOA followed by linear and then branched alkanes [59, 61]. However, in 3D models that employ SAPRC-11, a single model VOC species, ALK5, is used to describe the SOA formation from alkanes roughly larger than a carbon number of 6. In order to more accurately represent the SOA formation from alkanes, and specifically the carbon chain-length dependence, ALK5 is split by carbon number into seven separate species that

represent alkane emissions ranging from 6 through 13 carbon atoms (i.e., ALK_Cxx, where xx = 06 to 13). It should be noted that the split ALK_Cxx emissions generally decrease with increasing carbon number.

Typically, gas-phase organic emissions (including those for alkanes) are calculated by multiplying the total VOC emissions rate (e.g., tons day^{-1}) by a normalized VOC profile. The emissions are calculated for each source classification code (SCC) using a SCC-specific VOC profile for all grid cells at every hour. The emissions pre-processor developed at UCD (University of California, Davis) directly uses SAPRC model-species-specific VOC profiles (e.g., ALK1=0.1, ALK2=0.03, ALK3=0.01, etc.) and hence does not contain carbon-number specific information to build alkane emissions by carbon number. To do so, we used the California Air Resources Board's speciated database (http://www.arb.ca.gov/ei/speciate/vv10001/profphp/orgspecvv10001_list.php) to rebuild source-resolved, normalized VOC profiles that now included eight new alkanes species (C_6 to C_{13}) to replace the ALK5 species. Only ALK5 is considered since that is the only model species to include alkanes with significant SOA-forming potential. These updated VOC profiles were then used to build gridded emissions for C_6 to C_{13} alkanes; alkanes larger than C_{13} were lumped into the C_{13} model species because they accounted for less than 0.5% of the C_{6+} alkane emissions. While these emissions could easily have been resolved by alkane structure (linear, branched and cyclic), we did not do so because recent work has suggested that profiles used for emissions inventory building are relatively incomplete in determining emissions of higher carbon-number branched and cyclic alkanes [62]. Since the SOA yields for branched and cyclic alkanes are, respectively, lower and higher than those for linear alkanes, we assume that by lumping them together for each carbon number the effective SOA yield is closer to that of a linear alkane. At this point in time, the carbon-number resolved alkane emissions have been developed only for SoCAB. For the eastern US, where a similar speciated database is not available, we use findings from the work of Pye and Pouliot (2012) to determine a linear alkane that could represent SOA formation from ALK5. Pye and Pouliot (2012) determined that national emissions of alkanes higher than a carbon number of 6 would produce the same amount of SOA as 53% of *n*-dodecane equivalent emissions. Correcting for differences in SOA mass yields, we assume that the ALK5 behaves like a C_{10} linear alkane.

2.2.3   *Meteorology and Initial / Boundary Conditions*

The Weather Research and Forecasting (WRF) v3.4 model (www.wrf-model.org) is used to generate hourly meteorological fields for both episodes. The National Center for Environmental Protection's North American Mesoscale (NAM) analysis data are used to set the initial and boundary conditions for WRF. Results from the global model MOZART-4/NCEP are used to set gas- and particle-phase initial and hourly-varying boundary conditions; more details can be found in Emmons et al. (2010).

2.2.4   *Base SOA Model*

The "Base" SOA model is equivalent to that used in the Community Multiscale Air Quality (CMAQ) model version 4.7 [4]. This Base model is representative of current-generation SOA

models. Here, the SOA precursors in SAPRC-11 oxidize in the gas phase to form fixed semi-volatile or non-volatile products that partition into the particle phase [33]. SOA formation from aromatics is dependent on the abundance of NO_x, forming different product species upon reaction depending on the NO_x condition. Aromatic peroxy radicals (RO_2) react with HO_2 under low NO_x conditions to form non-volatile SOA while they reacted with NO under high NO_x conditions to form semi-volatile SOA. In addition, the Base model treats the acid enhancement of isoprene SOA [63] and irreversible particle-phase oligomerization [64], which converts semi-volatile condensed-phase species into non-volatile species. We do not consider SOA formation from IVOCs or via aqueous phase processing. SOA is assumed to absorptively partition into all OA, including POA. The SOA model species are allowed to dynamically partition to the particle-phase as per Kleeman and Cass (2001) (and corrected according to Aw and Kleeman (2003))

where   is the particle concentration in μg m^{-3} of the SOA model species m and for particle size bin *n*,   is the gas-phase diffusion coefficient in m^2 s^{-1},   is the particle radius in m, is the particle number concentration in m^{-3},   corrects for non-continuum effects ( ),   is the mean molecular speed of the gas molecules in m s^{-1},   is the accommodation coefficient,   is the gas concentration in μg m^{-3} of the SOA model species,   is the gas/particle partitioning coefficient in m^3 μg^{-1} and   is the total OA concentration in μg m^{-3}. Here, we use an accommodation coefficient of 0.1, which corresponds to an equilibration timescale of less than ~10 minutes (McVay et al., 2014). Changes in   with temperature are modeled using the Clausius-Clapeyron equation:

where   is the reference temperature (298K),   is the enthalpy of vaporization and   is the universal gas constant. We assume a constant   of 30 kJ mole^{-1} for all SOM model species for consistency with the treatment of species in the Base model. This may somewhat underestimate the actual sensitivity to temperature of individual species [66].

2.2.5 *Statistical Oxidation Model*

SOM Overview

SOM was used to model the multi-generational, gas-phase oxidation of SOA precursors and their subsequent products along with gas-particle partitioning of all species [46]. SOM uses a two-dimensional carbon-oxygen grid to track the evolution and properties of gas- and particle-phase

organic precursors and products. Each cell in the grid represents a model organic species with a molecular weight defined by the formula   . SOM assumes that the oxygen is bonded to carbon via a single covalent bond and hence the hydrogen number is the same as the species' remaining valence; we assume that the SOM species have a straight chain carbon backbone. A SOM species reflects the average properties (e.g. vapor pressure, reactivity) of all actual species with the same number of carbon (N_C) and oxygen (N_O) atoms that are produced from a given precursor class (e.g., aromatics, alkanes). All SOM species are assumed to be reactive towards OH radicals in the gas phase. These reactions lead to either functionalization or fragmentation, which results in movement through the carbon-oxygen grid. Chamber data are used to fit six precursor-specific adjustable parameters for each precursor class: four parameters that define the molar yields of the four functionalized, oxidized products, one parameter that determines the probability of functionalization or fragmentation, and one parameter that describes the relationship between N_C, N_O and vapor pressure. Each class of precursor species (e.g., aromatics, alkanes) has its own uniquely defined "grid" that describes its gas-phase photochemical oxidation and SOA formation. In the following sections, we describe more details about the SOM and its implementation in the UCD/CIT model.

Multi-generational Gas-Phase Oxidation and Gas/Particle Partitioning

Figure 2-1 shows a schematic of the carbon-oxygen grid and illustrates the oxidation of a typical SOA precursor and the movement of the product species in the SOM grid. For example, a saturated alkane with 8 carbon atoms (ALK_C08 or $C_8H_{18}O_0$ or *n*-octane; orange cell) reacts with OH to directly form 1 of 4 functionalized products with 1 to 4 oxygen atoms attached to the carbon backbone (yellow cells). In parallel, an oxygenated species (e.g. $C_8H_{15}O_3$) reacts to form directly functionalized products ($C_8H_{15}O_{4-7}$) and two fragment species.
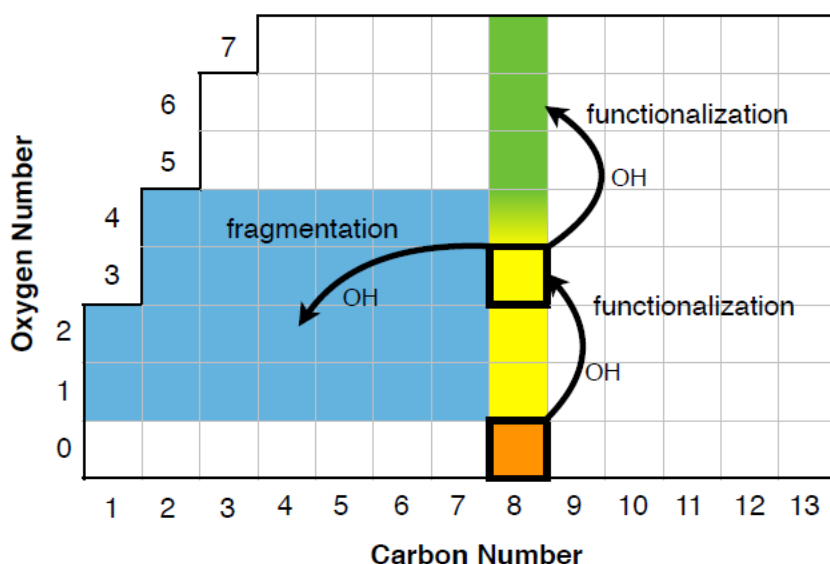
Figure 2-1: Schematic that demonstrates how the carbon-oxygen grid of the SOM captures the OH-driven multigenerational oxidation of gas-phase organics. Here, a hydrocarbon with 8 carbon atoms (C8H18O0; bordered orange cell) reacts with the OH radical and functionalizes to

form 4 products with 1, 2, 3 and 4 oxygen atoms (yellow cells). One of the products (C8H15O3, bordered yellow cell) further functionalizes to form 4 new products (green cells) or fragments while adding oxygen to form a host of products (blue cells).

The rate coefficients for the reaction of SOA precursors with OH are the same as those in SAPRC-11 (e.g., at 298 K ARO1 has a reaction rate coefficient of 6×10^{-12} cm^3 $molecule^{-1}$ s^{-1}). The reaction rate coefficients of non-precursor SOM species are functions of temperature (T) and carbon and oxygen number [67]:

where A_1 = -15.1, A_2 =-3.94, and A_3 = -0.797. It is assumed that the k_{OH} values for SOM species are the same in all precursor class grids, i.e. are not precursor specific, and thus describe the typical reactivities of oxidized hydrocarbon species. The particular dependence of k_{OH} on N_C and N_O was determined through comparison with results from the chemically-explicit GECKO model [9, 43].

Each compound has a probability of fragmenting, P_{frag}, or functionalizing, P_{func}, and $P_{func} + P_{frag}$ = 1, and functionalization has a probability of adding 1 to 4 oxygen atoms, p_{iO}, i = 1,4, $p_{1O} + p_{2O} + p_{3O} + p_{4O}$ = 1. The molar yield of each directly functionalized product, e.g. p_1, is therefore p_i = $P_{func} \times p_{iO}$, so the overall production of directly functionalized products can be written using n-octane as an example as:

Precursor-specific values of p_{1O}-p_{4O} and P_{func} are determined by fitting of the SOM to laboratory measurements.

In SOM, the probability of fragmentation of a given SOM species, P_{frag}, is dependent on the number of carbon and oxygen atoms and is parameterized as:

36

where m_{frag} is a fit parameter. Note that the fragmentation probability of species with zero oxygen atoms is zero in this formulation. In Figure 2-1, functionalized (green cells) and fragmented (blue cells) products from the oxidation of the model species $C_8H_{15}O_3$ are shown. In this case, the probability of fragmentation is $-$. When fragmentation occurs, two molecules are produced for which the total number of carbon atoms, summed over the two molecules, is conserved, but for which the total number of oxygen atoms is increased by two, with one oxygen being added to each fragment. Based on these criteria, all possible fragment species that can be formed from fragmentation of a given SOM species are identified. It is assumed that the formation of every species is equally probable such that the probability of forming a given fragment is $P_{frag}(N_C,N_O)/N_{fragments}(N_C,N_O)$, where $N_{fragments}(N_C,N_O)$ is the SOM species-specific number of possible fragments (note that this criterion differs from the original SOM parameterization in Cappa and Wilson (2012), where it was assumed that the individual fragments are generated with random probabilities.). We should note that the representation of the reaction chemistry in the SOM, in contrast to an explicit gas-phase mechanism like SAPRC, MCM or GECKO, is significantly simplified to capture the average chemistry. Further, each oxidation step in the SOM is an aggregation of numerous individual reaction steps, i.e. intermediate radical species are not explicitly simulated. For example, in reality each oxidation reaction is initiated through hydrogen abstraction to yield peroxy/alkoxy radicals. These radicals can go on to react (with HO_2, RO_2 or NO) or undergo isomerization to form low-volatility products such as organic nitrates, peroxides and hydroxy carbonyls, or can decompose leading to production of oxygenated fragments. These intermediate steps are not explicitly simulated, only the formation of the resulting stable product species.

The volatility of the model SOM species, and hence its propensity to partition to the particle phase, is defined by its N_C and N_O. The volatility is represented by the gas/particle partitioning coefficient (K_p) [68] and parameterized as:

where is the partitioning coefficient in $m^3 \mu g^{-1}$ for precursor-specific grid i, carbon number j, and oxygen number k, is the molecular weight of the hydrocarbon backbone in $gmole^{-1}$ (accounting only for carbon and hydrogen atoms) and is the decrease in volatility of the model species per addition of oxygen atom for grid i. This last term, ΔLVP_i, reflects the average change in vapor pressure due to the functional group added upon oxidation (e.g. alcohol, ketone) and is determined by fitting the SOM to chamber data. Differences in values of ΔLVP_i between different SOA precursors reflect differences in chemical reaction pathways between these precursors [46, 47]. The SOM model species are allowed to dynamically partition to the particle-phase as per equation 1.

In summary, as a VOC undergoes multi-generational oxidation the evolution of its oxidation products in the SOM grid is defined by six parameters: (i-iv) p_1-p_4, the yields of the four

products that add 1, 2, 3, and 4 oxygen atoms respectively, (v) m_{frag}, the parameter that characterizes the fragmentation probability, P_{frag}, and (vi) ΔLVP, the decrease in vapor pressure (or volatility) of the species per addition of an oxygen atom. Each of these parameters is determined through fitting of chamber experiments and then used in the regional model simulations.

While the SOM framework can be adapted to explicitly model other production and loss processes (e.g., oligomerization [69], heterogeneous reactions [70] in the atmosphere, in this work we consider parameterizations developed that consider only the multi-generational gas-phase oxidation of SOA precursors and their subsequent products. As with all existing SOA parameterizations that are used in 3D models, inherent in the parameterization are the effects of condensed-phase (and other unaccounted for) processes. As improved understanding of the kinetics and reaction chemistry of key heterogeneous and condensed-phase processes is developed they will be incorporated into the SOM framework.. The Base simulations include both acid-catalyzed isoprene SOA formation and irreversible oligomerization, while the SOM simulations include neither process. The gas-phase chemistry of the non-SOA forming VOCs is modeled using the gas-phase chemical mechanism, SAPRC-11. As noted above, only SOA formation from traditional VOC precursors is considered here, so as to be consistent with typical applications of CMAQ. However, the SOM framework is general and can incorporate SOA formation from non-traditional SOA precursors, such as SVOC and IVOC. As these SVOC and IVOC species are likely to resemble long-chain alkanes, they can be directly added to the "long alkanes" SOM grid, described in the next section.

SOM Grids and Parameterization

We use six SOM grids to represent the formation and evolution of SOA with a separate grid for each class of SOA precursors: long alkanes (ALK_C06 to ALK_C13), benzene, high-yield aromatics (ARO1), low-yield aromatics (ARO2), isoprene and mono and sesquiterpenes (TRP1 and SESQ). Table 1 lists the SOM parameters for each precursor class. Note that all SAPRC ALK_Cxx species are simulated together using a common grid. The SOM is parameterized for each grid, or precursor class, using data from experiments conducted in the Caltech environmental ("smog") chamber; the last column in Table 2-1 lists the references for the data. The parameters determined for *n*-dodecane are applied to C_6 through C_{13} alkanes since it was previously shown that the SOM framework captures the observed carbon chain-length dependence of SOA yields [59] for alkanes with good fidelity when a single set of parameters are used [13]. The parameters determined for α-pinene were also used for all sesquiterpenes, since these parameters were able to predict similar levels of SOA as those measured for a range of sesquiterpenes [71].

Table 2-1: SAPRC-11 Model Species, Corresponding SOM Grids, Surrogate Molecules, SOM parameters, O:C, Data Sources.

SAPRC-11 Species	SOM Grid	Surrogate to determine SOM fits	NO_x	$\mathit{\Delta LVP}$	P_{func}				m_{frag}	O:C (end-of-experiment)	Reference
ALK_C06 to ALK_C13	Long alkanes	n-dodecane	Low	1.54	0.717	0.278	0.0028	0.0022	0.122	0.34	Loza et al. (2014)
			High	1.39	0.927	0.0101	0.018	0.0445	0.098	0.36	
Benzene	Benzene	Benzene	Low	2.01	0.769	0.001	0.0505	0.18	2.01	0.71	Ng et al. (2007)
			High	1.7	0.0792	0.001	0.919	0.001	0.535	0.97	
ARO1	High-yield aromatics	Toluene	Low	1.84	0.561	0.001	0.001	0.438	0.01	0.61	Zhang et al. (2014)
			High	1.24	0.0029	0.001	0.001	1.01	0.222	1.02	
ARO2	Low-yield aromatics	m-xylene	Low	1.76	0.735	0.001	0.002	0.262	0.01	0.54	Ng et al. (2007)
			High	1.68	0.936	0.001	0.0021	0.0609	0.01	0.55	
Isoprene	Isoprene	Isoprene	Low	2.26	0.973	0.001	0.001	0.026	0.01	0.81	Chhabra et al. (2011)
			High	1.94	0.952	0.0011	0.0304	0.0163	0.0632	0.9	
TRP1/SESQ	Terpenes	α-pinene	Low	1.87	0.001	0.869	0.0776	0.0525	0.01	0.4	Chhabra et al. (2011), Griffin et al. (1999)
			High	1.62	0.068	0.633	0.275	0.0244	0.0353	0.5	

Two sets of six parameters were determined for all six grids by separately fitting experiments that were conducted under low NO_x (high yield) and high NO_x (low yield) conditions; the SOM parameters are listed in Table 2-1. The NO_x-dependence of SOA formation is consequently treated in a binary manner because the SOM in its current configuration does not allow for continuous variation in the dependence of SOA on NO_x. More details about the fitting process and the experimental chamber data can be found in Cappa et al. (2013)   and Zhang et al. (2014). Briefly, measurements of VOC decay during the chamber experiment were used to estimate OH concentrations that were then used to represent the oxidation of the SOM model species. Values of the six parameters were determined with the built-in curve fitting tool in IGOR Pro 6.3 (Wavemetrics, Lake Oswego, OR) by treating SOM as a user-defined function. The best fit was determined as that which gave the best agreement between simulated and observed SOA concentrations as a function of time, and where OA concentrations had been corrected for particle wall losses. The curve fitting tool used the Levenberg-Marquardt algorithm to minimize the Chi-square parameter. While important, the fitting did not consider the influence of organic gas/vapor losses to the chamber walls [67] and hence the fitted parameters represent the minimum potential of the precursor to form SOA; the influence of gas/vapor wall losses on the SOM parameters and consequently on regional SOA concentrations will be explored in a follow-up study. The fitting was undertaken assuming a monodisperse particle size distribution that matched the aerosol surface area in the chamber experiment and an accommodation coefficient of 1. Using an accommodation coefficient of 1 or 0.1 did not dramatically change the fitted parameters since the timescale to achieve gas/particle equilibrium is less than a few minutes for these conditions and much faster than the timescale of SOA formation in these experiments [67, 72].

It should be noted that the experimental data used here to determine the SOM fit parameters are not the same data as used in developing the parameters in the Base model [4]. This difference in datasets can be expected to lead to some differences in the resulting simulated SOA concentrations. The use of an alternative data set, with typically newer data, here is justified by the higher time resolution on the precursor decay, often-longer reaction times, and better quantification of chamber particle wall losses.

Implementation

The multi-generational gas-phase oxidation reactions of the SOM were directly added to the gas-phase mechanism of SAPRC-11 using the SAPRC mechanism compiler maintained by UC Davis. This allowed us to control the number of the SOM grids and the parameterizations for each SOM grid; the mechanism compiler is publically available at http://webwolf.engr.ucdavis.edu/data/mechanism_compiler/mechanism_generator_v1.html. The compiler accepts a .RXN SAPRC mechanism file [73] as input and generates a Fortran file that solves the right hand side of the differential equation for all gas-phase species including the SOM model species (see equation 10 below). Links to the Fortran output files (one for SOM (low yield) and one for SOM (high yield)) used in this work are also provided at the URL mentioned above. The rules described above that define the fate (production and loss) of any

given SOM species have been incorporated into the automated mechanism compiler. The formation of each grid species is governed by:

-----

where X is the number of carbon atoms, Z is the number of oxygen atoms (≥ 0), j_{max} is the maximum number of carbon atoms in a grid and k_{max} is the maximum number of oxygen atoms in a grid (specified here as 7). In the equation, we deliberately omit hydrogen from the representation of the SOM model species for clarity and also because the hydrogen number is not explicitly tracked in the SOM but rather determined by the remaining valence. The maximum number of oxygen atoms considered is restricted by physical limitations. For compounds with large N_C the addition of oxygen by a gas-phase reaction is constrained by the low volatility of the SOM species partitioning most of the compound into the condensed phase. For small N_C, large values of N_O give large N_O/N_C, which dictates extensive fragmentation. Tests using SOM in box model formulation indicate that $k_{max} = 7$ is a reasonable threshold such that changing k_{max} by one oxygen does not affect the results. Compounds with X carbon atoms that would theoretically have more than k_{max} oxygen atoms based on the rules governing the SOM are placed into the grid cell associated with the   species.

A separate operator was added to UCD/CIT to calculate dynamic gas/particle partitioning of the SOM model species. The numerical solutions for the gas-phase chemistry and gas/particle partitioning at each time step were performed using operator splitting. In all, 324 gas-phase species and 2592 (=324 species across 8 size bins) particle-phase SOM model species were added to the UCD/CIT model for the simulations reported here.

2.2.6   Simulations and Computational Considerations

We performed one simulation with the Base SOA model and two simulations with the SOM SOA model, one using parameters determined from fitting high NO_x (low yield) experiments and one using low NO_x (high yield) parameters. The SOM simulations will be referred to as SOM (low yield) or SOM (high yield). All simulations were performed for both domains: SoCAB and the eastern US. The simulations were performed on a computer cluster operated and maintained at the University of California, Davis. Each simulation was performed using Intel Core i5-3570s for a total of 40 core processors and shared memory of 40 GB. The simulations were performed for 19 days with the first 5 days used for spin up. For the SoCAB, each simulated day required approximately 4 hours of elapsed time so a 19-day episode was simulated in less than 4 days. For the eastern US, each simulated day required approximately 9 hours of elapsed time so a 19-day episode was simulated in about 8 days. SOM simulations typically required 8 times more computational time than the Base SOA model simulations.

2.3 Results

2.3.1 SOA Concentrations and Precursor-Resolved Composition

We plot the domain-wide, 14-day averaged SOA concentrations from the SOM (low yield) and SOM (high yield) simulations for SoCAB in Figure 2-2(a-b) and for the eastern US in Figure 2-3(a-b). In SoCAB, the predicted SOA concentrations varied between 0.3 and 1 $\mu g\ m^{-3}$ for the SOM (low yield) simulation. Higher concentrations of SOA were predicted on the coast northwest of the Los Angeles metropolitan area due to the partitioning of near-coast biogenic SOA into the marine POA emitted in the surf zone. In the eastern US, SOA concentrations from the SOM (low yield) simulation were highest in the southeast US (~2 $\mu g\ m^{-3}$) and collocated with large emissions of biogenic VOCs. In both domains, the SOA concentrations from the SOM (high yield) simulations were approximately 2-2.5 times higher than the SOA from the SOM (low yield) simulations. Spatially, the distribution of the SOA mass in the SOM (low yield) simulations resembled the distribution in the SOM (high yield) simulations. In Figures 2-2 and 2-3, the domain-wide, 14-day averaged precursor-resolved SOA concentrations from the SOM simulations for SoCAB and the eastern US are shown for comparison. In SoCAB, especially in the Los Angeles metropolitan area, more than 80% of the OA is (non-volatile) POA with comparably small contributions from aromatic and monoterpene SOA. Here, the POA was mostly a result of mobile and meat cooking emissions. In the eastern US, while there were POA hotspots around large metropolitan areas (e.g., Houston, TX and Chicago, IL) and along the coast (emissions of marine POA in the surf zone), about half to three-quarters of the OA was SOA. This SOA, especially in the southeast US, comes primarily from monoterpene and sesquiterpene oxidation.
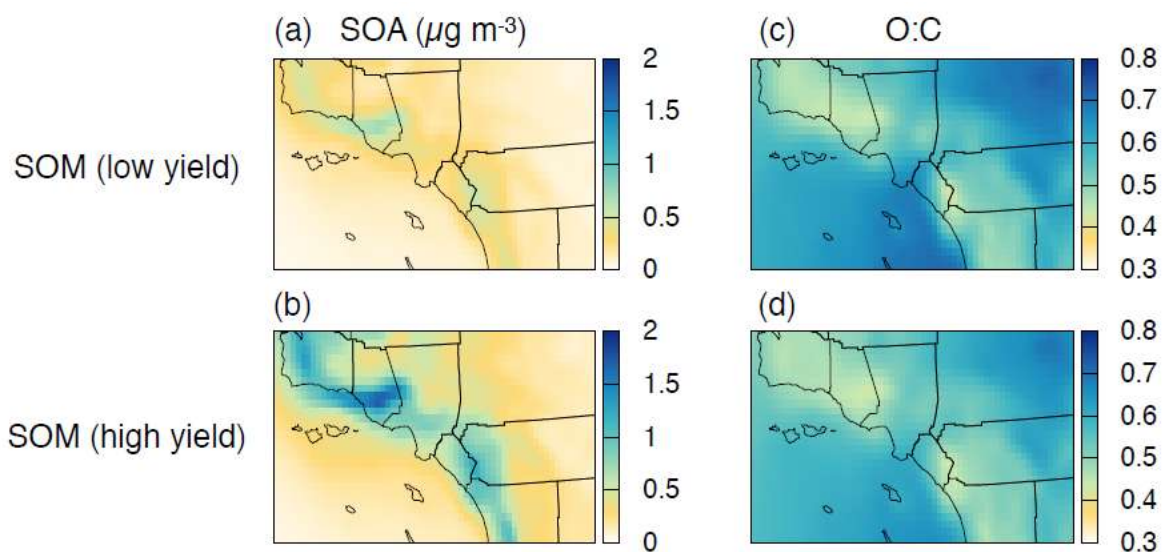
Figure 2-2: (a-b) 2-week averaged concentrations of SOA in $\mu g\ m^{-3}$ and (c-d) 2-week averaged ratio of O:C for southern California. (a,c) are predictions from the SOM (low yield) simulations and (b,d) are predictions from the SOM (high yield) simulations.
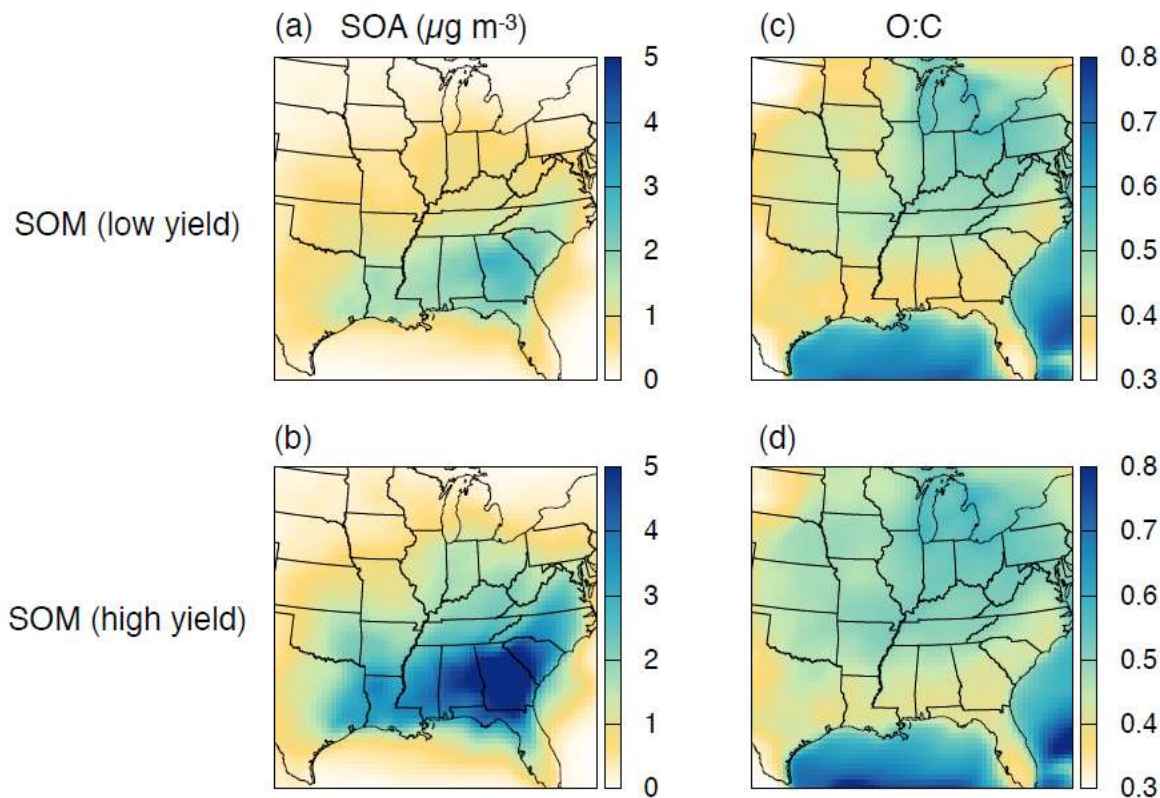
Figure 2-3: (a-b) 2-week averaged concentrations of SOA in µg m^{-3} and (c-d) 2-week averaged ratio of O:C for the eastern US. (a,c) are predictions from the SOM (low yield) simulations and (b,d) are predictions from the SOM (high yield) simulations.

Figure 2-4 shows the 2-week averaged, precursor-resolved SOA concentrations from the two SOM simulations and the Base simulations at two sites in SoCAB (Los Angeles: urban and Riverside: urban outflow) and at two sites in the eastern US (Atlanta: urban and Smoky Mountains: remote). While there are a few compositional differences, model predictions of total semi-volatile SOA concentrations at all four sites are similar between the SOM (low-yield) and Base simulation; here, semi-volatile SOA excludes acid-catalyzed isoprene SOA and all oligomers formed in the Base model. Similar results could arise from compensating effects of using SOA parameterizations based on newer chamber data than those used in the Base model, the lack of oligomerization reactions and differences in the precursor-specific sensitivity of multi-generational oxidation on SOA mass concentrations. The role of multi-generational oxidation on SOA mass can be explicitly tested only if the Base model is parameterized using the newer chamber data. Since the aim of this paper is to present the implementation of the SOM in a 3D air quality model, this and other hypotheses regarding the specific role of multi-generational oxidation will be examined in a follow up paper.
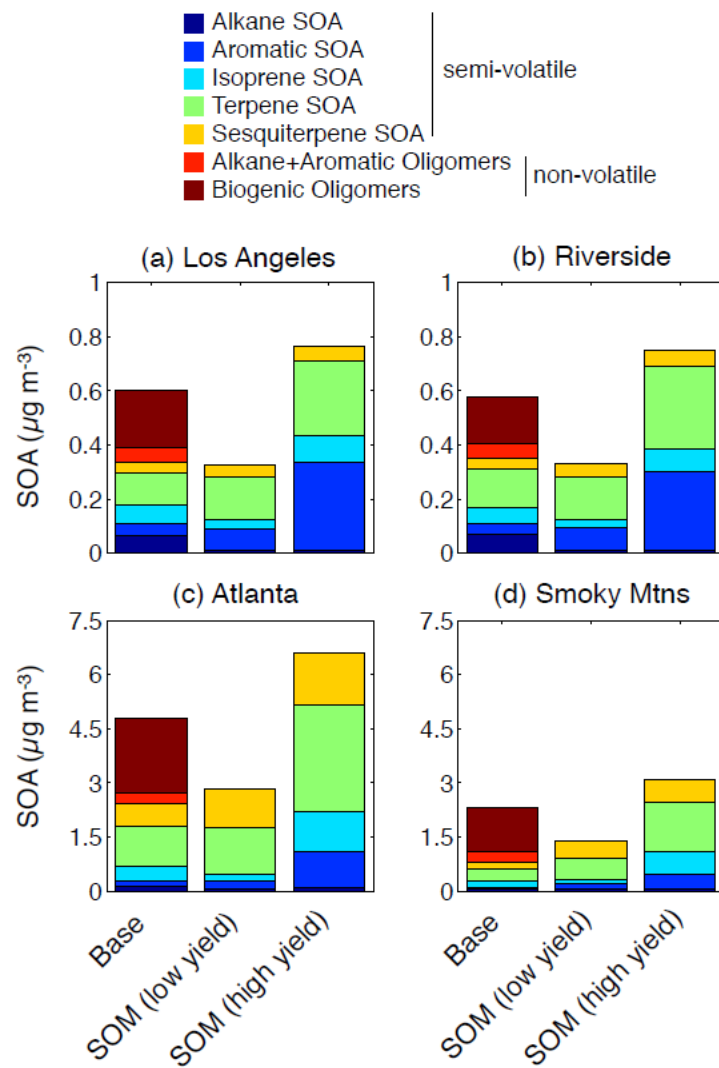
Figure 2-4: 2-week averaged SOA concentrations at Los Angeles (a), Riverside (b), Atlanta (c) and Smoky Mountains (d) for the Base and SOM simulations resolved by the SOA precursor.

Regardless, the Base model predictions of total semi-volatile SOA concentrations from the Base simulation at urban Los Angeles, Riverside and Atlanta are similar to those from the SOM (low yield) simulation (that was parameterized using high NO_x chamber data), most likely because urban areas have higher NO_x levels and, correspondingly, lower levels of SOA formation. While the total SOA concentrations were similar, the precursor-resolved composition of SOA (and possibly other important properties of SOA such as volatility) was modestly different between the Base and SOM (low yield) simulations. Alkane SOA concentrations decreased by an order of magnitude at all sites between the Base and SOM simulations, whether high or low yield. This implies that the SOA parameterization used for alkanes in the Base simulation (single model species, ALK5, assumed to have the same SOA potential as *n*-dodecane) might be over-predicting SOA formation from alkanes. This is perhaps not surprising, given that ALK5 emissions are heavily weighted towards smaller alkanes, while the assumed SOA potential corresponds to a longer chain alkane. Compared to the Base simulations, the relative contribution of aromatic, monoterpene and sesquiterpene SOA increased while that of alkane and isoprene

SOA decreased in the SOM simulations. Further, the Base simulations suggest that about 30-40% of the SOA in urban areas and slightly more than 50% of the SOA in remote areas exist as oligomerized products. Presumably, the SOA concentrations in the SOM simulations would have increased if oligomerization reactions had been included, although this hypothesis remains to be tested explicitly.

At all locations, the SOA composition is different between the SOM (low yield) and SOM (high yield) simulations. The differences in SoCAB are driven by the relatively larger enhancements in aromatic SOA compared to enhancements in SOA from other precursors. For example, aromatic SOA as a fraction of total SOA increased from 24% to 42% in central Los Angeles between the SOM (low yield) simulation and the SOM (high yield) simulation. Similarly, the differences in SOA composition in the eastern US are driven by the relatively larger enhancements in isoprene SOA compared to enhancements in SOA from other precursors. For example, isoprene SOA as a fraction of total SOA increased from 7% to 17% in Atlanta between the SOM (low yield) simulation and the SOM (high yield) simulation.

Predictions from the SOM model were compared to measurements made by the aerosol mass spectrometer (AMS) during the Study of Organic Aerosols at Riverside (SOAR) in the summer of 2005 [74, 75]. Over the two-week simulation, the SOM model under predicted total OA by 40% at this location. This suggests that important atmospheric processes and/or emissions sources upwind of Riverside are omitted from the model framework. The SOM model predicted an average SOA concentration of 0.50 μg m^{-3} (average of low yield and high yield), which is 10% of total OA. The campaign-averaged (30 day) oxygenated OA (OOA) concentration measured by the AMS (sum of the semi-volatile OOA, medium-volatility OOA and composite low-volatility OOA) was 7.1 μg m^{-3} (80% of total OA). Since the model-predicted OA at Riverside is dominated by POA (~90%), the O:C is controlled by the O:C of the emitted POA (~0.1-0.2) and is lower than the campaign-averaged O:C of 0.31 inferred from the AMS data. The under-prediction (in SOA concentrations and O:C) is typical of predictions in regional [4] and global models [76] and arises mostly from an incomplete understanding of the sources and pathways of OA. Numerous factors may contribute to the under prediction of O:C at Riverside, including missing emissions sources for SOA precursors, semi-volatile and reactive behavior of POA [3], SOA formation from unspeciated emissions [77], aqueous production of SOA in cloud, fog and aerosol water [78] and multi-generational aging [39]. The SOM model provides a framework to test these production pathways of OA as our understanding about these processes matures.

2.3.2   SOA in Carbon-Oxygen Space

The number of carbon and oxygen atoms of the SOA model species are explicitly tracked in the SOM and hence the O:C ratio of the SOA can be calculated. The 2-week averaged ratio of oxygen to carbon (O:C) of SOA from the SOM simulations is shown in Figure 2-2(c,d) for SoCAB and in Figure 2-3(c,d) for the eastern US. In both domains where the SOA concentrations were higher (>0.5 μg m^{-3} in SoCAB and >2 μg m^{-3} in the eastern US) and dominated by biogenic VOCs (northwest and south of the Los Angeles metropolitan area in SoCAB and the southeast US) the O:C of SOA ranged between 0.4 and 0.5. In these regions,

monoterpenes and sesquiterpenes account for a majority of the SOA mass and hence control the average O:C of SOA (see Table 2-1 that lists average O:C of SOA predicted by the SOM for the individual surrogate species). The O:C of SOA in the Los Angeles metropolitan area was higher (0.6-0.7) on account of a larger fraction of the SOA coming from aromatic oxidation. In very general terms, aromatic precursors have smaller N_C than mono- and sesquiterpenes, so the average O:C of the SOA from aromatics tends to be larger because a greater number of oxygen atoms must be added for the vapor pressures to become sufficiently low for substantial partitioning to the condensed phase [46, 61]. The O:C of SOA was also higher (0.5-0.8) in regions where the SOA concentrations were lower, probably as a result of sustained multi-generational oxidation tied with longer-range transport and dilution. Broadly, the O:C predictions for the SOA are in line with the O:C for worldwide ambient oxygenated OA measured using aerosol mass spectrometers (0.4-1.0) [31]. Spatially, there are few differences in the O:C between the SOM (low yield) and SOM (high yield) simulations over both domains. In SoCAB, the O:C decreased by 10% in the urban areas and increased by 3-5% in the forested regions between the SOM (low yield) and SOM (high yield) simulations. In the eastern US, the SOM (high yield) simulations predict a slightly higher O:C than the SOM (low yield) simulations; approximately 5-10% higher in the southeast US. The relatively minor changes in O:C of SOA, despite modest changes in the SOA composition, suggest that there could be compensating effects, i.e. differences in SOA composition are offset by differences in the O:C of the SOA arising from low yield versus high yield pathways.

Recently, high resolution time-of-flight chemical ionization mass spectrometry (HRToF-CIMS) has been used to resolve the composition of SOA in carbon and oxidation state space (for ambient OA that is dominated by carbon, hydrogen and oxygen, oxidation state = 2 × O:C – H:C) [79, 80]. The SOM enables us to visualize the product distribution of SOA in carbon and oxygen space and allows for a direct comparison with the measurements. While there are no measurements for the episodes simulated in this work, we can anticipate one area where such model-measurement comparisons in carbon-oxygen space could help our understanding of SOA. Figure 2-5 shows the SOA product distribution expressed in µg m^{-3} for Los Angeles and Atlanta in carbon-oxygen space. Here, the product distributions in the SOM grid from the SOM (low yield) simulations resemble each other at both locations. In these simulations, the majority of the SOA mass is spread between carbon numbers 3 and 10 and oxygen numbers 3 and 7 and the remainder at carbon number 15 and oxygen numbers 2 to 4 (associated with sesquiterpenes). While the product distributions from the SOM (high yield) simulations resemble each other too, they occupy a different space in the SOM grid. Here, the SOA mass is narrowly distributed in the oxygen number rows of 4 and 5 and carbon number column of 10 (associated with monoterpenes). Compared to the SOA mass in the SOM (low yield) simulations, the SOA mass at carbon number 15 (associated with sesquiterpenes) in the SOM (high yield) simulations is relatively lower. It is likely that the differences in product distributions between the SOM low and high yield simulations that represent SOA formation under high and low NO$_x$ respectively when combined with carbon-oxygen measurements might help us decipher the role of NO$_x$ on SOA formation.
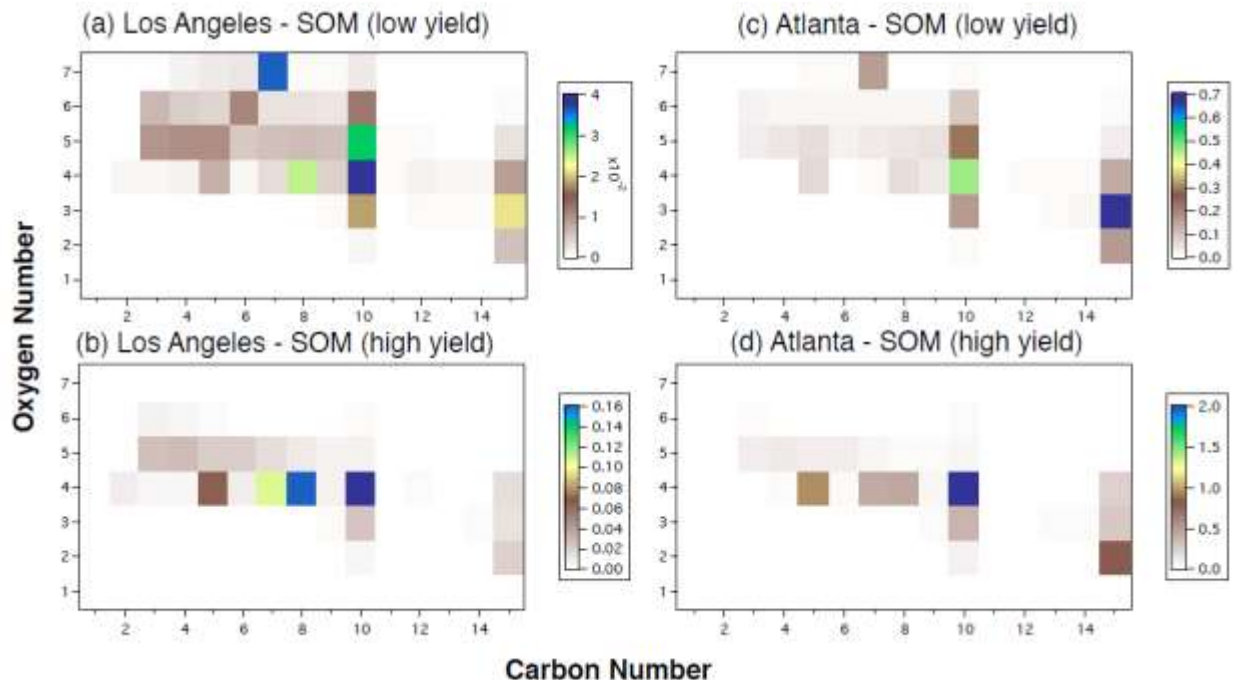
Figure 2-5: Predicted distribution of the SOA mass in µg m-3 in carbon and oxygen space for Los Angeles (a,b), and Atlanta (c,d)from the SOM (low yield) and SOM (high yield) simulations. Note the different color scales.

2.4 Summary and Future Work

The statistical oxidation model (SOM) of Cappa and Wilson (2012) is a comprehensive framework to model the atmospheric evolution of OA. In this work, we integrated the SOM with the gas-phase chemical mechanism SAPRC-11 [52] in the UCD/CIT air quality model and used it to model the multi-generational oxidation and gas/particle partitioning of SOA in the SoCAB and the eastern US. Preliminary results suggest that multi-generational oxidation modestly affects the chemical composition of SOA and hence possibly alters its environmental properties (volatility, deposition, toxicity, etc). The SOM allows for an explicit calculation of the oxygen-to-carbon ratio (O:C) and model predictions of O:C of the SOA appear to qualitatively agree with the O:Cs measured for ambient OA. With the SOM we are also able to quantify the distribution of the SOA mass in carbon and oxygen space and find that the predicted product distribution is different under the two simulated NO_x levels.

This work has focused on describing the implementation of the SOM in a 3D air quality model. The SOM offers a more realistic representation of the atmospheric evolution of SOA and provides a framework to incorporate many other processes, in addition to multi-generational oxidation, that are central to the OA system. In a follow-up study, we intend to use the SOM to systematically investigate the role of multi-generational oxidation (in conjunction with other important processes such as oligomerization and artifacts associated with vapor wall losses during chamber experiments) on the mass, composition and properties of SOA.

3 SIMULATING SECONDARY ORGANIC AEROSOL IN A REGIONAL AIR QUALITY MODEL USING THE STATISTICAL OXIDATION MODEL: ASSESSING THE INFLUENCE OF CONSTRAINED MULTI-GENERATIONAL AGEING

Online link:

3.1 Introduction

Organic aerosol (OA) is generally the dominant component of submicrometer-sized atmospheric particulate matter [81], which plays an important role in the energy budget of the earth [82] and the health effects of air pollution [83]. Despite its prominence, OA is the least understood component of atmospheric aerosol. Large-scale chemical transport models are the essential tool to simulate concentration distributions, which are needed to form strategies to mitigate, the climate and health impacts of atmospheric aerosols.

OA is a complex mixture of thousands of different compounds that have a wide range of properties [32]. OA can be directly emitted to the atmosphere in particulate form (so-called primary organic aerosol; POA) or it can be formed *in situ* by the oxidation of volatile organic compounds (VOCs) to yield lower volatility products that condense into the aerosol phase, so-called secondary organic aerosol (SOA). This latter route is generally the predominant one to form OA. Continuous oxidation of VOCs and their oxidation products yields a broad range of products, including those that have intermediate and low volatility. The importance of such "multi-generational oxidation" on SOA production has been widely established in laboratory chamber experiments [26, 38, 39, 84-86]. Multi-generational oxidation includes the initial formation of oxidized products of lower volatility as well as the loss of SOA mass after initial formation owing to fragmentation reactions. For example, experiments performed with the Potential Aerosol Mass (PAM) reactor, which aims to simulate prolonged VOC oxidation, are always associated with formation followed by destruction of OA mass [87]. Simulations that capture this behavior require inclusion of multi-generational oxidation. In addition to altering predicted SOA mass, inclusion of multi-generational oxidation is expected to alter the oxidation state of OA, which has important repercussions for OA properties (e.g., water uptake, toxicity) [81].

Traditionally, models of SOA formation in chamber experiments have represented SOA formation from VOCs using two to four surrogate products per VOC, the yields for which have been parameterized to reproduce observed levels of SOA [33]. These models generally assume that the surrogate products are non-reactive (i.e., do not undergo multi-generational oxidation). These models, whether implemented in "two-product" or "volatility basis set" (VBS) forms [88], generally under-predict ambient concentrations of SOA [4]. Some models have used simple chemical schemes to mimic the effects of multi-generational oxidation. While these schemes differ in their details, in essence, they assume that the vapors and the products of each surrogate

traditional VOC species react with the hydroxyl radical (OH) to form lower volatility products [3, 40, 89]. Such "ageing" schemes to account for multi-generational oxidation of traditional VOC products share similarities with reaction schemes applied to the oxidation of intermediate-volatility organic compounds (IVOCs) and POA vapors [3]. Note that oxidation of IVOCs and POA vapors is assumed to proceed only through these ageing-type reactions, whereas oxidation of the semi-volatile products of traditional VOC precursors is an augmentation to the existing two-product or VBS parameterization. Models that include these ageing schemes predict SOA mass concentrations that close the gap with measured ambient concentrations of OA mass. As a result, over the past five years, both research and regulatory groups have incorporated these schemes into their 3-D models (e.g., Environmental Protection Agency's Community Multiscale Air Quality Model (CMAQ) [90], PMCAMx [91, 92], WRF-CHEM [35, 92, 93]). These first order SOA schemes have three major mechanistic drawbacks. First, they typically do not account for laboratory evidence of fragmentation of oxygenated organic molecules that can lead to decreases in SOA concentrations [42, 86]. Second, they assume that the multi-generational oxidation of products of different anthropogenic VOCs (e.g., alkanes versus aromatics) or different biogenic VOCs (e.g., isoprene versus monoterpenes) share the same reaction mechanism. Finally (and most importantly), these schemes remain under-unconstrained in that they have not been rigorously tested against measurements of multi-generational products (or classes of products) under realistic ambient conditions, and they are typically added on top of existing parameterizations. These concerns apply specifically to the multi-generational oxidation schemes that are commonly applied to traditional VOCs, but these are also relevant to the oxidation schemes associated with IVOCs and POA vapors. Chemically explicit models have seldom been used in 3-D modeling (e.g. Johnson, Utembe [94], Chen, Mao [95], Ying and Li [96]) due to their heavy computational burden, although some studies have used reduced complexity forms for 3-D modeling (e.g. Utembe, Cooke [97], Lin, Penner [98]) or have implemented them for box modeling studies (e.g. Lee-Taylor, Madronich [10]).

In this work, we use the Statistical Oxidation Model (SOM) of Cappa and Wilson (2012) to model the multi-generational oxidation reactions inherent in SOA formation. The SOM provides an efficient framework to track the experimentally-constrained chemical evolution and gas/particle partitioning of SOA using a carbon and oxygen grid. In Jathar, Cappa [99], we detailed the coupling of the SOM with the gas-phase chemical mechanism SAPRC-11 [52] within the UCD/CIT regional air quality model and used the new model to make predictions over the South Coast Air Basin (SoCAB) in California and the eastern United States (US). Here, we use the UCD/CIT-SOM model to investigate the influence of constrained multi-generational oxidation on the mass concentrations and properties of SOA and contrast those results against predictions from a traditional two-product model and an unconstrained multi-generational oxidation model.

3.2   Model Description and Simulations

3.2.1   Air Quality Model

The UCD/CIT air quality model is a regional chemical transport model (CTM) [49] used here to simulate SOA formation for two geographically-distinct domains and time periods: (1) the state of California simulated at a grid resolution of 24 km followed by a nested simulation over the

SoCAB at a grid resolution of 8 km from July 20 to August 2, 2005, and (2) the eastern half of the US simulated at a grid resolution of 36 km from August 20th to September 2nd, 2006. Details about the latest version of the UCD/CIT model are provided in Jathar, Cappa [99] and summarized in Table 3-1. Briefly, anthropogenic emissions for California were based on the California Regional PM10/PM2.5 Air Quality Study (CRPAQS) inventory of 2000 but scaled to match conditions in 2005. FINN (Fire Inventory for National Center for Atmospheric Research) [56] and MEGAN (Model of Emissions of Gases and Aerosols from Nature) [57] were used to calculate wildfire and biogenic emissions in California. Anthropogenic and wildfire emissions for the eastern US were based on the 2005 National Emissions Inventory (NEI), and biogenic emissions were estimated using BEIS (Biogenic Emissions Inventory System) version 3. Hourly meteorological fields were generated using the Weather Research and Forecasting (WRF) v3.4 model (www.wrf-model.org). National Center for Environmental Protection's NAM (North American Mesoscale) analysis data were used to set the initial and boundary conditions for WRF. Gas- and particle-phase initial and hourly-varying boundary conditions were based on the results from the global model MOZART-4/NCEP [101]. Gas-phase chemistry was modeled using SAPRC-11. In all simulations, POA was treated as non-volatile, yet absorptive, as per the treatment in the regulatory Community Multiscale Air Quality (CMAQ) version 4.7 model [4]. As such, contributions of semi-volatile and intermediate volatility organic compound emissions (which are commonly assumed to originate from the evaporation of and co-emitted with POA) to the SOA burden were not considered in this study.

Table 3-1: Details of the Chemical Transport Model and Modeling Sytem Used in This Work

Domain	California	Eastern US
Resolution	24 km, nested 8 km	36 km
Grid cells	44 x 43; 63 x 30	65 x 65
Time Period	July 15 - Aug 2, 2005	Aug 15 - Sep 2, 2006
Meteorology	WRF v3.4 run with NAM reanalysis data	
Emissions	Anthropogenics: CARB (2000) Wildfires: NCAR Biogenics: MEGAN Gridded using UCD emissions processor	Anthropogenics+Wildfires: NEI (2005) Biogenics: MEGAN Gridded using SMOKE version 2.5
Gas-phase mechanism	SAPRC-11 (Carter and Heo, 2013)	
Inorganics	ISORROPIA (Nenes et al., 1998)	
Initial/Boundary conditions	MOZART-NCEP (Emmons et al., 2010)	
SOA model	2-product model, acid-catalyzed SOA from isoprene, oligomerization, (Carlton et al., 2010)	

3.2.2   SOA Models

Four types of SOA models are compared in this work: (1) A "Base" two-product model that is equivalent to the SOA model used in CMAQ and representative of SOA models used in most chemical transport [4] and global climate models [102]; (2) A modified version of the Base model, "BaseM", which uses the two-product framework, but in which the SOA formation

parameters were determined using newer chamber data; (3) A "SOM" model [13] in which multi-generational oxidation is accounted for through semi-explicit representation of progressive generations of gas-phase oxidation of the products and precursors of SOA, and that was parameterized based on the same dataset as the BaseM model; (4) A "cascading" oxidation model, wherein ageing of semi-volatile products was accounted for *a posteriori* using ageing rates derived from separate experiments. All of the SOA models utilize fully dynamic gas/particle partitioning for OA species as in Kleeman and Cass (2001) . The following sub-sections describe the four SOA models. To aid the reader, a conceptual schematic comparing various SOA models (e.g. 2-product, SOM, VBS) is provided in Figure. 3-1.
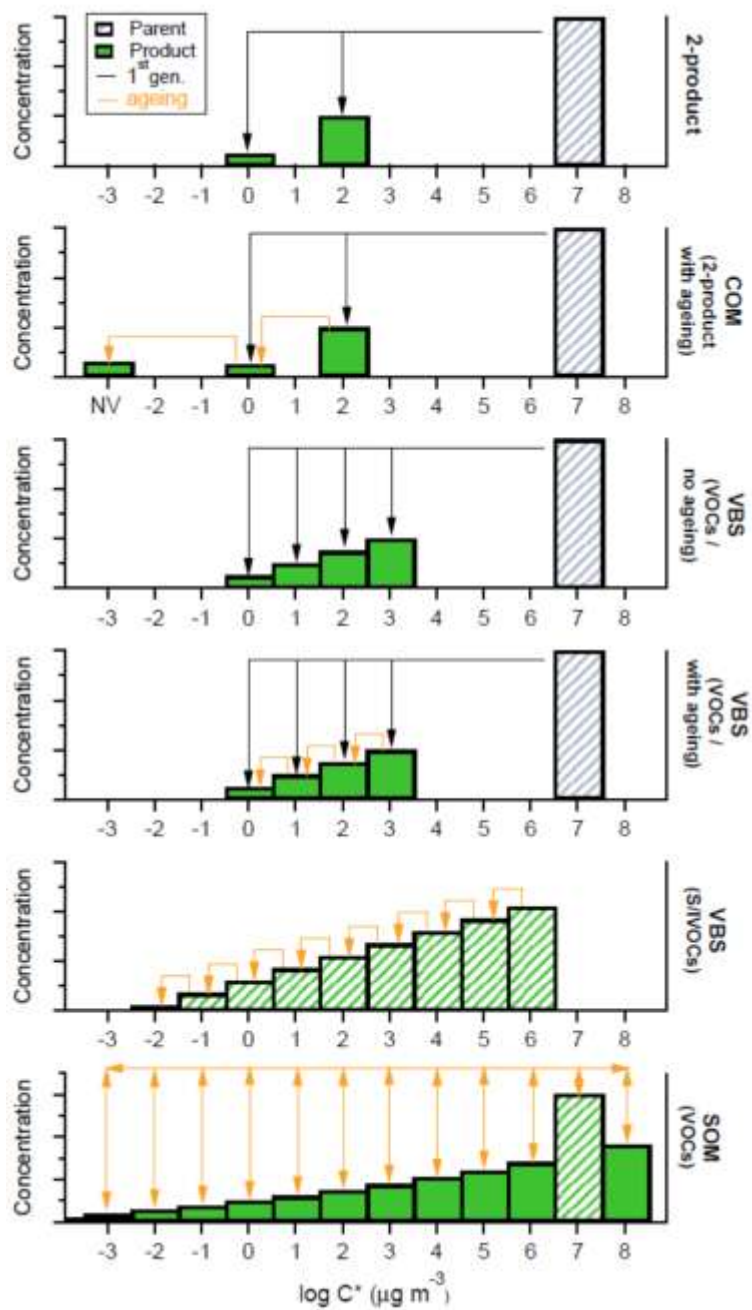
Figure 3-1: Schematic illustrating the differences between some of the different ways of modeling SOA. From top to bottom: the 2-product model; the COM-type model, i.e. 2-product with ageing; the VBS as applied to VOCs with no ageing; the VBS as applied to VOCs with additional ageing; the VBS as applied to S/IVOCs; and the SOM. The black arrows indicate the production of products directly from the parent VOC and the orange arrows indicate ageing reactions, i.e. reactions involving product species. For the SOM, all species are reactive and both functionalization and fragmentation are possible. In the other models that include ageing, only functionalization reactions are included, i.e. reactions that decrease compound vapor pressures.

Base

The Base model simulated SOA formation as per the pathways and parameters in CMAQ model version 4.7 [4] from the following gas-phase precursors: long alkanes (ALK5), benzene (BENZENE), low-yield aromatics (ARO1), high-yield aromatics (ARO2), isoprene, monoterpenes (TRP1) and sesquiterpenes (SESQ). The species in parentheses are the model species representing those compounds in SAPRC-11 (the gas-phase chemical mechanism used here). The pathways considered include: (1) oxidation of the above-mentioned precursors to form non-reactive semi-volatile products that partition into the particle-phase [33] (the so-called two-product model, where model parameters were previously determined from fitting chamber data); (2) acid enhancement of isoprene SOA [63]. SOA formation from aromatics is NO_x dependent; low levels of NO_x result in higher SOA formation and vice-versa. The Base model was extended to include particle-phase oligomerization [64], for which particle-phase semi-volatile components were converted to non-volatile components with $k_{oligomer} = 9.6 \times 10^{-6}$ s^{-1}. In summary, the Base model was run in two configurations, with and without oligomerization reactions: Base and Base-OLIG.

Base Modified

The "modified" version of the Base model, termed "BaseM" was created to facilitate a true evaluation of multi-generational oxidation in a two-product model framework. The BaseM model: (1) used recent chamber data [99] from California Institute of Technology to determine alternate two-product model parameters; and (2) did not include acid-catalyzed enhancement of isoprene SOA and oligomerization reactions. The two-product fit parameters and data sources are listed in Table 3-2. Note that the "long alkane" BaseM parameterization has been developed using experimental results for SOA formation from *n*-dodecane [103].

Table 3-2: SAPRC-11 Model Species, Surrogate Molecules and BaseM Parameters for Two Product Model

SAPRC-11 Species	Descriptor	Surrogate to determine BaseM fits	NO$_x$	Kp		α		Reference
ALK_C06	Long alkanes	n-dodecane	Low	0.200	0.010	0.001	0.016	Loza et al. (2014)
			High	0.200	0.010	0.001	0.020	
ALK_C07	Long alkanes	n-dodecane	Low	0.200	0.010	0.000	0.028	Loza et al. (2014)
			High	0.200	0.010	0.003	0.039	
ALK_C08	Long alkanes	n-dodecane	Low	0.200	0.010	0.000	0.088	Loza et al. (2014)
			High	0.200	0.010	0.005	0.079	
ALK_C09	Long alkanes	n-dodecane	Low	0.200	0.010	0.003	0.147	Loza et al. (2014)
			High	0.200	0.010	0.013	0.106	
ALK_C10	Long alkanes	n-dodecane	Low	0.200	0.010	0.009	0.232	Loza et al. (2014)
			High	0.200	0.010	0.024	0.158	
ALK_C11	Long alkanes	n-dodecane	Low	0.200	0.010	0.018	0.341	Loza et al. (2014)
			High	0.200	0.010	0.045	0.183	
ALK_C12	Long alkanes	n-dodecane	Low	0.200	0.010	0.035	0.447	Loza et al. (2014)
			High	0.200	0.010	0.070	0.228	
ALK_C13	Long alkanes	n-dodecane	Low	0.200	0.010	0.083	0.441	Loza et al. (2014)
			High	0.200	0.010	0.108	0.201	
Benzene	Benzene	Benzene	Low	0.283	0.026	0.281	0.127	Ng et al. (2007)
			High	100.000	0.013	0.074	0.642	
ARO1	High-yield aromatics	Toluene	Low	0.215	0.001	0.617	0.001	Zhang et al. (2014)
			High	18.502	0.023	0.021	0.537	
ARO2	Low-yield aromatics	m-xylene	Low	0.269	0.111	0.322	0.080	Ng et al. (2007)
			High	0.160	0.001	0.078	0.001	
Isoprene	Isoprene	Isoprene	Low	5.434	0.008	0.021	0.594	Chhabra et al. (2011)
			High	0.136	0.003	0.004	0.409	
TRP1/SESQ	Terpenes	α-pinene	Low	100.000	0.004	0.102	0.671	Chhabra et al. (2011), Griffin et al. (1999)
			High	0.549	0.009	0.046	0.489	

Statistical Oxidation Model

The SOM parameterizes multi-generational oxidation using a two-dimensional carbon-oxygen grid to track the evolution of gas- and particle-phase organic products arising from the oxidation of SOA precursors [46, 47, 67]. This evolution through the SOM grid is VOC-specific and defined by six parameters: (P1-P4) yields of the four products that add 1, 2, 3, and 4 oxygen atoms, respectively, without fragmentation; (P5) the probability of fragmentation; and (P6) the decrease in vapor pressure (or volatility) of the species per addition of oxygen atom. Details of the implementation and parameterization of the SOM model in the UCD-CIT are presented in [99]. Briefly, six SOM grids with precursor-specific parameter sets were used to represent SOA formation from the same precursor classes in the Base model. Parameter sets were separately determined from high NO_x (low yield) and low NO_x (high yield) chamber data as the SOM in its current configuration cannot yet account for continuous variation in NO_x. The SOM parameters were completely determined from explicit fitting to chamber data where the number of fit data points greatly exceeded the number of fitting parameters (6). Thus, the SOM model will be referred to as "constrained" multi-generational oxidation. The SOM parameters and data sources are listed in Table 2-1.

The SOM model parameters used in the present study were determined without accounting for losses of vapors to chamber walls, which can lead to a substantial underestimation of the actual SOA formation potential of a given precursor [67, 104]. A companion paper evaluates vapor wall-loss effects on the SOM results [105]. The SOM parameter fits were derived using dynamic gas-particle partitioning assuming an accommodation coefficient of unity, which tends to minimize the influence of vapor wall loss [72], and thus represents a conservative lower bound of SOA formation. The SOM model was additionally extended to consider the influence of oligomerization reactions by allowing irreversible conversion of particle-phase SOM species into a single non-volatile species using the same $k_{oligomer}$ as in the Base model, referred to as SOM-OLIG. Oligomerization reactions were added *a posteriori* to the SOM model, i.e. oligomerization reactions were not included as part of the data fitting and parameter determination and are included in the present study only as a sensitivity case.

Cascading Oxidation Model

Additional simulations were performed using a contemporary multi-generational oxidation scheme, the Cascading Oxidation Model (COM). The COM builds on the two-product Base model but allows for additional reaction of the semi-volatile products using the scheme of Baek et al. (2011). Briefly, the two semi-volatile products from a given precursor react with OH, with the highest volatility product converted into the lowest volatility product and the lowest volatility product converted to a non-volatile product (see SI Section on Cascading Oxidation Model). Like most other schemes that have thus far been used to represent multi-generational oxidation of SOA from traditional VOCs in 3-D models [35], COM does not consider fragmentation reactions, is not fit or constrained to experimental data, and adds these ageing reactions on top of

an existing parameterization. The COM model will be referred to as "unconstrained" multi-generational oxidation.

3.2.3   Simulations

Table 3-3 lists the simulations performed in this work. We performed two simulations with the Base model (with and without oligomerization), two with the BaseM model (low and high yield), four with the SOM model (low and high yield and with oligomerization accounted for) and one with the COM model. These nine simulations were performed for both domains: SoCAB and the eastern US. Simulations were performed for 19 days with the first 5 days used for spin up. For the SoCAB, each simulated day using the SOM required approximately 4 h of elapsed time (on 40 Intel i5-3570 processor cores) so a 19-day episode was simulated in less than 4 days. For the eastern US, each simulated day required approximately 9 h of elapsed time so a 19-day episode was simulated in about 8 days. The SOM simulations on account of the large number of model species were approximately four times slower than the BaseM simulations.

Table 3-3: Simulations Performed in this Work

Simulation	Description
Base	Equivalent to Carlton et al. (2010) without oligomerization
Base-OLIG	Equivalent to Carlton et al. (2010)
BaseM (low yield)	two-product model using new high NO_x data (low yield)
BaseM (high yield)	two-product model using new low NO_x data (high yield)
SOM (low yield)	New high NO_x data, no vapor wall losses
SOM (high yield)	New low NO_x data, no vapor wall losses
SOM-OLIG (low yield) and SOM-OLIG (high yield)	SOM with inclusion of oligomerization
COM	Base-OLIG model with added ageing reactions

3.3   Results

3.3.1   Base vs. BaseM

Although the main focus of the present study is on understanding the role of multi-generational oxidation in SOA models, it is useful to begin by considering differences between the predictions from Base and BaseM (two-product parameters fit to more recent data sets). The 14-day averaged, precursor-resolved SOA concentrations at two sites in the SoCAB (Los Angeles: urban, Riverside: urban outflow) and at two sites in the eastern US (Atlanta: urban, Smoky Mountains: remote) from Base and BaseM are compared in Figure 3-2. Base model predictions of total semi-volatile SOA concentrations (i.e. SOA exclusive of oligomers) at all four sites are similar to the BaseM (low yield) model predictions that were parameterized using high-NO_x chamber data. This outcome is perhaps not surprising at Los Angeles, Riverside and Atlanta since these urban areas have higher NO_x levels and, correspondingly, the Base simulations

effectively used high-NO$_x$ parameters. While there are slight increases in SOA from some precursors and decreases from others, BaseM, in comparison to Base, predicted negligible contributions from alkane SOA. The general agreement between Base and BaseM (low yield) in rural/remote areas like the Smoky Mountains (where more than three-quarters of the SOA comes from terpene oxidation) also resulted from increases in SOA from some precursors and decreases from others. These precursor-specific differences are a result of slight differences between the two-product yields for these species in Base [4] and BaseM. The comparison between Base and BaseM suggests that while the newer data might not dramatically affect the SOA concentrations in high-NO$_x$ (or urban) areas — at least those that still have marginal biogenic contributions — the newer data could increase SOA concentrations (factor of ~2) in low-NO$_x$ (or rural/remote) areas. One important difference is that the BaseM parameterizations for mono- and sesquiterpenes indicate a NO$_x$ dependence, whereas the Base parameterizations have no NO$_x$ dependence for these compounds. This has implications for the assessment of anthropogenic influences on biogenic SOA and whether biogenic SOA can, to some extent, be controlled [106]. Further, the substantial decrease in alkane SOA concentrations in BaseM compared to Base suggests that the Base alkane parameterization might be over-predicting SOA formation from alkanes, at least those that make up ALK5, making it an even smaller fraction of the total SOA mass.
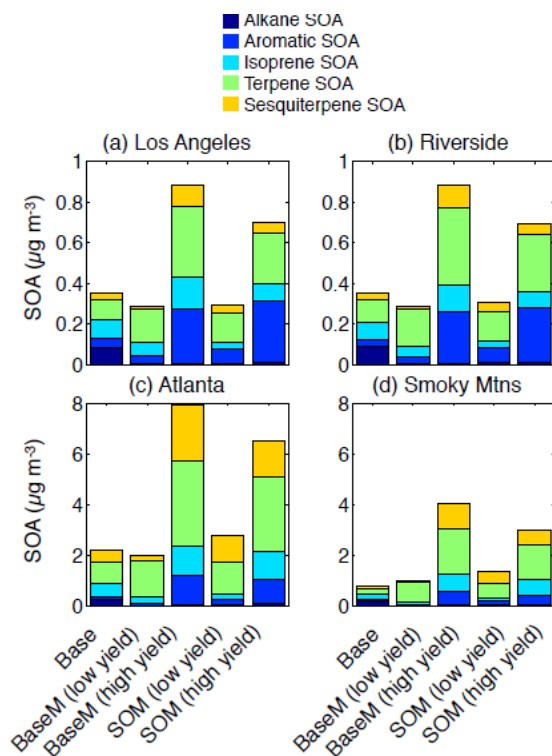
Figure 3-2: 14-day averaged SOA concentrations at Los Angeles (a), Riverside (b), Atlanta (c) and Smoky Mountains (d) for the Base, BaseM, and SOM simulations resolved by the precursor/ pathway.

3.3.2 *Effect of Constrained Multi-Generational Oxidation*

SOA Concentrations

Predictions from BaseM and SOM, which were parameterized using the same data, were used to investigate the influence of multi-generational oxidation. Domain-wide, 14-day averaged SOA concentrations from BaseM and SOM for the SoCAB and for the eastern US, along with the ratio of the SOA concentrations between SOM and BaseM, are shown in Figure 3-3. The SOA concentrations presented are averages of the low-yield and high-yield simulations. Consideration of either the low-yield or high-yield simulations individually affects the details, but not the general conclusions about multi-generational oxidation below, even though the SOA mass concentrations from the high-yield simulations are typically 2-4 times larger than from the low-yield simulations (see Figure 3-4). In both the SoCAB and the eastern US, the predicted spatial distribution of SOA is generally similar between BaseM and SOM, with only minor differences evident in some locations. For the SoCAB, the SOA concentrations in SOM are somewhat lower everywhere compared to BaseM, by 10-20% in the Los Angeles metropolitan area (marked by a red box) and by about 20-30% in regions dominated by biogenic SOA (e.g., Los Padres National Forest located in the northwest corner of the simulated domain). Similarly, the SOM predictions for SOA concentrations in the eastern US are 0-20% lower than BaseM predictions over most of the domain. The urban versus biogenic difference was not evident, probably owing to a coarser grid resolution (36 km for the eastern US versus 8 km for the SoCAB). It appears that multi-generational oxidation does not dramatically increase (from additional functionalization reactions) or decrease (from additional fragmentation reactions) the total SOA concentrations formed from the precursor compounds considered in either region.
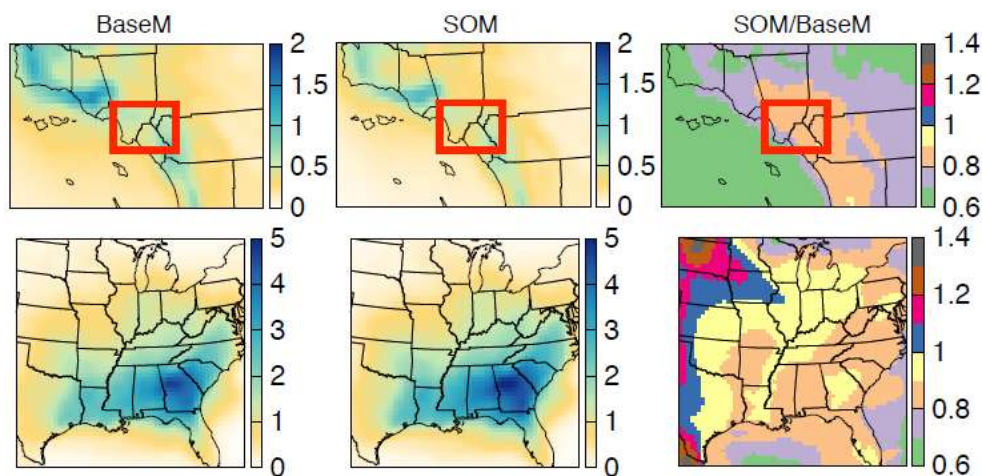
Figure 3-3: 14-day averaged SOA concentrations in SoCAB for the BaseM and SOM simulations. (c) Ratio of the 14-day averaged SOA concentration from the SOM simulation to that from the BaseM simulation. The BaseM and SOM results are averages of the low yield and high yield simulations. Red box indicates urban areas surrounding Los Angeles.
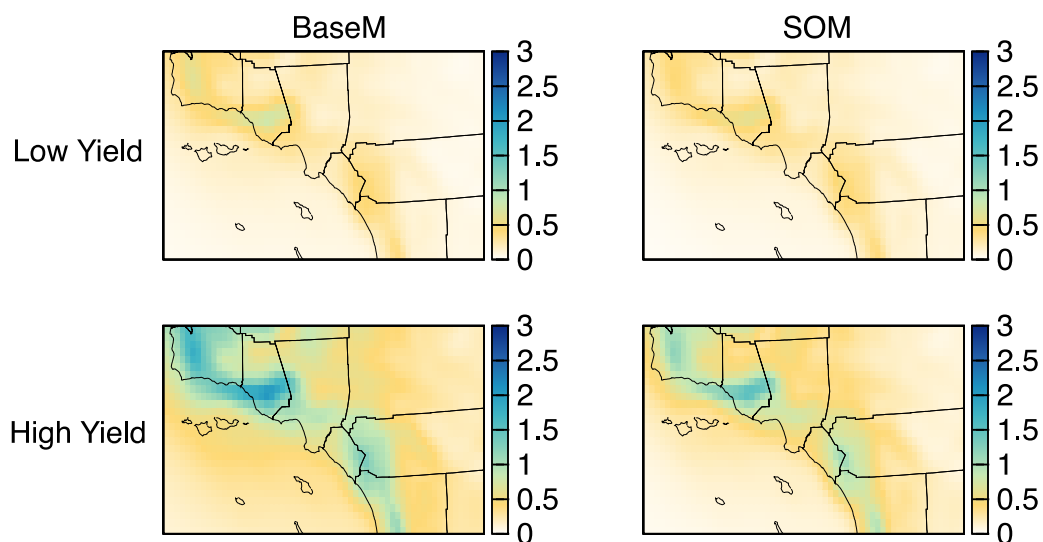
Figure 3-4: 14-day SOA concentrations in SoCAB for the BaseM and SOM simulations for the low-yield and high-yield parameterizations.

In Figure 3-2, at all sites, the SOM SOA concentrations are roughly the same or slightly higher than the BaseM SOA concentrations for the low-yield simulations but consistently lower for the high-yield simulations, by 18-25%. When averaged, the SOM SOA concentrations are slightly lower than the BaseM simulations, largely due to the lower predictions of SOA from mono-terpene and sesquiterpenes in the SOM high yield simulations. The low- versus high-yield distinction suggests that the SOM-predicted SOA is probably similar to BaseM-predicted SOA in urban areas (low yield or high NO_x) but lower in rural/remote areas (high yield or low NO_x).

The seemingly limited influence of multi-generational oxidation on total SOA concentrations runs counter to the findings from previous work that suggests multi-generational oxidation is an important source of SOA [3, 89, 91, 107, 108]. However, these previous efforts accounted for multi-generational VOC oxidation by adding ageing reactions for semi-volatile products on top of an existing parameterization, similar to the COM model, and thus may suffer from "double counting" to some extent (we will return to this point later). These results also indicate that the two-product model parameterization inherently captures some of the influence of multi-generational oxidation, at least over the timescales and conditions relevant for the SoCAB and the eastern US. This can be understood by considering that, although the two-product model assumes non-reactive products, the chamber-observed SOA formation is dependent on production from all reaction generations, even at short oxidation lifetimes (half to a full day of photochemistry); the extent to which multi-generational oxidation influences the two-product fit parameters will depend on the extent to which later generation products are responsible for the actual SOA formation in a given experiment. In summary, it is possible that the chamber-observed SOA formation accounts for the majority of the multi- generational oxidation reactions that contribute to SOA mass and hence, a two-product approach to model SOA formation would already include the mass-enhancement associated with multi-generational oxidation. However, such a two-product model may not necessarily accurately represent the chemical composition of SOA

The behavior of SOM vs. BaseM predictions is similar in the SoCAB and the eastern US, with minor differences likely related to the size of the domain and the average atmospheric lifetime of the simulated SOA, differences in the evolution of SOA from the various precursors, and the dominance of certain precursors in different domains. These precursor-specific SOA concentrations are visualized in Figure 3-2 and listed as domain-wide averages in Table 3-4. These results indicate that SOM typically produced more SOA from alkanes (although very little overall) but less from terpenes and isoprene in both the SoCAB and the eastern US, compared to BaseM. For aromatics and sesquiterpenes the concentrations are generally similar between the two models, although slightly greater for sesquiterpenes for the eastern US SOM simulations. The use of the SOM model that inherently accounts for multi-generational oxidation leads to more SOA mass for some compounds (due to enhanced functionalization) but less SOA mass for others (due to fragmentation) compared to a static representation of the semi-volatile products. SOA concentrations in chamber photo oxidation experiments have been observed to decrease at longer times for some VOCs, notably isoprene [26] and alpha-pinene [86]. Such behavior is captured by SOM but not by BaseM, which does not account for fragmentation. Consequently, SOA concentrations in BaseM can never decrease from reactions. The general similarity in the total simulated SOA from BaseM and SOM results in large part from offsetting trends associated with different SOA precursors. This suggests that the use of constrained multi-generational oxidation SOA models, such as SOM, over two-product models may help to provide a clearer picture of the sources of SOA in a given region, even if the different modeling approaches lead to similar total SOA mass concentrations.

Table 3-4: Reactions Added to SAPRC-11 to model multi-generational oxidation of SOA. For consistency, the names of the SAPRC-11 model species and the Base model species are kept the same as those described in CMAQ v4.7[4]. The species SV_ALK2, SV_ISO4, SV_TRP3 and SV_SQT2, denoted with an asterisk, are new non-volatile species added to SAPRC-11.

VOC	SAPRC-11 model species	Semi-volatile Base model species	Multi-generational aging reactions added to SAPRC11
Alkanes	ALK5	SV_ALK	SV_ALK + OH = SV_ALK2*
Benzene	BENZENE	SV_BNZ1, SV_BNZ2	SV_BNZ2 + OH = SV_BNZ1 SV_BNZ1 + OH = SV_BNZ3
High-yield aromatics	ARO1	SV_TOL1, SV_TOL2	SV_TOL2 + OH = SV_TOL1 SV_TOL1 + OH = SV_TOL3
Low-yield aromatics	ARO2	SV_XYL1, SV_XYL2	SV_XYL2 + OH = SV_XYL1 SV_XYL1 + OH = SV_XYL3
Isoprene	ISOPRENE	SV_ISO1, SV_ISO2	SV_ISO1 + OH = SV_ISO2 SV_ISO2 + OH = SV_ISO4*
Terpenes	TRP1	SV_TRP1, SV_TRP2	SV_TRP2 + OH = SV_TRP1 SV_TRP1 + OH = SV_TRP3*
Sesquiterpenes	SESQ	SV_SQT	SV_SQT + OH = SV_SQT2*

The simulated total OA concentrations (POA+SOA) are compared to ambient OA measurements made at the STN (Speciated Trends Network) and IMPROVE (Interagency Monitoring of Protected Visual Environments) air quality monitoring sites in the SoCAB and the eastern US. (IMPROVE sites tend to be remote and with lower OA concentrations compared to STN sites, which tend to be more urban.) Table 3-5 lists statistical metrics of fractional bias and fractional error that capture model performance for OA for all simulations for both domains at the STN and IMPROVE sites. Note that in the published paper corresponding to Chapter 3, the OM/OC ratio used for converting the filter-based OC measurements to OM mass concentrations was assumed to be 1.6 and blank corrections were not applied, whereas in the revised final report the OM/OC ratio for IMPROVE data was assumed to be 2.1 and blank corrections were applied to STN data. The exact choice of conversion factors is an "expert opinion" that evolved as the Chapters in the current project were developed, and the conversion factor of 1.6 vs. 2.1 represents typical variability in other published work. The conclusions of the model evaluation in the current project are not significantly affected by either the conversion factor of 1.6 vs. 2.1 or the choice of blank correction.

The simulated SOA fraction of total OA differs greatly between the SoCAB (~10%) and the eastern US (~80%). Consequently, changes in the amount of SOA simulated will have a larger influence on the total OA in the eastern US, and thus on the comparison with observations. Despite these differences, there is no substantial change in model performance between Base, BaseM and SOM in either domain, with all simulations under-predicting the total OA. In contrast, COM, which leads to substantial increases in the simulated SOA mass concentrations within both domains (see Section 3.3), improved model performance at the STN and IMPROVE sites for the SoCAB and at the STN sites for the eastern US.

Table 3-5: Fractional bias and fractional error at STN and IMPROVE sites for the SoCAB and the eastern US for the Base, BaseM (average of low- and high-yield), COM and SOM (average of low- and high-yield) simulations. Green, yellow, and orange shading represent 'good', 'average' and 'poor' model performance [109].

| Simulation | SoCAB | | | | Eastern US | | | |
| | STN | | IMPROVE | | STN | | IMPROVE | |
	Frac. Bias	Frac. Error	Frac. Bias	Frac. Error	Frac. Bias	Frac. Error	Frac. Bias	Frac. Error
Base	-56	58	-58	62	-70	85	-33	63
BaseM	-56	58	-54	58	-69	83	-32	61
SOM	-57	59	-58	61	-71	85	-36	62
COM	-23	41	2	43	12	62	65	81

SOA Volatility

The effective volatility of the SOA was characterized for the Base, BaseM and SOM simulations. SOA volatility influences the sensitivity of the SOA to dilution and temperature changes. Since Base, BaseM and SOM use model species that have very different volatilities, as characterized by the species saturation concentration, C^*, volatility distributions were developed in which individual species are grouped into logarithmically spaced bins of effective C^*, referred to as volatility basis set-equivalent (VBS$_{eq}$) distributions [88]. In Figure 3-5(a,c), we show the normalized, episode-averaged VBS$_{eq}$ distributions of SOA at Los Angeles and Atlanta for the Base, BaseM and SOM simulations. Qualitatively, the SOA VBS$_{eq}$ distributions for Base and BaseM are similar, with the bulk of the gas+particle mass being in the $C^* = 1$ to 1000 µg m^{-3} range. In sharp contrast, the SOA volatility distribution for the SOM simulation had a substantial fraction of SOA mass in the $C^* = 0.0001$ to 1 µg m^{-3} range, much lower than the Base/BaseM simulations. At atmospherically-relevant OA concentrations (1-10 µg m^{-3}), the mass in these low C^* bins would be exclusively in the particle-phase.
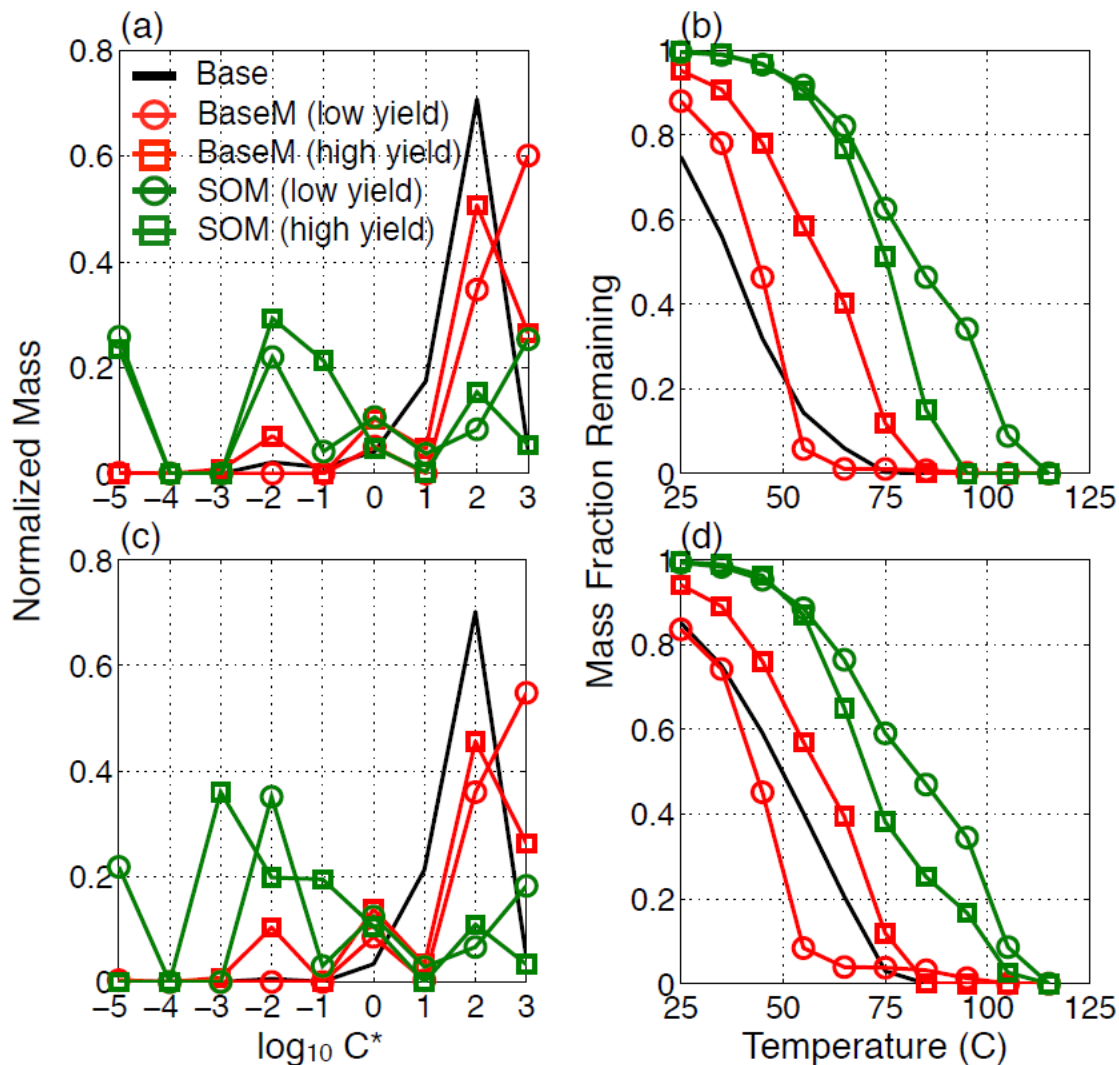
Figure 3-5: Volatility distributions of the 14-day averaged gas+particle SOA mass at Los Angeles (a) and Atlanta (c) for the Base, BaseM and SOM simulations. Thermograms that capture the volatility of the 14- day averaged gas+particle SOA mass at Los Angeles (b) and Atlanta (d) for the Base, BaseM and SOM simulations.

It is not possible to compare the simulated volatility distributions to ambient observations since direct measurement of volatility distributions has not been demonstrated for such low C^* species. However, the effective volatility of SOA particles has been experimentally assessed by considering the response of particles to heating in a thermodenuder [110, 111]. High volatility species generally evaporate at lower temperatures than low volatility species. The theoretical response of the predicted SOA mass, expressed as the mass fraction remaining (MFR), to heating in a thermodenuder over the range 25 to 105 °C was simulated using the model of Cappa (2010) . The C^* values varied with temperature according to the Clausius-Clapeyron equation and the enthalpy of vaporization was assumed to be a function of C^* with

. (See SI section Thermodenuder Model.) We plot the results in Figure 3-5(b,d). At both Los Angeles and Atlanta, differences in the predicted SOA volatility are quite evident. In general, the effective SOA volatility was higher in the Base and BaseM simulations than in the SOM

simulations. The SOA from the Base and BaseM simulations is almost entirely evaporated when heated to 70 °C, and some evaporation occurs even at 25 °C as a response to vapor stripping in the denuder. In contrast, the SOA from the SOM simulations did not entirely evaporate until 100 °C and exhibits a more gradual decrease with temperature. The SOM-simulated SOA TD evaporation is much more similar to the behavior observed in both laboratory experiments and field assessments of SOA volatility [110, 111, 113]. This suggests that SOM is producing SOA with more physically realistic properties even though the Base/BaseM and SOM simulations produced similar SOA concentrations.

Influence of Oligomerization

The Base-OLIG model includes an oligomerization pathway in which semi-volatile, condensed-phase material is converted to a non-volatile, yet absorptive material on a fixed timescale. This effectively "pumps" semi-volatile vapors to the particle phase and leads to increased SOA concentrations. It has the additional effect of making the SOA less sensitive to dilution and changes in temperature. To examine the influence of oligomerization, Figure 3-6 shows predictions of the precursor-resolved SOA concentrations from the Base, Base-OLIG, SOM and SOM-OLIG simulations for Los Angeles and Riverside, CA. The total SOA concentrations in Base-OLIG are ~60% higher than Base but the SOA concentrations in SOM-OLIG were only ~14% higher than SOM. This difference can be understood through the differences between the SOM and Base volatility distributions for semi-volatile species. For the Base model, a large fraction of the oxidation products have $C^* > 1$ μg m^{-3}, and thus a sizable fraction is in the gas-phase. This gas-phase material can be viewed as potential SOA, and as oligomers are formed this material is converted to actual SOA. For SOM, much of the material has $C^* \leq 1$ μg m^{-3}, and thus most of it is already in the particle phase. Consequently, when it is converted to oligomers only a marginal influence on the total SOA concentration results. Overall, it is evident that the influence of oligomerization on simulated SOA concentrations is tightly linked to the semi-volatile product distribution. This may influence the timescales of SOA formation, since in SOM production of lower volatility material is related to the timescales of gas-phase oxidation, whereas in Base, the specified oligomerization rate coefficient, which is largely under-constrained, controls the timescale of low (essentially non-) volatile material.
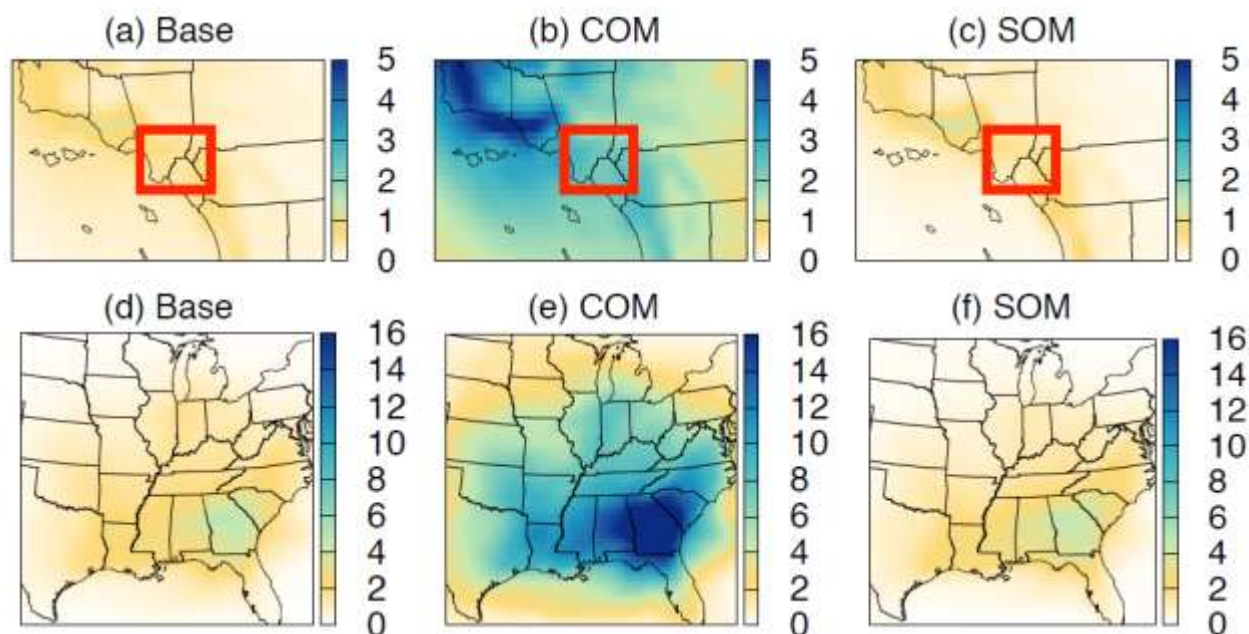
Figure 3-6:14-day averaged SOA concentrations at (a) Los Angeles and (b) Riverside for the Base, Base- OLIG, SOM, SOM-OLIG simulations resolved by the precursor/pathway.

3.3.3   Comparing Multi-Generational Oxidation to Unconstrained Schemes

The 14-day averaged SOA concentrations from the COM, Base, and SOM simulations for the SoCAB and the eastern US are compared in Figure 3-7. Recall that COM allows for conversion of the semi-volatile products in the Base model to lower-volatility products on top of the original 2-product parameterization. The COM simulations predict a factor of 4 to 8 increase in SOA concentrations over the Base and SOM simulations, attributable to the production of low-volatility and non-volatile SOA from the added oxidation reactions. Because COM, like many *ad hoc* ageing schemes [3, 40, 89, 114], lacks fragmentation and adds ageing reactions on top of an existing parameterization, and with sufficient oxidation all semi-volatile products will be converted into non-volatile SOA. This means that the ultimate SOA mass yield is equal to the sum of the mass yields of the individual products, independent of their vapor pressures. Given that SOM inherently accounts for multi-generational oxidation as part of the model parameterization, this comparison clearly suggests that the unconstrained schemes used in the COM simulations form too much SOA and that such schemes are not truly representative of multi-generational oxidation in the atmosphere.
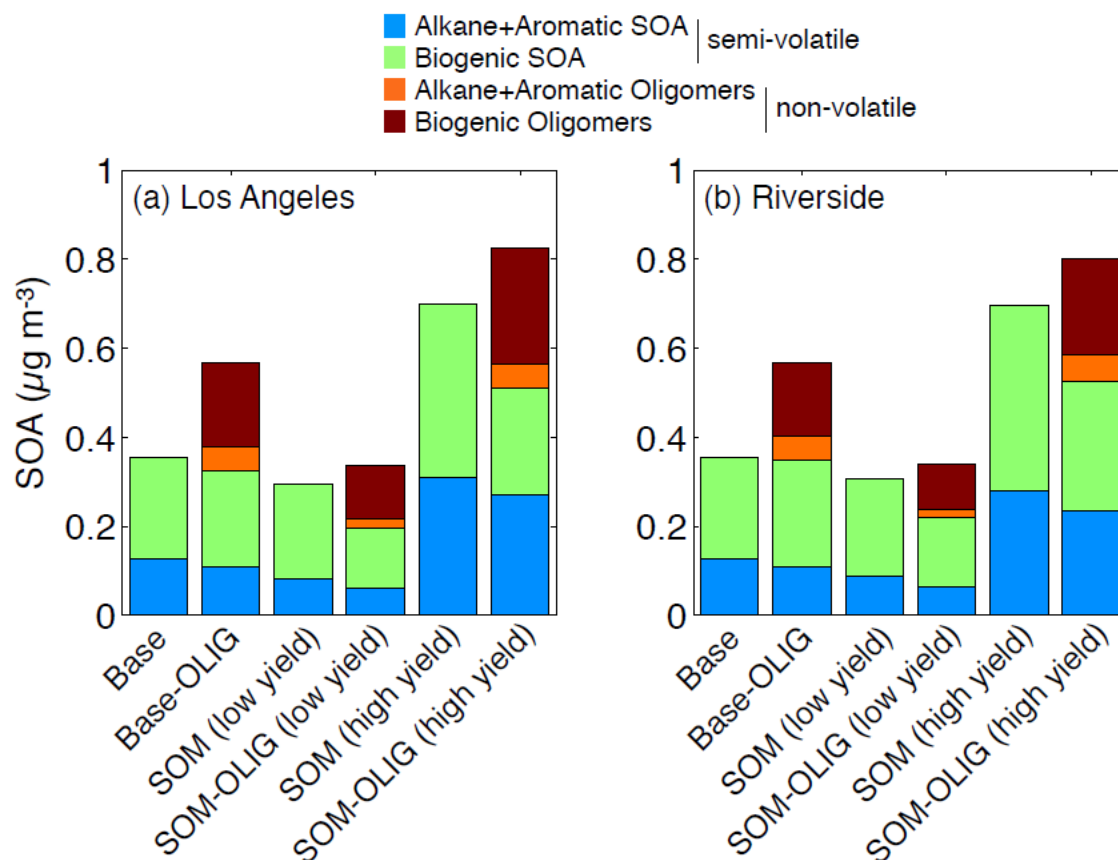
Figure 3-7:14-day averaged SOA concentrations in SoCAB (a-c) and the eastern US (d-f) for the Base, COM and SOM simulations. The SOM results are averages of the low-yield and high-yield simulations.

Some previous studies have defended the use of a COM-type model because its implementation improved model performance [35, 91, 115], as was also observed here (Table 3-5). However, given that COM-type models remain generally unconstrained and have been inconsistently applied to different VOC precursor types (e.g. ageing of anthropogenics but not biogenics) [35, 76, 91], and since recent testing of a COM-type scheme in the laboratory demonstrated that such schemes do, indeed, lead to over-prediction of SOA mass concentration [116], we suggest that this apparently improved agreement is more likely fortuitous than a true indication of improved representation of atmospheric chemistry. It should be noted that the current study specifically assesses the performance of a COM-type model on the SOA production from traditional VOCs only, exclusive of potential contributions of IVOCs and semi-volatile POA vapors to the SOA burden. Previous studies that have examined the influence of multi-generational oxidation of traditional VOCs using COM-type models have typically combined the effects of VOC ageing and IVOC and POA vapor oxidation (e.g. Murphy and Pandis [91];Jathar, Farina [117]) together and have not investigated the role of these effects. Consequently, our results, which isolate the influence of using a COM-type oxidation scheme, suggest COM-type models may be inappropriate for use in regional air quality models even though they can lead to improved model/measurement comparison (Table 3-5). They also imply that models that employed COM-like schemes have potentially underplayed the role of other important OA formation pathways such as aqueous (aerosol, fog, cloud) processing of water-soluble organics [118] and particle-

surface reactions [70, 119]. Future work to integrate semi-volatile POA treatments with constrained multi-generational ageing schemes like SOM is needed.

3.4 Discussion

When constrained using the same chamber data, the BaseM (traditional two-product model that does not resolve multi-generational oxidation) and SOM models predict roughly the same SOA mass concentrations and spatial distribution for regional air pollution episodes in the SoCAB and the eastern US. This suggests that the chamber data used to constrain the BaseM and SOM parameterizations presumably already includes a majority of the SOA mass that would be attributable to multi-generational oxidation. The extent to which multi-generational oxidation influences the production of SOA in a given chamber experiment depends on both the volatility and reactivity of the first-generation products and the time-scale of the experiment [120]. If SOA formation is dominated by first-generation products, then explicit accounting for multi-generational ageing will not be important. Alternatively, if most SOA is formed from second-generation products with little direct contribution from first-generation products, than a static representation (such as with the 2-product model) might be sufficient even when multi-generational ageing is, in fact, dominant. But if SOA formation is balanced between contributions from first, second and later generation products, then the extent to which a static representation will capture the influence of multi-generational ageing may be highly variable and sensitive to the experimental conditions and number of oxidation lifetimes. Consequently, the appropriateness of extrapolating static model parameterizations to longer (global atmospheric) timescales remains unclear. The results presented here indicate that the 2-product model does capture the influence of multi-generational ageing as part of the parameterization in terms of mass concentration, at least for the regional episodes considered, but it is also apparent that the simulated SOA properties (e.g. volatility) and the explicit contributions of various SOA types are not fully captured by such simple models.

The BaseM and SOM simulations show that the SOA concentrations in the SoCAB and eastern US vary by a factor of two when using parameterizations developed from low vs. high NO_x chamber experiments. Hence, we can argue that for the present simulations NO_x dependence is a much more important factor for SOA production than multi-generational oxidation. While most 3-D models include schemes to simulate the NO_x dependence of SOA formation, these schemes remain *ad hoc* as they are based on limited experimental measurements and also rely on the ability of the model to accurately predict radical concentrations (RO_2, HO_2) or VOC-to-NO_x ratios. In this work, the model predictions from the low- and high-yield simulations capture the NO_x-dependent uncertainty in SOA concentrations and we recommend that future work examine this issue in much more detail.

SOM predicts a modestly different composition of SOA than BaseM despite similar total mass concentrations of SOA. The composition predicted by SOM has a slightly higher contribution from alkanes, aromatics (anthropogenic) and sesquiterpenes and a lower contribution from isoprene and monoterpenes. These modest differences in the predicted composition of SOA have implications for understanding the sources of ambient aerosol and eventually the regulation of these sources to achieve compliance with National Ambient Air Quality Standards (NAAQS).

These more accurate SOA predictions resolved by chemical families should be tested in epidemiological studies to determine if they are associated with adverse health effects. Additionally, SOM predicted a much lower-volatility SOA than BaseM, and SOM predictions are in better qualitative agreement with ambient thermodenuder measurements of OA volatility. Since the SOA has a much lower volatility, there is very little enhancement (10-15%) with the inclusion of oligomerization reactions, implying that while oligomerization might affect composition, it may not be a source of additional SOA formation as the Base model suggests.

In this work, we consider POA as non-volatile and non-reactive and do not consider SOA contributions from IVOCs or semi-volatile POA vapors. Oxidation of IVOCs and semi-volatile POA vapors (i.e. SVOCs) can lead to the production of new SOA mass, but evaporation of POA leads to a decrease in the total OA mass. To some extent, these effects are offsetting (especially for SVOCs, which do not contribute new carbon mass to a model). To the extent that the loss of POA is balanced exactly by the formation of SOA from IVOCs and 'recycling' of semi-volatile POA vapors, the simulations here represent a scenario in which the total OA mass is conserved, although possibly with the wrong spatial distribution (Robinson et al., 2007). Most efforts to incorporate SOA formation from IVOCs and SVOCs have simulated their oxidation using a version of the VBS model in which multi-generational ageing is implicit, but highly underconstrained and structured in such a way that the ultimate (long time) SOA yield is greater than unity because all mass is converted to low-volatility products and oxygen addition is assumed. The SOM framework provides a way to explicitly account for the influence of multi-generational chemistry in SOA formation experiments that include semi-volatile POA vapors and IVOCs [121-134], and thus should be useful for constraining the contribution of these compound classes to the ambient OA budget. In addition, the simulations here do not consider the influence of vapor wall losses on SOA formation. Such losses can influence SOA yields in chambers, and consequently the parameterizations that result from fitting of such chamber data. The influence of vapor wall losses on simulated ambient SOA and OA concentrations within the SOM framework is examined in a companion paper [105]. Ultimately, models like the SOM can be applied to chamber experiments to better understand the role and contribution of POA, IVOCs and vapor wall-losses to total OA.

Finally, the comparison between the constrained SOM and the unconstrained COM (commonly used in large-scale models) suggests that COM may be double counting SOA formation. These simple ageing schemes should be refit to chamber data where all parameters can be matched to observed trends in a self-consistent manner.

4 SIMULATING SECONDARY ORGANIC AEROSOL IN A REGIONAL AIR QUALITY MODEL USING THE STATISTICAL OXIDATION MODEL: ASSESSING THE INFLUENCE OF VAPOR WALL LOSSES

Online link:

4.1 Introduction

Particulate organic matter, or organic aerosol (OA), is derived from primary emissions or from secondary chemical production in the atmosphere from the oxidation of volatile organic compounds (VOCs). OA makes up a substantial fraction of atmospheric submicron particulate matter [135], influencing the atmospheric fate and impact of PM on regional and global scales. Gas-phase oxidation of VOCs leads to the formation of oxygenated product species that can condense onto existing particles or nucleate with other species to form new particles [e.g. 136]. Much of the understanding regarding the formation of secondary organic aerosol (SOA) via condensation has been derived from experiments conducted in laboratory chambers. In a typical experiment, a precursor VOC is added to the chamber and exposed to an oxidant (e.g. OH, O_3 or NO_3). As both the precursor VOC and the oxidation products react with the oxidant, SOA is formed. The amount of SOA formed per amount of precursor reacted (i.e. the SOA mass yield) can then be quantified [e.g. 137]. Such SOA yield measurements form the basis of most parameterizations of SOA formation in regional air quality and global chemical-transport and climate models [138]. However, too often simulated SOA concentrations underestimate observed values, especially in polluted regions, and sometimes dramatically so [5, 139, 140]. There have been various efforts to account for model/measurement disparities including, most notably: (i) the addition of new SOA precursors in the form of so-called semi-volatile and intermediate volatility organic compounds, S/IVOCs, including treating primary organic aerosol as semi-volatile [3]; (ii) the addition of ad hoc "ageing" schemes on top of existing parameterizations of SOA from VOCs [141-143]; (iii) updating of aromatic SOA yields [144]; and (iv) production of SOA in the aqueous phase in aerosol-water, clouds and fogs [145]. More recently, concerns over the influence of vapor wall losses on the experimental chamber data used to develop the parameterizations have arisen [67, 146]. The influence of erroneously low SOA yields due to vapor wall losses on simulated SOA concentrations in three-dimensional regional models and properties is the focus of the current work.

Recent observations have demonstrated that organic vapors can be lost to Teflon chamber walls, and that the extent of loss is related to the compound vapor pressures with lower vapor pressure compounds partitioning more strongly to the walls than higher vapor pressure compounds [146-150]. These results suggest that vapor wall losses during SOA formation experiments could potentially bias observed SOA concentrations. Indeed, Zhang et al. [67] observed that SOA yields from toluene + OH photo oxidation depend explicitly on the seed particle surface area, all other conditions being equal. They interpreted these observations using a dynamic model of particle growth coupled with a parameterizable gas-phase chemical mechanism, the statistical

oxidation model (SOM) [13]. They determined that substantial vapor wall losses were most likely the cause of this dependence, with biases of up to a factor of ~4 for these experiments. Further, they estimated for this system that the vapor wall loss rate coefficient (k_{wall}) was ~2 x 10^{-4} s^{-1} for their 25 m^3 chamber. This value of k_{wall} is in reasonable agreement both with theoretical expectations—so long as the vapor-wall accommodation coefficient (α_{wall}) is >10^{-5}— and with results of Ziemann and colleagues [146, 147] who estimated k_{wall} ~ 6 x 10^{-4} s^{-1} for their 8 m^3 chamber. Kokkola, Yli-Pirilä [150] have also suggested vapor wall losses can impact SOA yields, although they determined a much larger k_{wall} of ~10^{-2} s^{-1} for their 4 m^3 chamber. Recent direct measurements of k_{wall} for a range of oxidized VOCs (OVOCs), produced from reactions of VOCs in traditional chambers, suggest that k_{wall} can vary by an order of magnitude (~ 2 x 10^{-6} – 3 x 10^{-5} s^{-1}) and that k_{wall} is dependent on the OVOC vapor pressure [148]; such low k_{wall} values implies that the α_{wall} is < 10^{-5} and controls the rate of vapor loss to the walls.

Although the exact value of k_{wall} is likely chamber-specific (which likely contributes to some of the above-mentioned variability in k_{wall}) and thus the exact influence of vapor wall losses on chamber SOA measurements remains somewhat uncertain, the preponderance of evidence suggests that such effects are important. Existing SOA parameterizations have typically not been determined with explicit accounting for vapor wall losses. Consequently, they likely underestimate actual SOA formation in the atmosphere where walls are much less important (although dry deposition of vapors may still be a factor [151]). Two recent efforts have attempted to estimate the influence of vapor wall losses on SOA concentrations in the atmosphere [152, 153]. One of the studies [153] builds on the existing two-product parameterization of SOA formation in the Community Multiscale Air Quality (CMAQ) model and simply scales the yields of the semi-volatile products up by factors of 4. In the two-product model, a given VOC reacts to form two semi-volatile products that partition to the condensed phase. The semi-volatile products are formed with mass yields, y_i, and partitioning coefficients, K_i, that have been determined by fitting the model to data from chamber experiments in which vapor wall losses were not accounted for. The other study [152] used a similar yield-scaling approach, but within the volatility basis set (VBS) four-product framework to represent SOA formation, and they scaled the mass yields for only the semi-volatile product species from aromatics. Not surprisingly, these simple *ad hoc* scaling methods demonstrated that increasing the yields of the semi-volatile products from their originally parameterized values increases the simulated SOA concentration, but quantitative interpretation of the results is difficult. This is an especially important consideration given that different SOA systems may exhibit different sensitivities to vapor wall losses, owing to differences in the product species volatility distribution and the extent to which multi-generational ageing influences the SOA formation. More robust assessment of the influence of vapor wall losses on simulated SOA concentrations in regional air quality models is thus needed.

In this study, the SOM SOA model [13] is utilized to examine the influence of vapor wall losses on simulated SOA concentrations and O:C atomic ratios in a 3D regional air quality model, specifically the UCD/CIT [49]. What distinguishes the present approach is that the potential influence of vapor wall losses is inherently accounted for during the development of the SOM SOA parameterization [67]. This can be contrasted with a simple scaling of an existing parameterization. The current approach allows for more detailed characterization of different precursor species, reaction conditions (e.g. NO$_x$ sensitivities) and the complex interplay of

various timescales (reaction, gas/wall partitioning and gas/particle partitioning). This also allows for examination of the extent to which different assumptions regarding the value of k_{wall} (i.e. the first-order rate constant for vapor loss to chamber walls) during development of the SOA parameterization impact simulations of ambient SOA concentrations. Further, the SOM framework simulates O:C atomic ratios in addition to OA mass concentrations, and thus allows for more detailed assessment of the simulated OA and comparison with observations. Our results demonstrate that accounting for vapor wall losses can have a substantial impact on simulated SOA concentrations and suggest that there may be regionally-specific differences.

4.2 Methods

4.2.1 Air Quality Model

Regional air quality simulations were performed using the UCD/CIT chemical transport model [49] for two geographical domains: (i) the Southern California Air Basin (SoCAB) and (ii) the eastern US. Details regarding the general model configuration and emissions inventory used have been previously discussed [154], and the reader is referred to that work for further information. Details specific to the current work are provided in the following sections. Model simulations were run for SoCAB from July 20 to August 2, 2005 and for the eastern US from August 20 to September 2, 2006. Model spatial resolution was higher in SoCAB (8 km x 8 km) than in the eastern US (36 km x 36 km) to account for the different domain sizes.

4.2.2 Statistical Oxidation Model for SOA

SOA formation from six VOC classes was simulated using the statistical oxidation model [13, 155], which was recently implemented in the UCD/CIT model [154]. The VOC classes considered are: long alkanes, benzene, high-yield aromatics (i.e. toluene), low-yield aromatics (i.e. m-xylene), isoprene and terpenes (including both mono- and sesquiterpenes). SOM is a parameterizable model that simulates the multi-generational oxidation of the product species formed from reaction of the SOA precursor VOCs. In SOM, a "species" is defined as a molecule with a specific number of carbon and oxygen atoms (N_C and N_O, respectively), and where the VOC-specific properties of these SOM species are determined through fitting to laboratory observations. Reactions of a SOM species lead to either functionalization (i.e. addition of oxygen atoms while conserving the number of carbon atoms) or fragmentation (i.e. the production of two species which individually have fewer carbon atoms but where the total carbon is conserved, and where each new species adds one additional oxygen atom). The particular tunable parameters in SOM are: the probability of adding one, two, three or four oxygen atoms per reaction, referred to as p_{XO}; the decrease in vapor pressure per added oxygen, referred to as ΔLVP; and the probability of fragmentation, which is related to the O:C atomic ratio of a given species as and where m_{frag} is the tunable parameter. SOA formation from the semi-volatile SOM species assumes that partitioning is described according to absorptive gas-particle partitioning theory [156], and the gas-particle mass transfer has been simulated using dynamic partitioning [49, 67, 154]. The parameters used in the current work have been determined by fitting to time-dependent data from SOA formation experiments conducted in the Caltech chamber both with and without accounting for vapor wall losses during the fitting process

(discussed further below); references for the specific experiments considered are provided in Table 4-1. The specific influence of considering multi-generational ageing on simulated SOA concentrations and properties is discussed in a companion paper [157]. The use of the SOM to represent SOA formation leads to an increase of about a factor of 2.5 or less in computer processing time required compared to use of the 2-product model.

Table 4-1: List of Best Fit SOM parameters determined by fitting SOM to experimental observations of SOA formation in the Caltech environmental chamber assuming that $k_{wall} = 1$ x 10^{-4} s^{-1} or 2.5 x 10^{-4} s^{-1}.

VOC Precursor Class	SAPRC-11 Species Name	VOC Surrogate	NO$_x$	m_{frag}	ΔLVP	p_{1O}	p_{2O}	p_{3O}	p_{4O}	Ref.^
				$k_{wall} = 1$ x 10^{-4} s^{-1}						
Long Alkanes	ALK5*	dodecane	low	0.677	1.57	0.97	0.023	0.003	0.004	[103, 155]
			high	0.186	1.45	0.961	0.001	0.002	0.036	
Benzene	Benzene	benzene	low	0.01	2.31	0.324	0.001	0.607	0.068	[23]
			high	0.73	1.47	0.018	0.001	0.981	0.001	
Toluene	ARO1	toluene	low	0.843	1.70	0.066	0.001	0.106	0.827	[67]
			high	5	1.37	0.865	0.001	0.065	0.069	
m-xylene	ARO2	m-xylene	low	0.236	1.97	0.001	0.123	0.8	0.075	[23]
			high	0.0389	1.46	0.001	0.001	0.905	0.093	
Isoprene	Isoprene	isoprene	low	0.01	2.20	0.097	0.13	0.748	0.025	[158]
			high	0.745	2.15	0.808	0.189	0.002	0.001	
Terpenes	TRP1/ SESQ+	α-pinene	low	0.156	1.89	0.316	0.554	0.087	0.043	[158]
			high	0.0588	1.92	0.064	0.865	0.063	0.008	
				$k_{wall} = 2.5$ x 10^{-4} s^{-1}						
Long Alkanes	ALK5*	dodecane	low	2	1.83	0.999	0.001	0.001	0.001	[103, 155]
			high	0.266	1.47	0.965	0.001	0.002	0.032	
Benzene	Benzene	benzene	low	0.0807	1.97	0.637	0.001	0.002	0.360	[23]
			high	0.824	1.53	0.008	0.001	0.991	0.001	
Toluene	ARO1	toluene	low	1.31	1.77	0.185	0.001	0.002	0.812	[67]
			high	4.61	1.42	0.856	0.001	0.002	0.141	
m-xylene	ARO2	m-xylene	low	1.08	2.05	0.102	0.001	0.878	0.019	[23]
			high	0.0671	1.46	0.001	0.001	0.942	0.056	
Isoprene	Isoprene	isoprene	low	0.0839	2.44	0.096	0.379	0.518	0.007	[158]
			high	5	1.78	0.874	0.039	0.085	0.001	
Terpenes	TRP1/ SESQ+	α-pinene	low	0.305	1.97	0.419	0.426	0.140	0.014	[158]
			high	0.16	1.91	0.500	0.422	0.070	0.008	

^These are the primary references for the experimental data. The data for the specific experiments used are presented in the supplemental material of [67]

*For SOM, the ALK5 class is separated into long alkane species grouped according to carbon number. See [154] for details.

+Although the same set of parameters are used to describe the formation of oxidation products and SOA from monoterpenes and sesquiterpenes, the SOA yield from sesquiterpenes is larger than for monoterpenes due to the larger number of carbon atoms comprising sesquiterpenes.

4.2.3 Accounting for Vapor Wall Losses

SOM

Vapor wall losses have been accounted for using SOM, as detailed in Zhang, Cappa [67]. Vapor wall loss is treated as a reversible, absorptive process with vapor uptake specified using a first-order rate coefficient (k_{wall}) and the desorption rate related to the effective saturation concentration, C^*, of the organic species and the effective absorbing mass of the walls [146]. Unique SOM fits (i.e. values of m_{frag}, ΔLVP and p_{XO}) have been determined for different assumed values of k_{wall}. Best-fit values are provided in Table 4-1. It should be noted that the influence of vapor wall losses is inherent in the fit parameters, and in the absence of walls (i.e. in the atmosphere) the predicted SOA formed will be larger when the fits account for vapor wall losses. A base case set of parameters with no vapor wall losses assumed during fitting (termed SOM-no) was determined using $k_{wall} = 0$. In Zhang, Cappa [67], an optimal value of $k_{wall} = 2$ x 10^{-4} s^{-1} was determined for the California Institute of Technology chamber based on simultaneous fitting of the SOM to a set of toluene photo oxidation experiments conducted at different seed particle concentrations. Unlike in Zhang et al. (2014), the values of k_{wall} used here were not determined during model fitting. This is because the absolute value of k_{wall} is not well constrained by a single experiment, and the simulations require vapor wall loss corrected parameters for VOCs besides toluene. Therefore, two specific bounding cases that account for vapor wall loss are instead considered based on the results from Zhang et al. (2014). Specifically, values of $k_{wall} = 1$ x 10^{-4} s^{-1} and 2.5 x 10^{-4} s^{-1} are considered, corresponding to a low vapor wall loss case (SOM-low) and high vapor wall loss case (SOM-high), respectively.

An important aspect of vapor wall loss is that the impact it has on SOA concentrations is dependent upon the timescale associated with vapor-particle equilibration (τ_{v-p}) [67, 72]. The τ_{v-p} is related to the accommodation coefficient associated with vapor condensation on particles, $\alpha_{particle}$. Above a vapor-particle accommodation coefficient of $\alpha_{particle} \sim 0.1$ variations in the exact value of $\alpha_{particle}$ does not influence the effects of vapor wall losses. This is not to say that vapor wall losses have no influence on the amount of SOA formed when $\alpha_{particle} \geq 0.1$, only that the net impact does not depend on $\alpha_{particle}$. Below this value, vapor-particle equilibration is slowed and the effects of loss of vapors to the walls are accentuated. Thus, a conservative estimate that minimizes the influence of vapor wall losses on SOA formation is obtained using $\alpha_{particle} \geq 0.1$. Here, data fitting and parameter determination was performed assuming that $\alpha_{particle} = 1$, and is thus a conservative estimate.

SOM was fit to time-dependent SOA formation experiments conducted in the California Institute of Technology chamber, following the methodologies described in Cappa, Zhang [155] and Zhang, Cappa [67]. Observed suspended particle concentrations have been corrected only for physical deposition on chamber walls, which is appropriate since vapor wall losses are accounted for separately by SOM. Best-fit values for the SOM parameters for the base case (SOM-no) are given in Jathar, Cappa [154] and values for SOM-low and SOM-high determined here are given in Table 4-1, along with the sources of the experimental data. Parameters have been separately determined for experiments conducted under low-NO_x and high-NO_x conditions since the SOA yields differ. Example results that illustrate the influence of vapor wall losses on simulated SOA yields are presented in Figure 4-1 for box model simulations that have been conducted using the best-fit parameters determined for toluene SOA (low-NO_x conditions), but where the simulations are run assuming there are no walls (i.e. by setting $k_{wall} = 0$).
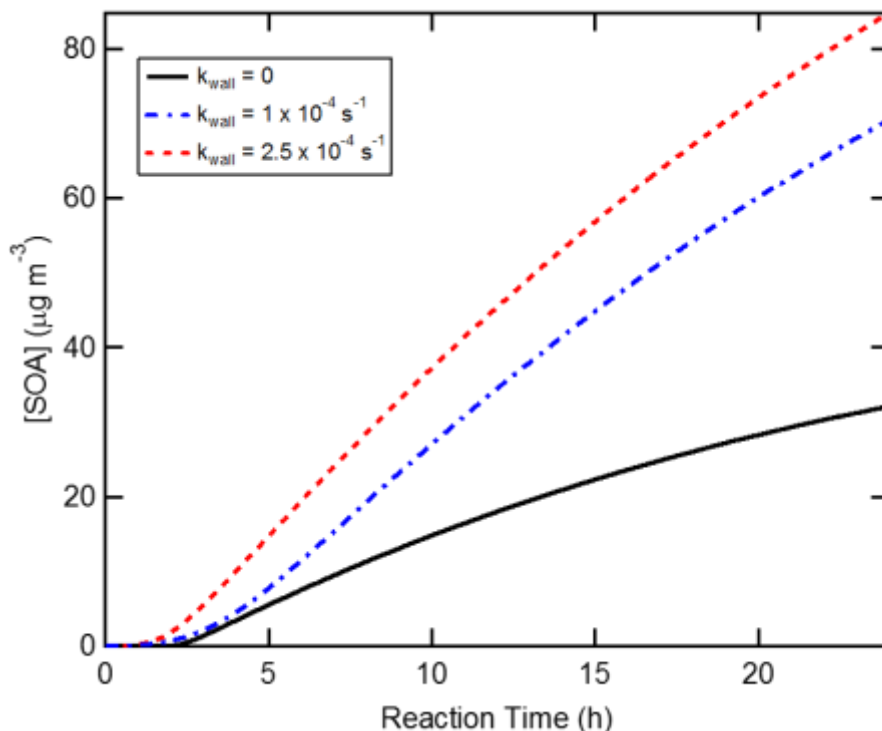
Figure 4-1: Box model simulations of SOA formation using SOM parameters determined from fitting low-NO$_x$ toluene + OH SOA data assuming $k_{wall} = 0$, 1 x 10^{-4} and 2.5 x 10^{-4} s^{-1}, but where the simulations are run with $k_{wall} = 0$ s^{-1}. Reaction conditions here are [toluene]$_{t=0}$ = 100 μg m^{-3} and [OH] = 2 x 10^6 molecules cm^{-3}.

Two Product Model

Ideally, SOA levels from the SOM-based simulations can be compared with similar results based on the commonly used two-product model. To do so involves determining new parameters for the two-product model in which vapor wall losses are explicitly accounted for. Therefore, vapor wall-loss corrected SOA yield curves (i.e. [SOA] versus [ΔHC], where ΔHC is the concentration of reacted hydrocarbon) were generated with SOM using the parameters determined by fitting SOM to the original chamber data when $k_{wall} > 0$, but now where k_{wall} is set to zero. The 2-product model could then be fit to these "corrected" yield curves to determine vapor wall-loss corrected yields and partitioning coefficients. These new fits would inherently account for the influence of vapor wall loss since the two-product model is being fit to the corrected "wall-less" data and thus differ from *ad hoc* scaling of yields. However, it was determined that the two-product fits were not sufficiently robust across the entire suite of compounds and vapor wall loss conditions considered to be implemented in the atmospheric model. An example for SOA from dodecane + OH under low-NO$_x$ reaction conditions is shown in Figure 4-2. We have determined that this lack of robustness is a result of the limited dynamic range of the 2-product model. This can be contrasted with the SOM, which includes many more species that span a wider, more continuous volatility range, making it more flexible when fitting the laboratory data. More specifically, the SOA concentrations from the chamber observations, both uncorrected and corrected, ranged from ~1-500 μg m^{-3}, often with few data points at concentrations less than ~10 μg m^{-3}. Thus, when fits were performed, inconsistent behavior between the different vapor wall

loss conditions was obtained over the atmospherically relevant concentration range (~0.1-20 μg m^{-3}). Attempts were made to fit the two-product model over a restricted concentration range or to fit using log([SOA]) instead of [SOA]. However, neither effort led to sufficiently robust results (although both did lead to improvements). This null result suggests that simple scaling of two-product yields [153] to account for the effects of vapor wall losses may not be appropriate. This may similarly apply to scaling of VBS parameters [152], although the greater flexibility of the VBS (commonly implemented with four products, instead of two) can potentially allow for unique "wall-less" fits to be determined [159]. The extent to which such alternative methods can robustly account for vapor wall losses that are computationally less intensive than SOM will be explored in future work.
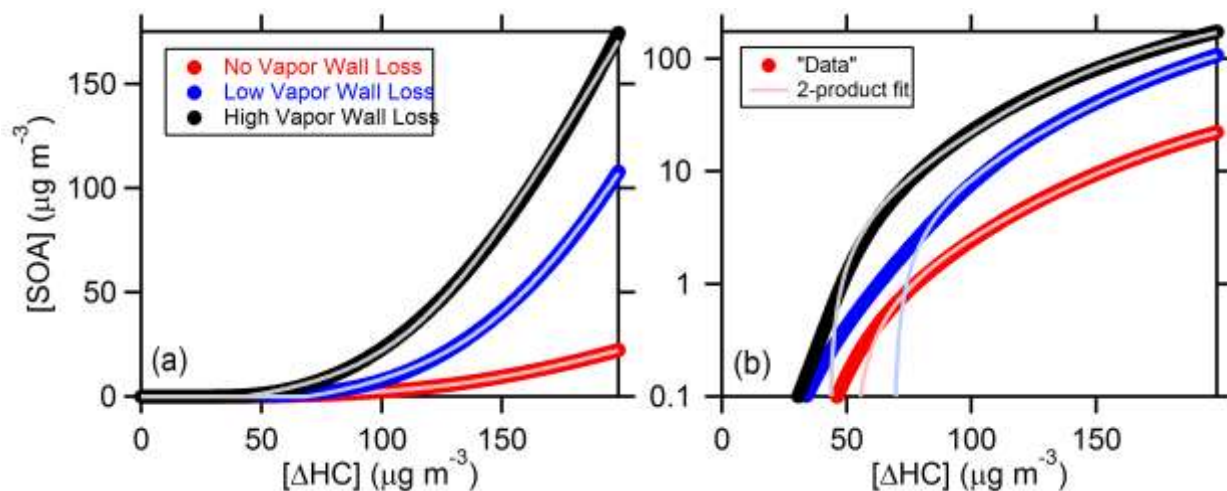
Figure 4-2: Example of 2-product fitting to SOA yield curves for dodecane + OH SOA formed under low-NO$_x$ conditions. The 2-product model was fit to simulated vapor wall-loss-corrected yield curves (circles) that were generated using the SOM model. The original SOM fits were performed using variable k_{wall} values to account for vapor wall losses, but the subsequent simulated yield curves were generated with $k_{wall} = 0$. The lines are colored according to the wall-loss condition used when SOM was fit to the chamber observations, no wall loss (red), low wall loss (blue) and high wall loss (black).The best 2-product fits are shown as solid lines. Panel (a) shows the curves and fits on a linear scale and panel (b) shows the same on a log scale. Note that on a linear scale the deviations between the fit curves and the "data" at low [SOA] is not visibly evident.

4.2.4   Primary Organic Aerosols and IVOCs

Primary organic aerosol (POA) derived from anthropogenic (e.g. vehicular activities, food cooking) or pyrogenic (e.g. wood combustion) sources are simulated assuming that the POA is non-volatile. This is the standard assumption in the CMAQ model framework [114], and thus is adopted here. It is known that some POA is semi-volatile, not non-volatile as assumed here. Had POA been treated within a semi-volatile framework [3], such that some fraction of the POA can evaporate (i.e. SVOCs) and react within the gas-phase and be converted to SOA (sometimes improperly referred to as "oxidized POA"), then the amount of POA would likely decrease (due to evaporation) and the amount of simulated SOA would increase (due to condensation of oxidized SVOC vapors); the total OA concentration (POA + SOA) may or may not increase as a

result, depending on the details of the parameterization and the atmospheric conditions. Additionally, nearly all modeling efforts in which POA is treated as semi-volatile have also included contributions from gas-phase IVOCs as an added class of SOA precursors; these two issues are rarely implemented independently in models, although their contributions can be separately tracked. Whereas simply treating POA as semi-volatile may or may not lead to an increase in the total OA concentration, the introduction of new SOA precursor mass in the form of IVOCs will inevitably lead to production of more SOA in the model. The relative importance of IVOCs will depend on the amount of added IVOC mass and the propensity of these IVOC vapors to form SOA in the model (i.e. their effective SOA yield). In the current study, we do not explicitly consider the potential for IVOCs to contribute to the ambient SOA burden, focusing instead on how vapor wall losses influence SOA formation from VOCs. We will aim to consider contributions from IVOCs and how they are influenced by vapor wall losses in future studies. Regardless, the implications of our particular treatment (non-volatile POA excluding IVOCs) are discussed below.

4.2.5   Model Simulations and Outputs

Six individual model simulations have been carried out to determine the spatial distribution of SOA concentrations. Each simulation used one of the SOM parameterizations, i.e. SOM-no, SOM-low or SOM-high with either the low- and high-NO_x parameters. Each precursor VOC is allowed to react with either OH, O_3 or NO_3 as characterized by an oxidant-specific rate coefficient, although the products and product distributions of the first-generation products are assumed to be oxidant independent. This simplification is identical to that employed in CMAQv4.7 [160]. Reactions of subsequent oxidized SOM products then occur only via reaction with OH radicals according to the SOM parameterization associated with that precursor VOC (as determined by fitting the photo oxidation experiments). Besides the absolute SOA concentration, SOM also allows for explicit calculation of the average (and precursor-specific) O:C and H:C atomic ratios and of the SOA volatility distribution, which characterizes the distribution of particulate and gas-phase mass concentrations with respect to C^*. To estimate the O:C of the total OA (POA + SOA), it is assumed that the non-volatile POA has a constant O:C = 0.2 and H:C = 2.0 [161]. Since the simulated $(O:C)_{total}$ is just a combination of $(O:C)_{SOA}$ and $(O:C)_{POA}$, assuming a different value for $(O:C)_{POA}$ would change the absolute value of $(O:C)_{total}$ but not any dependence on simulation conditions. This is similarly true for $(H:C)_{total}$.

As noted above, unique sets of SOM parameters were fit to experiments conducted under either low- or high-NO_x conditions assuming a particular value for k_{wall}. Since each simulation used a single set of SOM fit parameters (e.g. SOM-no fit to low-NO_x experiments) the SOA NO_x parameterization used in a given simulation is independent of the actual simulated ambient NO_x concentrations or NO/HO_2 ratio. Consequently, comparison between the simulations conducted using the low- and high-NO_x parameterizations gives an indication of the range expected from variability in NO_x levels, and the average between the two simulations provides a representation that is intermediate between these two extremes. Unless otherwise specified, reported values are for the average of the simulations run using the low- and high-NO_x parameterizations. This approach towards understanding the influence of NO_x is different than some previous approaches that attempted to account for the SOA NO_x dependence in a more continuously variable manner. For example, some simulations using the two-product approach have used the instantaneous

NO/HO$_2$ ratios predicted by the model to allow distinguishing between low- and high-NO$_x$ products and SOA yields for aromatic VOCs [160]. Similarly, instantaneous VOC/NO$_x$ ratios have been used with VBS-type models for aromatic VOCs to allow for interpolation between the two regimes [162]. Typically, these efforts have not considered the NO$_x$-dependence of monoterpene and sesquiterpene yields even though it is experimentally established that the NO$_x$ condition (and more specifically, the NO/HO$_2$ ratio) influences SOA yields for both aromatic and biogenic compounds [e.g. 22, 23]. For most VOCs, the functional dependence of the SOA yield on the VOC/NO$_x$ ratio or the NO/HO$_2$ ratio is not well established, making it difficult to understand how well the interpolation methods work. (SOA formation from isoprene is a notable exception [e.g. 163].) Further, modeled NO/HO$_2$ ratios may be off by orders of magnitude, most likely due to poor representation of HO$_2$ concentrations [160], making it difficult to understand how well the conditions of the laboratory translate to the model environment. By considering the low- and high-NO$_x$ parameterizations separately, i.e. the approach used in the current study, bounds on the overall influence of NO$_x$ on the simulated SOA can be established. However, this approach will not capture how the simulated SOA may vary due to spatial and temporal variations in the model NO$_x$ and oxidant fields. Future efforts will aim to account for the NO$_x$-dependence of SOA formation in a more continuously varying manner, and to account for recent updates to the detailed isoprene oxidation mechanism [164].

4.3   Results and Discussion

4.3.1   General Influence of Vapor Wall Losses on Simulated SOA

The spatial distribution of the SOM-no model SOA concentrations is shown for SoCAB and the eastern US using the average from the simulations carried out using the low- and high-NO$_x$ parameterizations (Figure 4-3 a-b). (Again, the low- and high-NO$_x$ designations here refer only to the experimental conditions under which the SOM parameters were determined, not the actual NO$_x$ conditions in the UCD/CIT model.) For SoCAB, predicted SOA concentrations are largest in and around downtown Los Angeles and in the forested regions of the Los Padres National Forest and the Santa Monica Mountains National Recreation Area in the NW quadrant. The spatial distribution of SOA is similar to that obtained using the conventional two-product SOA parameterization [154, 157]. For the eastern US, predicted SOA concentrations are largest in the southeast, in particular around Atlanta, Georgia. Overall, the simulated SOA concentrations with the SOM-no model are larger in the eastern US than in SoCAB, reflecting the relatively strong influence of biogenic emissions in this region.
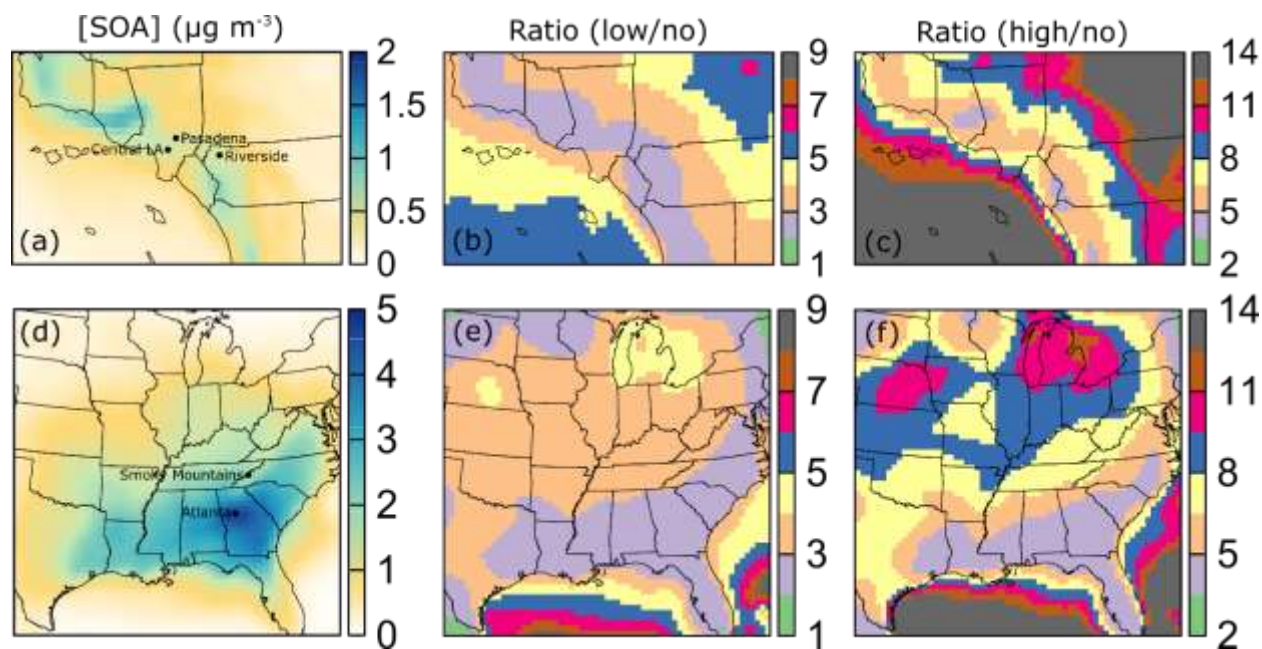
Figure 4-3: 14-day averaged SOA concentrations, in µg m^{-3}, for (a) SoCAB and (d) the eastern US for the SOM-no simulations. The averaging time periods are from July 20th to August 2nd, 2005 for SoCAB and from August 20th to September 2nd, 2006 for the eastern US. Panels (b,e) show the ratio between the SOA concentrations for the SOM-low and the SOM-no simulations and Panels (c,f) show the ratio between the SOM-high and SOM-no simulations. Results shown in all panels are the average of the low- and high-NO$_x$ simulations. Note that the color scale for the absolute SOA concentration is continuous whereas the color scale in the ratio plots is discrete.

The influence of vapor wall losses on the simulated ambient SOA concentrations is illustrated in Figure 4-3 c-f as the ratio between the SOA from the SOM-low and SOM-high simulations to the SOM-no (no wall losses) simulation. This ratio will be referred to generally as the wall loss impact ($R_{wall,low}$ or $R_{wall,high}$). Values of R_{wall} larger than one indicate that accounting for vapor wall losses as part of the SOM parameterization leads to an increase in the predicted SOA concentrations. In the SoCAB, the $R_{wall,low}$ varies from 1.5-4.5, while the $R_{wall,high}$ varies from 3 to more than 10. The largest ratios (indicating the largest impact of accounting for vapor wall losses) tend to occur in more remote locations as this is where concentrations are lower (Figure 4-4). However, the impact is still large in downtown Los Angeles and the greater LA region (average $R_{wall,low}$ ~2.5 and $R_{wall,high}$ ~5). In the eastern US, the simulated R_{wall} vary over a similar range as in SoCAB, with $R_{wall,low}$ varying from 1.5-5 and $R_{wall,high}$ from 3 to 10. There is again a general, although not exact, inverse relationship between R_{wall} and the absolute SOA concentrations; the greater scatter in the eastern US compared to SoCAB at low SOA concentrations likely reflects the larger spatial range considered. The smallest simulated R_{wall} values occur across the southeast and up the eastern seaboard ($R_{wall,low}$ ~2.5 and $R_{wall,high}$ ~5) while the largest values occur over the Great Lakes and Michigan, Nebraska, and the Gulf of Mexico and Atlantic Ocean; there is a steep increase going from land to sea. If R_{wall} values are calculated using the simulated SOA concentrations from either the low-NO$_x$ or high-NO$_x$

parameterizations individually, as opposed to the average values used above, very similar results are obtained (Figure 4-5).
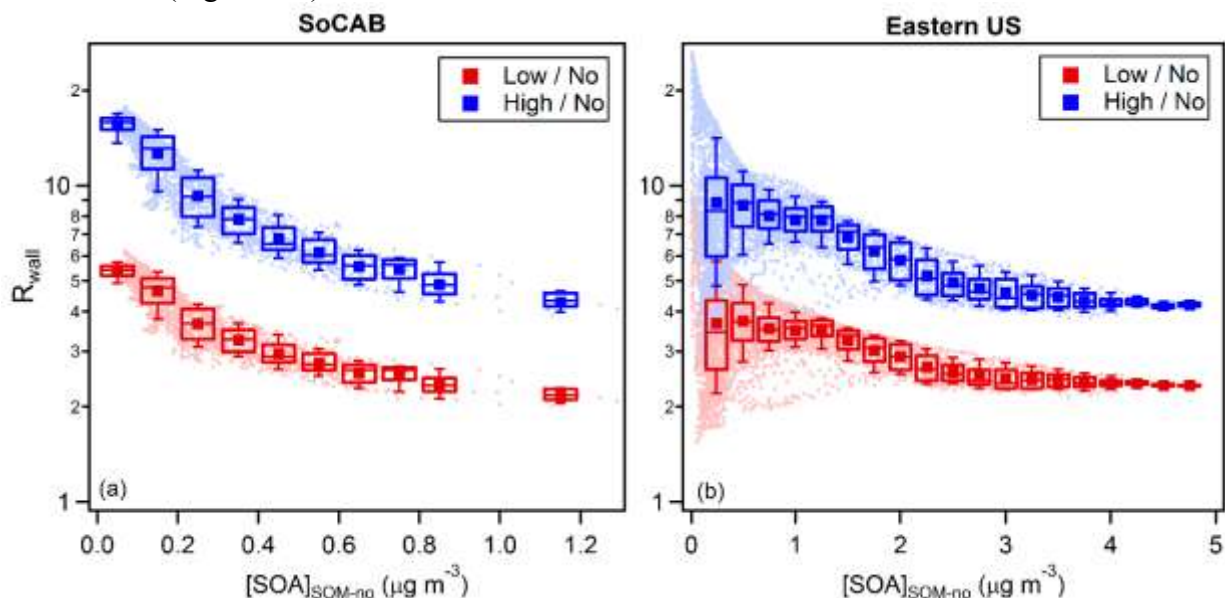
Figure 4-4: Variation of the ratio between simulated SOA concentrations from SOM-low (red) and SOM-high (blue) simulations to SOM-no simulations for (a) SoCAB and (b) the eastern US as a function of the absolute SOA concentration from the SOM-no simulations. Results shown are the average of the low- and high-NO_x simulations. Individual data points are shown along with box and whisker plots.
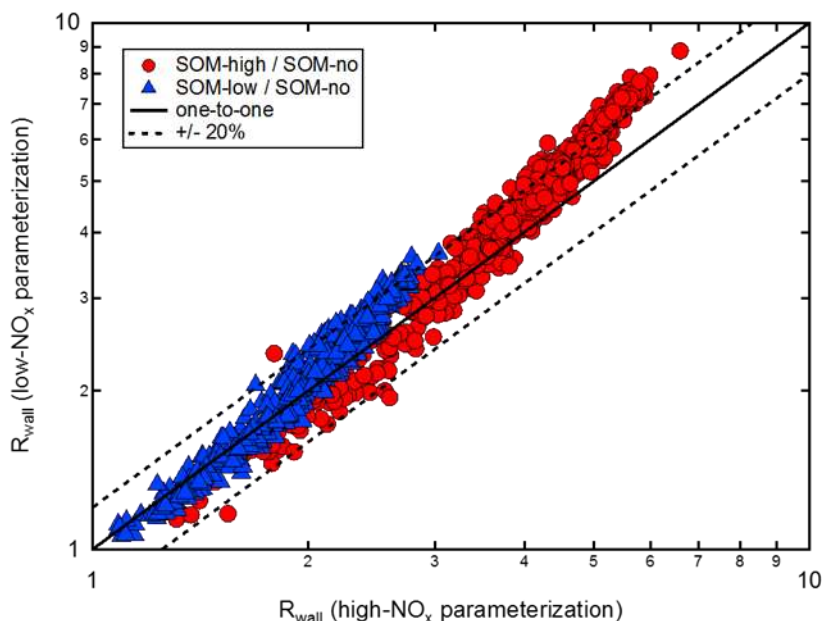
Figure 4-5: Comparison of R_{wall} values calculated for the low-NO_x parameterization (y-axis) or high-NO_x parameterization (x-axis) for the low vapor wall loss case (blue triangles) and high vapor wall loss case (red circles). The solid black line shows the 1-to-1 relationship and the dashed black lines the +/- 20% deviation from the 1-to-1 line.

Regional air quality models have historically overestimated the urban-to-regional gradient in total OA concentrations. Robinson, Donahue [3] showed that the simulated urban-to-regional gradient could be reduced and made more consistent with observations by treating POA as semi-volatile and adding SVOCs and IVOCs as SOA-forming species. The current results suggest a complementary explanation, namely that the urban-to-regional gradient can be reduced when vapor wall losses are accounted for since R_{wall} generally increases with decreasing SOA concentration and since POA is identical between the different model parameterizations. Consequently, larger R_{wall} are found outside of the major source regions, which decreases the urban-to-regional contrast. Indeed, the ratio between the predicted average SOA in downtown LA (urban) to that over the Pacific Ocean near the coast of LA (regional) and decreases from 2.3 (SOM-no) to 1.5 (SOM-low) to 1.3 (SOM-high), for example. Additionally, it has been suggested that the typical under prediction of SOA by air quality and chemical transport models relative to observations might increase with photochemical age [5]. The current results suggest the possibility that the SOA concentrations in more remote (lower concentration) regions may be underestimated in models to a greater extent in a relative sense than in high-source (higher concentration) regions due to a lack of accounting for vapor wall losses, although the absolute differences in SOA concentrations may be larger in regions where absolute concentrations are larger.

4.3.2   OA Composition and Concentrations

The simulated fraction of total OA that is SOA (f_{SOA}) is substantially smaller in SoCAB than in the eastern US, especially the southeast US (Figure 4-6). The predicted f_{SOA} values vary spatially within a given region, with the SOM-no simulations in the general range of ~0.1-0.3 for SoCAB and ~0.4-0.9 for the eastern US. This difference between regions results from the substantial POA emissions in SoCAB and the large emissions of biogenic VOCs across the southeast US. Consequently, accounting for vapor wall losses has a larger impact on the absolute total OA (SOA + POA) concentrations in the eastern US than it does in SoCAB, although the impact in both regions is substantial. For SoCAB, the predicted 24-h average f_{SOA} range increases to ~0.2-0.5 for SOM-low and to ~0.4-0.8 for SOM-high simulations. These model results can be compared with measurements from the 2005 SOAR field study in Riverside, CA, which overlaps with the simulation period. The observed f_{SOA} during SOAR ranged from ~0.6 in early morning to ~0.9 in midday, with a campaign-average of ~0.78 [165]. Measurements at Pasadena, CA during a later time period, June 2010 during the CalNex study, give similar results with the campaign-average f_{SOA} = 0.6 [166]. (Note that here we are equating SOA with the "oxygenated organic aerosol," or OOA factors that are obtained from positive matrix factorization of the measured OA time series, and equating POA with the sum of hydrocarbon-like OA (HOA), cooking-derived OA (COA), and "local" OA (LOA).) The SOM-high simulations in SoCAB are most consistent with these observations.
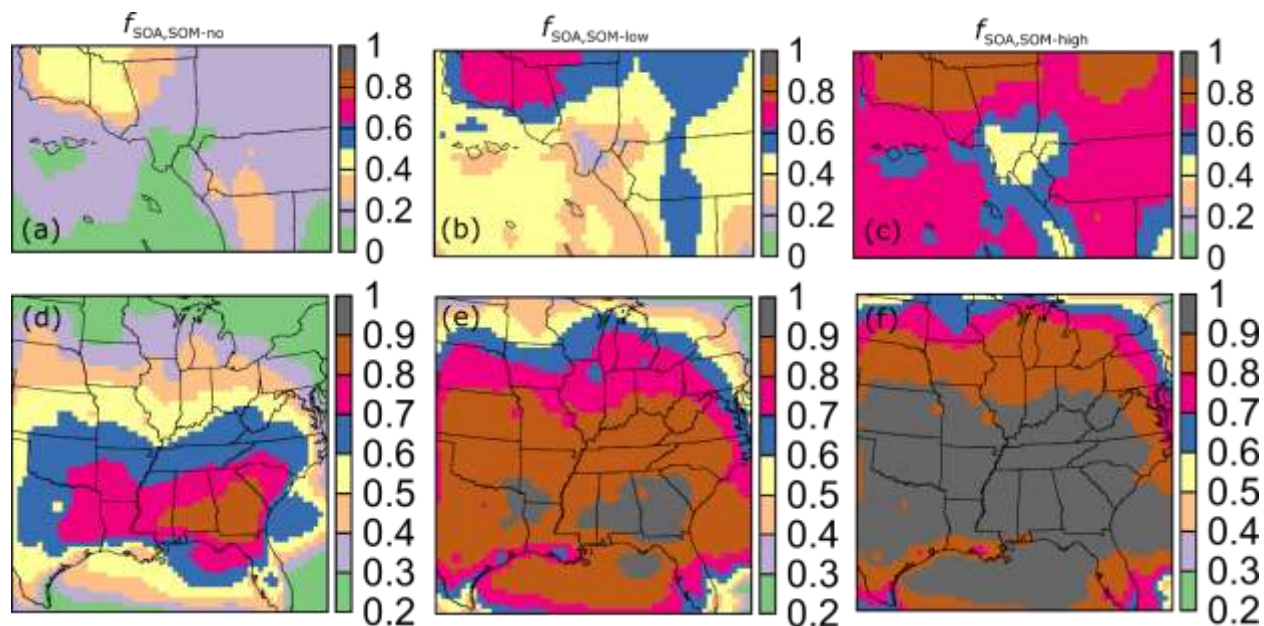
Figure 4-6: 14-day averaged f_{SOA}, the ratio between SOA and total OA concentrations, for (top panels, a, b, c) SoCAB and (bottom panels, d, e, f) the eastern US for the (a, d) SOM-no, (b, e) SOM-low and (c, f) SOM-high simulations.

For the eastern US, the predicted f_{SOA} range increases from 0.4-0.9 for SOM-no to ~0.7-0.9 for SOM-low and to ~0.8-1 for SOM-high. These predicted values can be compared with measurements made at a few locations in the southeastern US (specifically, sites in Alabama and Georgia), which show that the f_{SOA} in this region exhibits a strong seasonal dependence and some spatial variation [167]. The measurements in spring and summer indicate that the total OA is dominated by SOA, with f_{SOA} measurements ranging from 0.7 to 1 and with the smaller values observed at the more urban sites. The predicted f_{SOA} from the SOM-low and SOM-high simulations are most consistent with this range, with the f_{SOA} from the SOM-no simulations being on the low side, especially in comparison with the more rural sites.

The simulated total OA concentrations are compared to ambient OA measurements made at the STN (Speciated Trends Network) and IMPROVE (Interagency Monitoring of Protected Visual Environments) [168] air quality monitoring sites in SoCAB and the eastern US; the regional differences in f_{SOA} should be kept in mind for this model/measurement comparison. A map of sites is shown in Figure 4-7. STN sites tend to be more urban and have higher OA concentrations compared to IMPROVE sites, which tend to be more remote. OA concentrations are estimated as the measured organic carbon (OC) concentrations times 2.1 for IMPROVE sites and as 1.6 × ([OC] - 0.5 µg m^{-3}) for STN sites [169]. The -0.5 µg m^{-3} offset for the STN sites arises because the IMPROVE data are both artifact and blank corrected while the STN data are only artifact corrected [170]. The difference in scaling factors (2.1 versus 1.6) approximately accounts for differences in the OA/OC conversion between more urban and more rural networks [169]. Given the generally regional character of OA in much of the eastern US, it may be that the difference in OM/OC between the STN and IMPROVE sites may be smaller than assumed here (most likely with the 1.6 being too low, leading potentially to an underestimate in the OA at the STN sites).

We note that IMPROVE data may also be biased low by ~25% in the SE US summer due to evaporation after sampling [171].
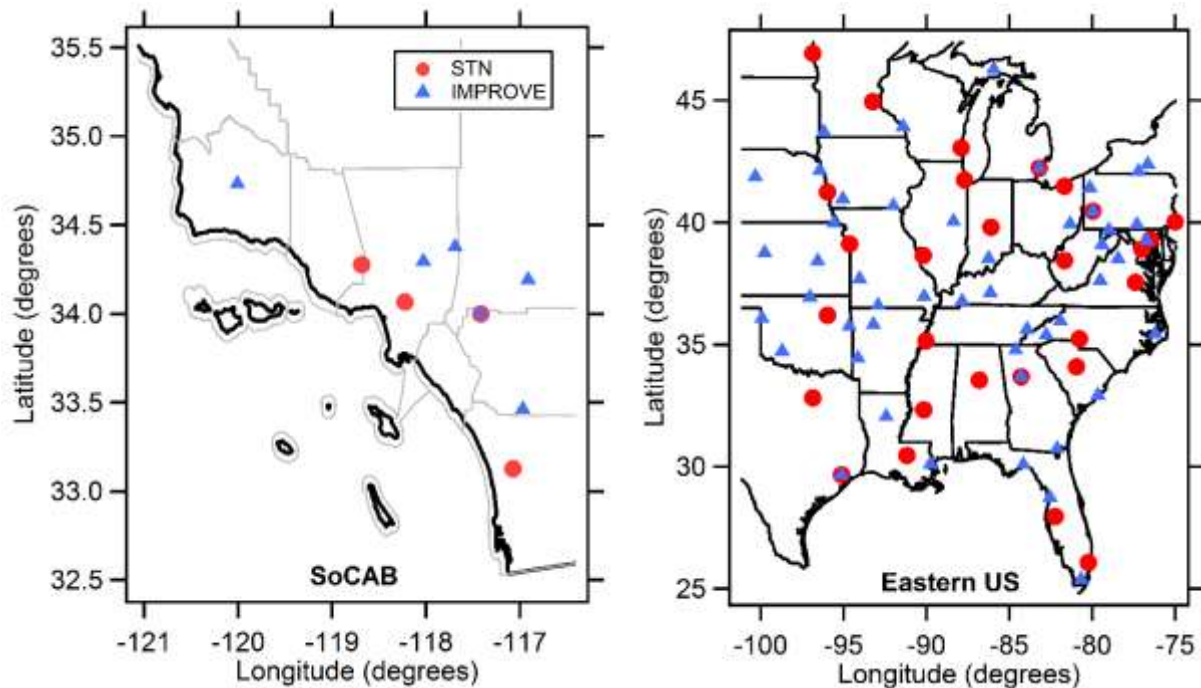
Figure 4-7: Map of STN and IMPROVE sites in the (left) SoCAB and (right) eastern US. STN sites are shown as red circles and IMPROVE sites as blue triangles.

Table 4-2 lists statistical metrics of fractional bias, normalized mean square error (NMSE) and the concordance correlation coefficients that capture model performance for OA for all simulations for both domains across the STN and IMPROVE monitoring networks. Fractional bias is calculated as:

$$\overline{\hspace{3cm}} \tag{1}$$

and the NMSE as

$$\overline{\hspace{2.5cm}} \tag{2}$$

where the subscripts *sim* and *obs* refer to the simulated and observed OA concentrations, respectively. The concordance correlation coefficients (ρ_c) are calculated as:

$$\overline{\hspace{3.5cm}} \tag{3}$$

where   and   indicate the mean,   and   are the variance and   is the covariance of the simulated and observed OA concentrations. Scatter plots are shown in Figure 4-8 and Figure 4-9; many more sites are considered in the eastern US than in the SoCAB given the larger geographical domain and distribution of sites. In both regions, the SOM-no simulations underpredict the STN and IMPROVE observations, especially in the SoCAB. The

negative bias of the SOM-no simulations is generally improved as vapor wall losses are accounted for. For both the STN and IMPROVE sites in the SoCAB the SOM-high simulations give best agreement. For the eastern US STN sites, an average of the SOM-low and SOM-high simulations provides the best agreement. For the eastern US IMPROVE sites, the SOM-low simulations provide the best agreement, although with some overprediction. (If the eastern US STN and IMPROVE measurements do underestimate the actual OA concentrations, the degree to which accounting for vapor wall losses improves the model-measurement comparison will increase.) The simulated anthropogenic/biogenic SOA split is found to be approximately the same at sites within both networks (e.g. Figure 4-10). This occurs even though the IMPROVE sites tend to be more remote than the STN sites in the eastern US, and reflects the regional character of SOA in that region. Ultimately, the comparisons suggest that accounting for vapor wall losses can improve model-measurement agreement, although there are differences in terms of whether the SOM-high simulations or SOM-low simulations produce the best agreement. That the OA concentrations for the SOM-high simulations remains slightly lower than the observations for STN sites in SoCAB could potentially result from the non-volatile treatment of POA, the exclusion of IVOCs in the current model or uncertainty in the POA emission inventory.
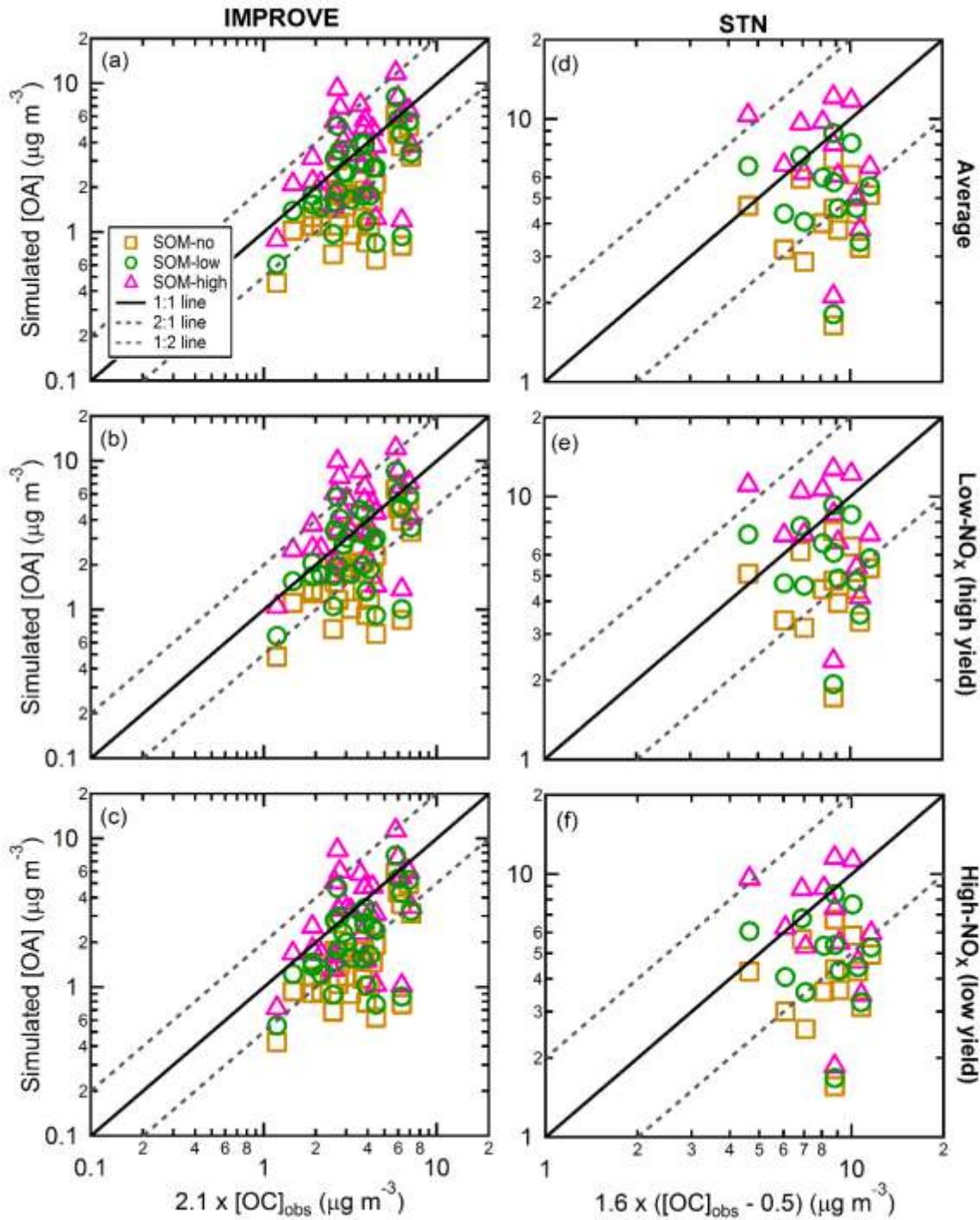
Figure 4-8: Scatter plots of simulated versus observed total OA (SOA + POA) concentrations for SoCAB for (left panels) IMPROVE and (right panels) STN sites. Simulation results are shown for SOM-no (orange), SOM-low (green) and SOM-high (pink). Results are reported from simulations run using the (top) average, (middle) low-NO_x / high-yield, and (bottom) high-NO_x / low-yield parameterizations.
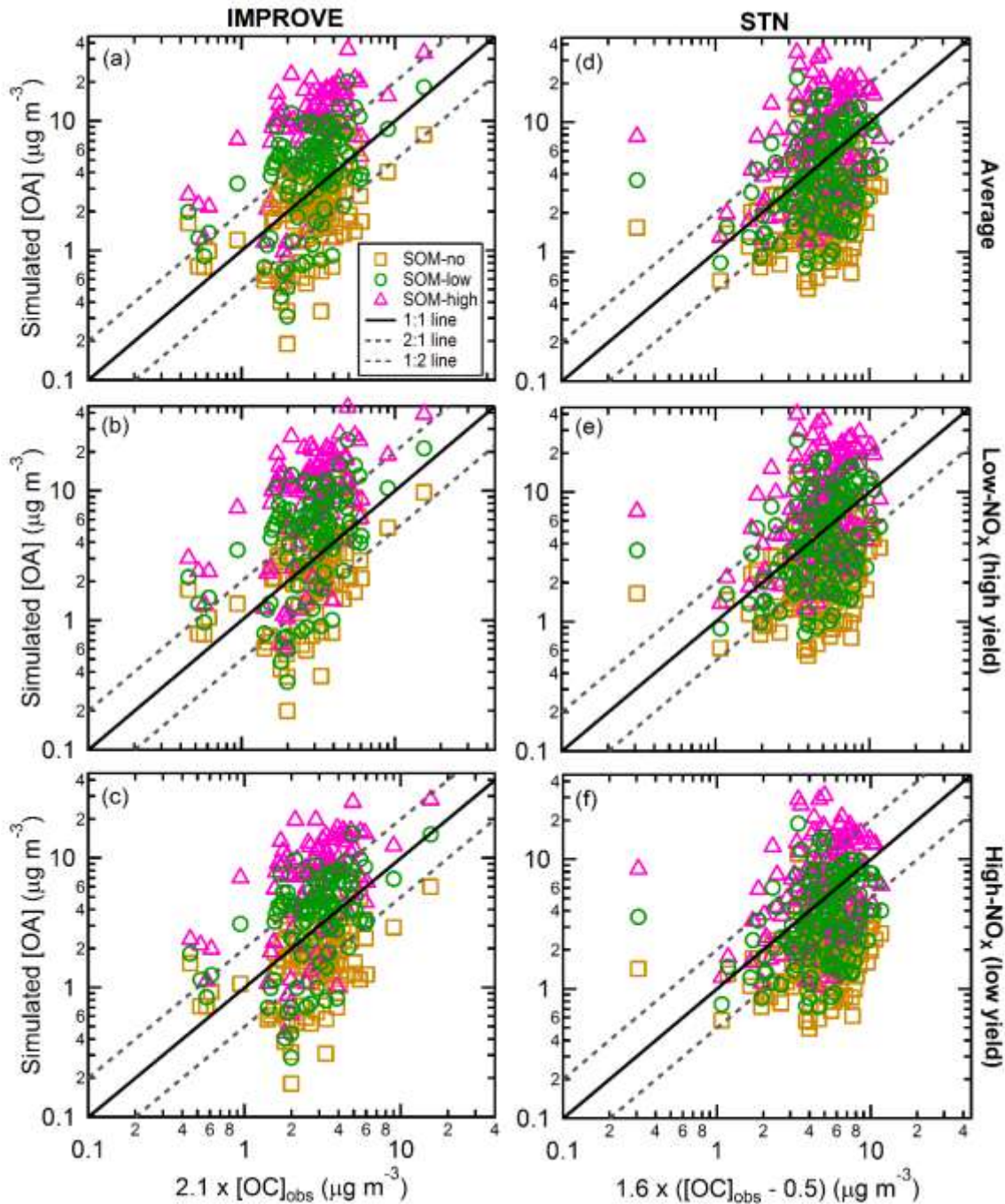
Figure 4-9 Scatter plots of simulated versus observed total OA (SOA + POA) concentrations for SoCAB for (left panels) IMPROVE and (right panels) STN sites. Simulation results are shown for SOM-no (orange), SOM-low (green) and SOM-high (pink). Results are reported from simulations run using the (top) average, (middle) low-NO_x / high-yield, and (bottom) high-NO_x / low-yield parameterizations. Only every other data point (one-in-two) is shown for visual clarity.
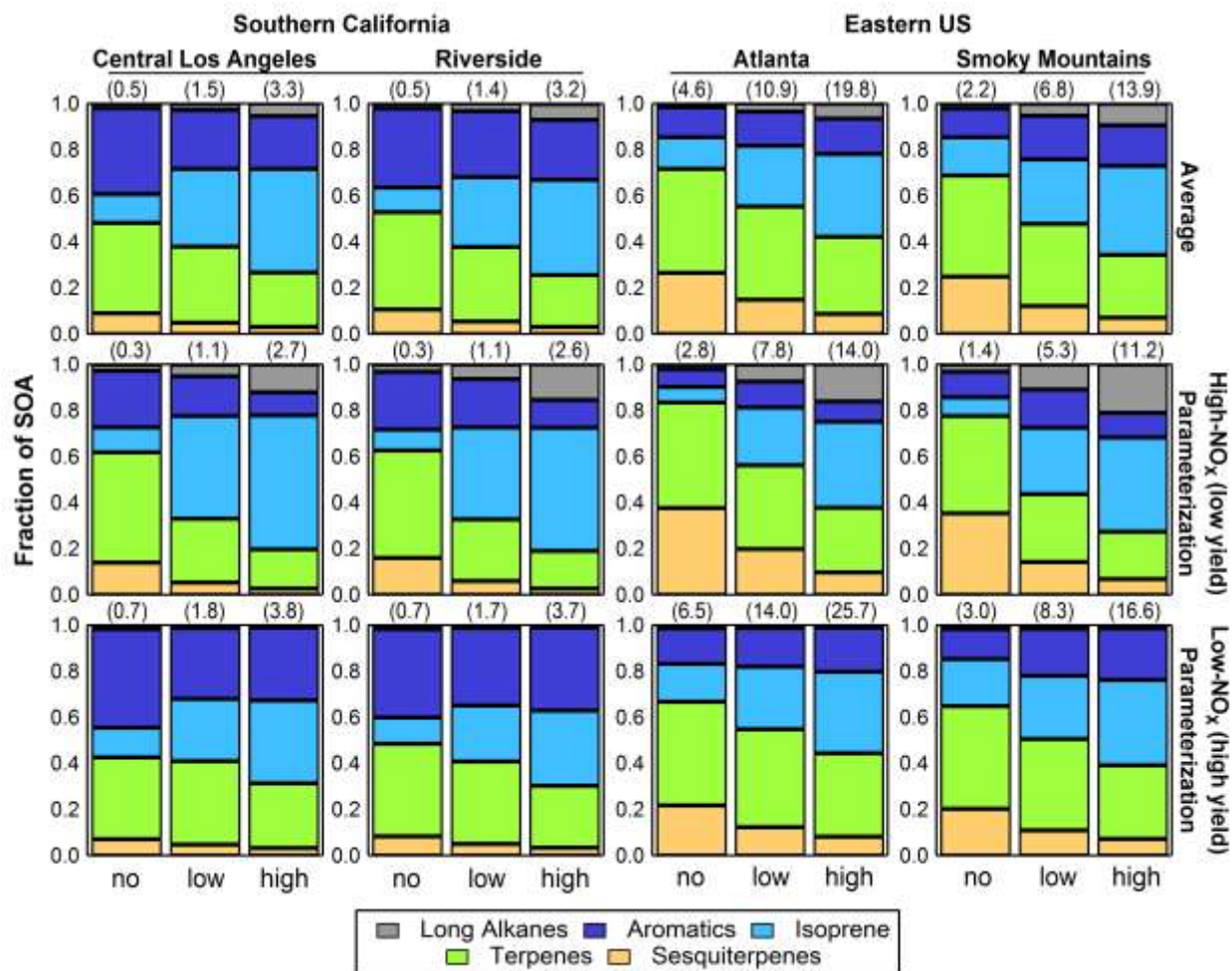
Figure 4-10: Bar charts showing the fractional contribution from the various VOC precursor classes to the total simulated SOA for two locations in SoCAB (central Los Angeles and Riverside) and two in the eastern US (Atlanta and the Smoky Mountains). Results are shown for (top) average, (middle) high-NO$_x$, low-yield and (bottom) low-NO$_x$, high-yield simulations. Each panel shows results from the 14-day average (left-to-right) SOM-no, SOM-low and SOM-high simulations. The average SOA concentration (in μg m^{-3}) is for each location and simulation is given in parentheses above each panel.

Table 4-2: Model Performance Metrics determined for the three simulation groupings (SOM-no, SOM-low and SOM-high) for the low-NO_x, high-NO_x and average parameterizations for STN and IMPROVE sites in SoCAB and the eastern US. Fractional bias is calculated as $2(C_{OA,sim}-C_{OA,obs})/(C_{OA,sim}+C_{OA,obs})$ and NMSE as $abs[(C_{OA,sim}-C_{OA,obs})^2/(C_{OA,sim}\times C_{OA,obs})]$, and the reported values are the averages over all data points as percentages. Note that a negative fractional bias indicates observed [SOA] > simulated [SOA], i.e. that the simulations are underpredicting. ρ_c are the concordance correlation coefficients from Eqn. 3.

Simulation	NOx parameterization	Southern California						Eastern US					
		STN[a]			IMPROVE[b]			STN[a]			IMPROVE[b,c]		
		Frac. Bias	NMSE	ρ_c	Frac. Bias	NMSE	ρ_c	Frac. Bias	NMSE	ρ_c	Frac. Bias	NMSE	ρ_c
SOM-no	low	-70	88	0.03	-75	114	0.36	-81	206	0.04	-55	105	0.31
	high	-61	69	0.02	-60	85	0.41	-58	166	0.12	-24	84	0.48
	average	-65	78	0.02	-67	97	0.39	-68	180	0.08	-38	89	0.43
SOM-low	low	-52	64	-0.21	-45	65	0.36	-26	154	0.08	15	85	0.15
	high	-39	49	-0.29	-27	47	0.27	-4	171	0.07	38	128	0.10
	average	-45	55	-0.25	-36	54	0.32	-14	160	0.08	28	105	0.12
SOM-high	low	-25	51	-0.03	-8	46	0.44	26	236	0.15	69	189	0.40
	high	-10	38	-0.08	16	43	0.46	45	298	0.15	86	295	0.25
	average	-17	43	-0.05	5	42	0.46	36	265	0.16	79	241	0.31

[a] Observed [OA] for STN sites estimated as 1.6([OC] – 0.5 µg m^{-3})

[b] Observed [OA] for IMPROVE sites estimated as 2.1[OC].

[c] Observed [OA] may be biased low by ~25% in the SE US summer due to evaporation after sampling (Kim et al., 2015).

The simulations can also be compared with observations of the OA-to-ΔCO concentration ratio (OA/ΔCO) during SOAR [165, 172], and where ΔCO indicates the background corrected CO concentration. Because CO is relatively long lived, normalization of the calculated and observed OA to the concurrent background-corrected CO helps to minimize the impacts of uncertainties in boundary layer dynamics and accounts for variability in emissions and transport to some extent [173]. The background-corrected CO concentration is calculated as $\Delta[CO] = [CO] - [CO]_{bgd}$. The estimated $[CO]_{bgd}$ for the observations is 105 ppb (with a plausible range from 85-125 ppb) [166]. In contrast, the $[CO]_{bgd}$ for the model is estimated to be 130 ppb based on the simulated [CO] over the open ocean west of Los Angeles. The observed diurnal profile of OA/ΔCO during SOAR exhibits a distinct peak around mid-day, corresponding to the peak in photochemical activity. This indicates a substantial influence of SOA production on the total OA concentration (Figure 4-11) [172]. The simulated OA/ΔCO diurnal profiles around Riverside for the SOM-high simulations are most consistent with the observations, exhibiting a distinct peak around mid-day that is similar to the observations (Figure 4-11). Unlike the observations, the diurnal OA/ΔCO profile for the SOM-no simulation exhibits almost no increase during mid-day and the SOM-low simulation exhibits only a slightly larger daytime increase. The slope of a one-sided linear fit to a graph of the observed [OA] versus [CO] during daytime (10 am to 8 pm) is 69 ± 2 $\mu g\ m^{-3}$ ppm^{-1} (Figure 4-11) when constrained to go through the assumed $[CO]_{bgd}$. This can be compared with the simulation results, which have constrained slopes of 23.0 ± 0.4, 34.0 ± 0.8 and 55 ± 2 $\mu g\ m^{-3}$ ppm^{-1} for SOM-no, SOM-low and SOM-high, respectively (Figure 4-11g-i). Clearly the SOM-high simulations are in best overall agreement with the SOAR observations. However, the maximum in the simulated OA/ΔCO peaks at a smaller value than was observed. The simulated peak also occurs slightly earlier than the maximum in the observations, which could be due to discrepancies in the transport to the Riverside site or to too fast SOA formation in the model. Nonetheless, these results clearly indicate that accounting for vapor wall losses has the potential to reconcile simulated SOA diurnal behavior with observations. Alternatively or complementarily, daytime increases in the OA/ΔCO ratio from SOA production can be achieved with the introduction of additional SOA precursor material such as S/IVOCs [152, 174], which are not considered here. The addition of S/IVOCs would increase the daytime OA/ΔCO for all of the simulations. The magnitude of the increase would depend on the amount of added S/IVOCs and the properties assigned to the S/IVOCs regarding their SOA formation timescale and yield. Consideration of SOA from S/IVOCs in the SoCAB using the SOM framework will be the subject of future work.
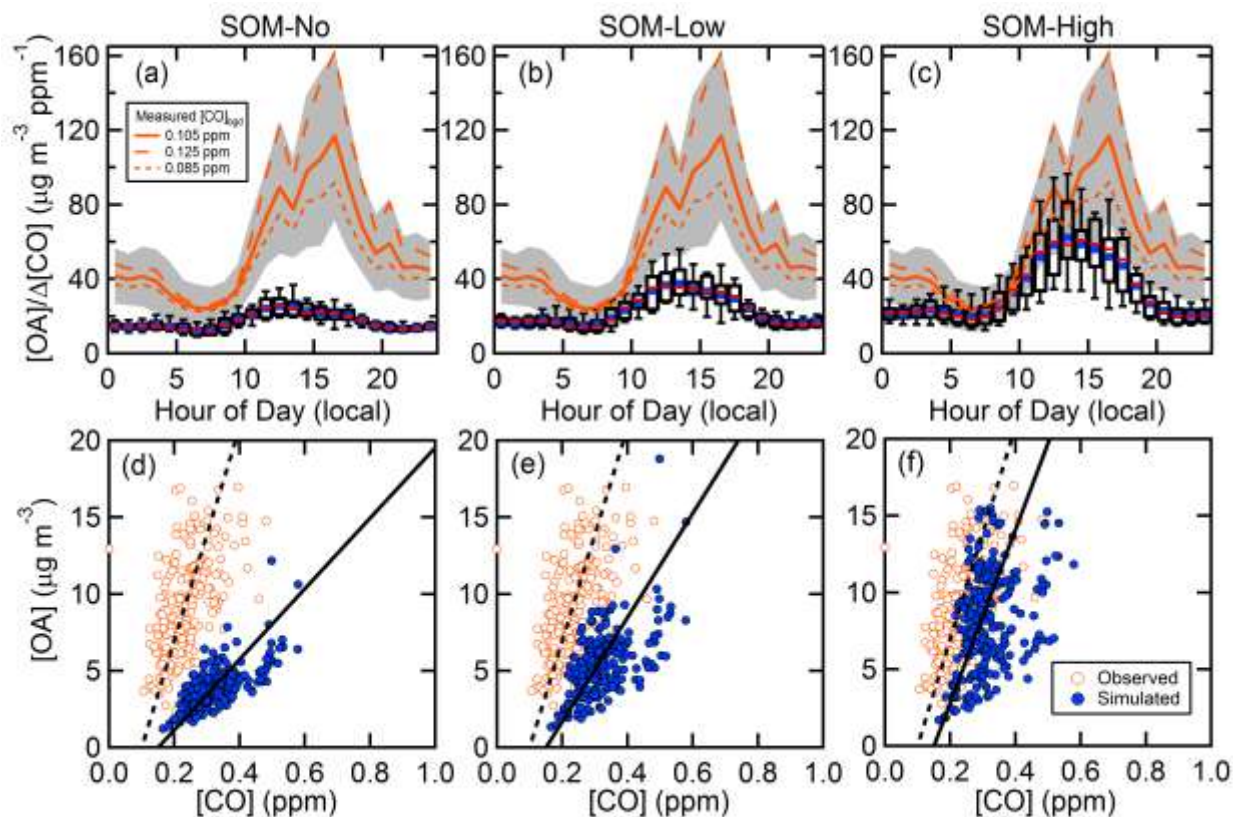
Figure 4-11: Simulated and observed diurnal profiles for the OA/ΔCO ratio (top panels) at Riverside, CA during the SOAR-2005 campaign for (a) SOM-no, (b) SOM-low and (c) SOM-high simulations. For the observations, the mean (solid orange line) and the 1σ variability range (grey band) are shown for $[CO]_{bgd}$ = 0.105 ppm, and only mean values are shown for $[CO]_{bgd}$ = 0.085 ppm (short dashed orange line) and $[CO]_{bgd}$ = 0.125 ppm (long dashed orange line). For the simulations, box and whisker plots are shown with the median (red –), mean (blue squares), lower and upper quartile (boxes), and 9th and 91st percentile (whiskers). The bottom panels (d-f) show scatter plots of [OA] versus [CO] for both the ambient measurements (open orange circles) and for the model results (blue circles) for daytime hours (10 am – 8 pm). The lines are linear fits where the x-axis intercept has been constrained to go through the assumed $[CO]_{bgd}$ (dashed = observed; solid = model). The derived slopes are 69 ± 2 (observed), 23.0 ± 0.4 (SOM-no), 34.0 ± 0.8 (SOM-low) and 55 ± 2 (SOM-high) μg m^{-3} ppm^{-1} and where the uncertainties are fit errors.

4.3.3   SOA Composition

Source / VOC Precursor Dependence

Accounting for vapor wall losses leads to regionally-specific changes in the simulated contributions from the different VOC classes (e.g. TRP1, ARO1) to the SOA burden, as illustrated in Figure 4-10 for two sites in SoCAB (central Los Angeles and Riverside) and two in the eastern US (Atlanta and the Smoky Mountains). Focusing first on contributions from the biogenic VOCs, at all locations accounting for vapor wall losses leads to an increase in the fractional contribution of isoprene SOA, typically at the expense of terpene and sesquiterpene SOA. This is true for both the low- and high-NO$_x$ simulations. Recent observations suggest that

isoprene SOA produced via the low-NO IEPOX (isoprene epoxydiol) pathway can be uniquely identified from analysis of aerosol mass spectrometer measurements when the relative contribution is sufficiently large (> ~5%) [e.g. 175, 176]. This observed IEPOX SOA accounts for around 30% (May) and 40% (August) of total SOA or around 20% (May) and 30% (August) of total OA in Atlanta in the summer [177], albeit not during the same time period as simulated here. IEPOX SOA was also found to account for 17% of total OA at a rural site in Alabama in 2013 [176]. The SOM-low and SOM-high simulation results for Atlanta are most consistent with the observations, with a predicted isoprene SOA fraction of 27% and 35%, respectively, compared to only 17% for the SOM-no simulations and where the reported values are for the simulations that use the low-NO_x parameterizations since this is the pathway that leads to IEPOX SOA. The related isoprene OA fractions are 10%, 21% and 31% for the SOM-no, -low and -high simulations, respectively. (These isoprene SOA fractions change only marginally for SOM-low and SOM-high simulations when the high-NO_x parameterizations are used, to 25% and 37%, respectively. The SOM-no simulations exhibit somewhat greater sensitivity to the NO_x parameterization, with the high-NO_x parameterization giving an SOA fraction of 7%.)

In SoCAB, the predicted average isoprene SOA fraction in central LA is relatively large for the SOM-low (36%) and SOM-high (47%) simulations, compared to the SOM-no simulations (12%). There is a large difference in SoCAB between the simulations that use the low-NO_x and high-NO_x parameterizations, with the isoprene SOA fractions being much larger with the high-NO_x parameterizations (e.g. 58% for high-NO_x versus 36% for low-NO_x for the SOM-high simulations). Measurements at Pasadena during the 2010 CalNex study did not distinctly identify IEPOX SOA, which is interpreted as the IEPOX SOA contribution being lower than ~5% of the OA [176]. It is possible that additional isoprene SOA had been formed under higher NOx conditions (compared to the southeast US) such that it is chemically different from IEPOX-SOA and was not identified as a uniquely isoprene-derived SOA component, instead contributing generically to the overall oxygenated OA pool. The concentration of isoprene SOA from specific high-NO_x pathways may, however, be limited at higher temperatures, such as found in summertime Pasadena, due to thermal decomposition of intermediate gas-phase species [178], although it is not clear to what extent this influenced the CalNex observations or would have affected the model results had it been explicitly considered. Additionally, it should be kept in mind that the ambient NO_x concentrations in SoCAB have decreased substantially from 2005-2013 [179]. Thus, although the CalNex measurements do not provide direct support for such a large isoprene SOA fraction, they also do not rule it out.

While the predicted isoprene SOA fraction increased, the predicted terpene and sesquiterpene SOA fractions decreased in the simulations that accounted for vapor wall losses. Additionally, the terpene SOA/sesquiterpene SOA ratio increased at all locations for the SOM-low and SOM-high simulations, in large part because the sesquiterpene yield is already large and thus accounting for vapor wall losses has a limited influence on the simulated sesquiterpene SOA concentrations.
There are some changes in the anthropogenic fraction of SOA when vapor wall losses are accounted for. The anthropogenic fraction of SOA is defined here as the sum of the SOA from long alkanes and aromatics, which are emitted from combustion of fossil fuels, divided by the sum of the total SOA, which additionally includes SOA from isoprene, monoterpenes and sesquiterpenes emitted by trees, plants and other natural sources. The ^{14}C isotopic signature of

fossil-derived VOCs is different from that of biogenically derived VOCs, and thus their respective contributions to SOA can be partially constrained via experimental analysis of the ^{14}C content of OA [180]. We assume the anthropogenic fraction is equivalent to the fossil fraction of SOA (termed $F_{SOA,fossil}$). At the two eastern US sites (Atlanta and Smokey Mountains) the average $F_{SOA,fossil}$ increases slightly from 14% (SOM-no) to 22% (SOM-low) and 25% (SOM-high). At the two SoCAB sites (downtown LA and Riverside) the predicted average $F_{SOA,fossil}$ decreases slightly, from 35% (SOM-no) to 29% (SOM-low) and 30% (SOM-high), respectively. In SoCAB the $F_{SOA,fossil}$ values differ between the low- and high-NO_x parameterizations, with $F_{SOA,fossil}$ typically larger for the low-NO_x parameterizations (e.g. 35% for low-NO_x and 25% for high-NO_x). In the eastern US, the predicted $F_{SOA,fossil}$ exhibit a stronger response to vapor wall losses for the high-NO_x parameterization than the low-NO_x parameterization, although the absolute values are reasonably similar. Of the anthropogenic SOA (aromatics + alkanes), the high-NO_x parameterizations indicate an increasing alkane SOA fraction as vapor wall losses are accounted for in both regions. In contrast, the low-NO_x parameterizations indicate minor contributions from alkane SOA for all of the simulations. In general, chamber SOA yields from aromatic compounds are larger for low-NO_x conditions [22], which could help to explain these differences.

The SoCAB $F_{SOA,fossil}$ values can be compared with estimates of the fossil fraction of "oxidized organic carbon" ($F_{OOC,fossil}$) from measurements made during CalNex in Pasadena [180]. It should be noted that while $F_{SOA,fossil}$ includes contributions from both oxygen and carbon mass the $F_{OOC,fossil}$ includes only the carbon mass. The fossil fraction of secondary organic carbon (SOC) can be calculated from the simulated SOA concentrations by accounting for the differences in the O:C atomic ratios of the different SOA types to facilitate more direct comparison between the simulations and observations. Specifically, the SOC mass concentration (C_{SOC}) is related to the SOA mass concentration (C_{SOA}) for a given SOA type through the relationship:

$$\overline{\quad\quad} \quad \overline{\quad\quad\quad\quad\quad\quad\quad} \quad \overline{\quad\quad\quad\quad} \tag{4}$$
$$\underline{\quad} \quad \underline{\quad}$$

where MW_C, MW_O, MW_H are the molecular weights of carbon, oxygen and hydrogen atoms, respectively. The O:C and H:C values of the different SOA types are not constant in the SOM due to the continuous evolution of the product distribution. However, for a given SOA type the simulated O:C and H:C values vary over a relatively narrow range [155] and thus an average value can be used. The resulting $F_{SOC,fossil}$ values are compared with the $F_{SOA,fossil}$ values in Table 4-3 and are found to be very similar. The $F_{OOC,fossil}$ values were determined from ^{14}C analysis of particles collected on filters to allow determination of the fossil fraction of the total carbonaceous material coupled with positive matrix factorization to allow separation of the contributions from the various fossil and non-fossil POA and SOA sources. The uncertainty in the fossil fraction of total OC was reported as 9%; the uncertainty in the $F_{OOC,fossil}$ will be larger. Zotter, El-Haddad [180] determined the nighttime $F_{OOC,fossil}$ was smaller than the peak daytime value and that the 24-h average best-estimate $F_{OOC,fossil}$ = 44%. This is somewhat larger than the average predicted $F_{SOC,fossil}$ (e.g. 31% for SOM-high). The difference between the observed $F_{OOC,fossil}$ and predicted $F_{SOC,fossil}$ could indicate a role for SOA formed from fossil-derived S/IVOC species in the atmosphere but which are not considered here.

Table 4-3: Comparison between calculated non-fossil fractions of secondary organic aerosol (SOA) and secondary organic carbon (SOC).

Vapor Wall Loss Case	NO$_x$ condition	Central LA		Riverside	
		SOA	SOC	SOA	SOC
SOM-no	high-NO$_x$	0.27	0.24	0.28	0.25
	low-NO$_x$	0.44	0.41	0.40	0.37
SOM-low	high-NO$_x$	0.22	0.23	0.27	0.28
	low-NO$_x$	0.32	0.30	0.35	0.33
SOM-high	high-NO$_x$	0.22	0.25	0.28	0.31
	low-NO$_x$	0.33	0.32	0.37	0.36
		Atlanta		Smokey Mountains	
		SOA	SOC	SOA	SOC
SOM-no	high-NO$_x$	0.10	0.08	0.14	0.12
	low-NO$_x$	0.17	0.15	0.15	0.13
SOM-low	high-NO$_x$	0.19	0.18	0.27	0.27
	low-NO$_x$	0.18	0.17	0.22	0.20
SOM-high	high-NO$_x$	0.25	0.27	0.32	0.35
	low-NO$_x$	0.20	0.19	0.24	0.23

Oxygen to Carbon Ratio

The O:C atomic ratios of the SOA have been calculated from the simulated distributions of compounds in N_C and N_O space; the O:C atomic ratio is an inherent property of the SOM model and (O:C)$_{SOA}$ values from box model simulations using SOM exhibit generally good agreement with observations [13, 155]. Few air quality models attempt to simulate O:C ratios for SOA [e.g. 181], although a dramatic expansion in observations of O:C ratios for ambient OA has recently occurred [161, 182, 183]. Comparison between intensive properties such as O:C, in addition to absolute OA concentrations, can provide further constraints on the transformation processes and OA sources in a given region. The simulated (O:C)$_{SOA}$ in the SOM-no simulations are generally larger in SoCAB than in the eastern US (Figure 14-12). The simulated (O:C)$_{SOA}$ from isoprene and aromatics individually are larger than those from mono- or sesquiterpenes due, in large part, to the smaller carbon backbone and the need to add more oxygens to produce sufficiently low volatility species that partition substantially to the particle phase [13, 26, 61]. Thus, the larger (O:C)$_{SOA}$ in SoCAB results from larger relative contributions from isoprene and aromatic compounds to the total SOA burden in this region. The (O:C)$_{SOA}$ is also generally larger in regions where SOA concentrations are smaller. This may reflect some relationship between SOA source and concentration, but it also reflects the role that continued multi-generational oxidation

has on the SOA composition, since lower concentrations can reflect greater dilution and overall more aged SOA.
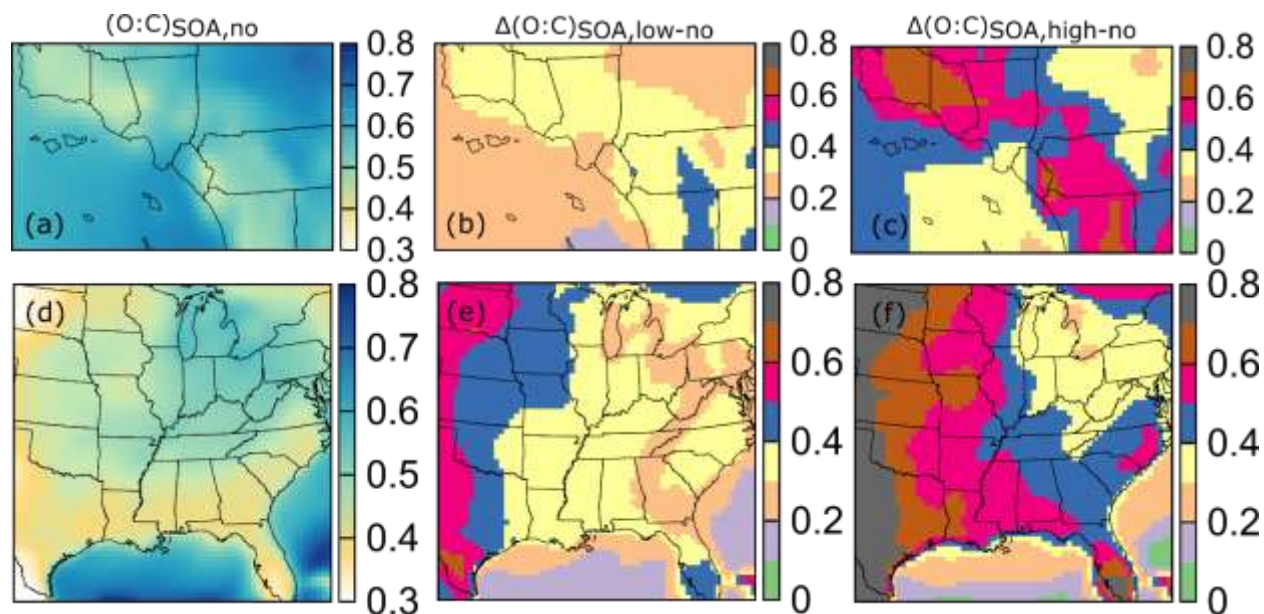
Figure 4-12: 14-day averaged O:C atomic ratios for SOA for (a) SoCAB and (d) the eastern US for the SOM-no simulations. The difference in O:C between the SOM-low or SOM-high and SOM-no simulations, termed Δ(O:C), is shown in panels (b-c) for SoCAB and (e-f) for the eastern US.

The $(O:C)_{SOA}$ for the SOM-low and SOM-high simulations are substantially larger than that from the SOM-no simulations in both SoCAB and the eastern US (Figure 14-12). This reflects two phenomena: (i) the increased relative contribution of isoprene to the total simulated SOA burden in the SOM-low and SOM-high simulations and (ii) differences in the SOM chemical pathways (i.e. the SOM parameters) that lead to the production of condensed-phase material between the parameterizations that do/do not include vapor wall losses. The influence of the latter has been confirmed through box model simulations, although the exact behavior is both precursor specific and somewhat dependent on the reaction conditions (e.g. [OH] and the initial precursor concentration). Overall, the former effect likely dominates since the difference in simulated $(O:C)_{SOA}$ between isoprene and monoterpenes is substantial [154].

The simulated O:C for the total OA also differs substantially between simulations (Figure 4-13), especially in regions where the simulated increase in f_{SOA} is largest (Figure 4-4). The simulated $(O:C)_{total}$ in both the SoCAB and eastern US increases substantially when vapor wall losses are accounted for. For example, the simulated $(O:C)_{total}$ values at Riverside were 0.22, 0.3 and 0.42 and at Atlanta were 0.45, 0.65 and 0.85 for SOM-no, SOM-low and SOM-high simulations, respectively. The increase in $(O:C)_{total}$ is mostly driven by an associated increase in f_{SOA}. The $(O:C)_{total}$ value is a weighted average of the $(O:C)_{SOA}$ and $(O:C)_{POA}$, with $(O:C)_{total} = (n_{O,SOA} + n_{O,POA})/(n_{C,SOA} + n_{C,POA})$ where n_O and n_C indicate the number of oxygen and carbon atoms, respectively, that comprise all SOA types and POA. For conceptual purposes, this exact expression for $(O:C)_{total}$ can be approximated as $(O:C)_{total} \sim f_{SOA}(O:C)_{SOA} + (1-f_{SOA})(O:C)_{POA}$, where $(O:C)_{SOA}$ represents the average over the different SOA types. Thus, changes in f_{SOA} lead

to changes in $(O:C)_{total}$, with some additional smaller changes due to variation in the weighted average $(O:C)_{SOA}$ between the various simulations (since each SOA type has a particular O:C range). The predicted eastern US $(O:C)_{total}$ are generally larger than in SoCAB due to the larger f_{SOA} in the eastern US and since $(O:C)_{SOA}$ is typically larger than $(O:C)_{POA}$. For example, the average $(O:C)_{total}$ in Atlanta for the SOM-no simulations was 0.4 whereas it was 0.22 in Riverside.
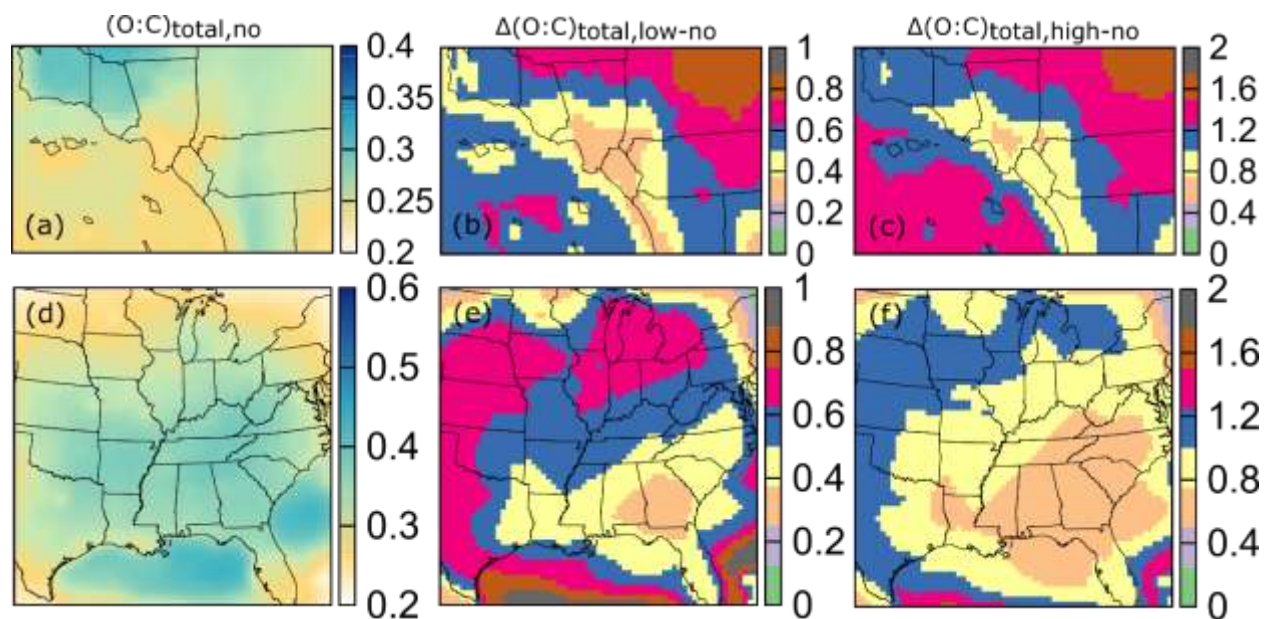
Figure 4-13: 14-day averaged O:C atomic ratios for total OA (POA + SOA) for (a) SoCAB and (d) the eastern US for the SOM-no simulations. The normalized difference in O:C, Δ(O:C), between the SOM-low or SOM-high and SOM-no simulations, where Δ(O:C) is defined as $((O:C)_{SOM\text{-}low/high}-(O:C)_{SOM\text{-}no})/(O:C)_{SOM\text{-}no})$, is shown in panels (b-c) for SoCAB and (e-f) for the eastern US. In all cases, the O:C for POA was assumed to be 0.2.

The simulated results at Riverside can be compared with bulk, campaign average $(O:C)_{total}$ values measured during the SOAR campaign using an Aerodyne high resolution time-of-flight aerosol mass spectrometer (HR-AMS), which determines $(O:C)_{total}$ with an absolute uncertainty of ±30% but with very high precision [144, 172]. Values reported here have been corrected according to Canagaratna, Jimenez [182]. The campaign-average observed $(O:C)_{total}$ was ~ 0.45. The SOM-high $(O:C)_{total}$ is in very good agreement with the observations, whereas $(O:C)_{total}$ is too small for both SOM-no and SOM-low. This good correspondence is, of course, sensitive to the assumed $(O:C)_{POA}$, here 0.2 based on [161]. If a smaller $(O:C)_{POA}$ had been assumed, then either a greater amount of SOA would be required or the simulated $(O:C)_{SOA}$ would need to be larger to match the SOAR measurements. Docherty, Aiken [165] determined there were three POA types during SOAR, with a weighted-average corrected O:C = 0.095, suggesting that the assumed 0.2 is too large. In contrast, Hayes, Ortega [166] determined a weighted-average corrected O:C = 0.25 for the three POA types identified at Pasadena during CalNex. It has been suggested that at least some of the difference in the $(O:C)_{POA}$ between SOAR and CalNex results from greater heterogeneous ageing of the Pasadena POA. Regardless of the exact $(O:C)_{POA}$, a strong improvement in the model-measurement agreement when vapor wall losses are accounted for is evident. Of additional consideration is the diurnal dependence of the $(O:C)_{total}$. The

observed (O:C)$_{total}$ exhibited a distinct diurnal dependence, with low values at night, a minimum at ~7 am and maximum values around midday (Figure 4-14). The simulated (O:C)$_{total}$ diurnal profile for the SOM-high simulations agrees reasonably well with the SOAR observations in terms of both the magnitude of the day-night difference and the absolute (O:C)$_{total}$ (Figure 4-14). In contrast, both the SOM-no and SOM-low exhibit only minor variations with time-of-day due to the controlling influence of (O:C)$_{POA}$.
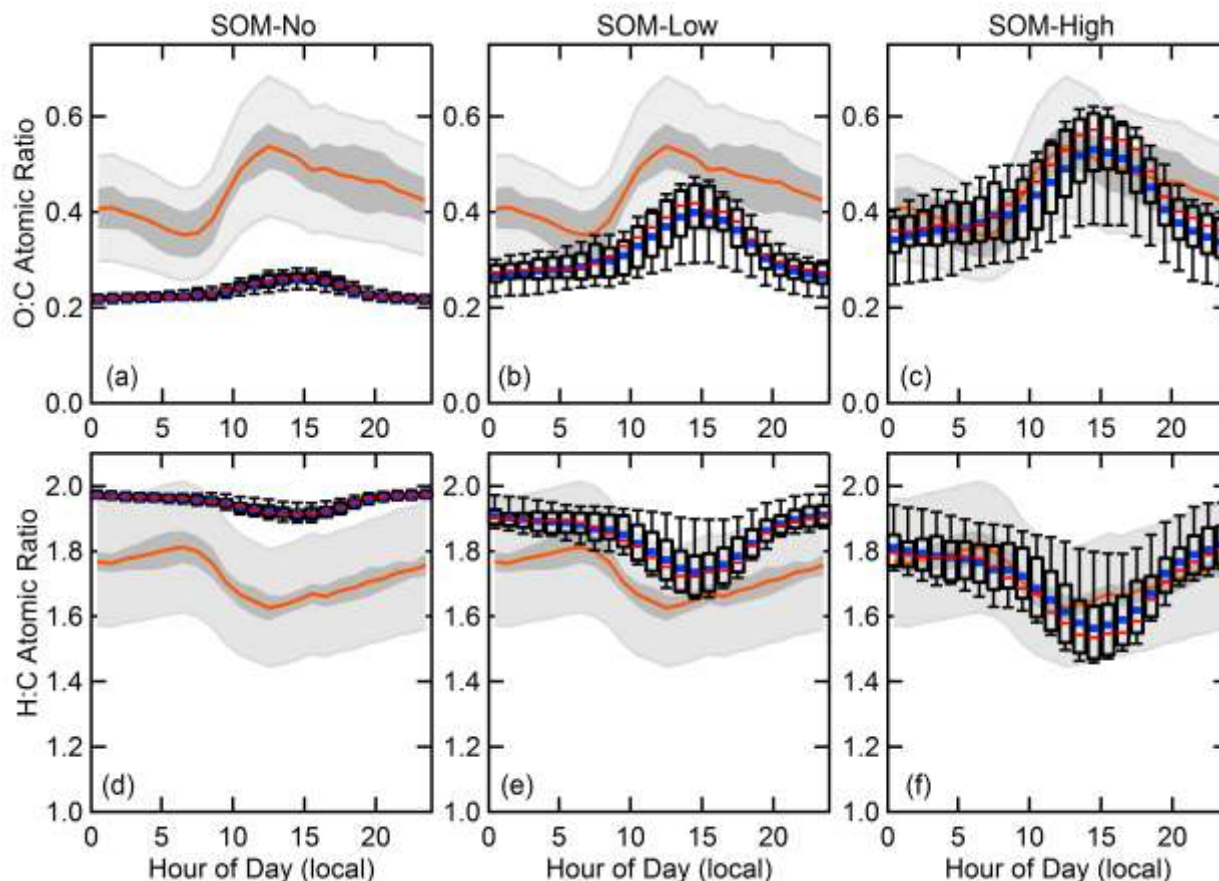
Figure 4-14: Simulated and observed diurnal profiles for the total OA O:C (panels a, b, c) and H:C (panels d, e, f) atomic ratios at Riverside, CA during the SOAR-2005 campaign for (a, d) SOM-no, (b, e) SOM-low and (c, f) SOM-high simulations. For the observations, the mean (orange line) and the 1σ variability range (dark grey band) are shown along with bands indicating the measurement uncertainty (light grey band), taken as ± 28% for O:C and 13% for H:C [182]. Observed values have been corrected according to Canagaratna, Jimenez [182]. For the simulations, box and whisker plots are shown with the median (red –), lower and upper quartile (boxes), and 9th and 91st percentile (whiskers). For reference, the assumed O:C for POA was 0.2 and for H:C was 2.0.

The simulated (O:C)$_{total}$ values in the eastern US can also be compared with recent observations, with the caveat that in this case the measurements were not made over the same time-period as the simulations were run. Nonetheless, measurements made in summer and winter of 2012 and 2013 at various locations in Alabama and Georgia indicate the O:C values for total OA were relatively constant, around 0.6-0.7, although it should be noted that these values were estimated

from measurements made using an Aerodyne aerosol chemical speciation monitor, which increases the uncertainty [167]. Measurements made around the southeast US using an HR-AMS onboard the NASA DC8 as part of the SEAC4RS field study indicate the average $(O:C)_{total} = 0.8$ when the plane was flying below 1 km [184]. As noted above, the simulated $(O:C)_{total}$ around Atlanta was 0.45 for SOM-no, increasing to ~0.65 for SOM-low and ~0.85 for SOM-high. As with the SoCAB comparison, the general level of agreement between the observed and simulated $(O:C)_{tot}$ was improved when vapor wall losses were accounted for.

The above simulations included SOA only from VOCs, neglecting contributions from S/IVOCs including oxidation of semi-volatile POA vapors. S/IVOCs and semi-volatile POA vapors are likely $\geq C_{14}$ carbon species [174, 185]. As such, little added oxygen is required to produce low-volatility species that will form SOA. Since these species also have relatively large number of carbon atoms, the O:C of the SOA formed from them will be relatively small, most likely with $(O:C)_{S/IVOC} < 0.2$ in the absence of strong heterogeneous oxidation [13, 61]; note that this range is lower than what was assumed for the non-volatile POA here. Consequently, had S/IVOCs been included in the simulations the $(O:C)_{total}$ would have likely decreased. The magnitude of the decrease would depend on the exact extent to which the S/IVOCs contributed to the overall SOA burden, the extent to which the simulated POA decreased (due to the semi-volatile treatment), and on the simulated $(O:C)_{S/IVOC}$. In the limit that SOA from S/IVOCs dominates the SOA budget, very little variation in the $(O:C)_{total}$ ratio with time of day would have likely been predicted because $(O:C)_{POA} \sim (O:C)_{S/IVOC}$. Additionally, the simulated daytime $(O:C)_{total}$ values would have likely been close to 0.2. A lack of diurnal variability and a small $(O:C)_{total}$ would both be inconsistent with the SOAR observations. Consequently, this implies that accounting for vapor wall losses has a stronger potential to allow for simultaneous reconciliation of the diurnal behavior of both the simulated OA/ΔCO and $(O:C)_{total}$ with observations than does consideration of oxidation of S/IVOCs alone. This is not to say that S/IVOC contributions to the SOA and total OA burden are not important, only that it seems unlikely that they could dominate the SOA budget. Ultimately, it seems likely that consideration of both vapor wall losses (as done here) and of SOA from S/IVOCs will be necessary to fully close the model/measurement gap.

4.4 Conclusions

The influence of chamber vapor wall losses on simulated SOA concentrations and properties has been assessed. The statistical oxidation model was used to parameterize SOA formation from laboratory chamber experiments both with and without accounting for vapor wall losses using data from experiments conducted under both high-NO_x and low-NO_x conditions. "Low" and a "high" vapor wall loss cases were considered in addition to the "no" vapor wall loss case. The best-fit SOM parameters under these different conditions were used as input to SOA simulations in the 3D UCD/CIT regional air quality model, in which SOM has been recently implemented [154]. Simulations were run for southern California and for the eastern US. Explicit accounting for vapor wall losses led to increases in simulated SOA concentrations, by a factor of ~2-5 for the "low" simulations and ~5-10 for the "high" simulations. The magnitude of the increase was inversely related to the simulated absolute SOA concentration. This suggests that the extent to which SOA concentrations are underpredicted may be greater in more remote regions.
This increase in simulated SOA when vapor wall losses are accounted for leads to a substantial increase in the simulated SOA fraction of total OA. This is especially seen in SoCAB where f_{SOA}

is very small for the base model but >50% for the simulations that account for vapor wall losses. The simulated f_{SOA} in SoCAB is found to agree reasonably well with observations when vapor wall losses are accounted for. Comparison of the OA/ΔCO from the SoCAB simulations with observations form the SOAR campaign [172] indicate that accounting for vapor wall losses leads to substantially improved agreement in terms of the diurnal behavior, in particular the magnitude of the daytime increase in OA/ΔCO. Accounting for vapor wall losses also leads to location-specific changes in the major contributing VOC precursors to the SOA burden. In general, accounting for vapor wall losses leads to an increase in the predicted relative contribution of isoprene SOA and a decrease in the relative contribution of monoterpene and sesquiterpene SOA. The relative contribution of total anthropogenic VOCs to SOA is reasonably insensitive to vapor wall losses, especially in SoCAB, although the apportionment between aromatic VOCs and alkanes does vary with vapor wall losses. The simulated anthropogenic SOA fraction is, however, somewhat smaller than suggested by ^{14}C observations during CalNex [180]. In general, the simulated O:C atomic ratio of the SOA increased for the low and high vapor wall loss simulations, compared to the base case. The simulated O:C of the total OA (SOA + POA) in both SoCAB and the eastern US are in better agreement with observations when vapor wall losses are accounted for.

Overall, the generally improved model performance when vapor wall losses are accounted for—in terms of both absolute and relative concentrations and in terms of SOA properties—suggests that accounting for this chamber effect in atmospheric simulations of SOA is important, although certainly requiring further examination. Our results qualitatively agree with other recent efforts to assess the influence of vapor wall losses on ambient SOA concentrations [152, 153], but as our accounting for vapor wall loss is inherent in the SOA parameterization the simulations here serve to provide a more robust assessment. The results presented here additionally suggest that there may be no need to invoke *ad hoc* "ageing" schemes for aromatics [141] to achieve increases in simulated SOA concentrations in urban environments. Further, these results suggest that that the contribution of S/IVOCs to urban SOA might be somewhat limited, albeit still important, although this issue certainly requires further investigation.

5 REACTIVITY ASSESSMENT OF VOLATILE ORGANIC COMPOUNDS USING MODERN CONDITIONS

5.1 Introduction

The incremental reactivity (IR) of a chemical compound (sometimes called ozone formation potential) generally refers to the amount of additional ozone that is produced for each unit of the compound that is introduced into a representative atmospheric system. IR depends both on the inherent properties of the compound being studied and on the conditions under which that compound will react. Several variations of IR have been defined by modifying the NOx concentrations of the representative atmosphere. These variations include the Maximum Incremental Reactivity (MIR) scale for high NOx conditions, the Maximum Ozone Incremental Reactivity (MOIR) corresponding to the NOx concentrations that produce the highest total ozone concentrations, and the Equal Benefits Incremental Reactivity (EBIR) for low NOx conditions. The MIR is the most commonly used version of the incremental reactivity but the MOIR likely corresponds better with current ambient conditions in major California cities.

California tabulates MIR values for more than 1000 chemical compounds to guide emissions reduction programs that seek to reduce ambient ozone concentrations. MIRs are calculated using the SAPRC chemical mechanism [186] in a series of box model calculations representing 39 cities across the United States. The box model format was chosen for computational efficiency since numerous calculations are required to assess all the compounds of interest in each of the representative cities. The input data required for box model calculations in each city include meteorological parameters, emission rates, and initial / boundary concentrations. The box model then predicts the ozone formation after 10 hrs of chemical reaction time under nominal conditions and with the addition of a small amount of the target compound.

The original MIR values were calculated with the SAPRC90 chemical mechanism. These MIRs have been recalculated periodically after updates to the SAPRC99 and SAPRC2007 chemical mechanisms. All of these calculations used input data representing meteorology, emissions, and initial / boundary conditions from the original conditions representing the year 1988. Air quality has changed significantly in the United States in the decades since that date. Emissions of criteria air pollutants and their precursors have been greatly reduced following the implementation of regulations and new control technologies [29, 187] . Since the 1980's there has been an average of 68% reduction in the ambient concentrations of the six criteria air pollutants. SIPs, which include regulations and other materials used to meet clean air standards and associated Clean Air Act requirements [188], have aided in the observed reduction of anthropogenic emissions. These changes directly influence the emissions and initial / boundary conditions needed for MIR calculations. They also potentially influence the season during which ozone episodes occur, which influences the meteorological parameters used in the calculations.

The purpose of this study is to update the IR values for all the compounds tracked by the state of California using contemporary meteorological parameters, emission rates, and initial / boundary conditions representing the year 2010. In addition, a modernized VOC composition, or "surrogate" background profile, will be developed for multiple cities across the US. Basecase IR values and MIR values will be recalculated for each compound and compared to previous values

calculated using 1988 conditions. Overall trends will be discussed along with implications for the best interpretation of the revised values.

5.2   Methods

The incremental reactivity (IR) of a volatile organic compound (VOC) is defined as the change in ozone concentration that results from adding a small amount of the VOC to a representative atmospheric system divided by the amount of VOC added (equation 2) [186]:

$$\overline{\qquad} \tag{E2}$$

where IR_i is the incremental reactivity of a VOC_i,   is the change in ozone and   is the amount of VOC_i added to the system.   The base case scenario at each location calculates a specific VOC or mixture's reactivity which yields information on how potent a specific VOC is in producing ozone for "regular atmospheric conditions". The MIR scenario looks at the IR sensitivity to NOx by adjusting the initial NOx concentrations and emissions in order to yield the highest IR of the base reactive organic gas (ROG) mixture [186] which usually occurs at high NOx values. Both base case IR and MIR values will be reported in the current study.

5.2.1   City Locations

Thirty-nine cities across the continental United States were selected in order to update the scenarios that drive the reactivity calculation using the SAPRC box model. Figure 5-1 illustrates the location of each study city. Two California cities, Bakersfield and Fresno, were added to the 2010 analysis while Tampa, FL and Chicago, IL were omitted. Bakersfield and Fresno were added due to their impact on California air quality and high number of ozone non-attainment days. Tampa and Chicago were removed as they did not have high ozone events on days that corresponded with other surrounding cities in 2010.

Daily 1-hour maximium ozone measurements for the year of 2010 were obtained from the EPA AQS datamart daily summaries. Multiple monitors in each city were averaged to calculate the daily maximum ozone concentration. .   The data were inspected to identify periods with high ozone events in each target city. An ozone event was considered for each city when ozone levels reached the non-attainment value of 70 ppb. Some cities were selected in a cluster of city ozone events due to their proximity to one another. A cluster of cities were used in order to ensure the ozone event was due to atmospheric subsidence or a high pressure system resulting in a layer of warm air trapping pollutants at the surface. In certain cases, some cities that were included in a cluster did not reach a maximum ozone concentration of 70 ppb but did reach up to 60ppb. Table 5-1 shows the date of investigation for each city in 2010, the date that was investigated in the calendar year 1988, and the population in 2010 and 1988.
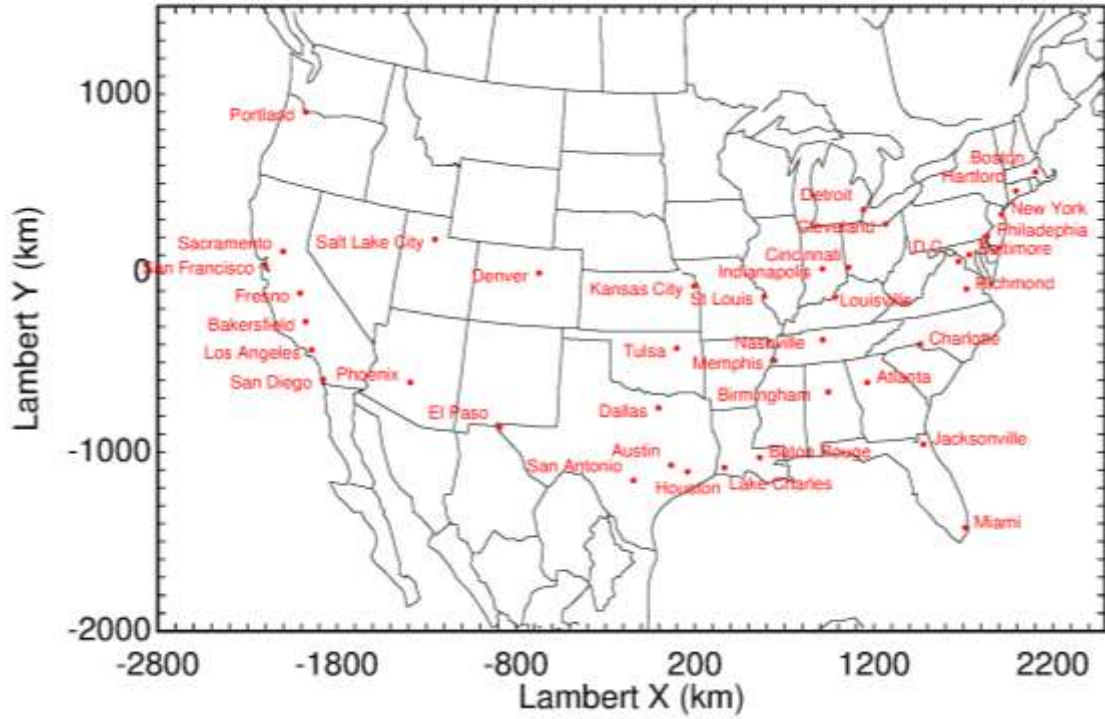
Figure 5-1: Map of 39 cities used for IR calculations throughout the continental United States.

Table 5-1: List of 39 Cities under investigation and the associated ozone event date in 2010 and 1988

	City	2010 Date	1988 Date	2010 Population	1988 Population
1	Atlanta	2-Apr	6-Jun	422765	394175
2	Austin	28-Aug	9-Sep	815260	497154
3	Bakersfield	25-Aug	N/A	348938	185405
4	Baltimore	10-Aug	7-Jul	621210	735632
5	Baton Rouge	10-Oct	26-Apr	229584	222684
6	Birmingham	8-Oct	31-Jul	212107	265515
7	Boston	2-Sep	16-Jun	620451	572479
8	Charlotte	2-Apr	8-Jun	738710	430023
9	Cincinnati	10-Aug	18-Aug	296904	364649
10	Cleveland	29-Aug	5-Jul	396009	505672
11	Dallas	27-Aug	9-Sep	1201000	1011000
12	Denver	16-Jul	26-Jul	603421	468139
13	Detroit	29-Aug	2-Aug	711299	1029000
14	El Paso	13-Jul	7-Sep	651665	519480
15	Fresno	25-Aug	N/A	497090	357662
16	Hartford	2-Sep	8-Jul	125312	137296
17	Houston	10-Oct	26-Aug	2103000	1707000
18	Indianapolis	28-Aug	28-Jul	830952	731,278
19	Jacksonville	1-Apr	7-May	823291	635,230
20	Kansas City	28-Aug	7-Aug	460639	435187
21	Lake Charles	9-Oct	26-Jul	72268	71543
22	Los Angeles	26-Sep	3-Sep	3796000	3490000
23	Louisville	10-Aug	13-Jun	300000	269592
24	Memphis	9-Oct	24-Jun	647609	619396
25	Miami	1-Apr	22-Apr	400769	316746
26	Nashville	8-Oct	22-Jun	1800000	1048154
27	New York City	1-Sep	22-Jun	8190000	7322000
28	Philadelphia	10-Aug	29-Jul	1529000	1581000
29	Phoenix	23-Jun	9-Sep	1449000	992511
30	Portland	25-Aug	29-Jun	585286	487849
31	Richmond	31-Aug	10-Jul	204351	203463
32	Sacramento	25-Aug	23-Jul	1422000	398256
33	Salt Lake City	21-Aug	22-Jul	186505	160076
34	San Antonio	28-Aug	26-Sep	1334000	999290
35	San Diego	26-Sep	3-Oct	1306000	1118000
36	San Francisco	25-Aug	20-May	805704	723496
37	St. Louis	28-Aug	8-Jul	319257	395857
38	Tulsa	27-Aug	22-Jul	392443	368320

| 39 | Washington DC | 30-Aug | 30-Jul | 604453 | 605321 |

5.2.2 Meteorological Inputs

Meteorology parameters were updated using the Weather Research and Forecasting model (WRFv3.6) and WRF preprocessing system (WPSv3.6). Parameters were generated within 3 nested domains with horizontal resolutions of 36km, 12km, and 4km, respectively. Each domain had 31 telescoping vertical levels up to a top height of 12km. Four dimensional data assimilation (FDDA) or "FDDA nudging" was used in order to yield meteorology results that better correlated to the observed data [189]. The meteorological parameters of interest for the SAPRC reactivity model are temperature, planetary boundary layer height, and absolute humidity. Figures 5-2 through 5-4 illustrate the updated 10 hour values across the 39 cities used in the reactivity box model.
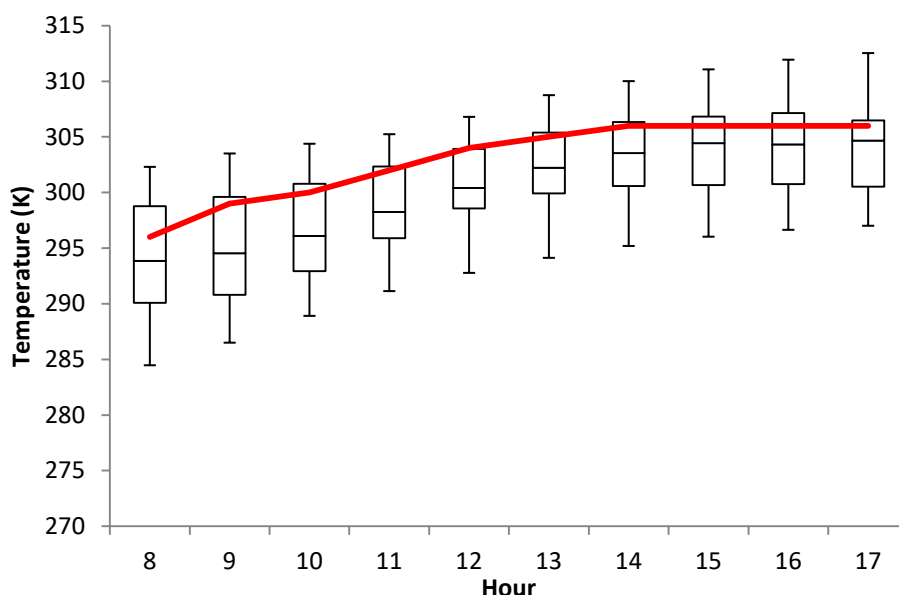
Figure 5-2: Temperature (K) in 39 cities across the United States over the 2D box model 10 hour time frame. The box and whisker plots represent 2010 and the red line represents the median temperature in 1988.

101
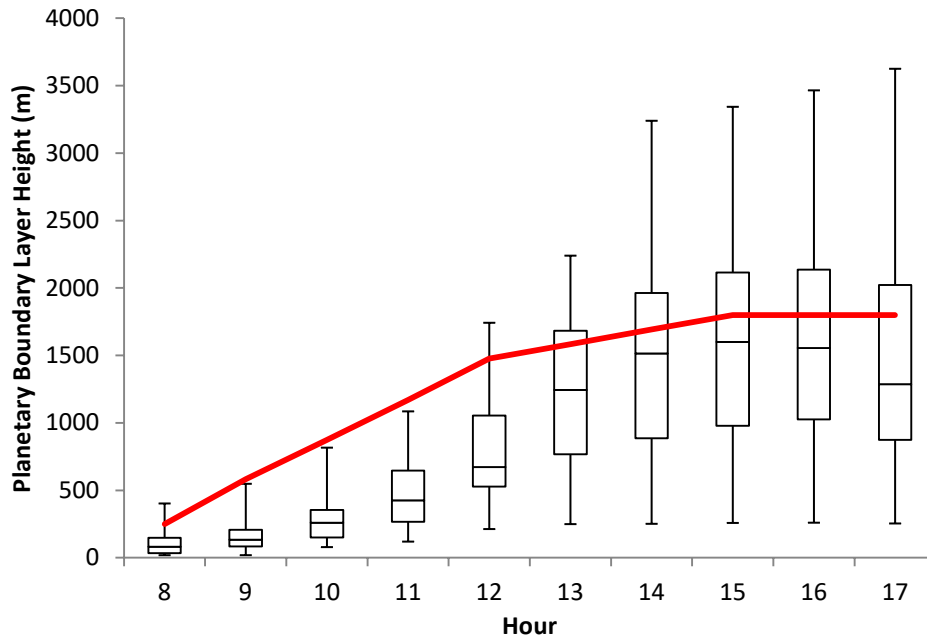
Figure 5-3: Boundary layer height (m) in 39 cities across the United States over the 2D box model 10 hour time frame. The box and whisker plots represent 2010 and the red line represents the median boundary layer height in 1988.
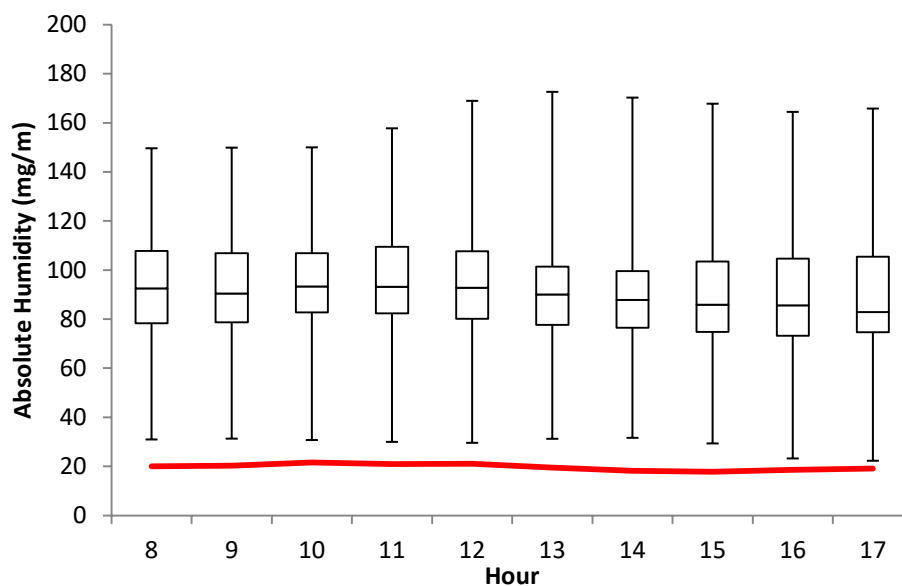
Figure 5-4: Absolute humidity (mg m^{-3}) in 39 cities across the United States over the 2D box model 10 hour time frame. The box and whisker plots represent 2010 and the red line represents the median absolute humidity in 1988.

Figures 5-2 through 5-4 show that the 2010 median temperature and boundary layer height were lower than corresponding values representing the 1988 simulations, while median absolute humidity in 2010 was higher than in 1988. Approximately 9 of the 39 cities considered in the analysis had ozone events in the spring and fall (April and October) in 2010 as opposed to the summer (June, July, August and September) in 1988, resulting in these changes. 1988 meteorology conditions for temperature and relative humidity were based on local measurements while the planetary boundary layer heights were developed base on upper air soundings recommended by the EPA EKMA guidance documents (Carter, 1994). The differences in temperature and relative humidity between 1988 and 2010 scenarios are primarily due to seasonal changes. The differences in boundary layer height, however, may be due to improvement in model technology.

5.2.3   Emissions Inputs

Anthropogenic emissions were updated for 2010 conditions using the Sparse Matrix Operator Kernel Emissions (SMOKEv3.7) modeling system while biogenic emission rates were updated using the Model of Emissions of Gases and Aerosols from Nature (MEGANv2.1). For the current study, the 2011 National Emission Inventory (NEI) data was used to represent all area, point, and mobile sources for each of the 39 cities. Meteorological data and a gridded map projection of the domains for each city were taken from the corresponding WRF simulations using the meteorology-chemistry interface processor (MCIP). Source apportionment profiles were designed by assigning a specific source classification code within each of SMOKE's four source sectors (area, mobile, non-road and point) to one of the following tracked groups: biomass, diesel, gasoline, food cooking, natural gas and all other emissions.

The gridded geo-referenced emission factors and land cover variables required for MEGAN calculations were created using the MEGANv2.1 pre-processr tool and and the ESRI_GRID leaf area index and plant functional type files available at the Community Data Portal[190]. 1988 scenario hourly emission data for anthropogenic emissions were obtained from the 1985 NAPAP emissions inventory (Carter, 1994) while 1988 biogenic emissions were determined based on best approximation (Carter, 1994).

Figures 5-5 through 5-8 represent the updated 10 hour emissions rates per capita across the 39 cities used in the reactivity box model. Per capita emissions rates were plotted to view the effects of emissions control programs in the presence of changing population between 1988 and 2010. Figure 5-5 shows that per capita non-methane organic hydrocarbon emissions have significantly decreased during the commute hours (hour 8-10) but have decreased only slightly during non-commute hours between 1988 and 2010. This trend can also be observed for the other species (NOx and CO) in figures 5-6 and 5-7. Figure 5-8 shows that the estimated median emissions rates of isoprene across the 39 target cities have increased during the warmer afternoon hours using the state of the science understanding in 2010 vs. 1988.
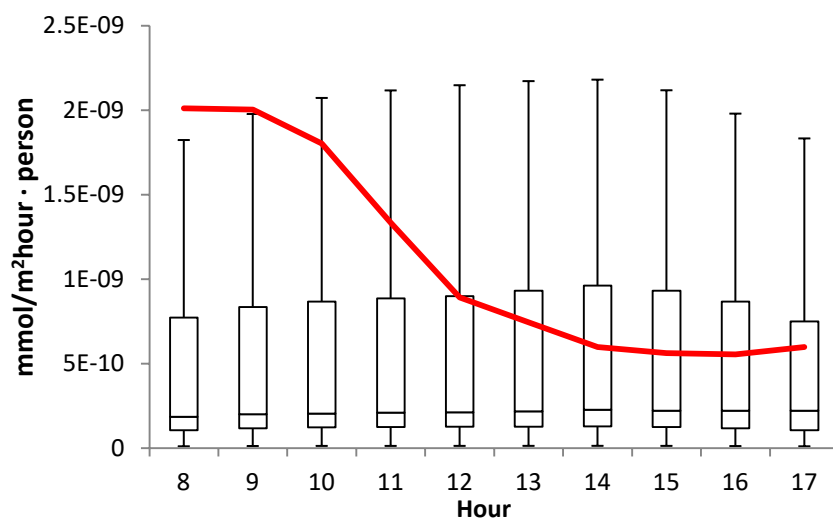
Figure 5-5: Non-methane organic carbon emission rates per capita (mmol/m2 hour·person) in 39 cities across the United States over the 2D box model 10 hour time frame. The box and whisker plots represent 2010 and the red line represents the median emission rate in 1988.
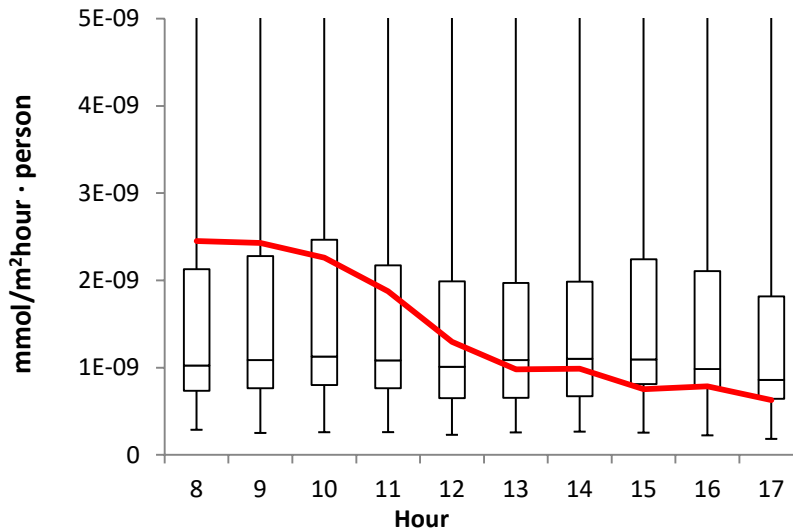
Figure 5-6: NOx emission rates per capita (mmol/m2 hour·person) for NOx in 39 cities across the United States over the 2D box model 10 hour time frame. The box and whisker plots represent 2010 and the red line represents the median emission rate in 1988.
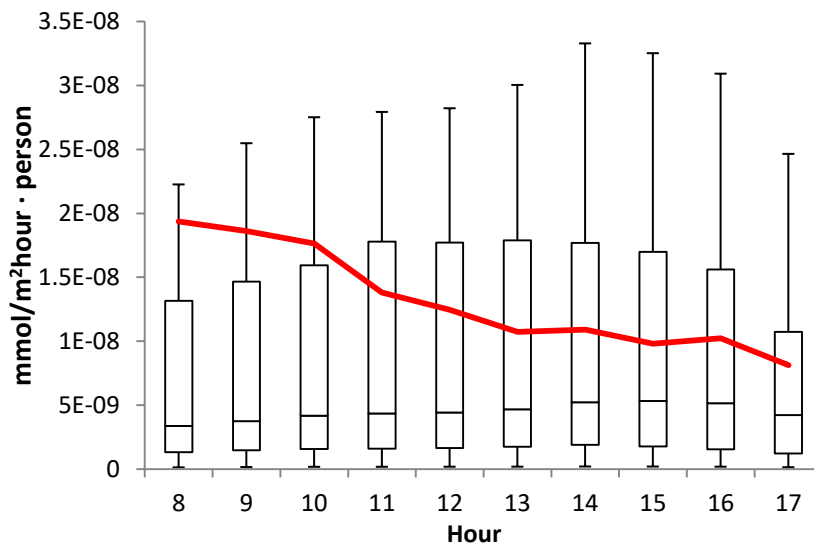
Figure 5-7: CO emission rates per capita (mmol/m2 hour·person) in 39 cities across the United States over the 2D box model 10 hour time frame. The box and whisker plots represent 2010 and the red line represents the median emission rate in 1988.
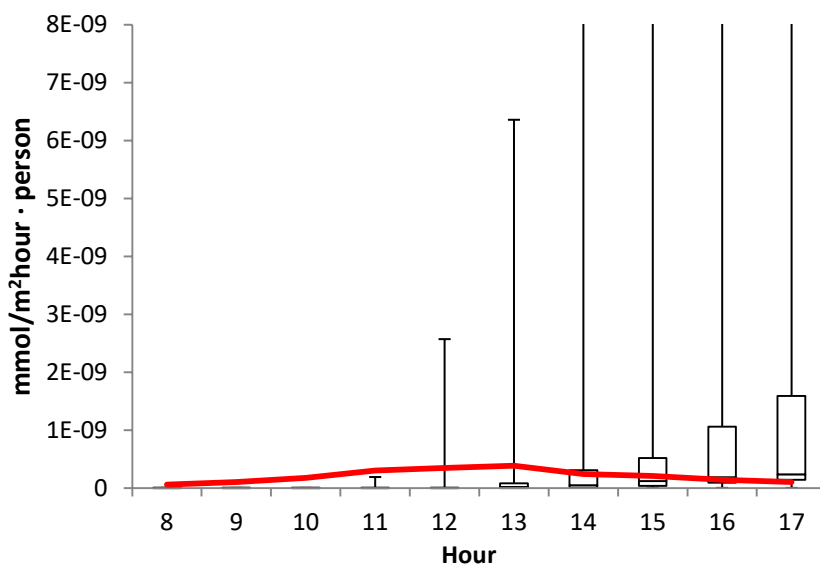
Figure 5-8: Isoprene emission rates per capita (mmol/m2 hour) in 39 cities across the United States over the 2D box model 10 hour time frame. The box and whisker plots represent 2010 and the red line represents the median emission rate in 1988.

5.2.4   VOC Composition

The aloft and ground (base) VOC composition profiles used in the SAPRC reactivity box model were determined by running UCD/CIT chemical transport model (CTM) simulations for the 39 cities of interest. Similar to CMAQ, the UCD/CIT reactive CTM predicts the evolution of gas and particle phase pollutants in the atmosphere in the presence of emissions, transport, deposition, chemical reaction and phase change [191] as represented by equation (1)

$$\overline{}$$

(E1)

where C_i is the concentration of gas or particle phase species i at a particular location as a function of time t, u is the wind vector, K is the turbulent eddy diffusivity, E_i is the emissions rate, S_i is the loss rate, R_i^{gas} is the change in concentration due to gas-phase reactions, R_i^{part} is the change in concentration due to particle-phase reactions and R_i^{phase} is the change in concentration due to phase change [191]. A total of 50 particle-phase chemical species are included in each of 15 discrete particle sizes that range from 0.01-10 μm particle diameter [191]. The model can be configured with the SAPRC90, SAPRC07, SAPRC11, or SAPRC16 chemical mechanisms. SAPRC11 was used for the calculations in the current study.

106

The UCD/CIT model combined the meteorology and emissions produced by WRF and SMOKE, respectively, in order to simulate a complete air quality episode that was then used to determine the "aloft" chemical composition above the boundary layer height and the "base" chemical composition below the boundary layer height for each of the cities. Figure 5-9 illustrates the averaged 1988 VOC aloft composition [186] and the averaged 2010 VOC aloft composition. The 2010 composition has a reduced proportion of alkanes (due to a reduction in anthropogenic emissions) and an increased proportion of ketones (due to relatively constant or increasing biogenic VOCs) relative to conditions in 1988. Ketones were not included in the original 1988 aloft chemical composition profile (Carter 1994). Ketones are a combination of the SAPRC11 species MEK, PROD2 and MVK which include ketones and other non-aldehyde oxygenated products which react with OH radicals faster than 5×10^{-13} but slower than 5×10^{-12} cm^3 $molec^{-2}$ sec^{-1} (MEK), ketones and other non-aldehyde oxygenated product which react with OH radicals faster than 5×10^{-12} cm^3 $molec^{-2}$ sec^{-1} (PROD2) and methyl vinyl ketones (MVK). The following profile is averaged over all 39 cities in order to compare to the average 1988 aloft and base composition profile. VOC fractions per city varied across the US depending on their location. Ketone fractions were lower in the western United States versus the east.

Figure 5-10 illustrates the averaged 1988 VOC base composition and the averaged 2010 VOC base composition profiles. The 2010 composition shows an increase in alkenes, which is primarily in response to the addition of biogenic VOCs, and a decrease in aromatics. Overall, the maximum incremental reactivity of the updated VOC profile decreased when used in the 1988 (see figure 5-24) scenario and will be discussed further in this chapter. Table 5-2 illustrates the averaged 2010 aloft and base composition profiles and standard deviation in order to report the variability amongst each city profile in the continental US.

Sullivan et al (2011) performed a study on updating the base VOC profile by using a combination of measurements from photochemical assessment monitoring stations (PAMS), 1997 Southern California Ozone Study (SCOS) and the 2005 national emissions inventory. This profile was developed solely for the Los Angeles region and therefor was not representative of the entire United States. The study also found that the new profile (PAMS/SCOS/Emis) exhibited an increase in biogenic hydrocarbons and a reduction of aromatics (Sullivan 2011).

1988 VOC % Aloft Composition

1.87
9.63
9.96
5.73
72.75

- Alkanes
- Alkenes
- Aromatics
- Acetylene
- Aldehydes

2010 VOC % Aloft Composition

29.66
39.92
18.94
9.47
1.67
0.29

- Alkanes
- Alkenes
- Aromatics
- Acetylene
- Aldehydes
- Ketones
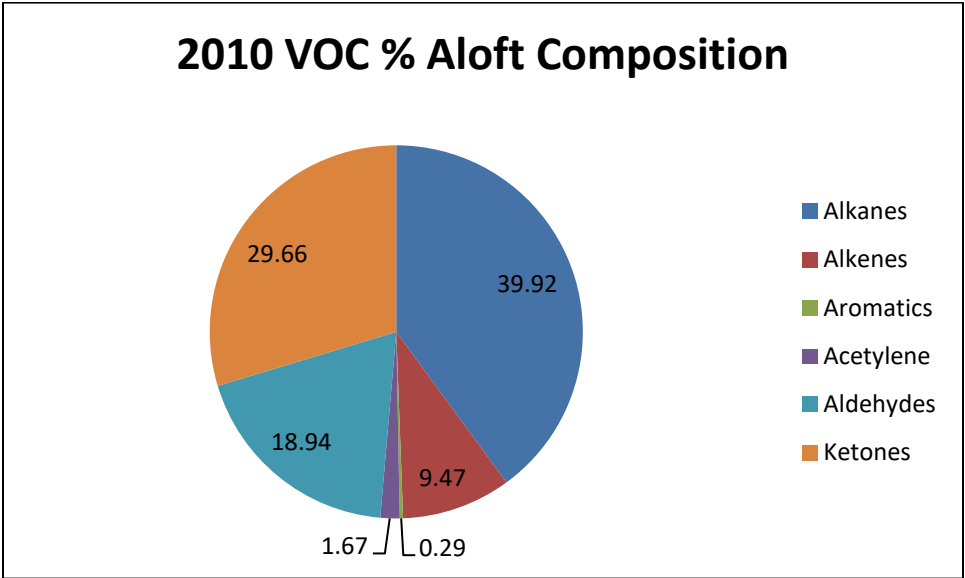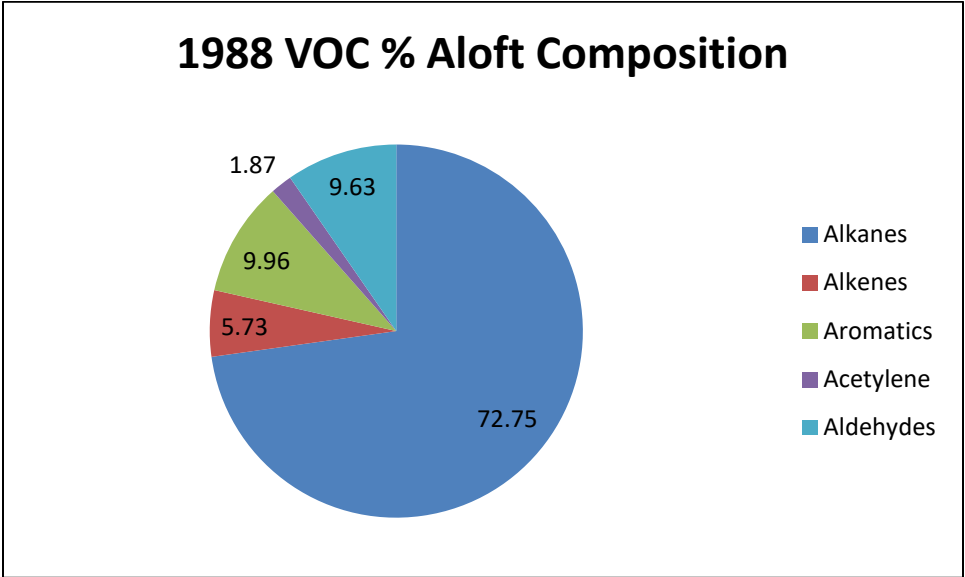
Figure 5-9: Aloft VOC Composition (by percentage) for averaged city scenarios in 1988 (top) and 2010 (bottom).
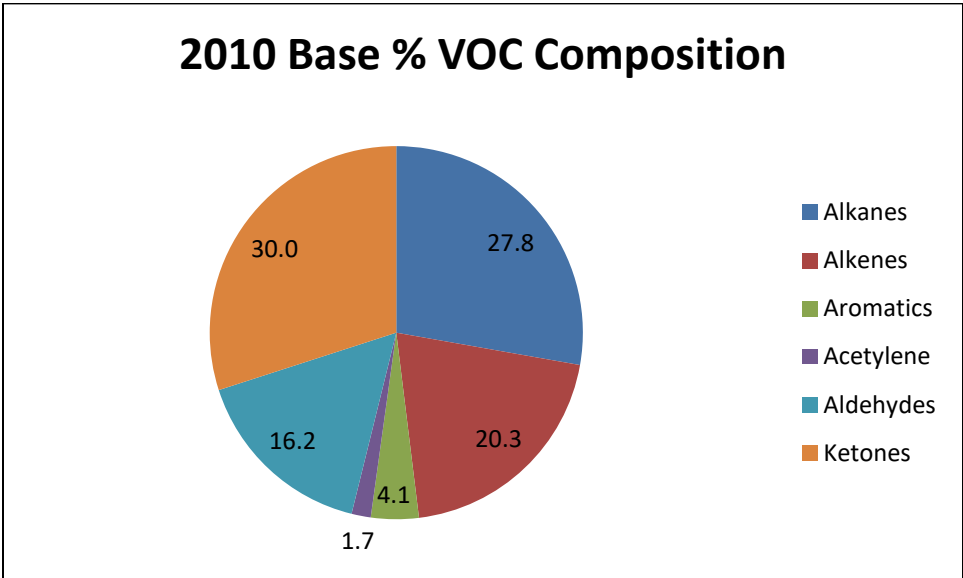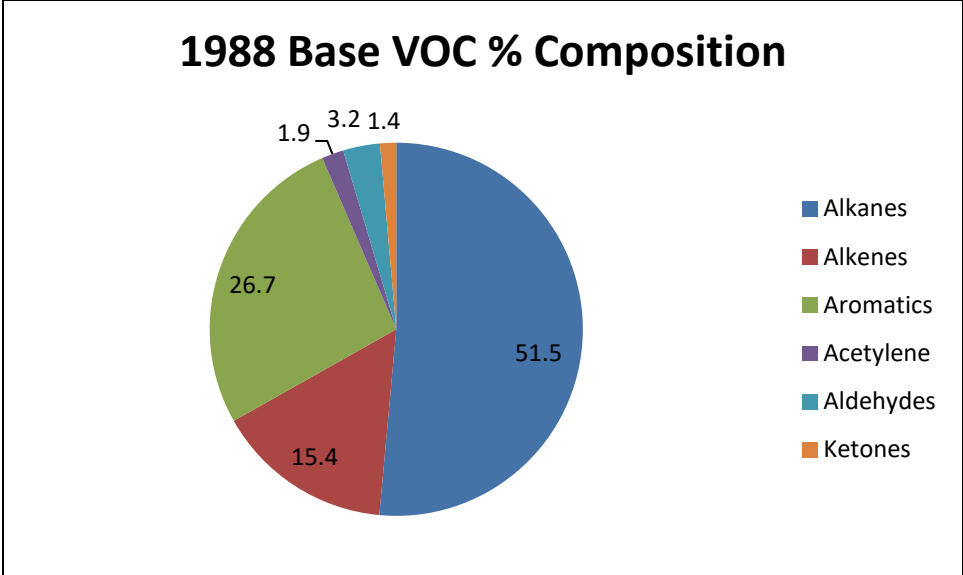
Figure 5-10: Base VOC Composition (by percentage) for averaged city scenarios in 1988 (top) and 2010 (bottom).

Table 5-2: 2010 Aloft and Base VOC composition profile and standard devation across all 39 cities in the continental US.

	Aloft VOC Profile		Base VOC Profile	
	Mean (% fraction)	Standard Deviation ± (% Fraction)	Mean (% Fraction)	Standard Deviation ± (% Fraction)
Alkanes	39.92	13.50	27.80	13.93
Alkenes	9.47	2.52	20.30	3.91
Aromatics	0.29	0.12	4.14	0.09
Acetylene	1.67	0.56	1.67	0.41
Aldehydes	18.94	6.56	16.18	3.67
Ketones	29.66	7.68	30.01	7.55

The modeling scenarios for the SAPRC box model were updated using the stated 2010 meteorology, emission rates and VOC composition profiles. The box model uses two vertical levels, one above the mixing depth and other below, and is limited to one photochemical cycle over 10 hours. Pollutants are either present initially, entrained from the "aloft" level or emitted throughout the day. Table 5-2 illustrates a summary of conditions in each city scenario used in the SAPRC box model compared to 1988 conditions. The first column states the city, followed by the maximum ozone concentration calculated by the box model, the ratio of the VOC/NOx input base flux in 2010 and 1988, the aloft ozone concentration in 2010 and 1988 and lastly the aloft VOC concentration in 2010. The aloft VOC concentration in 1988 was set at a constant 30ppb for each city scenario. The calculated maximum ground-level ozone, aloft ozone and aloft VOC concentration decreased across all of the 39 cities in comparison to the 1988 scenario whereas the input ratio of VOC/NOx varied per city.

Table 5-3: Summary of conditions of the 2010 scenario vs 1988 scenarios for the selected study dates.

City	2010 Max Ozone (ppb)	1988 Max Ozone (ppb)	2010 Base VOC/NOx ratio	1988 Base VOC/NOx ratio	2010 Aloft O3 (ppb)	1988 Aloft O3 (ppb)	2010 Aloft VOC (ppb)
Atlanta	65.9	158	16.35	7.25	55.5	63	8.52
Austin	72.1	155	4.73	9.3	55.7	85	9.41
Bakersfield	83.2	N/A	11.39	N/A	68.5	N/A	6.99
Baltimore	93.5	279	17.71	5.15	59.4	84	11.24
Baton Rouge	67.2	210	13.25	6.8	43.2	62	4.55
Birmingham	68.3	214	5.91	6.94	50.7	81	5.21
Boston	91.8	176	20.93	6.5	66.5	105	9.51
Charlotte	68.4	130	8.4	7.79	54.1	92	7.41

Cincinnati	78.82	177	14.59	6.37	48.5	70	6.173
Cleveland	75.8	214	20.04	6.62	44.1	89	5.94
Dallas	73.4	163	8.04	4.74	52.1	75	13.21
Denver	60.6	165	11.36	6.33	55.8	57	8.41
Detroit	73.9	210	7.31	6.82	58.5	68	6.83
El Paso	71.6	156	12.97	6.59	49.3	65	7.72
Fresno	96.2	N/A	10.62	N/A	61.9	N/A	7.87
Hartford	83.7	150	17.32	8.39	63.1	78	8.31
Houston	68.3	267	5.92	6.08	55.7	65	12.59
Indianapolis	60.3	179	4.86	6.64	49.2	52	5.64
Jacksonville	74.3	136	4.53	7.62	54.1	40	7.82
Kansas City	61.24	138	4.37	7.09	49.2	65	5.93
Lake Charles	67.6	251	11.1	7.42	60.3	40	9.31
Los Angeles	69.5	488	6.43	7.59	65.22	100	14.52
Louisville	74.6	185	7.09	5.53	54.7	75	4.16
Memphis	70.1	197	4.16	6.78	51	58	11.04
Miami	72.14	117	4.12	9.63	54.2	57	3.98
Nashville	71.97	146	4.22	8.05	49.2	50	6.28
New York City	75.4	306	16.95	8.09	62.1	103	13.31
Philadelphia	83.4	208	14.52	6.19	58.2	53	11.47
Phoenix	75.9	236	12.33	7.58	52.4	60	7.41
Portland	70.2	146	14.54	6.46	45.3	66	5.72
Richmond	72.1	205	11.75	6.18	55.6	64	9.88
Sacramento	83.7	178	13.4	6.59	51.3	60	6.312
Salt Lake City	88.7	164	13.08	8.47	63.4	85	7.41
San Antonio	70.1	118	8.04	3.92	58.3	60	10.23
San Diego	100.82	169	12.87	7.09	40.2	90	6.45
San Francisco	71.2	156	4.84	4.78	53.8	70	6.23
St. Louis	63.2	264	1.51	6.08	48.4	82	10.55
Tulsa	65.42	197	5.55	5.31	56.3	70	8.12
Washington DC	75.43	248	4.59	5.32	47.4	99	9.41

5.3 Results

5.3.1 Model Performance

Ozone concentrations predicted by the UCD/CIT CTM were compared to measured ozone values in each city in order to indirectly assess the accuracy of the calculated aloft VOC concentration. Figure 5-11 summarizes the comparison between simulated daily 1-hr maximum ozone values and measured daily 1-hr maximum ozone values in each city. Overall, the model slightly under predicted the ozone in comparison to the measurements with a mean fractional bias of -0.0393.
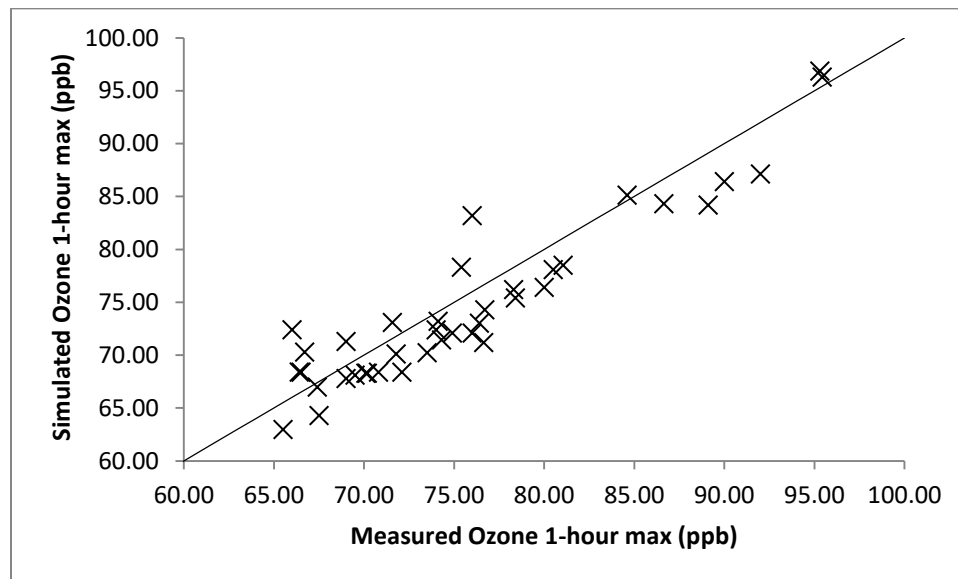
Figure 5-11: UCD/CIT predictions for 8-hour average ozone compared to measured 8-hour ozone in 39 cities during 2010.

Figure 5-12 compares the simulated daily 1 hr maximum ozone concentrations for the SAPRC box model and the measured daily 1 hour maximum concentrations. The SAPRC box model also underpredicts ozone in comparision to the measurements with a mean fractional bias of -0.059. Figure 5-13 compares the 2D box model daily maximum ozone values to the UCD/CIT simulated daily maximum ozone values. The results of these comparisons illustrate the uncertainty introduced by using box model calculations as opposed to full 3D reactive chemical transport model calculations for ozone formation. These differences result from the simplification inherent in the box model including averaging over the entire horizontal domain and using only 2 vertical levels to represent vertical gradients. As a general summary, both the full UCD/CIT model and the 2D box model slightly under predicted ozone but both calculations are in reasonable agreement with the measured values.

112
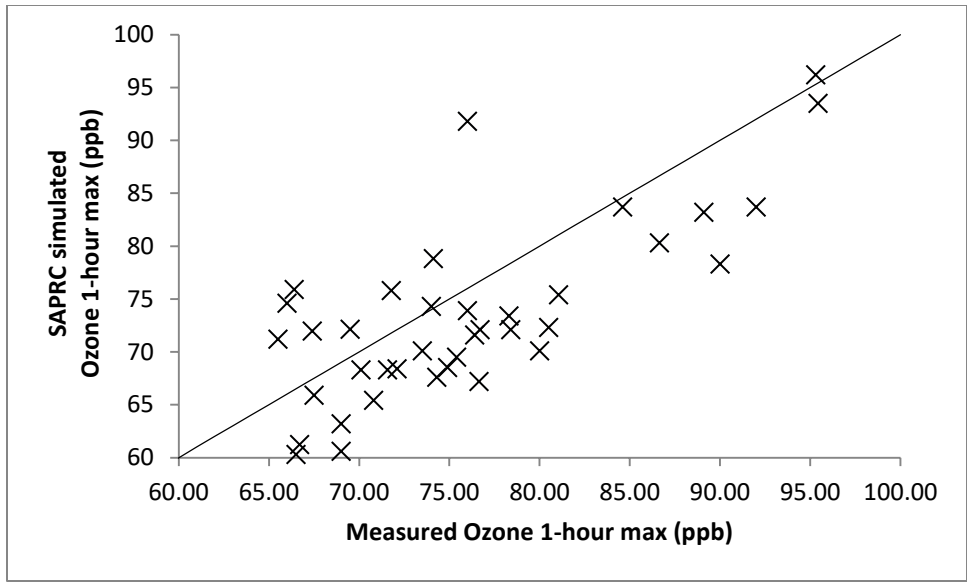
Figure 5-12: SAPRC box model predictions for daily maximum ozone vs. measurements for 39 cities in 2010.
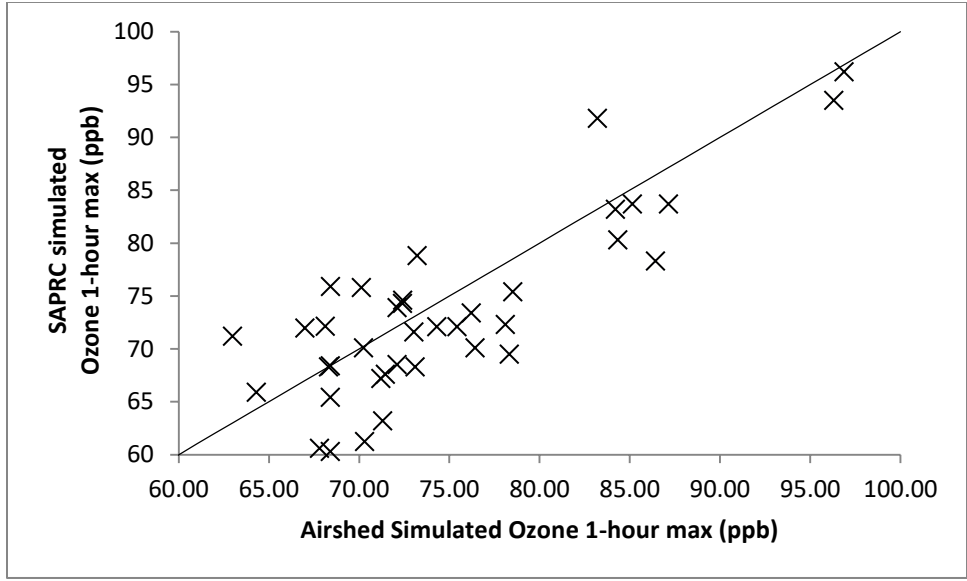
Figure 5-13: Comparison between UCD/CIT simulated daily maximum and 2D box model daily maximum ozone values.

5.3.2   Reactivity Values

The incremental reactivity for 1,192 VOCs were determined for the base case IR and MIR scenarios. Figure 5-14 shows that the 2010 VOC base case IR was slightly higher (17.3%) than the 1988 base case reactivity. VOCs tested across the 39 representative cities produced median values of 0 to 7 g of ozone per g of VOC under 2010 conditions but only -1 to 5 g of ozone per g of VOC under 1988 conditions.
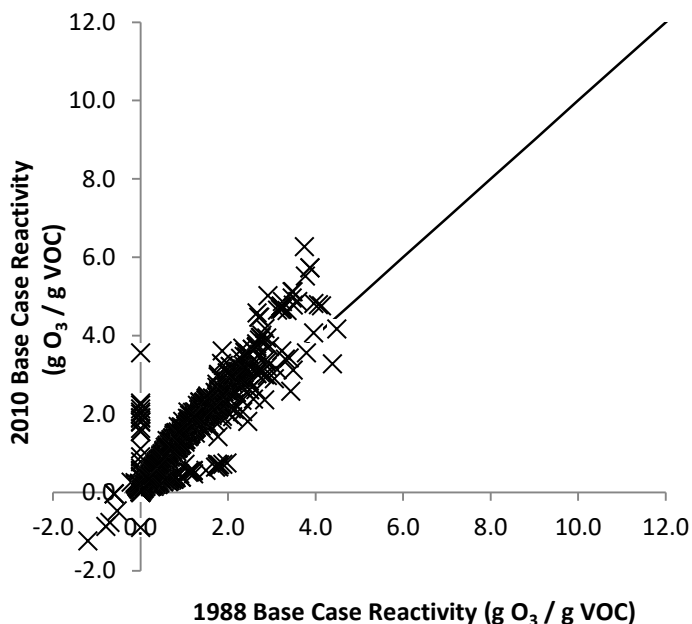
Figure 5-14: Correlation of 1988 base case median reactivity and 2010 base case median reactivity for 1,192 different VOCs.

The base case calculations for each compound produce different IR values for each city that was considered in the analysis. The variance of the IR results across all cities was generally related to the median base case IR in a non-linear manner. Figure 5-15 compares the median value and variance across the 39 cities of the VOC base case IR for the conditions in 2010. The IR variance across the cities gets larger for compounds with higher median IR. These findings suggest that results should be stratified regionally to determine if there are clear patterns that would suggest different behavior in different cities.

A sensitivity analysis was performed to see which variable impacted the change in IR from 1988 to 2010 scenarios. Figures 5-16 through 5-18 illustrate how the 1988 IR values change when each 2010 variable (meteorology, emissions and VOC composition) is utilized in place of the 1988 variable. The emissions variable sensitivtity test incorporated updates to the initial ground VOC and NOx concentrations as a fraction of those concentrations are emitted throughout the

day. The analysis reveals that the increased base case IR under 2010 conditions is driven mainly by changes in the meteorological conditions and VOC composition profiles. Figure 5-16 illustrates a 27.7% increase attributable to meteorology which accounts for the majority of the increase between 2010 IR and 1988 IR.

1988 meteorology conditions for temperature and relative humidity were based on local measurements while the planetary boundary layer heights were developed base on upper air soundings recommended by the EPA EKMA guidance documents (Carter, 1994). The differences in temperature and relative humidity between 1988 and 2010 scenarios are primarily due to seasonal changes. The differences in boundary layer height, however, may be due to improvement in model technology. The addition of biogenic VOCs increased the alkene fraction of the 2010 aloft and base VOC composition. The 1988 composition profiles may have only included the anthropogenic hydrocarbons, missing large fractions from biogenic VOCs.
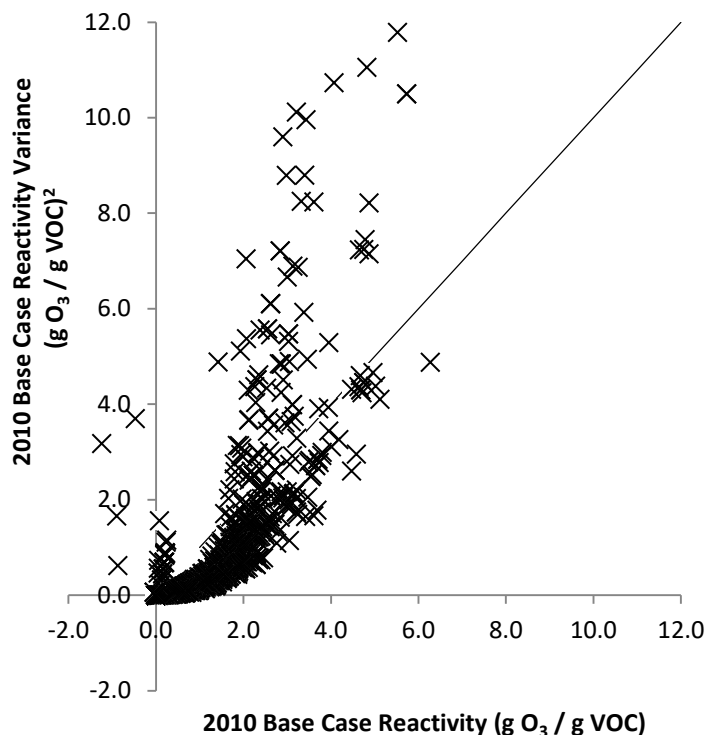
Figure 5-15: Comparison between 2010 base case IR median and 2010 base case IR variance across 39 cities.
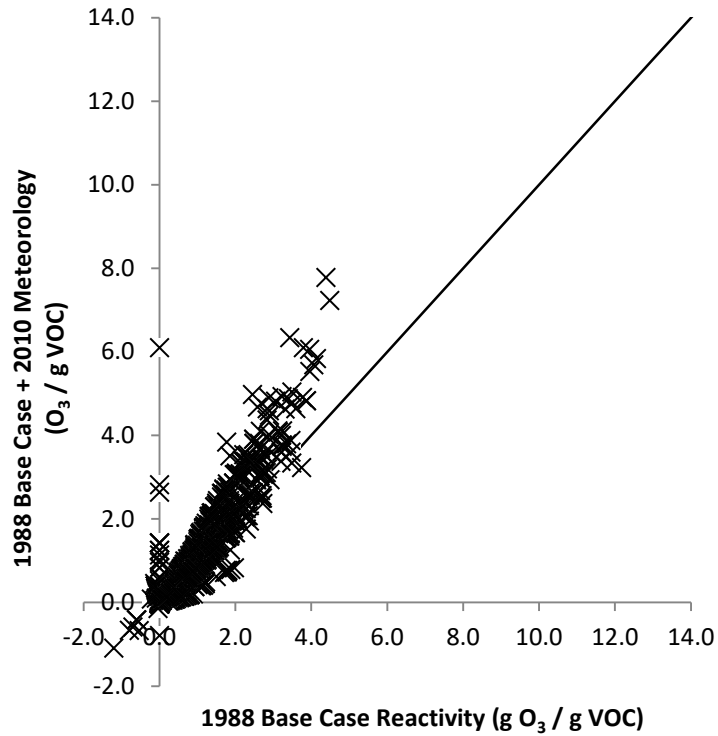
Figure 5-16. Effect of updating meteorology from 1988 conditions to 2010 conditions on median IR for 1192 different VOCs. Regression slope of 1.277 indicates a 27.7 % increase from the 1988 conditions.
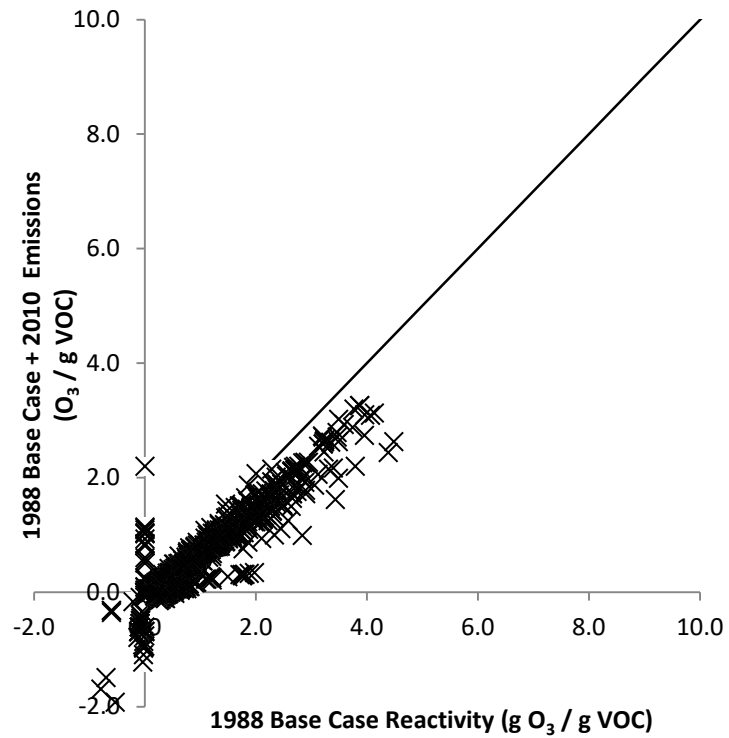
Figure 5-17. Effect of updating emissions from 1988 conditions to 2010 conditions on median IR for 1192 different VOCs.
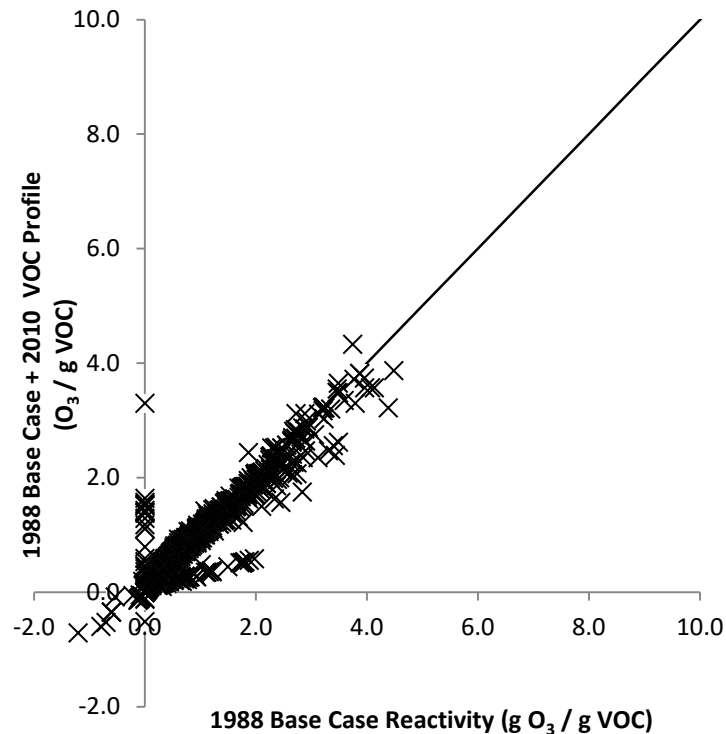
Figure 5-18. Effect of updating VOC profile from 1988 conditions to 2010 conditions on median IR for 1192 different VOCs.

The maximum incremental reactivity (MIR) scenario was derived for high NOx conditions where VOC emissions reductions are the most efficient path for ozone reduction. Many cities in the 1990s had high NOx concentrations which made MIR the most relevant IR metric. Figure 5-19 compares the MIR values for the 1,192 tested VOCs under the 1988 conditions and the 2010 conditions, showing that MIR values generally decrease by approximately 41.1% in the updated scenarios. Figure 5-20 plots the variance of MIR values across the 39 target cities as a function of median MIR value for the conditions in 2010. Little variance is observed for compounds with low MIRs but variance increases exponentially for compounds with higher median MIR values. Once again, this finding suggests that regional trends should be examined to determine if regional IR rankings should be developed.

 A sensitivity analysis was performed to see which variable impacted the change in MIR from 1988 to 2010 scenarios. Figures 5-21 through 5-23 illustrate how the 1988 MIR values change when each 2010 variable (meteorology, emissions and VOC composition) is utilized in place of the 1988 variable. The analysis reveals that this change is driven by a combination of changes to meteorology (seasonal shift), the initial/emitted VOC and NOx concentrations, and the aloft VOC profile which creates a less reactive atmosphere for the MIR scale.   The different behavior of the base case IR and MIR reflects the different effects of meteorological conditions and VOC composition on ozone formation at different ratios of NOx/VOC.
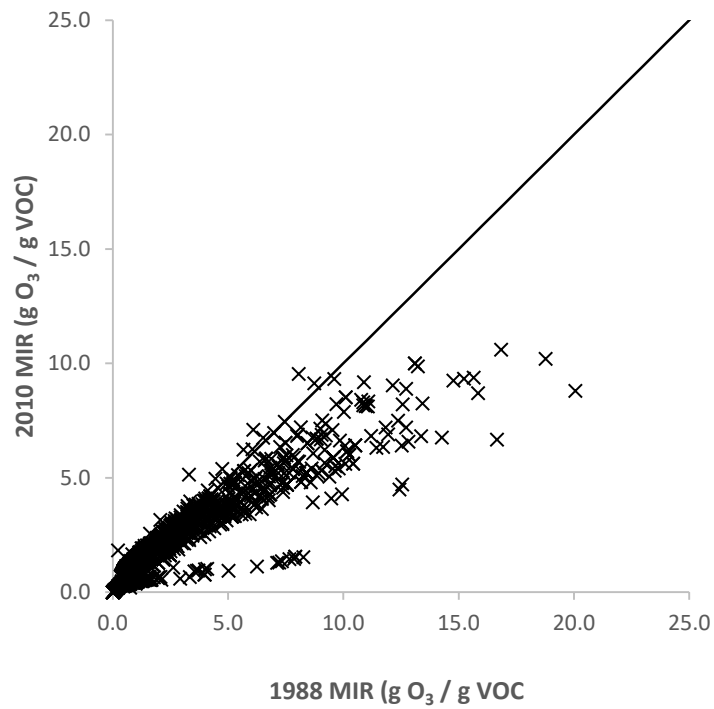
Figure 5-19: Correlation of 1988 MIR median reactivity and 2010 MIR median reactivity for 1192 different VOCs. Regression slope of 0.589 indicates a 41.1 % decrease from the 1988 conditions.
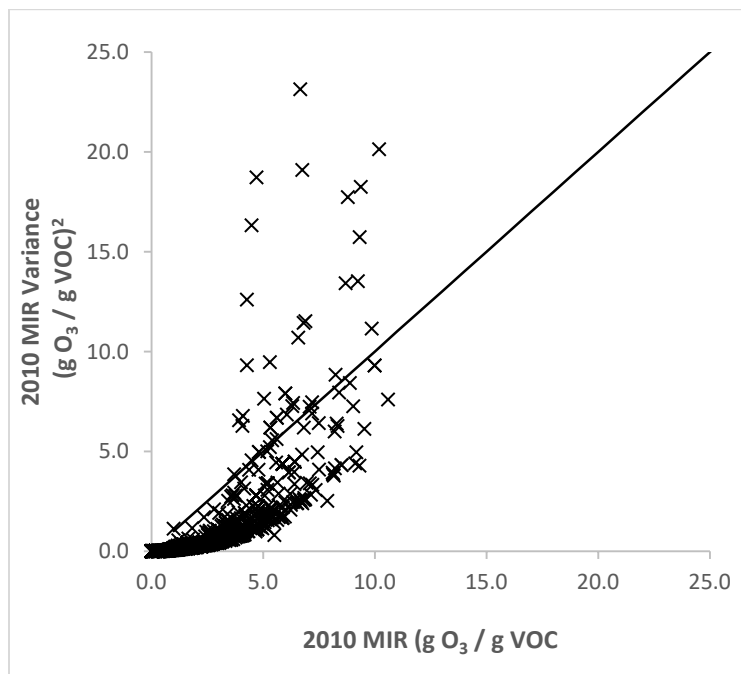
Figure 5-20: Correlation of 2010 MIR median reactivity and 2010 MIR variance.
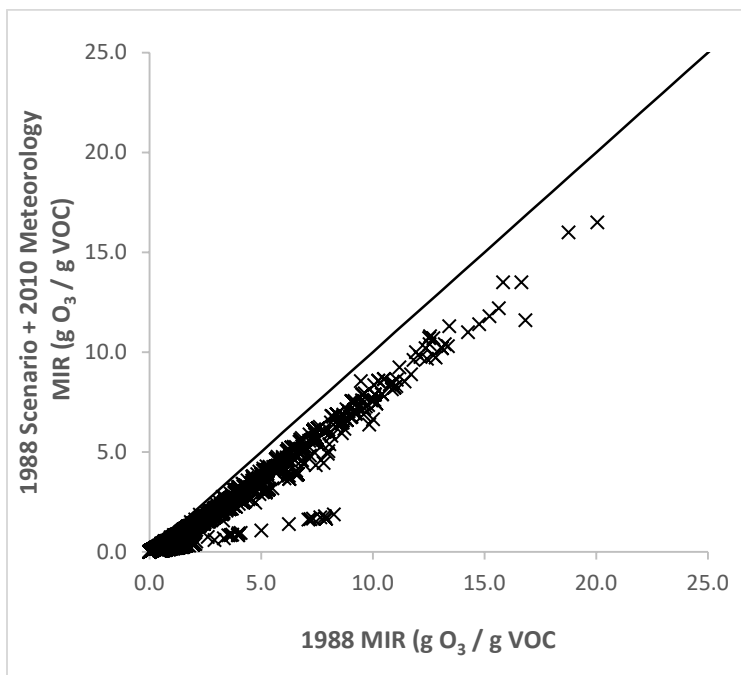
Figure 5-21. Effect of updating meteorology from 1988 conditions to 2010 conditions on MIR median reactivity for 1192 different VOCs. Regression slope of 0.783 indicates a 21.7 % decrease from the 1988 conditions.
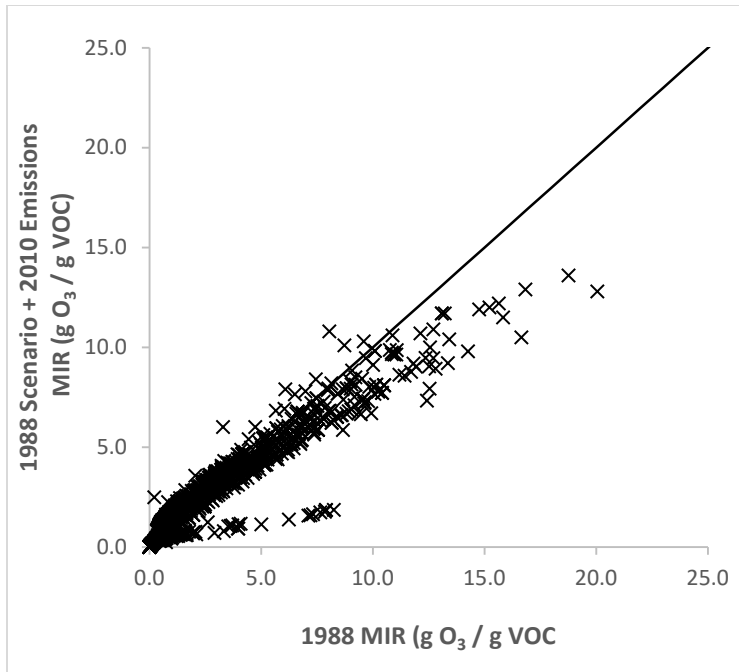
Figure 5-22. Effect of updating emissions from 1988 conditions to 2010 conditions on MIR median reactivity for 1192 different VOCs. Regression slope of 0.741 indicates a 25.9 % decrease from the 1988 conditions.
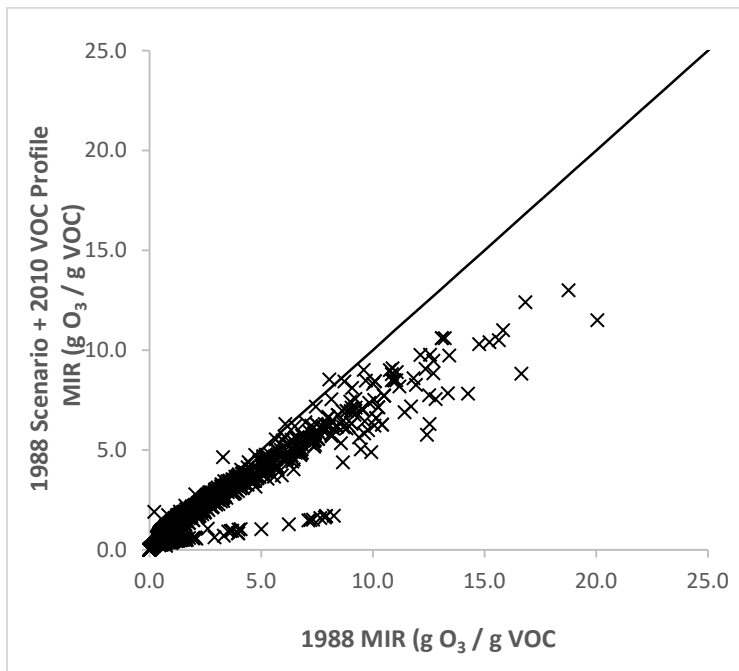
Figure 5-23. Effect of updating VOC profile from 1988 conditions to 2010 conditions on MIR median reactivity for 1192 different VOCs. Regression slope of 0.669 indicates a 33.1 % decrease from the 1988 conditions.

Each VOC was ranked based on its median reactivity under conditions in 1988 and 2010. Table 5-4 summarizes 15 VOCs with the highest base case IR under conditions from 1988 while Table 5-5 summarizes the 15 VOCs with the highest base case IR under conditions from 2010. A total of 10 out of 15 compounds appear in both lists, indicating that the changing conditions in 2010 had a slight effect on relative IR rankings.

Table 5-4: Top 15 base case IR values (g O3/ g VOC) and their associated VOCs under conditions in 1988.

VOC or Mix	Reactivity (g O3/ g VOC)	Rank
methacrylic acid	4.48	1
biacetyl	4.38	2
trans-2-butene	4.13	3
C4 internal alkenes	4.06	4
cis-2-butene	3.96	5
2-butyne	3.96	6
cis-1,3-pentadiene	3.87	7
trans-1,3-pentadiene	3.87	8
methyl methacrylate	3.79	9
1,3-butadiene	3.77	10
methylamine	3.74	11
C4 alkenes	3.59	12
propene	3.49	13
2-methyl-2-butene	3.49	14
1,2-propadiene (allene)	3.48	15

Table 5-5: Top 15 base case IR values (g O3/ g VOC) and their associated VOCs under conditions in 2010.

VOC or Mix	Median (g O_3/ g VOC)	2010 Rank
methylamine	6.27	1
cis-1,3-pentadiene	5.73	2
trans-1,3-pentadiene	5.73	3
1,3-butadiene	5.52	4
1,2-propadiene (allene)	5.12	5
1-buten-3-yne(vinyl acetylene)	5.12	6
isopropyl amine	5.02	7
1,2-butadiene	4.96	8
3-methyl-1,2-butadiene	4.87	9
C4 alkenes	4.87	10
cis-2-butene	4.82	11
C4 internal alkenes	4.79	12
propene	4.78	13
trans-2-butene	4.76	14
1-butene	4.75	15

Table 5-6 summarizes 15 VOCs with the highest base case MIR under conditions from 1988 while Table 5-7 summarizes the 15 VOCs with the highest base case MIR under conditions from 2010. A total of 8 out of 15 compounds appear in both lists, indicating that the changing conditions in 2010 did not had a slight effect on relative MIR rankings.

Table 5-6: Top 15 MIR values (g O3/ g VOC) and their associated VOCs under conditions in 1988.

VOC or Mix	Median (g O$_3$/ g VOC)	1988 Rank
biacetyl	20.06	1
methacrylic acid	18.77	2
2-butyne	16.84	3
methyl glyoxal	16.66	4
methyl methacrylate	15.84	5
trans-2-butene	15.65	6
C4 internal alkenes	15.23	7
cis-2-butene	14.77	8
2-methyl-2-butene	14.27	9
acrylic acid	13.43	10
trans-3-methyl-2-pentene	13.37	11
1,3-butadiene	13.23	12
cis-1,3-pentadiene	13.1	13
trans-1,3-pentadiene	13.1	14
cis-3-methyl-2-pentene	12.82	15

Table 5-7: Top 15 MIR values (g O3/ g VOC) and their associated VOCs under conditions in 2010.

VOC or Mix	Median (g O_3/ g VOC)	2010 Rank
2-butyne	10.60	1
methacrylic acid	10.20	2
cis-1,3-pentadiene	10.00	3
trans-1,3-pentadiene	10.00	4
1,3-butadiene	9.87	5
methylamine	9.54	6
trans-2-butene	9.38	7
C4 internal alkenes	9.33	8
1,2-butadiene	9.32	9
cis-2-butene	9.25	10
1-buten-3-yne (vinyl acetylene)	9.18	11
1,2-propadiene (allene)	9.13	12
propene	9.04	13
C4 alkenes	8.89	14
biacetyl	8.80	15

Table 5-8 summarizes VOCs whose MIR changed by more than 5 g O_3/ g VOC from 1988 to 2010. The specific chemical mechanism used in the SAPRC box model was the same for both the 1988 and 2010 case therefore the ambient conditions (meteorology, emissions and VOC composition) drove the differences observed in MIR. The differences in the meteorology and VOC composition profiles (aloft and base) are most likely the primary causes for the observed changes. In both the aloft and base VOC composition profiles the fraction of alkenes greatly increased from 1988 to 2010 due to the addition of biogenic VOCs. Relative humidity in general was higher and temperature lower in 2010 versus 1988 which may lead to large changes in MIR for some compounds.

Table 5-8: List of VOC or mixtures whose MIR values changed by more than 5 g O_3/ g VOC.

VOC or Mixture	1988 Median MIR (g O_3 / g VOC)	2010 Median MIR (g O_3 / g VOC)	Absolute Change (g O_3/ g VOC)
1,3,5-trimethyl benzene	11.94	6.90	5.04
1-methyl cyclopentene	11.72	6.35	5.37
2,3-dimethyl-2-butene	12.43	4.49	7.94
2,3-dimethyl-2-pentene	9.938	4.28	5.66
2-butyne	16.84	10.60	6.24
2-methyl-2-butene	14.27	6.76	7.51
2-methyl-2-pentene	11.43	6.31	5.12
acrylic acid	13.43	8.25	5.18
Aromatic 100®	7.658	1.45	6.21
biacetyl	20.06	8.80	11.26
Unspeciated C10 Aromatics	7.331	1.36	5.98
Unspeciated C11 Aromatics	7.214	1.30	5.92
Unspeciated C12 Aromatics	6.251	1.12	5.13
cis-2-butene	14.77	9.25	5.52
cis-3-methyl-2-pentene	12.82	6.58	6.24
C4 internal alkenes	15.23	9.33	5.90
Unspeciated C8 Aromatics	7.913	1.55	6.36
Unspeciated C9 Aromatics	8.262	1.53	6.73
chloroacetaldehyde	12.53	6.41	6.12
ethyl methacrylate	12.72	7.20	5.52
formaldehyde	9.472	4.10	5.37
glyoxal	12.55	4.71	7.84
CARB Hydrocarbon Bin 21	7.906	1.55	6.35
CARB Hydrocarbon Bin 22	7.863	1.46	6.41
CARB Hydrocarbon Bin 23	7.125	1.29	5.84
methacrylic acid	18.77	10.20	8.57
methyl glyoxal	16.66	6.67	9.99
methyl methacrylate	15.84	8.70	7.14
trans-2-butene	15.65	9.38	6.27
trans-3-methyl-2-pentene	13.37	6.82	6.55

Forty eight (48) additional VOCs were added to the reactivity calculation at the requests of CARB staff. In the current IR and MIR scale, values are calculated for 1,192 compounds of which 741 have mechanisms that are explicitly derived for that compound (Carter, 2009 ARB Final Report #07-339). The remaining compounds are estimated by assuming they have behave in the same fashion as explicitly resolved molecules with similar chemical structure. Thirtyfive (35) of the 48 requested additional VOCs were assigned to explicit compounds based on similar chemical structure. The SAPRC reactivity calculation was performed on each of the 35

additional compounds over each of the 39 cities based on the reaction rates of similar explicit compounds, the molecular weight of the actual compound, and the total number of carbons of the actual compound. Table 5-9 illustrates the median base IR and MIR values of the additional VOCs over the 39 cities and the explicit VOC it was assigned to based on chemical structure.

Thirteen (13) of the 48 requested VOCs were in a form of a mixture and the specific percentage, or ratio, of that mixture was not provided. For this reason the authors could not assign a specific explicit mixture to the 13 additional VOCs and calculate a single reactivity value. Rather, an estimated average value and range for that mixture was suggested based on the compounds that are in each specific mixture. Tables 5-10 and 5-11 illustrate the 13 VOC mixtures and a suggested IR and MIR range, respectively.

Table 5-9: Additional VOCs IR and MIR values for 2010 scenario and corresponding assigned explicit VOC.

New Compound	Assigned Explicit Compound	Median IR (g O$_3$ / g VOC)	Median MIR (g O$_3$ / g VOC)
1,1,1,3,5,5,5-Heptamethyl-3-Octyl-Trisiloxane	cyclosiloxane D4 (octamethylcyclotetrasiloxane)	0.01	-0.04
1,2-Octanediol	1,4-butanediol	1.11	1.85
1,2-Pentanediol	1,4-butanediol	1.55	2.59
1,3-Propanediol	1,4-butanediol	2.13	3.55
1,5-Pentanediol	1,4-butanediol	1.55	2.59
2-Propoxy-1-Propanol	n-propoxy-propanol	2.23	3.85
2-Pyrrolidone	n-methyl-2-pyrrolidone	2.05	3.45
3-Ethylheptamethyltrisiloxane	cyclosiloxane D4 (octamethylcyclotetrasiloxane)	0.01	-0.04
Butyl Benzyl Phthalate	dibutyl phthalate	0.5	1.09
Dimethylcyclopolysiloxane	cyclosiloxane D5 (decamethylcyclopentasiloxane)	0.01	-0.02
Dodecamethylcyclohexasiloxane	cyclosiloxane D5 (decamethylcyclopentasiloxane)	0.01	-0.03
Octamethylcyclotetrasiloxane	cyclosiloxane D5 (decamethylcyclopentasiloxane)	0.01	-0.04
Decamethyltetrasiloxane	cyclosiloxane D5 (decamethylcyclopentasiloxane)	0.01	-0.04
Dibutyl Adipate	diisopropyl adipate	0.56	1.23
Diethylenetriamine	triethyl amine	2.28	3.93
Diisopropylamine	tert-butyl amine	-0.9	0.73
Dimethicone	hexamethyl-disiloxane	0.08	0.02
Dimethyl phthalate	diethyl phthalate	0.78	1.7
Dipropylene Glycol Dibenzoate	2-ethyl-hexyl benzoate	0.42	0.83

Dodecamethylhexacyclosiloxane	cyclosiloxane D4 (octamethylcyclotetrasiloxane)	0.01	-0.02
Dodecamethylpentasiloxane	cyclosiloxane D4 (octamethylcyclotetrasiloxane)	0.01	-0.02
Ethyl Cyanoacrylate	2-ethyl-hexyl acrylate	1.81	3.57
Ethyl Nonafluorobutyl Ether	ethoxy-perfluoro-isobutane	0.01	0.01
Ethylene Glycol Monohexyl Ether	ethylene glycol diethyl ether; 1,2-diethoxyethane	1.63	2.63
Hexamethyldisiloxane	cyclosiloxane D4 (octamethylcyclotetrasiloxane)	0.02	-0.05
Hydroxyethyl Methacrylate	2-methyl-2,4-pentanediol	0.91	1.44
Isododecane	n-dodecane	0.62	1.05
Isohexadecane	N-C16	0.54	0.94
m-Aminophenol	phenol	0.21	1.61
Methacyrlate Monomer	methyl methacrylate	3.56	8.7
Methylene Glycol	ethylene glycol	1.89	3.23
Octamethyltrisiloxane	cyclosiloxane D4 (octamethylcyclotetrasiloxane)	0.01	-0.04
Phenyl Trimethicone	hexamethyl-disiloxane	0.03	0.01
Tetrahydrofurfuryl Methacrylate	isobutyl methacrylate	1.79	4.06
Trifluoroethyl Methacrylate	isobutyl methacrylate	1.91	4.33

Table 5-10: Additional VOC mixture IR values for 2010 scenario and corresponding assigned explicict VOC.

New Mixture	IR (g O_3/ g VOC)	Range		Group of explicit compounds used to determine IR range
		min IR (g O_3/ g VOC)	max IR (g O_3/ g VOC)	
C10-11 Isoparaffin	0.6695	0.559	0.78	2 methyl "alkanes" extrapolated; need proportion of mixture
C10-13 Isoparaffin	0.4845	0.213	0.78	2 methyl "alkanes" extrapolated; need proportion of mixture
C13-14 Isoparaffin	0.1265	0.04	0.213	2 methyl "alkanes" extrapolated; need proportion of mixture
C7-8 Isoparaffin	1.155	1.07	1.24	average of 2-methyl hexane and 2-methyl heptane
Cyclomethicone	0.01005	0.0095	0.0106	cyclosiloxane (D4 and D5), D6 extrapolated; need proportions of mixture
Dibasic Ester (DBE-3)	1.645	1.48	1.81	average of dimethyl adipate and dimethy glutarate
Diethylethanolamine	2.21	N/A	N/A	ethanoloamine
Glutamic Acid	0	N/A	N/A	Approx. 0 – straight into aerosol phase; not volatile

New Mixture	MIR (g O₃/ g VOC)	min MIR (g O₃/ g VOC)	max MIR (g O₃/ g VOC)	Group of explicit compounds used to determine MIR range
Propane/Isobutane/n-Butane	2.012	0.983	3.12	average of Propane/Isobutane/n-Butane; need proportions of mixture
Siloxanes	0.75975	0.0095	1.51	siloxane range; need proportions and which siloxanes of interest for mixture
Dimethylpolysiloxane	0.75975	0.0095	1.51	siloxane range; need proportions of mixture
Polydimethylsiloxane	0.75975	0.0095	1.51	siloxane range; need proportions of mixture
Stilbenzene Derivates	1.79		1.79	Benzene; need to know which derivates of interest for mixture

Table 5-11: Additional VOC mixture MIR values for 2010 scenario and corresponding assigned explicit VOC.

New Mixture	MIR (g O₃/ g VOC)	min MIR (g O₃/ g VOC)	max MIR (g O₃/ g VOC)	Group of explicit compounds used to determine MIR range
C10-11 Isoparaffin	1.1835	1.077	1.29	2 methyl "alkanes" extrapolated; need proportion of mixture
C10-13 Isoparaffin	1.002	0.735	1.29	2 methyl "alkanes" extrapolated; need proportion of mixture
C13-14 Isoparaffin	0.6495	0.564	0.735	2 methyl "alkanes" extrapolated; need proportion of mixture
C7-8 Isoparaffin	1.685	1.58	1.79	average of 2-methyl hexane and 2-methyl heptane
Cyclomethicone	-0.0341	-0.0382	-0.03	cyclosiloxane (D4 and D5), D6 extrapolated; need proportions of mixture
Dibasic Ester (DBE-3)	1.87	0.482	1.87	avreage of dimethyl adipate and dimethy glutarate
Diethylethanolamine	6.96	N/A	N/A	ethanoloamine
Glutamic Acid	0	N/A	N/A	Approx. 0 – straight into aerosol phase; not volatile
Propane/Isobutane/n-Butane	1.103333333	0.6	1.39	average of Propane/Isobutane/n-Butane; need proportions of mixture
Siloxanes	0.0205	-0.575	0.0205	siloxane range; need proportions and which siloxanes of interest for mixture
Dimethylpolysiloxane	0.0205	-0.575	0.0205	siloxane range; need proportions of mixture
Polydimethylsiloxane	0.0205	-0.575	0.0205	siloxane range; need proportions of mixture
Stilbenzene Derivates	0.716		0.716	Benzene; need to know which derivates of interest for mixture

Figures 5-24 through 5-26 and 5-27 through 5-29 illustrate the base case IR and MIR, respectively, for all VOCs under 2010 conditions. Certain VOCs/mixtures are not represented graphically as either their reactivity was determined to be zero or they were one of the additional reactivities calculated for 2010 only. Table 5-12 represents a complete, master list of all VOCs (or mixtures) along with the number correlated to the box and whisker plots, median IR value (g O_3/g VOC) in 1988 and 2010, rank in 1988 and rank in 2010 for base IR. Table 5-13 represents a complete, master list of all VOCs (or mixtures), median MIR value (g O_3/g VOC) in 1988 and 2010, rank in 1988 and rank in 2010 for MIR
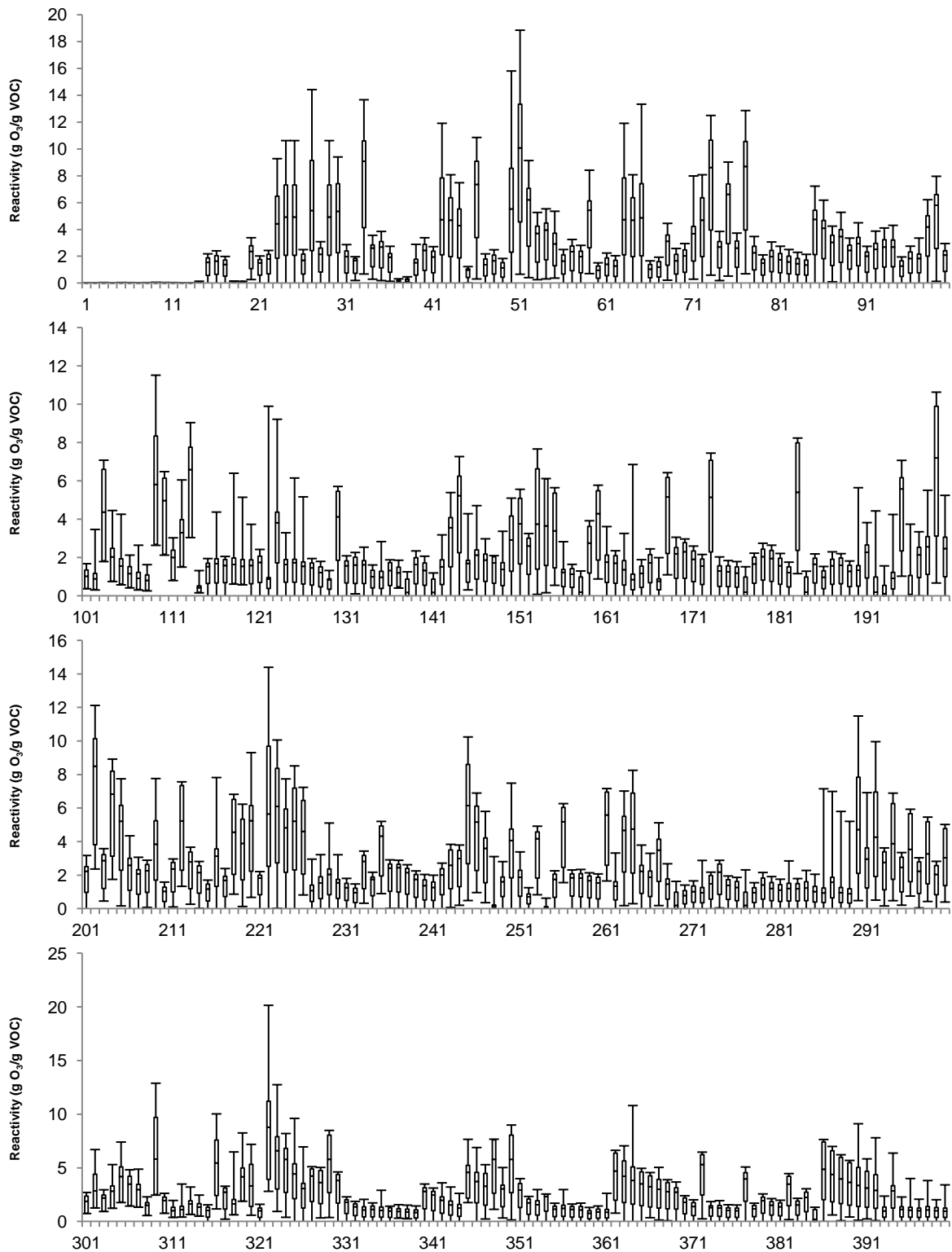
Figure 5-24: Box and whisker plots for VOC #1-400 representing 39 cities VOC reactivity for 2010 base case scenario. VOC's are stated as a number and can be referred to its specific name in the table 5-8.
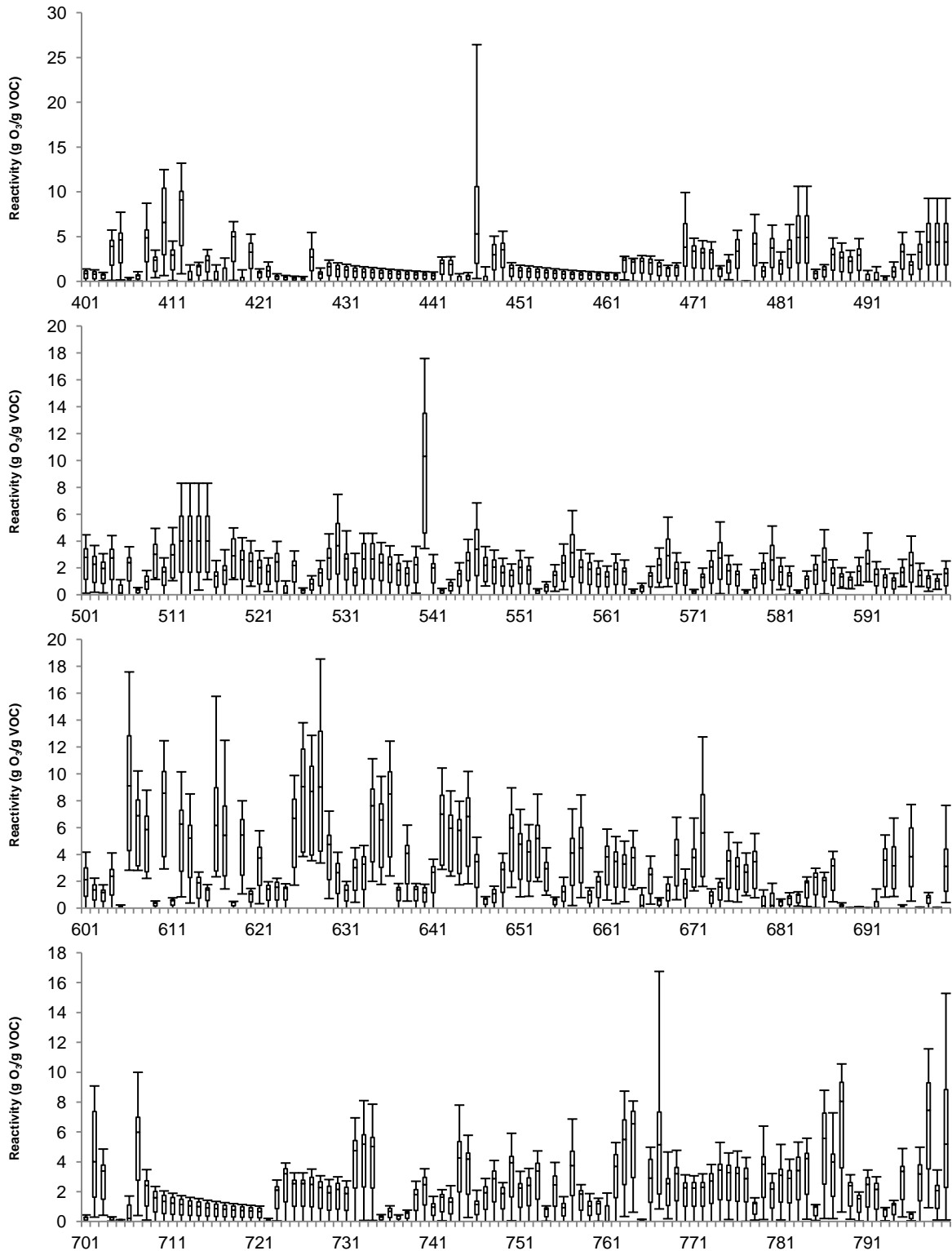
Figure 5-25: Box and whisker plots for VOC #401-800 representing 39 cities VOC reactivity for 2010 base case scenario. VOC's are stated as a number and can be referred to its specific name in the 5-8.
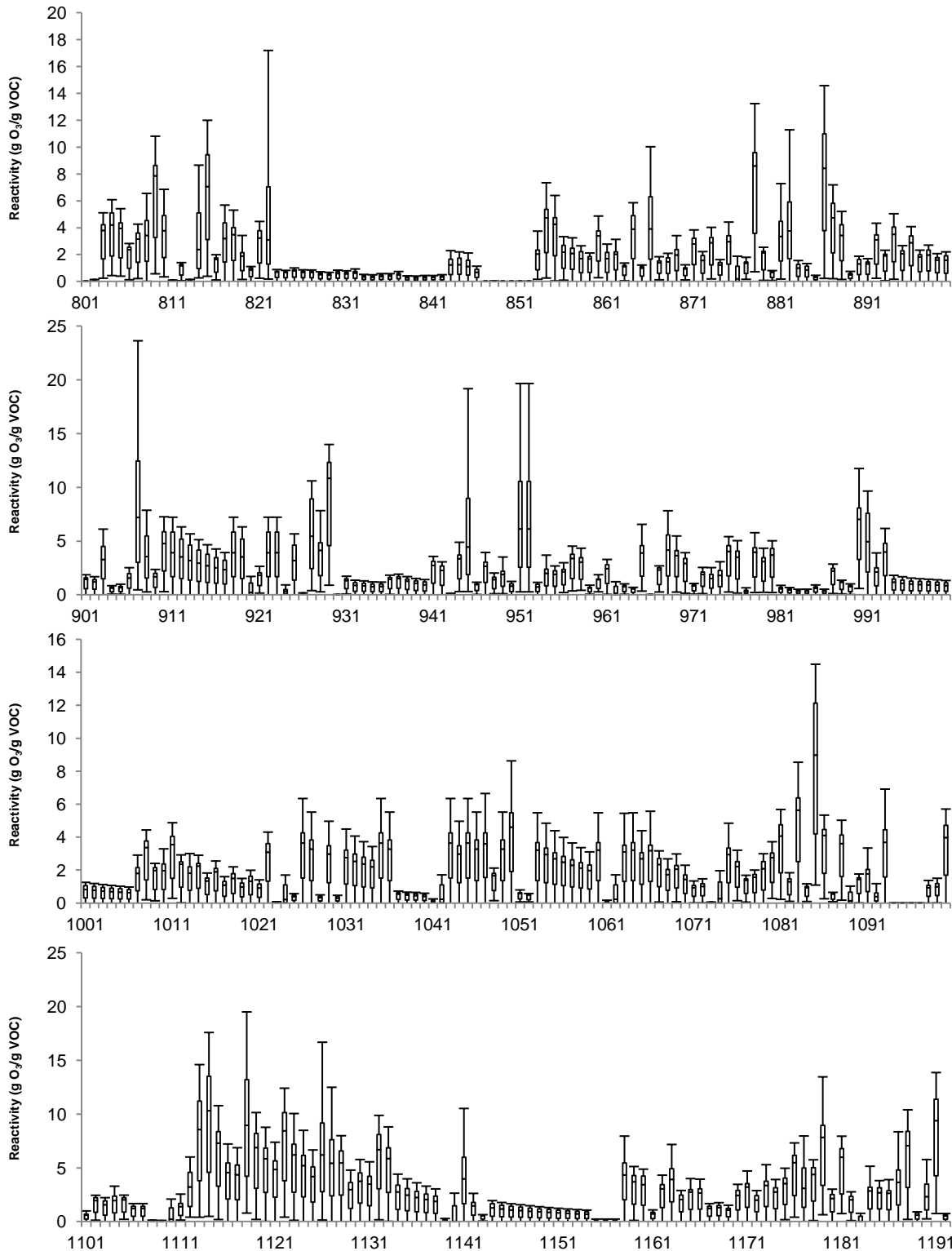
Figure 5-26: Box and whisker plots for VOC #801-1116 representing 39 cities VOC reactivity for 2010 base case scenario. VOC's are stated as a number and can be referred to its specific name in the table 5-8.
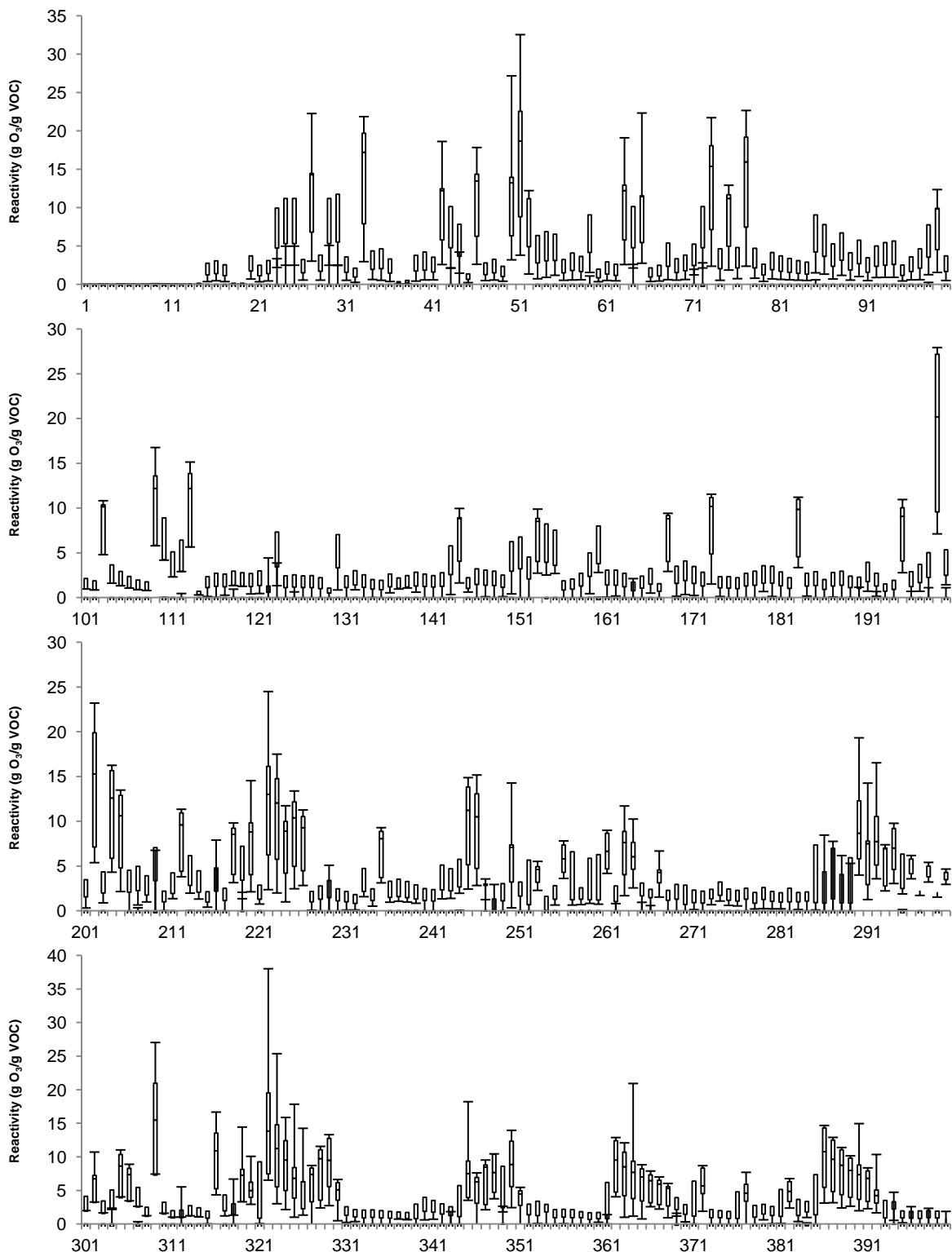
Figure 5-27: Box and whisker plots for VOC #1-400 representing 39 cities VOC reactivity for 2010 MIR scenario. VOC's are stated as a number and can be referred to its specific name in the table 5-9.

135
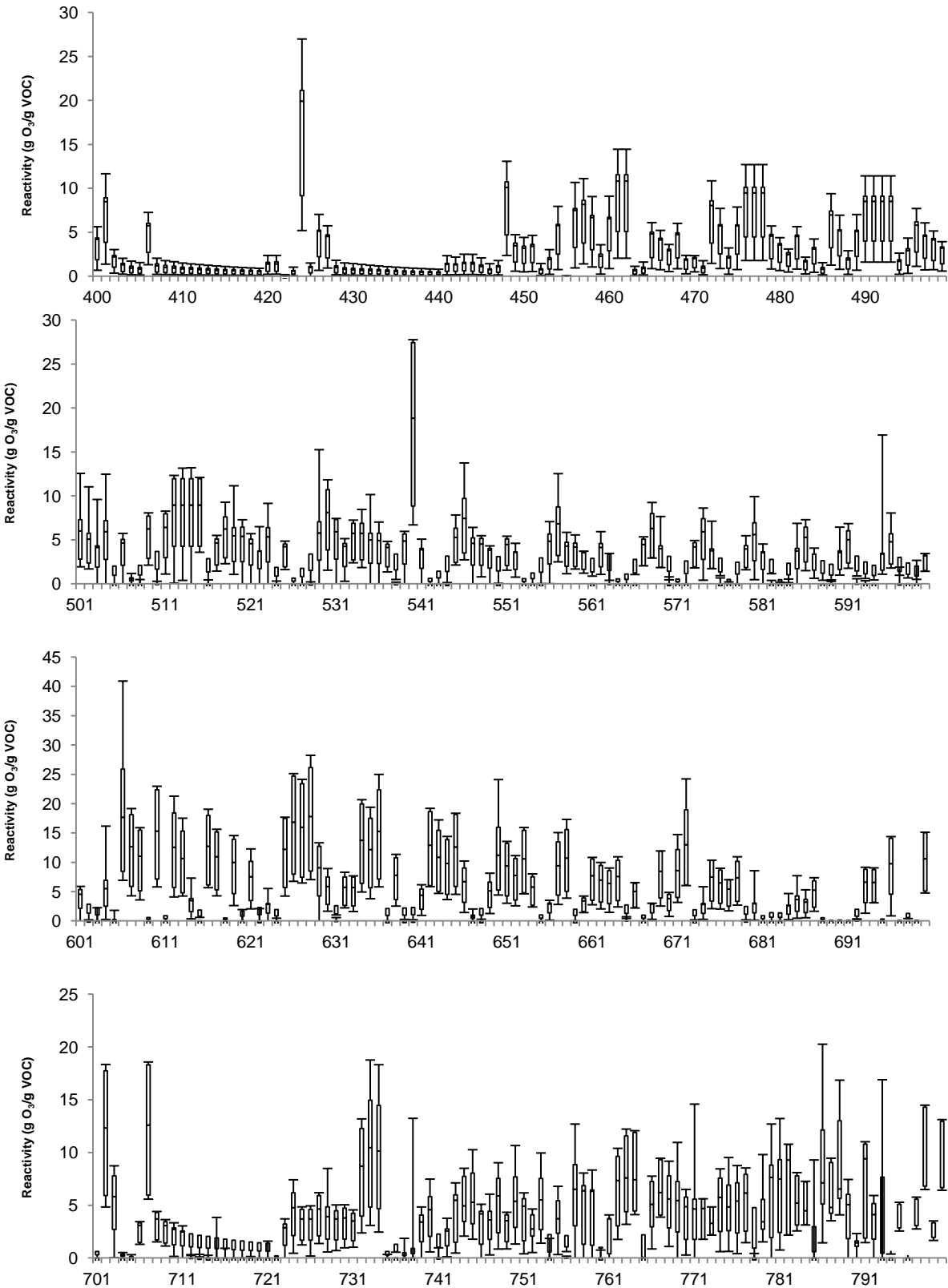
Figure 5-28: Box and whisker plots for VOC #400-799 representing 39 cities VOC reactivity for 2010 MIR scenario. VOC's are stated as a number and can be referred to its specific name in the table 5-9.

136
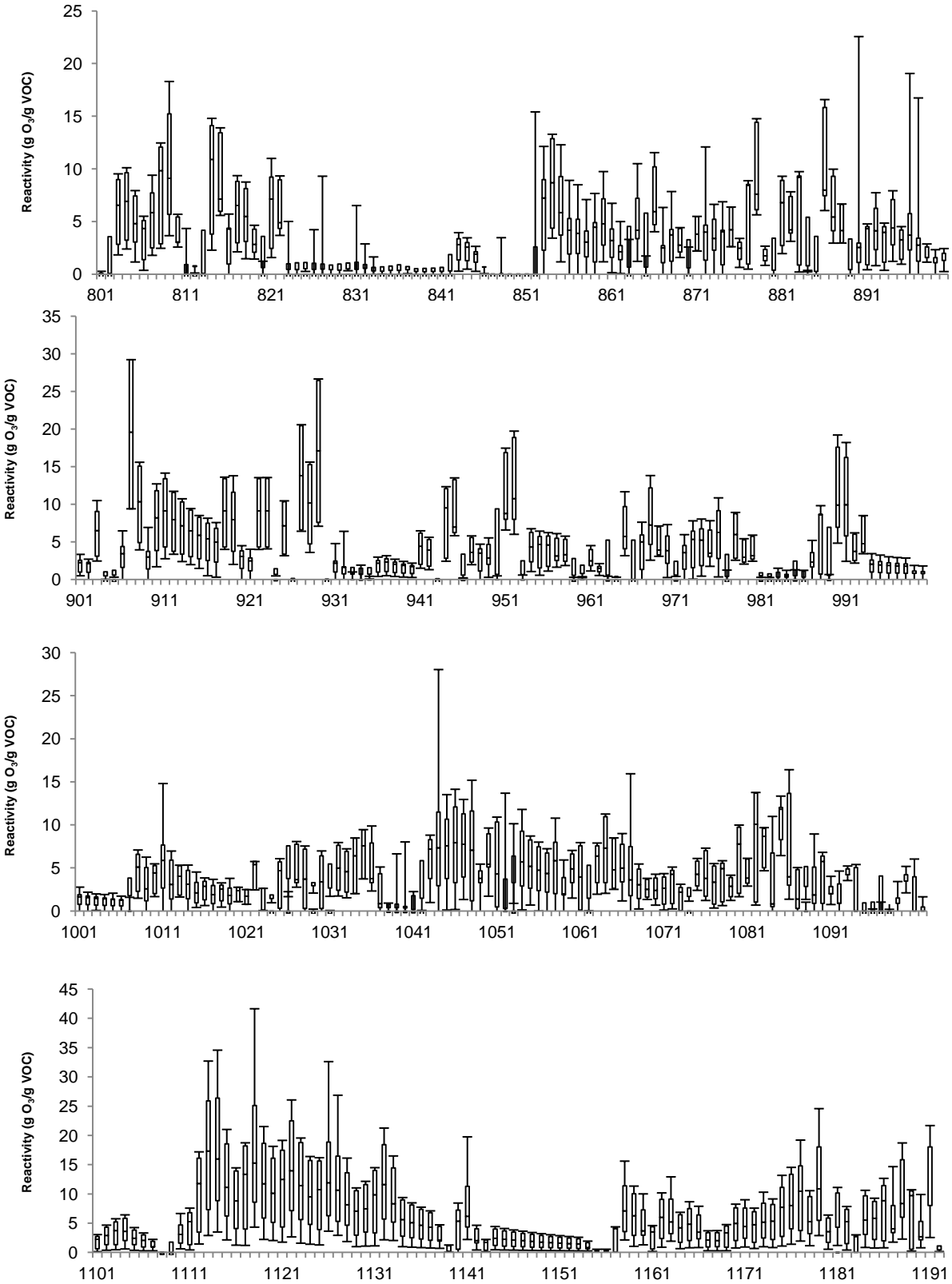
Figure 5-29: Box and whisker plots for VOC #801-1105 representing 39 cities VOC reactivity for 2010 MIR scenario. VOC's are stated as a number and can be referred to its specific name in the table 5-9.

Table 5-12: List of VOC or mixture name, median IR value in 1988 and 2010 (g O_3 / g VOC), and rank (most reactive = 1 least = 1192) in 2010 and 1988 for base case IR.

#	VOC / Mix	1988 Median IR (g O_3/ g VOC)	2010 Median IR (g O_3/ g VOC)	1988 Rank	2010 Rank
1	Dodecamethylpentasiloxane	N/A	0.01	1155	1174
2	Dimethylcyclopolysiloxane	N/A	0.01	1156	1173
3	1,1,1,3,5,5,5-Heptamethyl-3-Octyl-Trisiloxane	N/A	0.01	1157	1162
4	Dodecamethylhexacyclosiloxane	N/A	0.01	1158	1176
5	decamethyltetrasiloxane	N/A	0.01	1159	1163
6	3-Ethylheptamethyltrisiloxane	N/A	0.01	1160	1166
7	cyclosiloxane D4 (octamethylcyclotetrasiloxane)	0.00	0.01	1113	1169
8	cyclosiloxane D5 (decamethylcyclopentasiloxane)	0.00	0.01	1114	1167
9	hexamethyldisiloxane	N/A	0.02	1161	1160
10	Octamethylcyclotetrasiloxane	N/A	0.01	1162	1161
11	octamethyltrisiloxane	N/A	0.01	1163	1165
12	Dodecamethylcyclohexasiloxane	N/A	0.01	1164	1170
13	1,1,1-trichloroethane	0.00	0.00	1099	1177
14	1,1,2-trichloroethane	0.04	0.05	1083	1148
15	1,1,2-trimethyl cyclopentane	0.55	0.97	708	680
16	1,1,3-trimethyl cyclohexane	0.55	1.00	703	654
17	1,1,3-trimethyl cyclopentane	0.49	0.87	770	734
18	1,2-dibromoethane	0.04	0.05	1079	1149
19	1,1-dichloroethane	0.04	0.06	1080	1144
20	1,1-dichloroethene	0.85	1.28	492	506
21	1,1-dimethyl cyclopentane	0.52	0.92	744	715
22	1,1-dimethyl cyclohexane	0.61	1.11	661	600
23	pentamethyl benzene	2.03	2.57	127	138
24	1,2,3,4-tetramethyl benzene	2.29	2.86	90	104
25	1,2,3,5-tetramethyl benzene	2.29	2.86	91	105
26	1,2,3-trimethyl cyclohexane	0.52	1.03	735	636
27	1,2,3-trimethyl benzene	2.90	2.98	36	93
28	1,2,3-trimethyl cyclopentane	0.80	1.32	524	491
29	1,2,4,5-tetramethyl benzene	2.29	2.86	92	106
30	1,2,4-trimethyl benzene	2.26	3.09	102	79
31	1,2,4-trimethyl cyclopentane	0.70	1.23	590	529

32	1,2-epoxy butane	0.59	0.96	678	685
33	1,2-butadiene	3.46	4.96	16	8
34	1,2-butandiol	0.94	1.40	441	455
35	1,2-pentanediol	N/A	1.55	1165	406
36	1,2-octanediol	N/A	1.11	1166	601
37	1,2-dichloroethane	0.09	0.11	1070	1127
38	1,2-dichloropropane	0.12	0.15	1068	1118
39	1,2-diacetyl benzene	0.55	0.93	706	702
40	1,2-dimethyl cyclopentane	0.85	1.48	486	431
41	1,2-dimethyl cyclohexane	0.61	1.20	670	551
42	1,2-dimethyl-3-ethyl benzene	2.49	2.62	69	129
43	1,2-dimethyl-4-ethyl benzene	1.96	2.72	141	119
44	1,2-dimethyl cyclohexene	1.64	2.41	202	156
45	1,2-propylene glycol diacetate	0.35	0.57	898	925
46	1,2-pentadiene	2.74	3.95	49	31
47	1,3,5-triethyl cyclohexane	0.46	0.84	790	755
48	1,3,5-trimethyl cyclohexane	0.51	0.99	752	656
49	1,3,5-tripropyl cyclohexane	0.41	0.70	843	844
50	1,3,5-trimethyl benzene	2.89	3.21	37	65
51	1,3-butadiene	3.77	5.52	10	4
52	1,3-butadiyne	2.37	3.47	83	53
53	1,3-propanediol	N/A	2.13	1167	215
54	1,3-butanediol	1.46	2.22	242	202
55	1,3-dichloropropene mixture	1.16	1.63	348	376
56	1,3-diethyl cyclohexane	0.55	0.99	707	657
57	1,3-dimethyl cyclopentane	0.82	1.42	505	451
58	1,3-dimethyl cyclohexane	0.61	1.20	660	552
59	1,3-dioxolane	2.00	2.79	134	116
60	1,3-diethyl-5-pentyl cyclohexane	0.32	0.60	932	899
61	1,3-diethyl-5-methyl cyclohexane	0.47	0.87	786	737
62	1,3-diethyl-5-propyl cyclohexane	0.44	0.79	803	784
63	1,3-dimethyl-2-ethyl benzene	2.49	2.62	70	130
64	1,3-dimethyl-4-ethyl benzene	1.96	2.72	142	120
65	1,3-dimethyl-5-ethyl benzene	2.48	2.84	71	111
66	1,3-propyl-5-butyl cyclohexane	0.35	0.63	896	881
67	1,3-dipropyl-5-ethyl cyclohexane	0.42	0.74	828	816
68	1,4-butanediol	1.14	1.80	359	327
69	1,4-diethyl cyclohexane	0.54	1.00	721	647
70	1,4-dimethyl cyclohexane	0.66	1.23	620	530
71	1,4-dioxane	1.19	2.04	344	248
72	1,4-dimethyl-2-ethyl benzene	1.96	2.72	143	121

73	1,4-pentadiene	3.20	4.67	30	21
74	1,5-pentanediol	N/A	1.55	1168	407
75	1-amino-2-propanol	2.34	3.68	85	41
76	1-(butoxyethoxy)-2-propanol	0.96	1.44	436	444
77	1-butene	3.21	4.75	27	15
78	1-decene	0.88	1.29	471	499
79	1-decanol	0.50	0.90	757	721
80	1-undecene	0.77	1.12	539	593
81	1-dodecene	0.68	0.97	604	677
82	1-tridecene	0.61	0.88	663	729
83	1-tetradecene	0.56	0.81	702	774
84	1-pentadecene	0.52	0.75	739	807
85	butanal	2.01	2.63	132	127
86	pentanal (valeraldehyde)	1.72	2.27	187	191
87	1-hexanol	1.08	1.72	399	350
88	hexanal	1.48	1.94	237	273
89	1-heptanol	0.85	1.41	485	454
90	heptanal	1.26	1.66	308	368
91	1-octanol	0.68	1.19	606	554
92	octanal	1.08	1.43	392	447
93	1-nonene	1.04	1.49	407	423
94	1-nonene-4-one	1.13	1.48	366	432
95	1-ethyl-2-propyl cyclohexane	0.37	0.77	880	797
96	1-ethyl-4-methyl cyclohexane	0.58	1.10	686	606
97	1-ethyl naphthalene	0.67	1.07	614	615
98	1-heptene	1.57	2.18	209	209
99	1-hexene	2.05	3.21	123	66
100	5-methyl-1-heptanol	0.74	1.21	559	545
101	1-methyl-2-hexyl cyclohexane	0.29	0.64	964	880
102	1-methyl-2-octyl cyclohexane	0.25	0.56	1006	933
103	1-methyl-3,5-diethyl benzene	2.19	2.55	108	144
104	1-methyl-3-ethyl cyclopentane	0.67	1.27	612	510
105	1-methyl-3-isopropyl cyclohexane	0.49	0.94	772	694
106	1-methyl-4-pentyl cyclohexane	0.35	0.71	899	832
107	trans-1-methyl-4-heptyl cyclohexane	0.26	0.58	1002	917
108	1-methyl-4-nonyl cyclohexane	0.23	0.52	1031	958
109	1-methyl cyclopentene	3.12	3.13	32	74
110	1-methyl cyclohexene	2.03	2.80	129	115
111	1-methyl naphthalene	0.73	1.18	567	560
112	1-octene	1.27	1.77	305	335
113	1-pentene	2.47	3.54	73	49

114	2,2,3,3-tetramethyl butane	0.17	0.25	1063	1060
115	2,2,3-trimethyl butane	0.56	0.89	701	723
116	2,2,3-trimethyl pentane	0.61	1.00	667	648
117	2,2,4-trimethyl pentane	0.62	0.90	652	720
118	2,2,4-trimethyl hexane	0.59	1.00	680	649
119	2,2,4-trimethyl heptane	0.55	0.95	714	692
120	2,2,5-trimethyl hexane	0.56	0.95	700	689
121	2,2,5-trimethyl heptane	0.61	1.05	669	629
122	neopentane	0.35	0.49	902	974
123	2,2-dimethylpropanal (pivaldehyde)	1.63	2.10	205	230
124	2,2-dimethyl butane	0.64	0.93	638	708
125	2,2-dimethyl pentane	0.58	1.03	683	637
126	2,2-dimethyl hexane	0.52	0.93	743	709
127	2,2-dimethyl heptane	0.49	0.89	768	724
128	2,2-dimethyl octane	0.40	0.75	848	814
129	2,2-dimethoxy-propane	0.28	0.49	976	971
130	2,3,3-trimethyl-1-butene	1.45	2.28	249	188
131	2,3,3-trimethyl pentane	0.57	0.89	691	725
132	2,3,4,6-tetramethyl heptane	0.53	0.98	731	664
133	2,3,4-trimethyl pentane	0.55	0.97	712	673
134	2,3,5,6,8-pentamethyl-nonyl acetate	0.33	0.59	923	908
135	2,3,5,7-tetramethyl-octyl acetate	0.31	0.59	944	911
136	2,3,5,7-tetramethyl octane	0.42	0.79	832	779
137	2,3,5-trimethyl-hexyl acetate	0.38	0.74	868	817
138	2,3,5-trimethyl phenol	-0.09	0.17	1133	1108
139	2,3,5-trimethyl hexane	0.57	1.01	692	642
140	2,3,6-trimethyl 4-isopropyl heptane	0.43	0.78	824	786
141	2,3,6-trimethyl phenol	-0.09	0.17	1134	1109
142	2,3,6-trimethyl heptane	0.47	0.92	781	711
143	2,3-butanediol	1.22	2.05	327	239
144	2,3-dimethyl-1-pentene	1.78	2.99	171	91
145	2,3-dimethyl butane	0.55	0.98	715	661
146	2,3-dimethyl pentane	0.74	1.25	561	517
147	2,3-dimethyl hexane	0.63	1.12	647	594
148	2,3-dimethyl heptane	0.54	1.07	719	616
149	2,3-dimethyl octane	0.43	0.85	817	747
150	2,3-dimethyl naphthalene	1.16	1.63	349	377
151	2,3-dimethyl-1-butene	1.34	2.10	284	231
152	dimethylpentanol (2,3-dimethyl-	0.96	1.49	435	424

	1-pentanol)				
153	2,3-dimethyl-2-butene	2.84	2.36	42	165
154	2,3-dimethyl-2-pentene	2.33	2.06	86	238
155	2,3-dimethyl-2-hexene	2.10	1.93	118	277
156	2,3-dimethylbutyl acetate	0.40	0.75	856	813
157	2,3-dimethyl-heptyl acetate	0.35	0.70	894	846
158	2,3-dimethyl phenol	-0.10	0.19	1136	1091
159	2,4,4-trimethyl-1-pentene	0.95	1.56	439	401
160	2,4,4-trimethyl-2-pentene	1.75	2.42	180	155
161	2,4,4-trimethyl hexane	0.67	1.06	619	625
162	2,4,4-trimethyl heptane	0.60	1.04	673	632
163	2,4,5,6,8-pentamethyl nonane	0.45	0.81	796	777
164	2,4,6,8-tetramethyl-nonyl acetate	0.27	0.53	990	951
165	2,4,6,8-tetramethyl nonane	0.38	0.73	870	818
166	2,4,6-trimethyl heptane	0.58	1.04	684	633
167	2,4-pentanedione	0.31	0.45	938	990
168	2,4-dimethyl-1-pentene	1.77	2.95	174	95
169	2,4-dimethyl pentane	0.79	1.28	528	507
170	2,4-dimethyl hexane	0.86	1.39	483	458
171	2,4-dimethyl heptane	0.64	1.16	632	567
172	2,4-dimethyl octane	0.47	0.96	785	684
173	2,4-dimethyl-2-pentene	2.39	2.86	79	107
174	2,4-dimethylpentyl acetate	0.43	0.80	822	778
175	2,4-dimethylhexyl acetate	0.39	0.77	859	796
176	2,4-dimethyl-heptyl acetate	0.37	0.73	883	819
177	2,4-dimethyl phenol	-0.10	0.19	1137	1092
178	2,5,5-trimethyl heptane	0.61	1.01	665	643
179	2,5-dimethyl hexane	0.74	1.23	560	531
180	2,5-dimethyl heptane	0.66	1.19	622	555
181	2,5-dimethyl octane	0.48	0.97	776	670
182	2,5-dimethyl-heptyl acetate	0.38	0.75	871	809
183	2,5-dimethyl furan	2.26	3.03	103	85
184	2,5-dimethyl phenol	-0.10	0.19	1138	1093
185	trimethylnonanolthreoerythro (2,6,8-trimethyl-4-nonanol)	0.56	0.98	697	662
186	2,6,8-trimethyl 4-isopropyl nonane	0.29	0.60	965	900
187	2,6-dimethyl heptane	0.48	0.96	773	681
188	2,6-dimethyl octane	0.49	0.97	769	666
189	2,6-dimethyl nonane	0.38	0.79	872	781
190	dimethyl heptanol (2,6-dimethyl-2-heptanol)	0.43	0.82	815	760

191	2,6-dimethyl-4-heptanol	0.82	1.35	511	474
192	2,6-dimethyl phenol	-0.10	0.19	1139	1094
193	2,6-di-tert-butyl-p-cresol	-0.05	0.11	1126	1128
194	2,7-dimethyl 3,5-diisopropyl heptane	0.26	0.56	999	935
195	2-amino-1-butanol	1.89	3.24	148	63
196	2-amino-2-ethyl-1,3-propanediol	-0.04	0.08	1125	1134
197	2-butoxyethyl acetate	0.77	1.19	537	556
198	2-butyl tetrahydrofuran	0.94	1.44	444	445
199	2-butyne	3.96	4.07	6	29
200	C12 2-alkenes	1.10	1.46	379	437
201	2-pentanol	0.77	1.27	540	511
202	2-pentenes	3.23	4.68	23	19
203	2-hexanol	0.95	1.66	438	369
204	2-hexenes	2.65	3.70	62	39
205	2-heptenes	2.28	2.93	97	97
206	2-octanol	0.93	1.49	453	425
207	2-chlorotoluene	0.67	1.22	616	538
208	2-ethyl-1,3-hexanediol	0.81	1.29	514	500
209	2-ethyl-1-butene	1.42	2.15	256	214
210	2-ethyl-hexyl benzoate	0.39	0.61	861	896
211	2-ethyl-1-hexanol	0.87	1.37	473	469
212	2-ethyl furan	2.07	2.95	122	96
213	2-ethyl hexanoic acid	1.20	1.61	334	389
214	2-ethyl-hexyl acrylate	0.81	1.22	512	539
215	2-ethyl-hexyl acetate	0.36	0.71	885	833
216	2-methoxy-1-(2-methoxy-1-methylethoxy)-propane; dipropylene glycol dimethyl ether	0.96	1.81	437	320
217	2-methyl-1-butyl acetate	0.60	0.96	676	682
218	2-methyl-1-butene	1.73	2.53	186	148
219	2-methyl-1-pentene	1.45	2.18	248	210
220	2-methyl-1-hexene	1.78	3.01	173	88
221	2-methyl-2,4-pentanediol	0.62	1.00	653	653
222	2-methyl-2-butene	3.49	3.12	14	75
223	2-methyl-2-pentene	2.85	3.38	40	58
224	mesityl oxide (2-methyl-2-penten-4-one)	1.84	2.66	157	126
225	2-methyl-2-hexene	2.43	2.91	76	101
226	2-methyl-2-heptene	2.14	2.55	113	145
227	2-methyl 3,5-diisopropyl heptane	0.31	0.64	940	877
228	2-methyl-3-ethyl heptane	0.47	0.93	780	703

229	2-methyl-3-hexanone	0.71	1.21	580	546
230	2-methylpentyl acetate	0.48	0.93	778	707
231	2-methylhexyl acetate	0.39	0.77	863	798
232	2-methyloctyl acetate	0.27	0.59	982	907
233	2-methyl-1-butanol	1.04	1.63	410	378
234	isobutane	0.65	0.99	630	658
235	2-methyl propanal	1.81	2.38	164	163
236	isopentane	0.83	1.38	500	463
237	2-methyl pentane	0.76	1.45	545	443
238	2-methyl hexane	0.67	1.29	613	501
239	2-methyl heptane	0.53	1.07	727	617
240	2-methyl octane	0.42	0.85	831	750
241	2-methyl nonane	0.36	0.78	889	790
242	2-methyl naphthalene	0.73	1.18	568	561
243	2-methoxy-1-propanol	0.94	1.40	440	456
244	2-methyl-hexanal	1.26	1.68	309	361
245	2-methyl furan	2.42	3.46	77	54
246	2-methyl-trans-3-hexene	2.25	2.90	104	102
247	2-pyrrolidone	N/A	2.05	1169	240
248	2-nitropropane	0.07	0.11	1074	1126
249	2-methyoxy-1-propyl acetate	0.53	0.88	729	731
250	2-Propoxy-1-Propanol	N/A	2.23	1170	196
251	2-propyl cyclohexanone	0.62	1.13	654	584
252	Dipropylene Glycol Dibenzoate	N/A	0.42	1171	1006
253	2-propoxy-ethanol	1.49	2.35	234	170
254	dimethicone	N/A	0.08	1172	1135
255	3,3-diethyl pentane	0.61	1.07	659	618
256	3,3-dimethyl-1-pentene	1.91	2.72	146	122
257	3,3-dimethyl pentane	0.65	1.09	627	608
258	3,3-dimethyl hexane	0.61	1.12	666	595
259	3,3-dimethyl heptane	0.55	1.03	709	638
260	3,3-dimethyl octane	0.51	0.95	750	693
261	3,3-dimethyl-1-butene	2.04	3.00	125	89
262	3,4-diethyl hexane	0.43	0.81	823	767
263	3,4-dimethyl-1-pentene	1.75	2.48	182	150
264	3,4-dimethyl-cis-2-pentene	2.37	2.62	82	131
265	3,4-dimethyl hexane	0.79	1.31	532	495
266	3,4-dimethyl heptane	0.62	1.15	651	571
267	3,4-diethyl-2-hexene	1.33	1.86	288	304
268	3,4-dimethyl-hexyl acetate	0.47	0.89	779	727
269	3,4-dimethyl phenol	-0.10	0.19	1140	1095

270	3,5,7,9-tetramethyl-decyl acetate	0.24	0.50	1017	967
271	3,5,7-trimethyl-octyl acetate	0.34	0.65	905	873
272	3,5,7-trimethyl-nonyl acetate	0.32	0.60	927	904
273	3,5-diethyl heptane	0.53	0.92	733	712
274	3,5-dimethyl heptane	0.79	1.33	527	486
275	3,5-dimethyl-hexyl acetate	0.48	0.85	774	742
276	3,5-dimethyl-heptyl acetate	0.44	0.79	808	783
277	3,5-dimethyl phenol	N/A	0.19	1173	1096
278	3,6,8-trimethyl-nonyl acetate	0.30	0.59	952	914
279	2,6-diethyl octane	0.47	0.84	783	751
280	3,6-dimethyl decane	0.37	0.73	877	822
281	3,6-dimethyl undecane	0.34	0.68	906	855
282	3,6-dimethyl-heptyl acetate	0.39	0.74	864	815
283	3,6-dimethyl-octyl acetate	0.39	0.72	860	824
284	3,7-diethyl nonane	0.42	0.76	834	803
285	3,7-dimethyl dodecane	0.31	0.62	941	885
286	3,7-dimethyl tridecane	0.28	0.57	980	924
287	3,7-dimethyl-1-octanol	0.55	0.94	710	695
288	3,8-diethyl decane	0.27	0.59	981	912
289	3,9-diethyl undecane	0.26	0.55	1001	938
290	1,2,3-C10 trisubstituted benzenes	2.64	2.62	64	132
291	C10 3-alkenes	1.33	1.73	289	345
292	1,2,3-C11 trisubstituted benzenes	2.32	2.35	89	171
293	C11 3-alkenes	1.24	1.62	316	384
294	1,2,3-C12 trisubstituted benzenes	2.08	2.13	121	216
295	C12 3-alkenes	1.11	1.46	372	438
296	1,2,3-C13 trisubstituted benzenes	1.87	1.94	150	274
297	C13 3-alkenes	1.01	1.33	423	487
298	1,2,3-C14 trisubstituted benzenes	1.71	1.79	191	329
299	C14 3-alkenes	0.92	1.22	456	540
300	1,2,3-C15 trisubstituted benzenes	1.57	1.66	212	370
301	C15 3-alkenes	0.85	1.13	487	585
302	1,2,3-C16 trisubstituted benzenes	1.44	1.57	250	397
303	3-pentanol	0.77	1.23	542	532
304	3-octanol	1.04	1.59	409	394
305	3-octenes	1.85	2.39	155	160
306	3-nonenes	1.55	2.01	216	252
307	3-carene	1.11	1.61	371	390
308	3-(chloromethyl)-heptane	0.51	0.93	754	710
309	3-chloropropene	2.88	3.32	39	59
310	3-ethyl 2-methyl pentane	0.70	1.16	592	568

311	3-ethyl-6,7-dimethyl-nonyl acetate	0.33	0.60	921	901
312	3-ethyl-6-methyl-octyl acetate	0.36	0.66	893	863
313	3-ethylpentyl acetate	0.55	0.97	705	671
314	3-ethyl-hexyl acetate	0.46	0.82	793	765
315	3-ethyl-heptyl acetate	0.32	0.64	930	879
316	3-ethyl-2-pentene	2.74	3.05	47	82
317	3-ethyl pentane	0.98	1.59	431	395
318	3-ethyl heptane	0.57	1.00	693	650
319	3-ethoxy-1-propanol	1.56	2.27	214	192
320	Trifluoroethyl Methacrylate	N/A	1.91	1174	282
321	3-isopropyl-heptyl acetate	0.30	0.62	950	890
322	3-methyl-1,2-butadiene	3.24	4.87	22	9
323	3-methyl-1-butene	2.38	3.57	80	46
324	3-methyl-1-pentene	2.22	3.09	106	80
325	3-methyl-1-hexene	1.72	2.32	189	177
326	3-methyl-2-hexanone	1.20	1.82	341	314
327	3-methyl-2-isopropyl-1-butene	1.50	2.36	231	166
328	3-methyl butanoic acid	1.47	1.97	240	266
329	3-methyl-cis-3-hexene	2.74	3.12	48	76
330	3-methylbutanal (isovaleraldehyde)	1.66	2.12	196	222
331	3-methylpentyl acetate	0.59	1.06	677	626
332	3-methylhexyl acetate	0.46	0.83	794	758
333	3-methyl-heptyl acetate	0.34	0.67	904	861
334	3-methyl decane	0.33	0.71	917	838
335	3-methyl undecane	0.30	0.64	955	878
336	3-methyl dodecane	0.28	0.60	979	902
337	3-methyl tridecane	0.26	0.57	1000	927
338	3-methyl tetradecane	0.25	0.54	1014	946
339	3-methyl pentadecane	0.23	0.51	1028	961
340	3-methyl pentane	0.98	1.63	430	379
341	3-methyl hexane	0.82	1.46	504	439
342	3-methyl heptane	0.66	1.21	621	547
343	3-methyl octane	0.51	0.94	747	698
344	3-methyl nonane	0.39	0.78	865	789
345	3-methyl cyclopentene	1.82	2.40	163	157
346	3-methoxy-1-propanol	1.43	2.01	253	253
347	3-methoxy-1-butanol	1.25	1.78	310	333
348	3-methyl furan	2.27	3.16	101	70
349	3 methoxy-3 methyl-1-butanol	1.15	1.67	357	365
350	3-methyl-trans-3-hexene	2.69	3.12	54	77

351	4,4-dimethyl-1-pentene	1.21	1.64	329	374
352	4,4-dimethyl heptane	0.60	1.07	674	619
353	4,4-dimethyl octane	0.55	0.97	713	674
354	4,4-diethyl-3-oxahexane	0.85	1.36	484	471
355	4,5-dimethyl-hexyl acetate	0.37	0.70	875	839
356	4,5-dimethyl-heptyl acetate	0.41	0.75	844	810
357	4,6-dimethyl-heptyl acetate	0.37	0.71	876	836
358	4,6-dimethyl-octyl acetate	0.37	0.68	881	851
359	4,7,9-trimethyl-decyl acetate	0.24	0.49	1021	972
360	4,7-dimethyl-nonyl acetate	0.29	0.57	963	928
361	4,8-dimethyl tetradecane	0.25	0.53	1013	949
362	1,2,4-C10 trisubstituted benzenes	1.96	2.72	144	123
363	1,2,4-C11 trisubstituted benzenes	1.74	2.44	185	152
364	1,2,4-C12 trisubstituted benzenes	1.57	2.22	211	203
365	1,2,4-C13 trisubstituted benzenes	1.42	2.03	255	251
366	1,2,4-C14 trisubstituted benzenes	1.31	1.88	293	298
367	1,2,4-C15 trisubstituted benzenes	1.22	1.74	328	342
368	1,2,4-C16 trisubstituted benzenes	1.13	1.62	365	385
369	4-octanol	0.97	1.57	433	398
370	4-ethyl heptane	0.61	1.09	658	609
371	4-ethyl octane	0.44	0.86	804	739
372	4-methyl-1-pentene	1.99	2.84	136	112
373	4-methylpentyl acetate	0.43	0.79	816	780
374	4-methylhexyl acetate	0.42	0.78	830	788
375	4-methyl-heptyl acetate	0.33	0.64	922	874
376	4-methyloctyl acetate	0.31	0.63	946	883
377	4-methyl cyclohexene	1.54	2.11	218	226
378	4-methyl decane	0.35	0.73	901	821
379	4-methyl heptane	0.64	1.18	635	562
380	4-methyl octane	0.50	0.93	759	705
381	4-methyl nonane	0.43	0.85	814	748
382	4-nonene	1.53	2.01	222	254
383	4-propyl heptane	0.51	0.95	748	691
384	4-propyl cyclohexanone	0.86	1.34	482	482
385	4-vinyl phenol	-0.02	0.20	1119	1087
386	1,3,5-C10 trisubstituted benzenes	2.48	2.84	72	113
387	1,3,5-C11 trisubstituted benzenes	2.19	2.55	109	146
388	1,3,5-C12 trisubstituted benzenes	1.97	2.31	139	179
389	1,3,5-C13 trisubstituted benzenes	1.78	2.12	172	223
390	1,3,5-C14 trisubstituted benzenes	1.63	1.96	203	269
391	1,3,5-C15 trisubstituted benzenes	1.50	1.81	233	321

392	1,3,5-C16 trisubstituted benzenes	1.38	1.69	264	359
393	5-ethyl-3,6,8-trimethyl-nonyl acetate	0.33	0.59	915	909
394	5-methyl-2-hexanone	1.03	1.62	416	386
395	5-methylhexyl acetate	0.37	0.70	878	842
396	5-methyl-heptyl acetate	0.33	0.65	914	867
397	5-methyloctyl acetate	0.30	0.62	953	888
398	5-methyl undecane	0.32	0.66	931	862
399	5-methyl dodecane	0.28	0.61	971	893
400	6-methyl tridecane	0.27	0.58	986	916
401	6-methyl tetradecane	0.26	0.55	1003	939
402	7-methyl pentadecane	0.23	0.52	1029	959
403	acetic acid	0.27	0.41	985	1007
404	acetal (1,1-diethoxyethane)	1.34	2.12	279	224
405	acetaldehyde	2.03	2.56	126	143
406	acetone	0.12	0.18	1067	1102
407	acetylene	0.26	0.37	997	1025
408	acrolein	2.28	2.69	96	124
409	acrylonitrile	0.90	1.26	466	515
410	acrylic acid	3.23	3.61	26	44
411	adipic acid (hexanedioic acid)	1.20	1.67	339	366
412	1,2-propadiene (allene)	3.48	5.12	15	5
413	allylbenzene	-0.02	0.21	1120	1083
414	amyl acetate (n-pentyl acetate)	0.53	1.00	732	652
415	amyl cinnamal	0.89	1.29	467	502
416	a-methyl styrene	-0.02	0.21	1121	1084
417	2-amino-2-methyl-1-propanol	-0.54	-0.47	1148	1188
418	alpha-methyl tetrahydrofuran	1.74	2.76	184	118
419	anethol (p-propenyl-anisole)	0.00	0.05	1115	1150
420	alpha-pinene	1.33	1.85	287	307
421	Base ROG Mixture	1.16	0.54	352	944
422	Aromatic 100®	1.80	0.70	167	841
423	Regular mineral spirits	0.71	0.32	582	1042
424	Reduced Aromatics Mineral Spirits	0.53	0.27	730	1055
425	Dearomatized Alkanes, mixed, predominately C10-C12	0.42	0.24	833	1062
426	Synthetic isoparaffinic alkane mixture, predominately C10-C12	0.37	0.23	874	1067
427	a-terpineol	1.25	1.51	312	418
428	butyl benzyl phthalate	N/A	0.50	1175	968
429	C10 bicycloalkanes	0.52	0.98	738	659

430	C11 bicycloalkanes	0.43	0.83	821	757
431	C12 bicycloalkanes	0.40	0.76	855	801
432	C13 bicycloalkanes	0.36	0.70	892	840
433	C14 bicycloalkanes	0.33	0.65	920	869
434	C15 bicycloalkanes	0.31	0.62	933	889
435	C16 bicycloalkanes	0.29	0.58	959	919
436	C17 bicycloalkanes	0.28	0.54	977	942
437	C18 bicycloalkanes	0.26	0.51	996	962
438	C19 bicycloalkanes	0.25	0.49	1012	976
439	C20 bicycloalkanes	0.24	0.46	1025	986
440	C21 bicycloalkanes	0.22	0.44	1036	997
441	C22 bicycloalkanes	0.21	0.42	1043	1004
442	C8 bicycloalkanes	0.69	1.23	596	533
443	C9 bicycloalkanes	0.64	1.15	639	572
444	benzaldehyde	-0.79	-0.87	1153	1190
445	benzene	0.00	0.38	1103	1021
446	biacetyl	4.38	3.28	2	61
447	ß-methyl styrene	0.00	0.06	1117	1142
448	ß-phenethyl alcohol (2-phenyl ethyl alcohol)	1.09	1.69	384	360
449	beta-pinene	1.27	1.99	306	263
450	branched C10 alkanes	0.46	0.92	792	714
451	branched C11 alkanes	0.36	0.76	884	804
452	branched C12 alkanes	0.34	0.69	907	849
453	branched C13 alkanes	0.30	0.64	958	876
454	branched C14 alkanes	0.29	0.60	968	905
455	branched C15 alkanes	0.26	0.56	994	934
456	branched C16 alkanes	0.24	0.52	1020	952
457	branched C17 alkanes	0.23	0.49	1033	970
458	branched C18 alkanes	0.21	0.47	1044	984
459	branched C19 alkanes	0.20	0.44	1048	996
460	branched C20 alkanes	0.19	0.42	1053	1003
461	branched C21 alkanes	0.18	0.40	1056	1012
462	branched C22 alkanes	0.17	0.38	1061	1020
463	branched C5 alkanes	0.84	1.38	497	464
464	branched C6 alkanes	0.75	1.24	553	522
465	branched C7 alkanes	0.78	1.33	534	488
466	branched C8 alkanes	0.73	1.27	566	512
467	branched C9 alkanes	0.53	1.02	728	639
468	n-butyl acetate	0.46	0.88	795	732
469	n-butyl butyrate	0.52	0.94	737	697
470	butyl methacrylate	2.15	2.11	112	227

471	di-n-butyl ether	1.25	1.89	314	290
472	n-butoxy-2-propanol (propylene glycol n-butyl ether)	1.20	1.78	340	334
473	2-butoxy-ethanol	1.16	1.80	353	328
474	butyl propionate	0.44	0.85	807	745
475	butanoic acid	0.82	1.22	510	541
476	benzyl alcohol	1.23	1.91	318	283
477	hexafluoro-benzene	0.00	0.03	1112	1156
478	methoxybenzene; anisole	1.53	2.43	224	154
479	Unspeciated C10 Aromatics	1.75	0.67	181	859
480	butylbenzenes	1.43	2.16	251	213
481	C10 monosubstituted benzenes	0.74	1.14	558	577
482	C10 disubstituted benzenes	1.36	2.10	271	232
483	C10 trisubstituted benzenes	2.29	2.86	93	108
484	C10 tetrasubstituted benzenes	2.29	2.86	94	109
485	decyl cyclohexane	0.25	0.54	1005	943
486	2-decanone	0.42	0.81	837	769
487	C10 cyclic olefins or di-olefins	1.35	1.76	278	337
488	C10 alkenes	1.17	1.57	346	399
489	C10 terminal alkenes	0.88	1.29	470	503
490	C10 internal alkenes	1.32	1.73	290	346
491	C10 alkyl phenols	-0.08	0.16	1131	1115
492	C10 styrenes	-0.02	0.18	1118	1101
493	Unspeciated C10 Alkanes	0.44	0.26	809	1056
494	Unspeciated C11 Aromatics	1.79	0.65	170	870
495	pentyl benzenes	1.28	1.93	303	278
496	C11 monosubstituted benzenes	0.69	1.06	595	627
497	C11 disubstituted benzenes	1.23	1.90	319	289
498	C11 trisubstituted benzenes	2.13	2.57	115	139
499	C11 tetrasubstituted benzenes	2.03	2.57	128	140
500	C11 pentasubstituted benzenes	2.13	2.57	116	141
501	C11 cyclic olefins or di-olefins	1.25	1.65	311	372
502	C11 alkenes	1.01	1.35	422	475
503	C11 terminal alkenes	0.77	1.12	538	596
504	C11 internal alkenes	1.24	1.62	317	387
505	C11 alkyl phenols	-0.07	0.14	1129	1121
506	C11 tetralins or indanes	0.69	1.35	593	476
507	Unspeciated C11 Alkanes	0.37	0.22	879	1068
508	Unspeciated C12 Aromatics	1.49	0.56	235	931
509	hexyl benzenes	1.14	1.76	361	338
510	C12 monosubstituted benzenes	0.65	1.00	628	651
511	C12 disubstituted benzenes	1.10	1.73	380	347

512	C12 trisubstituted benzenes	1.83	2.33	159	173
513	C12 tetrasubstituted benzenes	1.83	2.33	160	174
514	C12 pentasubstituted benzenes	1.83	2.33	161	175
515	C12 hexasubstituted benzenes	1.83	2.33	162	176
516	cis-1,2-dichloroethene	0.64	0.84	640	752
517	C12 monosubstituted naphthalene	0.74	1.07	564	620
518	C12 disubstituted naphthalenes	1.16	1.63	350	380
519	C12 naphthalenes	0.94	1.46	443	440
520	C12 cyclic olefins or di-olefins	1.11	1.48	373	433
521	C12 alkenes	0.90	1.22	463	542
522	C12 terminal alkenes	0.68	0.97	600	678
523	C12 internal alkenes	1.11	1.46	374	441
524	C12 alkyl phenols	-0.07	0.13	1128	1123
525	C12 tetralins or indanes	0.69	1.24	599	523
526	Unspeciated C12 Alkanes	0.34	0.20	908	1086
527	Unspeciated C13 Aromatics	1.21	0.47	332	983
528	C13 monosubstituted benzenes	0.62	0.97	655	675
529	C13 disubstituted benzenes	1.02	1.60	417	392
530	C13 trisubstituted benzenes	1.66	2.13	197	217
531	cis-1,3-dichloropropene	1.06	1.56	404	402
532	C13 monosubstituted naphthalene	0.61	0.98	662	660
533	C13 disubstituted naphthalenes	1.07	1.49	402	426
534	C13 trisubstituted naphthalenes	1.07	1.49	403	427
535	C13 naphthalenes	0.86	1.34	477	483
536	C13 cyclic olefins or di-olefins	1.00	1.35	424	477
537	C13 alkenes	0.82	1.11	508	602
538	C13 terminal alkenes	0.62	0.88	650	730
539	C13 internal alkenes	0.99	1.33	428	489
540	cis-1,3-pentadiene	3.87	5.73	7	2
541	C13 tetralins or indanes	0.63	1.14	644	578
542	Unspeciated C13 Alkanes	0.31	0.19	935	1098
543	Unspeciated C14 Aromatics	0.93	0.39	450	1016
544	C14 monosubstituted benzenes	0.59	0.92	681	716
545	C14 disubstituted benzenes	0.94	1.48	448	434
546	C14 trisubstituted benzenes	1.58	1.97	207	267
547	C14 naphthalenes	0.80	1.24	525	524
548	C14 cyclic olefins or di-olefins	0.93	1.23	451	534
549	C14 alkenes	0.75	1.01	552	644
550	C14 terminal alkenes	0.56	0.81	698	775
551	C14 internal alkenes	0.92	1.22	457	543

552	C14 tetralins or indanes	0.59	1.05	682	630
553	Unspeciated C14 Alkanes	0.29	0.18	962	1104
554	Unspeciated C15 Aromatics	0.77	0.34	543	1037
555	C15 monosubstituted benzenes	0.56	0.86	699	740
556	C15 disubstituted benzenes	0.86	1.38	481	465
557	C15 trisubstituted benzenes	1.40	1.82	260	315
558	C15 naphthalenes	0.74	1.15	556	573
559	C15 cyclic olefins or di-olefins	0.86	1.14	480	579
560	C15 alkenes	0.69	0.94	598	699
561	C15 terminal alkenes	0.52	0.75	740	808
562	C15 internal alkenes	0.85	1.13	488	586
563	C15 tetralins or indanes	0.54	0.98	717	663
564	Unspeciated C15 Alkanes	0.28	0.17	978	1111
565	Unspeciated C16 Aromatics	0.67	0.30	607	1046
566	C16 monosubstituted benzenes	0.53	0.81	726	768
567	C16 disubstituted benzenes	0.80	1.29	520	504
568	C16 trisubstituted benzenes	1.34	1.70	280	355
569	C16 naphthalenes	0.69	1.08	597	613
570	C16 tetralins or indanes	0.47	0.92	784	717
571	Unspeciated C16 Alkanes	0.26	0.16	1004	1114
572	C17 monosubstituted benzenes	0.50	0.76	758	802
573	C17 disubstituted benzenes	0.76	1.21	550	548
574	C17 trisubstituted benzenes	1.22	1.60	325	393
575	C17 naphthalenes	0.65	1.01	631	645
576	C17 tetralins or indanes	0.44	0.86	802	741
577	Unspeciated C17 Alkanes	0.24	0.15	1019	1119
578	C18 monosubstituted benzenes	0.47	0.72	782	825
579	C18 disubstituted benzenes	0.71	1.14	585	580
580	C18 trisubstituted benzenes	1.15	1.50	354	420
581	C18 naphthalenes	0.61	0.95	664	690
582	C18 tetralins or indanes	0.45	0.81	797	772
583	Unspeciated C18 Alkanes	0.23	0.14	1032	1122
584	C19 monosubstituted benzenes	0.45	0.68	800	853
585	C19 disubstituted benzenes	0.67	1.08	611	614
586	C19 trisubstituted benzenes	1.09	1.42	386	452
587	C19 naphthalenes	0.58	0.90	688	722
588	C19 tetralins or indanes	0.42	0.77	826	799
589	C20 monosubstituted benzenes	0.42	0.65	825	871
590	C20 disubstituted benzenes	0.64	1.02	636	640
591	C20 trisubstituted benzenes	1.04	1.35	412	478
592	C20 naphthalenes	0.55	0.85	711	743

593	C20 tetralins or indanes	0.40	0.73	846	823
594	C21 monosubstituted benzenes	0.40	0.62	849	891
595	C21 disubstituted benzenes	0.61	0.97	668	667
596	C21 trisubstituted benzenes	1.02	1.28	418	508
597	C21 naphthalenes	0.51	0.81	753	773
598	C21 tetralins or indanes	0.38	0.69	867	848
599	C22 monosubstituted benzenes	0.38	0.59	866	910
600	C22 disubstituted benzenes	0.58	0.93	689	706
601	C22 trisubstituted benzenes	0.94	1.23	442	535
602	C22 naphthalenes	0.50	0.77	762	795
603	C22 tetralins or indanes	0.37	0.66	882	864
604	ethyl benzene	0.84	1.39	494	459
605	ethyl bromide	0.07	0.10	1073	1131
606	cis-2-butene	3.96	4.82	5	11
607	cis-2-hexene	2.65	3.73	60	37
608	cis-2-heptene	2.33	3.15	87	72
609	ethyl chloride	0.16	0.22	1064	1069
610	cis-2-pentene	3.23	4.71	24	18
611	n-propyl bromide	0.20	0.34	1051	1035
612	cis-3-hexene	2.71	3.52	52	51
613	cis-3-heptene	2.28	2.93	98	98
614	propyl cyclohexane	0.64	1.15	637	574
615	n-propyl formate	0.44	0.81	813	771
616	cis-3-methyl-2-pentene	3.31	3.40	21	57
617	cis-3-methyl-2-hexene	2.66	3.03	57	86
618	1-nitropropane	0.14	0.25	1065	1058
619	4,4-dimethyl-cis-2-pentene	2.09	2.98	120	94
620	n-butyl bromide	0.41	0.61	845	892
621	cis-4-octene	1.51	2.04	228	249
622	1-chlorobutane	0.55	0.83	716	756
623	butyl cyclohexane	0.49	0.96	764	686
624	n-butyl formate	0.47	0.87	787	735
625	cis 4-methyl-2-pentene	2.55	3.65	66	42
626	C4 alkenes	3.59	4.87	12	10
627	C4 terminal alkenes	3.21	4.75	28	16
628	C4 internal alkenes	4.06	4.79	4	12
629	C4 aldehydes	2.01	2.63	133	128
630	cis-5-decene	1.15	1.55	355	408
631	pentyl cyclohexane	0.41	0.82	840	762
632	di-n-pentyl ether	1.17	1.70	347	356
633	pentyl alcohol	1.23	1.89	323	291

634	C5 alkenes	2.84	4.18	41	27
635	C5 terminal alkenes	2.47	3.54	74	50
636	C5 internal alkenes	3.23	4.68	25	20
637	n-pentyl propionate	0.41	0.83	842	759
638	C5 aldehydes	1.72	2.27	188	193
639	hexyl acetates	0.46	0.85	791	744
640	hexyl cyclohexane	0.34	0.72	912	826
641	1,2-dihydroxyhexane	0.93	1.53	449	413
642	C6 cyclic olefins or di-olefins	2.81	3.80	44	35
643	C6 alkenes	2.25	3.21	105	67
644	C6 terminal alkenes	2.05	3.21	124	68
645	C6 internal alkenes	2.65	3.70	63	40
646	C6 aldehydes	1.48	1.94	238	275
647	Unspeciated C6 Alkanes	0.73	0.40	573	1011
648	heptyl cyclohexane	0.31	0.65	942	868
649	2-heptanone	1.09	1.71	389	352
650	C7 cyclic olefins or di-olefins	2.38	3.21	81	69
651	C7 alkenes	1.95	2.61	145	133
652	C7 terminal alkenes	1.57	2.18	210	211
653	C7 internal alkenes	2.28	2.92	99	99
654	C7 aldehydes	1.27	1.66	304	371
655	Unspeciated C7 Alkanes	0.72	0.38	576	1019
656	Unspeciated C8 Aromatics	1.76	0.71	179	835
657	isomers of ethylbenzene	1.51	2.40	230	158
658	C8 disubstituted benzenes	1.79	2.60	169	135
659	octyl cyclohexane	0.29	0.61	967	894
660	2-octanone	0.67	1.19	608	557
661	C8 cyclic olefins or di-olefins	1.58	2.09	208	233
662	C8 alkenes	1.40	1.92	261	281
663	C8 terminal alkenes	1.27	1.77	307	336
664	C8 internal alkenes	1.53	2.05	225	241
665	C8 alkyl phenols	-0.10	0.19	1141	1097
666	C8 aldehydes	1.11	1.43	375	448
667	Unspeciated C8 Alkanes	0.66	0.35	624	1031
668	Unspeciated C9 Aromatics	1.97	0.75	138	812
669	isomers of propyl benzene	1.54	2.29	219	185
670	C9 monosubstituted benzenes	0.63	1.07	648	621
671	C9 disubstituted benzenes	1.37	2.21	268	206
672	C9 trisubstituted benzenes	2.66	3.25	58	62
673	nonyl cyclohexane	0.27	0.58	988	921
674	2-nonanone	0.53	0.97	723	668

675	C9 cyclic olefins or di-olefins	1.55	2.04	215	250
676	C9 alkenes	1.29	1.73	301	348
677	C9 terminal alkenes	1.04	1.49	408	428
678	C9 internal alkenes	1.55	2.01	217	255
679	C9 alkyl phenols	-0.09	0.17	1135	1110
680	C9 styrenes	-0.02	0.21	1122	1085
681	Unspeciated C9 Alkanes	0.50	0.29	761	1047
682	camphor	0.24	0.49	1018	975
683	cyclobutanone	0.33	0.59	919	913
684	cyclopentanone	0.62	1.13	656	587
685	cyclopentanol	0.81	1.30	518	496
686	cyclohexanone	0.67	1.24	617	525
687	cyclohexanol	1.10	1.82	377	316
688	benzotrifluoride	0.07	0.15	1072	1120
689	methyl chloride	0.02	0.02	1090	1157
690	nitromethane	0.04	0.06	1084	1145
691	chloroform	0.01	0.02	1092	1159
692	Cinnamic alcohol	0.00	0.06	1116	1146
693	cinnamic aldehyde	1.37	1.98	267	265
694	citronellol (3,7-dimethy-6-octen-1-ol)	1.57	1.71	213	353
695	p-dichlorobenzene	0.00	0.10	1109	1129
696	2-(chloro-methyl)-3-chloro-propene	1.69	2.25	194	195
697	dichloromethane	0.03	0.03	1089	1152
698	trichloroethylene	0.31	0.44	939	994
699	perchloroethylene	0.02	0.03	1091	1155
700	chloroacetone	1.86	1.86	154	305
701	monochlorobenzene	0.00	0.18	1108	1105
702	chloroacetaldehyde	2.58	2.38	65	164
703	vinyl chloride	1.29	1.89	300	292
704	TLEV Exhaust -- CNG	0.31	0.15	936	1116
705	carbon monoxide	0.03	0.06	1085	1143
706	C7 alkyl phenols	-0.11	0.22	1142	1070
707	crotonaldehyde	2.53	3.22	68	64
708	2-ethoxyethyl acetate	0.83	1.38	503	466
709	C10 cycloalkanes	0.51	0.97	746	676
710	C11 cycloalkanes	0.42	0.82	827	766
711	C12 cycloalkanes	0.38	0.76	873	805
712	C13 cycloalkanes	0.35	0.70	897	847
713	C14 cycloalkanes	0.33	0.65	924	872
714	C15 cycloalkanes	0.31	0.61	937	895

715	C16 cycloalkanes	0.28	0.56	974	929
716	C17 cycloalkanes	0.26	0.53	992	950
717	C18 cycloalkanes	0.25	0.50	1008	966
718	C19 cycloalkanes	0.24	0.48	1024	980
719	C20 cycloalkanes	0.22	0.45	1035	991
720	C21 cycloalkanes	0.21	0.43	1041	998
721	C22 cycloalkanes	0.20	0.41	1046	1008
722	cyclopropane	0.06	0.09	1075	1132
723	cyclobutane	0.72	1.24	578	526
724	cyclopentane	1.10	1.88	378	299
725	cyclohexane	0.81	1.52	515	414
726	C6 cycloalkanes	0.81	1.52	516	415
727	cycloheptane	0.78	1.49	536	429
728	C7 cycloalkanes	0.83	1.39	501	460
729	cyclooctane	0.74	1.17	555	565
730	C8 cycloalkanes	0.61	1.32	672	492
731	C9 cycloalkanes	0.63	1.13	649	588
732	cyclohexene	1.79	2.51	168	149
733	cyclopentadiene	2.18	2.86	110	110
734	cyclopentene	2.11	2.78	117	117
735	Exxon Exxol® D95 Fluid	0.31	0.19	945	1100
736	dimethyl sebacate	0.20	0.43	1047	1000
737	dimethyl succinate	0.13	0.21	1066	1075
738	dimethyl glutarate	0.19	0.35	1054	1032
739	dimethyl adipate	0.70	1.07	589	622
740	glycol ether DPnB (dipropylene glycol n-butyl ether) (1-[2-butoxy-1-methylethoxy]-2-propanol)	0.91	1.36	459	472
741	dibutyl phthalate	0.38	0.56	869	936
742	3-pentanone	0.56	0.97	696	672
743	dimethyl phthalate	N/A	0.78	1176	787
744	diethylenetriamine	N/A	2.28	1177	189
745	diethylene glycol	1.49	2.36	236	167
746	diethyl phthalate	0.45	0.68	801	854
747	diethylene glycol mono(2-ethylhexyl) ether	0.72	1.12	577	597
748	2-(2-butoxyethoxy)-ethanol	1.02	1.56	419	403
749	2-(2-butoxyethoxy) ethyl acetate	0.65	1.04	626	634
750	2-(2-ethoxyethoxy) ethanol	1.35	2.30	274	183
751	2-(2-ethoxyethoxy) ethyl acetate	0.74	1.30	557	497
752	2-(2-hexyloxyethoxy) ethanol	0.92	1.35	458	479
753	2-(2-propoxyethoxy) ethanol	1.24	1.89	315	293

754	diacetone alcohol	0.27	0.50	984	969
755	di-isobutyl ketone (2,6-dimethyl-4-heptanone)	1.08	1.43	394	449
756	Dibutyl Adipate	N/A	0.56	1178	930
757	Diethylethanolamine	N/A	2.00	1179	260
758	di-isopropyl ketone	0.63	1.10	646	607
759	diisopropyl adipate	0.48	0.63	777	882
760	diisopropyl carbonate	0.45	0.70	798	843
761	Diisopropylamine	N/A	-0.90	1180	1191
762	d-limonene	1.42	2.09	257	234
763	dimethylaminoethanol	2.01	3.04	131	84
764	dimethyl amine	1.87	3.61	151	45
765	dimethyl carbonate	0.04	0.07	1077	1137
766	dimethyl naphthalenes	1.16	1.63	351	381
767	dimethyl sulfoxide (DMSO)	1.85	3.29	156	60
768	dihydroxy acetone	1.12	1.48	368	435
769	dipropylene glycol ethyl ether	1.12	1.81	367	322
770	dipropylene glycol methyl ether acetate isomers	0.76	1.25	546	518
771	dipropylene glycol methyl ether acetate isomer #1	0.76	1.23	547	536
772	dipropylene glycol methyl ether acetate isomer #2	0.78	1.27	535	513
773	dipropylene glycol n-propyl ether isomer #1	1.00	1.49	426	430
774	dipropylene glycol methyl ether: 2-(2-methoxypropoxy)-1-propanol	1.15	2.00	356	261
775	dipropylene glycol isomer (1-[2-hydroxypropyl]-2-propanol)	1.21	1.87	330	300
776	dipropylene glycol methyl ether: 1-methoxy-2-(2-hydroxypropoxy)-propane	1.10	1.87	382	301
777	ethyl 3-ethoxy propionate	1.09	1.57	385	400
778	TLEV Exhaust -- E-85	1.02	0.72	420	827
779	ethylene glycol diethyl ether; 1,2-diethoxyethane	1.30	2.22	297	204
780	2-(2-ethylhexyloxy) ethanol	0.82	1.27	507	514
781	2-n-hexyloxyethanol	1.07	1.79	400	330
782	Ethylene Glycol Monohexyl Ether	N/A	1.63	1181	382
783	2-phenoxyethanol; ethylene glycol phenyl ether	1.23	1.96	320	270
784	ethyl n-butyl ether	1.50	2.40	232	159
785	ethyl acetate	0.33	0.57	918	923

786	ethyl acrylate	2.16	3.06	111	81
787	ethyl acetylene	1.84	2.30	158	184
788	ethyl amine	2.72	4.47	50	25
789	ethyl tert-butyl ether	0.85	1.37	489	470
790	ethyl butyrate	0.57	0.92	690	713
791	ethyl cyclopentane	0.82	1.52	509	416
792	ethyl cyclohexane	0.69	1.32	594	493
793	ethyl formate	0.27	0.46	989	988
794	ethylene glycol diacetate	0.35	0.67	895	858
795	ethylene glycol	1.34	1.89	283	294
796	ethane	0.18	0.29	1059	1048
797	ethyl cyanoacrylate	N/A	1.81	1182	323
798	ethene	2.88	3.94	38	33
799	ethyl lactate	0.85	1.20	491	553
800	ethyl methacrylate	3.06	2.90	33	103
801	Ethyl Nonafluorobutyl Ether	N/A	0.01	1183	1171
802	nitroethane	0.04	0.07	1081	1138
803	1-ethoxy-2-propanol	1.35	2.11	277	228
804	diethyl ether	1.46	2.31	244	180
805	2-ethoxy-ethanol	1.39	2.19	263	208
806	ethanol	0.79	1.38	531	467
807	diethanol-amine	1.06	1.72	405	351
808	triethanolamine	1.32	1.93	292	279
809	ethanolamine	2.66	4.58	56	24
810	ethyl isopropyl ether	1.34	2.01	285	256
811	ethylene oxide	0.03	0.05	1088	1151
812	ethyl propionate	0.39	0.70	858	845
813	formic acid	0.04	0.07	1082	1139
814	formaldehyde	1.77	1.42	176	453
815	furan	2.75	3.95	46	32
816	gamma-butyrolactone	0.54	0.96	718	683
817	geraniol	1.43	1.75	254	341
818	glutaraldehyde	1.48	1.91	239	284
819	glycolic acid	0.80	1.09	522	610
820	glyceryl triacetate	0.28	0.51	973	960
821	glycerol	1.14	1.86	360	306
822	glyoxal	2.45	1.81	75	324
823	CARB Hydrocarbon Bin 1	0.79	0.42	529	1005
824	CARB Hydrocarbon Bin 2	0.72	0.39	579	1015
825	CARB Hydrocarbon Bin 3	0.89	0.47	468	982
826	CARB Hydrocarbon Bin 4	0.78	0.41	533	1010

827	CARB Hydrocarbon Bin 5	0.80	0.39	523	1018
828	CARB Hydrocarbon Bin 6	0.59	0.32	679	1041
829	CARB Hydrocarbon Bin 7	0.53	0.29	725	1049
830	CARB Hydrocarbon Bin 8	0.65	0.37	629	1028
831	CARB Hydrocarbon Bin 9	0.67	0.35	610	1033
832	CARB Hydrocarbon Bin 10	0.81	0.37	513	1023
833	CARB Hydrocarbon Bin 11	0.36	0.21	891	1077
834	CARB Hydrocarbon Bin 12	0.32	0.20	925	1088
835	CARB Hydrocarbon Bin 13	0.41	0.23	839	1065
836	CARB Hydrocarbon Bin 14	0.44	0.23	806	1064
837	CARB Hydrocarbon Bin 15	0.64	0.27	641	1053
838	CARB Hydrocarbon Bin 16	0.27	0.17	987	1112
839	CARB Hydrocarbon Bin 17	0.25	0.16	1009	1113
840	CARB Hydrocarbon Bin 18	0.31	0.18	947	1106
841	CARB Hydrocarbon Bin 19	0.30	0.18	954	1107
842	CARB Hydrocarbon Bin 20	0.40	0.20	854	1090
843	CARB Hydrocarbon Bin 21	1.76	0.71	177	834
844	CARB Hydrocarbon Bin 22	1.88	0.72	149	828
845	CARB Hydrocarbon Bin 23	1.71	0.64	190	875
846	CARB Hydrocarbon Bin 24	0.93	0.39	455	1017
847	1,1,1,2-tetrafluoroethane; HFC-134a	0.00	0.00	1101	1179
848	1,1-difluoroethane; HFC-152a	0.01	0.02	1094	1158
849	1,1,1,3,3-pentafluoropropane	0.00	0.00	1104	1180
850	methoxy-perfluoro-n-butane	0.00	0.00	1106	1182
851	ethoxy-perfluoro-isobutane	0.00	0.01	1097	1172
852	ethoxy-perfluoro-n-butane	0.00	0.01	1098	1175
853	hydroxy acetone	0.87	1.18	472	563
854	hydroxyl-methacrolein	1.91	2.57	147	142
855	hydroxypropyl acrylate	1.62	2.36	206	168
856	hexyl cinnamal	0.84	1.21	496	549
857	hydroxycitronella	0.90	1.19	465	558
858	cis-hydrindane; bicyclo[4.3.0]nonane	0.54	1.05	720	631
859	isoamyl acetate (3-methyl-butyl acetate)	0.54	1.01	722	646
860	isoamyl alcohol (3-methyl-1-butanol)	1.29	1.85	302	308
861	2,6,8-trimethyl-4-nonanone (isobutyl heptyl ketone)	0.71	1.02	581	641
862	di-isobutyl ether	0.60	1.17	675	566
863	isobutyl acetate	0.39	0.66	857	865

864	isobutyl acrylate	1.41	2.21	258	207
865	isobutyl isobutyrate	0.34	0.60	910	903
866	isobutyl methacrylate	2.14	2.26	114	194
867	isobutyric acid	0.53	0.78	734	785
868	8-methyl-1-nonanol (isodecyl alcohol)	0.50	0.89	760	728
869	isopropyl benzene (cumene)	0.68	1.15	601	575
870	isopropyl alcohol	0.32	0.52	926	955
871	triisopropanolamine	1.03	1.55	415	409
872	isobutyl cyclohexane; (2-methylpropyl) cyclohexane	0.49	0.96	765	687
873	isobutyl alcohol	1.06	1.65	406	373
874	isoamyl isobutyrate	0.40	0.77	851	800
875	indane	0.86	1.68	478	362
876	indene	-0.02	0.21	1123	1079
877	isopropyl acetate	0.51	0.77	755	794
878	isopropyl amine	2.91	5.02	35	7
879	isopropyl cyclopropane	0.70	1.25	591	519
880	isopropyl formate	0.23	0.39	1026	1013
881	diisopropyl ether	1.18	1.83	345	312
882	isobutene	1.63	2.07	204	237
883	isododecane	N/A	0.62	1184	886
884	isohexadecane	N/A	0.54	1185	947
885	Exxon Isopar® M Fluid	0.30	0.18	956	1103
886	isoprene (2-methyl-1,3-butadiene)	3.13	4.65	31	22
887	lumped C5+ unsaturated carbonyl species	1.81	2.61	166	134
888	isophorone (3,5,5-trimethyl-2-cyclohexenone)	1.31	1.89	296	295
889	Kerosene	0.64	0.28	643	1052
890	C10 ketones	0.42	0.81	838	770
891	C10 cyclic ketones	0.42	0.79	829	782
892	C5 ketones	1.23	1.81	321	325
893	C5 cyclic ketones	0.61	1.13	671	589
894	C6 ketones	1.38	2.05	265	242
895	C6 cyclic ketones	0.67	1.24	618	527
896	C7 ketones	1.09	1.71	390	354
897	C7 cyclic ketones	0.58	1.09	685	611
898	C8 ketones	0.67	1.19	609	559
899	C8 cyclic ketones	0.52	0.97	742	679
900	C9 ketones	0.53	0.97	724	669

901	C9 cyclic ketones	0.47	0.87	788	736
902	lauryl pyrrolidone	0.44	0.69	811	850
903	linalool	1.47	1.82	241	317
904	TLEV Exhaust -- LPG	0.73	0.35	572	1030
905	TLEV Exhaust -- M-85	0.45	0.37	799	1027
906	methyl cis-9-pentadecenoate	0.70	0.93	586	700
907	methacrylic acid	4.48	4.17	1	28
908	malic acid	2.03	1.99	130	264
909	methyl amyl acetate (4-methyl-2-pentanol acetate)	0.64	1.00	633	655
910	2-methyl-3-butene-2-ol	1.70	2.55	192	147
911	m-C10 disubstituted benzenes	1.65	2.23	198	197
912	m-C11 disubstituted benzenes	1.45	2.01	245	257
913	m-C12 disubstituted benzenes	1.31	1.82	294	318
914	m-C13 disubstituted benzenes	1.19	1.68	342	363
915	m-C14 disubstituted benzenes	1.09	1.55	387	410
916	m-C15 disubstituted benzenes	1.01	1.44	421	446
917	m-C16 disubstituted benzenes	0.93	1.34	452	484
918	1-methyl-3-n-propyl benzene	1.65	2.23	199	198
919	1-methyl-3-n-butyl benzene	1.45	2.01	246	258
920	m-cresol	-0.11	0.22	1143	1071
921	2-methoxyethyl acetate	0.62	0.98	657	665
922	m-cymene; 1-methyl-3-(1-methylethyl) benzene	1.65	2.23	200	199
923	m-diethyl benzene	1.65	2.23	201	200
924	methylene diphenylene diisocyanate	-0.09	0.21	1132	1080
925	3-isopropyl cumene; 1,3-di-isopropyl benzene	1.31	1.82	295	319
926	methyl acetate	0.05	0.09	1076	1133
927	methyl acrylate	2.83	3.00	43	90
928	methyl acetylene	1.86	2.36	153	169
929	methylamine	3.74	6.27	11	1
930	methyl bromide	0.01	0.01	1095	1164
931	methyl butyrate	0.50	0.76	756	806
932	methyl decanoate	0.26	0.54	993	945
933	methyl undecanoate	0.25	0.52	1007	953
934	methyl tridecanoate	0.23	0.48	1034	981
935	methyl pentadecanoate	0.23	0.48	1027	977
936	methyl pentanoate; methyl valerate	0.51	0.86	751	738
937	methyl hexanoate	0.51	0.91	749	718

938	methyl heptanoate	0.43	0.77	820	792
939	methyl octanoate	0.35	0.67	900	860
940	methyl nonanoate	0.29	0.58	961	918
941	methyl cyclopentane	0.94	1.64	445	375
942	methyl cyclohexane	0.74	1.39	563	461
943	methyl formate	0.04	0.07	1078	1140
944	Methylene Glycol	N/A	1.89	1186	296
945	methyl glyoxal	3.43	2.58	18	137
946	methyl isobutyrate	0.31	0.58	934	922
947	methyl indanes	0.77	1.50	541	421
948	methyl ethyl ketone	0.55	0.84	704	754
949	methyl lactate	0.81	1.11	517	603
950	methyl dodecanoate (methyl laurate)	0.24	0.51	1022	964
951	Methacyrlate Monomer	N/A	3.56	1187	47
952	methyl methacrylate	3.79	3.56	9	48
953	methyl myristate (methyl tetradecanoate)	0.22	0.46	1038	989
954	methyl naphthalenes	0.73	1.18	569	564
955	menthol	0.66	1.11	623	604
956	methoxy-acetone	0.86	1.23	474	537
957	1-methoxy-2-propanol	1.21	1.87	331	302
958	2-methoxy ethanol	1.08	1.59	395	396
959	methanol	0.25	0.37	1010	1024
960	dimethyl ether	0.52	0.82	745	761
961	methoxypropanol acetate	0.86	1.40	475	457
962	methylparaben (4-Hydroxybenzoic acid, methyl ester)	-0.08	0.15	1130	1117
963	methyl propionate	0.29	0.46	969	987
964	methyl pivalate	0.18	0.34	1058	1034
965	methacrolein	1.76	2.18	178	212
966	methane	0.01	0.01	1096	1168
967	dimethoxy methane	0.76	1.36	544	473
968	m-ethyl toluene	1.70	2.39	193	161
969	4-methyl-2-pentanone	1.40	1.95	262	272
970	4-methyl-2-pentanol (methyl isobutyl carbinol)	1.04	1.68	411	364
971	methyl isopropyl carbonate	0.30	0.48	949	978
972	methyl isopropyl ketone	0.74	1.12	562	598
973	methyl linoleate (methyl cis,cis-9,12-octadecadienoate)	0.68	0.89	605	726
974	methyl linolenate (methyl	0.83	1.04	502	635

	cis,cis,cis-9,12,15-octadecatrienoate)				
975	methyl n-butyl ether	1.45	2.29	247	186
976	methyl n-butyl ketone	1.38	2.05	266	243
977	m-nitrotoluene	0.10	0.21	1069	1082
978	2-(2-methoxyethoxy) ethanol	1.36	2.31	269	181
979	2-pentanone	1.23	1.81	322	326
980	morpholine	1.08	2.05	397	244
981	composite mineral spirit (naphthas or lactol spirits) (CARB Profile ID 802)	0.76	0.33	548	1038
982	Safety-Kleen Mineral Spirits "A" (Type I-B, 91% Alkanes)	0.52	0.27	741	1054
983	Safety-Kleen Mineral Spirits "B" (Type II-C)	0.34	0.21	911	1081
984	Safety-Kleen Mineral Spirits "C" (Type II-C)	0.34	0.21	909	1078
985	thinning solvent/mineral spirits (Cal Poly SLO 1996)	0.79	0.37	526	1026
986	Safety-Kleen Mineral Spirits "D" (Type II-C)	0.36	0.21	888	1076
987	methyl tert-amyl ether (TAME)	0.83	1.26	499	516
988	methyl t-butyl ether	0.40	0.68	852	852
989	methyl tert-butyl ketone	0.30	0.45	948	993
990	methylvinyl ketone	2.95	3.72	34	38
991	m-xylene	2.22	2.82	107	114
992	naphthalene	0.84	1.29	498	505
993	n-butyl acrylate	1.52	2.22	227	205
994	n-decane	0.36	0.73	887	820
995	n-undecane	0.32	0.68	928	856
996	n-dodecane	0.29	0.62	966	887
997	n-tridecane	0.27	0.59	983	906
998	n-tetradecane	0.26	0.58	991	920
999	n-pentadecane	0.24	0.56	1016	937
1000	n-C16	0.25	0.54	1015	948
1001	n-C17	0.23	0.50	1030	965
1002	n-C18	0.22	0.48	1037	979
1003	n-C19	0.21	0.45	1045	992
1004	n-C20	0.20	0.43	1050	999
1005	n-C21	0.19	0.41	1055	1009
1006	n-C22	0.17	0.39	1062	1014
1007	n-propyl benzene	0.63	1.07	645	623
1008	n-propyl alcohol	1.12	1.97	369	268

1009	n-butane	0.67	1.16	615	569
1010	n-butyl benzene	0.72	1.14	574	581
1011	n-butyl alcohol	1.25	2.05	313	245
1012	n-pentane	0.73	1.39	565	462
1013	n-pentyl benzene	0.68	1.06	603	628
1014	n-hexane	0.71	1.34	583	485
1015	n-hexyl acetate	0.40	0.82	853	763
1016	n-heptane	0.56	1.15	695	576
1017	n-heptyl acetate	0.33	0.68	913	857
1018	n-octane	0.46	0.93	789	704
1019	n-octyl acetate	0.29	0.61	960	897
1020	n-nonane	0.40	0.82	847	764
1021	n-nonyl acetate	0.26	0.57	998	926
1022	n-methyl-2-pyrrolidone	1.10	1.76	383	339
1023	nitrobenzene	0.00	0.03	1111	1154
1024	m-Aminophenol	N/A	0.21	1188	1074
1025	Oxo-Decyl Acetate	0.35	0.24	903	1063
1026	o-C10 disubstituted benzenes	1.34	2.13	281	218
1027	o-C11 disubstituted benzenes	1.19	1.91	343	285
1028	Oxo-Dodecyl Acetate	0.30	0.20	951	1089
1029	o-C12 disubstituted benzenes	1.09	1.74	391	343
1030	Oxo-Tridecyl Acetate	0.29	0.19	970	1099
1031	o-C13 disubstituted benzenes	0.99	1.61	427	391
1032	o-C14 disubstituted benzenes	0.91	1.48	460	436
1033	o-C15 disubstituted benzenes	0.84	1.38	493	468
1034	o-C16 disubstituted benzenes	0.79	1.28	530	509
1035	1-methyl-2-n-propyl benzene	1.35	2.13	275	219
1036	1-butyl-2-methyl benzene	1.20	1.91	335	286
1037	Oxo-Hexyl Acetate	0.48	0.34	775	1036
1038	Oxo-Heptyl Acetate	0.42	0.30	835	1045
1039	Oxo-Octyl Acetate	0.41	0.28	841	1051
1040	Oxo-Nonyl Acetate	0.36	0.25	890	1059
1041	o-dichlorobenzene	0.00	0.10	1110	1130
1042	o-cresol	-0.11	0.22	1144	1072
1043	o-cymene; 1-methyl-2-(1-methylethyl) benzene	1.34	2.13	282	220
1044	1,3-di-n-propyl benzene	1.08	1.74	398	344
1045	o-diethyl benzene	1.35	2.13	276	221
1046	1-ethyl-2-n-propyl benzene	1.20	1.91	336	287
1047	o-ethyl toluene	1.35	2.05	272	246
1048	Hydroxyethyl Methacrylate	N/A	0.91	1189	719
1049	o-tert-butyl toluene; 1-(1,1-	1.20	1.91	337	288

	dimethylethyl)-2-methyl benzene				
1050	o-xylene	1.75	2.68	183	125
1051	peroxyacetic acid	0.21	0.33	1042	1039
1052	propylene carbonate	0.18	0.28	1060	1050
1053	p-C10 disubstituted benzenes	1.13	1.85	362	309
1054	p-C11 disubstituted benzenes	1.04	1.70	413	357
1055	p-C12 disubstituted benzenes	0.94	1.56	446	404
1056	p-C13 disubstituted benzenes	0.86	1.43	476	450
1057	p-C14 disubstituted benzenes	0.81	1.32	519	494
1058	p-C15 disubstituted benzenes	0.74	1.21	554	550
1059	p-C16 disubstituted benzenes	0.71	1.12	584	599
1060	1-methyl-4-n-propyl benzene	1.13	1.85	363	310
1061	p-trifluoromethyl-chloro-benzene	0.03	0.06	1087	1141
1062	p-cresol	-0.11	0.22	1145	1073
1063	1-methyl-4-isopropyl benzene (p-cymene)	1.08	1.79	396	331
1064	p-diethyl benzene	1.13	1.85	364	311
1065	1,4 di-isopropyl benzene	0.94	1.56	447	405
1066	p-ethyl toluene	1.11	1.87	376	303
1067	1-tert-butoxy-2-propanol	0.85	1.35	490	480
1068	2-tert-butoxy-1-propanol	0.58	0.94	687	696
1069	1-methoxy-2-propyl acetate	0.76	1.14	549	582
1070	1-phenoxy-2-propanol	0.49	0.85	763	749
1071	Final LEV -- Phase 2	1.09	0.51	388	963
1072	TLEV exhaust – phase 2	1.20	0.56	333	932
1073	Phenyl Trimethicone	N/A	0.03	1190	1153
1074	phenol	-0.13	0.25	1146	1061
1075	p-isobutyl toluene; 1-methyl-4-(2-methylpropyl) benzene	1.04	1.70	414	358
1076	pentaerythritol	0.82	1.25	506	520
1077	propyl acetate	0.44	0.81	812	776
1078	n-propyl butyrate	0.52	0.93	736	701
1079	propyl cyclopentane	0.65	1.30	625	498
1080	propylene glycol	0.99	1.52	429	417
1081	n-propoxy-propanol	1.51	2.23	229	201
1082	propionic acid	0.49	0.78	767	791
1083	propionaldehyde	2.37	3.12	84	78
1084	propane	0.31	0.52	943	956
1085	propene	3.49	4.78	13	13
1086	di-n-propyl ether	1.43	2.29	252	187
1087	propylene oxide	0.20	0.31	1049	1043
1088	1-propoxy-2-propanol (propylene	1.34	2.00	286	262

	glycol n-propyl ether)				
1089	propylparaben	-0.07	0.13	1127	1125
1090	n-propyl propionate	0.44	0.85	805	746
1091	phthalic anhydride	0.64	1.07	634	624
1092	p-toluene isocyanate	-0.22	0.26	1147	1057
1093	p-xylene	1.36	2.11	270	229
1094	3,3-dichloro-1,1,1,2,2-pentafluoropropane;HCFC-225ca	0.00	0.00	1100	1178
1095	1,3-dichloro-1,1,2,2,3-pentafluoropropane;HCFC-225cb	0.00	0.00	1102	1181
1096	1,1,1,3,3-pentafluorobutane; HFC-365mfc	0.00	0.00	1105	1183
1097	1,1,1,2,2,3,4,5,5,5-decafluoropentane; HFC-43-10mee	0.00	0.00	1107	1184
1098	final LEV – RFA	1.12	0.52	370	954
1099	TLEV Exhaust -- RFA	1.20	0.55	338	941
1100	sabinene	1.46	2.28	243	190
1101	stillbenzene derivates	N/A	0.38	1191	1022
1102	sec-butyl acetate	0.73	1.11	570	605
1103	sec-butyl cyclohexane	0.49	0.96	766	688
1104	sec-butyl benzene	0.72	1.14	575	583
1105	sec-butyl alcohol	0.68	1.13	602	590
1106	substituted C7 ester (C12)	0.42	0.72	836	829
1107	substituted C9 ester (C12)	0.43	0.72	818	830
1108	hexamethyl-disiloxane	0.03	0.08	1086	1136
1109	hydroxymethyl-disiloxane	0.01	0.05	1093	1147
1110	styrene	-0.03	0.23	1124	1066
1111	trans-1,2-dichloroethene	0.64	0.84	642	753
1112	trans-1,3-dichloropropene	1.30	1.83	298	313
1113	trans-1,3-hexadiene	3.21	4.75	29	17
1114	trans-1,3-pentadiene	3.87	5.73	8	3
1115	trans-1,4-hexadiene	2.77	4.01	45	30
1116	trans-2,2-dimethyl 3-hexene	1.86	2.44	152	153
1117	trans-2,5-dimethyl 3-hexene	1.77	2.34	175	172
1118	trans-2-butene	4.13	4.76	3	14
1119	trans-2-hexene	2.65	3.79	61	36
1120	trans-2-heptene	2.33	3.14	88	73
1121	trans-2-octene	1.96	2.59	140	136
1122	trans-2-pentene	3.35	4.64	20	23
1123	trans-3-hexene	2.68	3.49	55	52
1124	trans-3-heptene	2.28	2.92	100	100

1125	trans-3-octene	1.81	2.39	165	162
1126	trans-3-methyl-2-pentene	3.40	3.43	19	55
1127	trans-3-methyl-2-hexene	2.66	3.03	59	87
1128	trans-4,4-dimethyl-2-pentene	2.09	2.99	119	92
1129	trans-4-decene	1.32	1.73	291	349
1130	trans-4-octene	1.53	2.05	226	247
1131	trans-4-nonene	1.53	2.01	223	259
1132	trans-4-methyl-2-pentene	2.55	3.65	67	43
1133	trans-4-methyl-2-hexene	2.39	3.16	78	71
1134	trans-5-undecene	1.23	1.62	324	388
1135	trans-5-dodecene	1.10	1.46	381	442
1136	trans-5-tridecene	1.00	1.33	425	490
1137	trans-5-tetradecene	0.91	1.22	461	544
1138	trans-5-pentadecene	0.84	1.13	495	591
1139	tert-butyl acetate	0.08	0.13	1071	1124
1140	tert-butyl amine	-1.21	-1.24	1154	1192
1141	1-(1,1-dimethylethyl)-3,5-dimethylbenzene	2.00	2.31	135	182
1142	tert-butyl benzene	0.49	0.87	771	733
1143	tert-butyl alcohol	0.19	0.31	1052	1044
1144	C12 tricycloalkanes	0.40	0.77	850	793
1145	C13 tricycloalkanes	0.36	0.71	886	837
1146	C14 tricycloalkanes	0.33	0.66	916	866
1147	C15 tricycloalkanes	0.32	0.62	929	884
1148	C16 tricycloalkanes	0.30	0.58	957	915
1149	C17 tricycloalkanes	0.28	0.55	975	940
1150	C18 tricycloalkanes	0.26	0.52	995	957
1151	C19 tricycloalkanes	0.25	0.49	1011	973
1152	C20 tricycloalkanes	0.24	0.47	1023	985
1153	C21 tricycloalkanes	0.22	0.44	1039	995
1154	C22 tricycloalkanes	0.21	0.42	1040	1002
1155	2,4-toluene diisocyanate	-0.60	-0.04	1149	1185
1156	2,6-toluene diisocyanate	-0.60	-0.04	1150	1186
1157	toluene diisocyanate (mixed isomers)	-0.60	-0.04	1151	1187
1158	triethyl amine	1.54	2.32	220	178
1159	triethylene glycol	1.35	2.09	273	235
1160	terpene (monoterpenes)	1.29	1.93	299	280
1161	triethyl citrate	0.28	0.43	972	1001
1162	tetraethylene glycol	1.08	1.76	393	340
1163	triethylene diamine	1.41	2.09	259	236
1164	3,6,9,12-tetraoxa-hexadecan-1-ol	0.73	1.13	571	592

1165	2,5,8,11-tetraoxatridecan-13-ol	0.90	1.63	464	383
1166	tetralin (1,2,3,4-tetrahydronaphthalene)	0.80	1.50	521	422
1167	2,2,4-trimethyl-1,3-pentanediol monoisobutyrate and isomers (texanol®)	0.43	0.72	819	831
1168	3-hydroxy-2,2,4-trimethylpentyl-1-isobutyrate	0.44	0.75	810	811
1169	1-hydroxy-2,2,4-trimethylpentyl-3-isobutyrate	0.39	0.61	862	898
1170	2-[2-(2-butoxyethoxy) ethoxy] ethanol	0.89	1.35	469	481
1171	2-[2-(2-ethoxyethoxy) ethoxy] ethanol	1.07	1.89	401	297
1172	tripropylene glycol n-butyl ether	0.70	1.09	587	612
1173	2-[2-(2-methoxyethoxy) ethoxy] ethanol	1.14	1.96	358	271
1174	2-[2-(2-propoxyethoxy) ethoxy] ethanol	0.98	1.55	432	411
1175	tetrahydro-2-furanmethanol (tetrahydrofurfuryl alcohol)	1.22	1.94	326	276
1176	tetrahydrofuran	1.98	3.05	137	83
1177	Tetrahydrofurfuryl Methacrylate	N/A	1.79	1192	332
1178	tetrahydropyran	1.53	2.46	221	151
1179	trimethyl amine	2.70	4.47	53	26
1180	trimethyl cyclohexanol	0.75	1.25	551	521
1181	trimethylene oxide	2.29	3.42	95	56
1182	2,2,4-trimethyl-1,3-pentanediol	0.70	1.16	588	570
1183	tolualdehyde	-0.70	-0.77	1152	1189
1184	toluene	0.93	1.67	454	367
1185	tripropylene glycol	0.97	1.51	434	419
1186	tripropylene glycol monomethyl ether	0.86	1.54	479	412
1187	Terpinolene	1.68	2.12	195	225
1188	trans,trans-2,4-hexadiene	2.72	3.89	51	34
1189	2,2,4-trimethyl-1,3-pentanediol diisobutyrate	0.18	0.36	1057	1029
1190	vinyl acetate	0.91	1.24	462	528
1191	1-buten-3-yne (vinyl acetylene)	3.46	5.12	17	6
1192	VMP Naphtha	0.57	0.32	694	1040

Table 5-13: List of VOC or mixture name, median MIR value in 1988 and 2010 (g O_3 / g VOC), and rank (most reactive = 1 least = 1192) in 2010 and 1988 for MIR (g O_3/ g VOC).

#	VOC or Mix	1988 MIR (g O_3 / g VOC)	2010 MIR (g O_3 / g VOC)	1988 Rank	2010 Rank
1	Dodecamethylpentasiloxane	N/A	-0.02	1160	1181
2	Dimethylcyclopolysiloxane	N/A	-0.02	1161	1182
3	1,1,1,3,5,5,5-Heptamethyl-3-Octyl-Trisiloxane	N/A	-0.04	1162	1188
4	Dodecamethylhexacyclosiloxane	N/A	-0.02	1163	1180
5	decamethyltetrasiloxane	N/A	-0.04	1164	1189
6	3-Ethylheptamethyltrisiloxane	N/A	-0.04	1165	1186
7	cyclosiloxane D4 (octamethylcyclotetrasiloxane)	-0.06	-0.03	1146	1183
8	cyclosiloxane D5 (decamethylcyclopentasiloxane)	-0.07	-0.03	1150	1185
9	hexamethyldisiloxane	N/A	-0.05	1166	1191
10	Octamethylcyclotetrasiloxane	N/A	-0.04	1167	1190
11	octamethyltrisiloxane	N/A	-0.04	1168	1187
12	Dodecamethylcyclohexasiloxane	N/A	-0.03	1169	1184
13	1,1,1-trichloroethane	0.01	0.00	1137	1170
14	1,1,2-trichloroethane	0.09	0.08	1116	1146
15	1,1,2-trimethyl cyclopentane	1.20	1.55	756	697
16	1,1,3-trimethyl cyclohexane	1.25	1.66	740	650
17	1,1,3-trimethyl cyclopentane	1.06	1.42	803	755
18	1,2-dibromoethane	0.10	0.09	1114	1144
19	1,1-dichloroethane	0.07	0.08	1118	1147
20	1,1-dichloroethene	1.88	1.97	577	572
21	1,1-dimethyl cyclopentane	1.05	1.36	807	778
22	1,1-dimethyl cyclohexane	1.29	1.70	726	638
23	pentamethyl benzene	8.40	5.21	88	125
24	1,2,3,4-tetramethyl benzene	9.56	5.88	58	81
25	1,2,3,5-tetramethyl benzene	9.56	5.88	59	82
26	1,2,3-trimethyl cyclohexane	1.14	1.74	774	631
27	1,2,3-trimethyl benzene	12.37	7.50	22	32
28	1,2,3-trimethyl cyclopentane	1.74	2.11	599	537
29	1,2,4,5-tetramethyl benzene	9.56	5.88	60	83
30	1,2,4-trimethyl benzene	9.19	6.22	69	72
31	1,2,4-trimethyl cyclopentane	1.64	2.00	621	564
32	1,2-epoxy butane	0.96	1.15	839	874
33	1,2-butadiene	9.60	9.32	57	9
34	1,2-butandiol	2.33	2.40	502	482

35	1,2-pentanediol	N/A	2.59	1170	446
36	1,2-octanediol	N/A	1.85	1171	604
37	1,2-dichloroethane	0.22	0.19	1107	1134
38	1,2-dichloropropane	0.30	0.28	1102	1127
39	1,2-diacetyl benzene	2.29	2.04	509	548
40	1,2-dimethyl cyclopentane	1.96	2.38	565	487
41	1,2-dimethyl cyclohexane	1.30	1.92	722	579
42	1,2-dimethyl-3-ethyl benzene	10.51	6.42	37	62
43	1,2-dimethyl-4-ethyl benzene	7.81	5.39	107	110
44	1,2-dimethyl cyclohexene	5.72	4.16	194	209
45	1,2-propylene glycol diacetate	0.64	0.74	977	1032
46	1,2-pentadiene	8.15	7.21	96	35
47	1,3,5-triethyl cyclohexane	1.04	1.55	813	698
48	1,3,5-trimethyl cyclohexane	1.17	1.75	764	629
49	1,3,5-tripropyl cyclohexane	0.88	1.32	872	796
50	1,3,5-trimethyl benzene	11.94	6.90	24	42
51	1,3-butadiene	13.23	9.87	12	5
52	1,3-butadiyne	6.05	6.25	183	70
53	1,3-propanediol	N/A	3.55	1172	283
54	1,3-butanediol	3.49	3.79	351	259
55	1,3-dichloropropene mixture	4.32	3.45	283	301
56	1,3-diethyl cyclohexane	1.20	1.75	757	630
57	1,3-dimethyl cyclopentane	1.87	2.28	580	502
58	1,3-dimethyl cyclohexane	1.39	1.97	691	573
59	1,3-dioxolane	5.21	4.92	223	148
60	1,3-diethyl-5-pentyl cyclohexane	0.67	1.10	961	902
61	1,3-diethyl-5-methyl cyclohexane	1.06	1.60	804	675
62	1,3-diethyl-5-propyl cyclohexane	0.97	1.46	836	733
63	1,3-dimethyl-2-ethyl benzene	10.51	6.42	38	63
64	1,3-dimethyl-4-ethyl benzene	7.81	5.39	108	111
65	1,3-dimethyl-5-ethyl benzene	10.25	6.00	42	76
66	1,3-propyl-5-butyl cyclohexane	0.76	1.18	917	855
67	1,3-dipropyl-5-ethyl cyclohexane	0.92	1.38	854	771
68	1,4-butanediol	2.82	3.00	431	375
69	1,4-diethyl cyclohexane	1.25	1.81	738	614
70	1,4-dimethyl cyclohexane	1.48	2.05	668	543
71	1,4-dioxane	2.74	2.81	438	412
72	1,4-dimethyl-2-ethyl benzene	7.81	5.39	109	112
73	1,4-pentadiene	9.70	8.22	54	24
74	1,5-pentanediol	N/A	2.59	1173	447
75	1-amino-2-propanol	5.66	6.23	200	71

76	1-(butoxyethoxy)-2-propanol	2.23	2.65	518	435
77	1-butene	10.10	8.52	46	18
78	1-decene	2.30	2.56	507	452
79	1-decanol	1.14	1.40	772	762
80	1-undecene	1.98	2.25	558	508
81	1-dodecene	1.73	2.00	601	565
82	1-tridecene	1.55	1.81	651	615
83	1-tetradecene	1.39	1.66	688	651
84	1-pentadecene	1.30	1.55	718	699
85	butanal	6.27	4.83	172	151
86	pentanal (valeraldehyde)	5.32	4.15	212	210
87	1-hexanol	2.56	2.94	468	389
88	hexanal	4.56	3.56	267	280
89	1-heptanol	1.91	2.26	569	504
90	heptanal	3.88	3.07	322	363
91	1-octanol	1.55	1.89	650	592
92	octanal	3.31	2.68	369	427
93	1-nonene	2.70	2.95	446	386
94	1-nonene-4-one	3.25	3.05	381	367
95	1-ethyl-2-propyl cyclohexane	0.75	1.37	919	774
96	1-ethyl-4-methyl cyclohexane	1.34	1.91	708	585
97	1-ethyl naphthalene	2.87	2.52	425	459
98	1-heptene	4.23	4.20	288	205
99	1-hexene	5.69	5.30	197	122
100	5-methyl-1-heptanol	1.72	2.02	607	558
101	1-methyl-2-hexyl cyclohexane	0.58	1.15	1005	875
102	1-methyl-2-octyl cyclohexane	0.50	1.01	1048	945
103	1-methyl-3,5-diethyl benzene	9.06	5.33	71	116
104	1-methyl-3-ethyl cyclopentane	1.60	2.04	633	549
105	1-methyl-3-isopropyl cyclohexane	1.02	1.57	816	689
106	1-methyl-4-pentyl cyclohexane	0.73	1.27	929	819
107	trans-1-methyl-4-heptyl cyclohexane	0.53	1.06	1030	920
108	1-methyl-4-nonyl cyclohexane	0.46	0.95	1063	972
109	1-methyl cyclopentene	11.72	6.35	26	67
110	1-methyl cyclohexene	6.80	4.67	151	174
111	1-methyl naphthalene	3.15	2.77	390	418
112	1-octene	3.40	3.48	357	292
113	1-pentene	7.49	6.53	119	58
114	2,2,3,3-tetramethyl butane	0.34	0.38	1096	1098
115	2,2,3-trimethyl butane	1.17	1.25	766	825
116	2,2,3-trimethyl pentane	1.29	1.47	727	731

117	2,2,4-trimethyl pentane	1.31	1.43	714	752
118	2,2,4-trimethyl hexane	1.35	1.58	703	684
119	2,2,4-trimethyl heptane	1.24	1.51	741	720
120	2,2,5-trimethyl hexane	1.21	1.45	753	737
121	2,2,5-trimethyl heptane	1.35	1.63	704	658
122	neopentane	0.69	0.70	945	1041
123	2,2-dimethylpropanal (pivaldehyde)	5.08	3.90	238	240
124	2,2-dimethyl butane	1.23	1.32	746	797
125	2,2-dimethyl pentane	1.18	1.36	761	779
126	2,2-dimethyl hexane	1.08	1.32	796	798
127	2,2-dimethyl heptane	1.07	1.35	801	784
128	2,2-dimethyl octane	0.87	1.21	874	839
129	2,2-dimethoxy-propane	0.50	0.56	1045	1066
130	2,3,3-trimethyl-1-butene	4.60	3.71	265	265
131	2,3,3-trimethyl pentane	1.08	1.31	795	800
132	2,3,4,6-tetramethyl heptane	1.14	1.61	775	669
133	2,3,4-trimethyl pentane	1.07	1.40	799	763
134	2,3,5,6,8-pentamethyl-nonyl acetate	0.66	1.08	965	908
135	2,3,5,7-tetramethyl-octyl acetate	0.63	1.05	984	923
136	2,3,5,7-tetramethyl octane	0.93	1.42	852	756
137	2,3,5-trimethyl-hexyl acetate	0.80	1.18	907	856
138	2,3,5-trimethyl phenol	1.96	1.29	561	808
139	2,3,5-trimethyl hexane	1.16	1.54	767	705
140	2,3,6-trimethyl 4-isopropyl heptane	0.94	1.39	850	767
141	2,3,6-trimethyl phenol	1.96	1.29	562	809
142	2,3,6-trimethyl heptane	1.01	1.50	829	725
143	2,3-butanediol	2.72	3.23	444	335
144	2,3-dimethyl-1-pentene	5.28	4.78	217	156
145	2,3-dimethyl butane	1.01	1.20	824	845
146	2,3-dimethyl pentane	1.44	1.76	676	628
147	2,3-dimethyl hexane	1.25	1.70	736	639
148	2,3-dimethyl heptane	1.13	1.60	782	676
149	2,3-dimethyl octane	0.89	1.37	866	775
150	2,3-dimethyl naphthalene	5.16	3.30	226	330
151	2,3-dimethyl-1-butene	4.84	3.58	253	278
152	dimethylpentanol (2,3-dimethyl-1-pentanol)	2.31	2.44	503	471
153	2,3-dimethyl-2-butene	12.43	4.49	21	184
154	2,3-dimethyl-2-pentene	9.94	4.28	51	198
155	2,3-dimethyl-2-hexene	8.67	3.93	82	234
156	2,3-dimethylbutyl acetate	0.77	1.02	911	940
157	2,3-dimethyl-heptyl acetate	0.73	1.12	927	887

158	2,3-dimethyl phenol	2.19	1.44	521	740
159	2,4,4-trimethyl-1-pentene	3.40	2.62	356	439
160	2,4,4-trimethyl-2-pentene	6.40	4.21	168	202
161	2,4,4-trimethyl hexane	1.43	1.66	679	652
162	2,4,4-trimethyl heptane	1.41	1.70	686	640
163	2,4,5,6,8-pentamethyl nonane	0.96	1.50	837	726
164	2,4,6,8-tetramethyl-nonyl acetate	0.56	0.97	1015	965
165	2,4,6,8-tetramethyl nonane	0.84	1.34	891	790
166	2,4,6-trimethyl heptane	1.36	1.74	698	632
167	2,4-pentanedione	1.03	0.84	815	1000
168	2,4-dimethyl-1-pentene	5.30	4.78	214	157
169	2,4-dimethyl pentane	1.63	1.92	626	580
170	2,4-dimethyl hexane	1.84	2.19	586	519
171	2,4-dimethyl heptane	1.47	1.90	669	587
172	2,4-dimethyl octane	1.06	1.54	805	706
173	2,4-dimethyl-2-pentene	9.62	5.31	56	120
174	2,4-dimethylpentyl acetate	0.95	1.26	848	822
175	2,4-dimethylhexyl acetate	0.86	1.26	884	823
176	2,4-dimethyl-heptyl acetate	0.80	1.23	906	832
177	2,4-dimethyl phenol	2.19	1.44	522	741
178	2,5,5-trimethyl heptane	1.33	1.58	711	685
179	2,5-dimethyl hexane	1.54	1.94	653	576
180	2,5-dimethyl heptane	1.41	1.89	685	593
181	2,5-dimethyl octane	1.05	1.56	806	694
182	2,5-dimethyl-heptyl acetate	0.80	1.20	902	846
183	2,5-dimethyl furan	8.13	5.31	97	121
184	2,5-dimethyl phenol	2.19	1.44	523	742
185	trimethylnonanolthreoerythro (2,6,8-trimethyl-4-nonanol)	1.34	1.54	710	707
186	2,6,8-trimethyl 4-isopropyl nonane	0.63	1.11	982	895
187	2,6-dimethyl heptane	1.07	1.53	800	712
188	2,6-dimethyl octane	1.11	1.59	788	682
189	2,6-dimethyl nonane	0.81	1.30	900	801
190	dimethyl heptanol (2,6-dimethyl-2-heptanol)	1.02	1.25	821	826
191	2,6-dimethyl-4-heptanol	1.86	2.15	582	523
192	2,6-dimethyl phenol	2.19	1.44	524	743
193	2,6-di-tert-butyl-p-cresol	1.21	0.80	751	1014
194	2,7-dimethyl 3,5-diisopropyl heptane	0.56	1.03	1016	935
195	2-amino-1-butanol	5.11	4.99	230	143
196	2-amino-2-ethyl-1,3-propanediol	0.84	1.66	889	653
197	2-butoxyethyl acetate	1.73	2.05	604	544

198	2-butyl tetrahydrofuran	2.26	2.77	512	419
199	2-butyne	16.84	10.60	3	1
200	C12 2-alkenes	2.96	2.86	409	402
201	2-pentanol	1.69	1.92	612	581
202	2-pentenes	10.97	8.14	31	27
203	2-hexanol	2.04	2.37	549	492
204	2-hexenes	8.84	6.71	77	52
205	2-heptenes	6.64	5.83	158	90
206	2-octanol	2.10	2.46	538	467
207	2-chlorotoluene	2.96	2.73	408	424
208	2-ethyl-1,3-hexanediol	1.88	2.14	578	526
209	2-ethyl-1-butene	5.20	3.70	224	267
210	2-ethyl-hexyl benzoate	1.04	1.21	814	840
211	2-ethyl-1-hexanol	2.09	2.31	539	498
212	2-ethyl furan	7.42	5.19	124	132
213	2-ethyl hexanoic acid	3.42	3.33	355	323
214	2-ethyl-hexyl acrylate	2.59	2.41	462	477
215	2-ethyl-hexyl acetate	0.77	1.16	910	867
216	2-methoxy-1-(2-methoxy-1-methylethoxy)-propane; dipropylene glycol dimethyl ether	2.39	2.59	495	448
217	2-methyl-1-butyl acetate	1.15	1.37	771	776
218	2-methyl-1-butene	6.57	4.49	163	185
219	2-methyl-1-pentene	5.39	3.77	210	260
220	2-methyl-1-hexene	5.22	4.78	222	158
221	2-methyl-2,4-pentanediol	1.50	1.58	661	686
222	2-methyl-2-butene	14.27	6.76	9	49
223	2-methyl-2-pentene	11.43	6.31	27	69
224	mesityl oxide (2-methyl-2-penten-4-one)	6.82	4.69	150	173
225	2-methyl-2-hexene	9.80	5.41	53	108
226	2-methyl-2-heptene	8.58	4.80	85	155
227	2-methyl 3,5-diisopropyl heptane	0.67	1.16	963	868
228	2-methyl-3-ethyl heptane	1.02	1.50	817	727
229	2-methyl-3-hexanone	1.60	1.94	635	577
230	2-methylpentyl acetate	1.05	1.35	809	785
231	2-methylhexyl acetate	0.82	1.18	894	857
232	2-methyloctyl acetate	0.57	0.98	1006	960
233	2-methyl-1-butanol	2.48	2.54	477	457
234	isobutane	1.27	1.32	733	799
235	2-methyl propanal	5.51	4.35	208	192
236	isopentane	1.53	1.79	656	619

237	2-methyl pentane	1.61	1.93	631	578
238	2-methyl hexane	1.37	1.79	695	620
239	2-methyl heptane	1.13	1.58	781	687
240	2-methyl octane	0.86	1.36	886	780
241	2-methyl nonane	0.74	1.29	921	810
242	2-methyl naphthalene	3.15	2.77	391	420
243	2-methoxy-1-propanol	3.12	2.46	394	468
244	2-methyl-hexanal	3.70	3.09	334	360
245	2-methyl furan	8.69	6.07	81	75
246	2-methyl-trans-3-hexene	6.59	5.76	161	94
247	2-pyrrolidone	N/A	3.45	1174	302
248	2-nitropropane	0.12	0.14	1113	1140
249	2-methyoxy-1-propyl acetate	1.14	1.21	773	841
250	2-Propoxy-1-Propanol	N/A	3.85	1175	244
251	2-propyl cyclohexanone	1.49	1.92	666	582
252	Dipropylene Glycol Dibenzoate	N/A	0.83	1176	1006
253	2-propoxy-ethanol	3.72	3.87	330	242
254	dimethicone	N/A	0.02	1177	1162
255	3,3-diethyl pentane	1.29	1.57	728	690
256	3,3-dimethyl-1-pentene	5.10	4.99	231	144
257	3,3-dimethyl pentane	1.26	1.45	734	738
258	3,3-dimethyl hexane	1.32	1.61	713	670
259	3,3-dimethyl heptane	1.20	1.54	755	708
260	3,3-dimethyl octane	1.16	1.53	768	713
261	3,3-dimethyl-1-butene	5.98	5.34	185	115
262	3,4-diethyl hexane	0.95	1.27	846	820
263	3,4-dimethyl-1-pentene	5.01	4.63	244	178
264	3,4-dimethyl-cis-2-pentene	9.39	5.05	65	142
265	3,4-dimethyl hexane	1.61	1.99	632	569
266	3,4-dimethyl heptane	1.30	1.74	720	633
267	3,4-diethyl-2-hexene	3.59	3.59	343	276
268	3,4-dimethyl-hexyl acetate	1.05	1.40	811	764
269	3,4-dimethyl phenol	2.19	1.44	525	744
270	3,5,7,9-tetramethyl-decyl acetate	0.52	0.94	1034	979
271	3,5,7-trimethyl-octyl acetate	0.74	1.17	924	864
272	3,5,7-trimethyl-nonyl acetate	0.68	1.11	949	896
273	3,5-diethyl heptane	1.13	1.67	777	648
274	3,5-dimethyl heptane	1.66	2.15	618	524
275	3,5-dimethyl-hexyl acetate	1.05	1.40	808	765
276	3,5-dimethyl-heptyl acetate	0.92	1.34	856	791
277	3,5-dimethyl phenol	N/A	1.44	1178	745

278	3,6,8-trimethyl-nonyl acetate	0.64	1.05	973	924
279	2,6-diethyl octane	0.99	1.48	834	729
280	3,6-dimethyl decane	0.76	1.28	916	818
281	3,6-dimethyl undecane	0.70	1.20	942	847
282	3,6-dimethyl-heptyl acetate	0.80	1.21	905	842
283	3,6-dimethyl-octyl acetate	0.81	1.21	901	843
284	3,7-diethyl nonane	0.90	1.35	864	786
285	3,7-dimethyl dodecane	0.63	1.11	987	897
286	3,7-dimethyl tridecane	0.55	1.03	1017	936
287	3,7-dimethyl-1-octanol	1.29	1.51	725	721
288	3,8-diethyl decane	0.55	1.07	1019	914
289	3,9-diethyl undecane	0.51	1.01	1037	946
290	1,2,3-C10 trisubstituted benzenes	10.51	6.42	39	64
291	C10 3-alkenes	3.60	3.48	340	293
292	1,2,3-C11 trisubstituted benzenes	9.19	5.65	68	99
293	C11 3-alkenes	3.28	3.16	373	344
294	1,2,3-C12 trisubstituted benzenes	8.24	5.08	93	138
295	C12 3-alkenes	2.96	2.86	410	403
296	1,2,3-C13 trisubstituted benzenes	7.38	4.57	127	181
297	C13 3-alkenes	2.69	2.60	448	442
298	1,2,3-C14 trisubstituted benzenes	6.73	4.18	155	207
299	C14 3-alkenes	2.44	2.39	487	483
300	1,2,3-C15 trisubstituted benzenes	6.15	3.84	181	246
301	C15 3-alkenes	2.24	2.21	515	514
302	1,2,3-C16 trisubstituted benzenes	5.66	3.55	205	284
303	3-pentanol	1.70	1.90	611	588
304	3-octanol	2.37	2.76	496	422
305	3-octenes	5.10	4.74	232	165
306	3-nonenes	4.22	4.00	290	225
307	3-carene	3.38	2.91	360	393
308	3-(chloromethyl)-heptane	1.00	1.36	830	781
309	3-chloropropene	12.57	8.21	18	25
310	3-ethyl 2-methyl pentane	1.42	1.77	683	626
311	3-ethyl-6,7-dimethyl-nonyl acetate	0.67	1.07	958	915
312	3-ethyl-6-methyl-octyl acetate	0.74	1.15	926	876
313	3-ethylpentyl acetate	1.18	1.51	759	722
314	3-ethyl-hexyl acetate	0.96	1.33	844	793
315	3-ethyl-heptyl acetate	0.65	1.05	972	925
316	3-ethyl-2-pentene	10.08	5.61	48	103
317	3-ethyl pentane	2.02	2.34	552	495
318	3-ethyl heptane	1.13	1.63	778	659

319	3-ethoxy-1-propanol	4.21	3.95	294	233
320	Trifluoroethyl Methacrylate	N/A	4.33	1179	193
321	3-isopropyl-heptyl acetate	0.61	1.01	997	947
322	3-methyl-1,2-butadiene	10.77	8.41	36	20
323	3-methyl-1-butene	7.26	6.35	135	68
324	3-methyl-1-pentene	6.37	5.71	169	97
325	3-methyl-1-hexene	4.55	4.56	269	182
326	3-methyl-2-hexanone	2.67	2.98	454	376
327	3-methyl-2-isopropyl-1-butene	4.04	3.99	306	229
328	3-methyl butanoic acid	5.02	4.08	243	217
329	3-methyl-cis-3-hexene	10.16	6.16	44	73
330	3-methylbutanal (isovaleraldehyde)	5.19	3.92	225	237
331	3-methylpentyl acetate	1.24	1.54	742	709
332	3-methylhexyl acetate	0.95	1.30	849	802
333	3-methyl-heptyl acetate	0.69	1.08	944	909
334	3-methyl decane	0.66	1.18	967	858
335	3-methyl undecane	0.59	1.11	1001	898
336	3-methyl dodecane	0.55	1.05	1021	926
337	3-methyl tridecane	0.51	1.00	1042	954
338	3-methyl tetradecane	0.48	0.95	1058	970
339	3-methyl pentadecane	0.45	0.91	1067	985
340	3-methyl pentane	1.91	2.18	570	520
341	3-methyl hexane	1.73	2.12	605	534
342	3-methyl heptane	1.31	1.78	716	623
343	3-methyl octane	1.02	1.51	818	723
344	3-methyl nonane	0.78	1.29	909	811
345	3-methyl cyclopentene	5.36	4.64	211	176
346	3-methoxy-1-propanol	3.96	3.56	316	281
347	3-methoxy-1-butanol	4.02	3.20	307	339
348	3-methyl furan	7.16	5.59	139	104
349	3 methoxy-3 methyl-1-butanol	2.83	2.94	428	390
350	3-methyl-trans-3-hexene	10.16	6.16	45	74
351	4,4-dimethyl-1-pentene	3.24	3.32	384	327
352	4,4-dimethyl heptane	1.37	1.73	696	637
353	4,4-dimethyl octane	1.22	1.61	750	671
354	4,4-diethyl-3-oxahexane	2.02	2.12	553	535
355	4,5-dimethyl-hexyl acetate	0.77	1.12	914	888
356	4,5-dimethyl-heptyl acetate	0.82	1.20	896	848
357	4,6-dimethyl-heptyl acetate	0.80	1.18	904	859
358	4,6-dimethyl-octyl acetate	0.78	1.20	908	849
359	4,7,9-trimethyl-decyl acetate	0.50	0.90	1049	989

360	4,7-dimethyl-nonyl acetate	0.59	1.01	1003	948
361	4,8-dimethyl tetradecane	0.49	0.96	1052	969
362	1,2,4-C10 trisubstituted benzenes	7.81	5.39	110	113
363	1,2,4-C11 trisubstituted benzenes	6.86	4.78	147	159
364	1,2,4-C12 trisubstituted benzenes	6.15	4.32	180	196
365	1,2,4-C13 trisubstituted benzenes	5.55	3.91	207	238
366	1,2,4-C14 trisubstituted benzenes	5.07	3.59	239	277
367	1,2,4-C15 trisubstituted benzenes	4.65	3.31	262	328
368	1,2,4-C16 trisubstituted benzenes	4.29	3.07	285	364
369	4-octanol	2.20	2.60	520	443
370	4-ethyl heptane	1.30	1.77	721	627
371	4-ethyl octane	0.90	1.41	860	758
372	4-methyl-1-pentene	5.89	5.21	189	126
373	4-methylpentyl acetate	0.87	1.16	876	869
374	4-methylhexyl acetate	0.86	1.20	883	850
375	4-methyl-heptyl acetate	0.68	1.05	953	927
376	4-methyloctyl acetate	0.63	1.03	981	937
377	4-methyl cyclohexene	4.37	3.97	280	231
378	4-methyl decane	0.70	1.21	943	844
379	4-methyl heptane	1.34	1.78	709	624
380	4-methyl octane	0.99	1.47	833	732
381	4-methyl nonane	0.88	1.38	870	772
382	4-nonene	4.22	4.00	291	226
383	4-propyl heptane	1.05	1.54	810	710
384	4-propyl cyclohexanone	1.99	2.39	556	484
385	4-vinyl phenol	1.56	1.55	646	700
386	1,3,5-C10 trisubstituted benzenes	10.25	6.00	43	77
387	1,3,5-C11 trisubstituted benzenes	9.06	5.33	72	117
388	1,3,5-C12 trisubstituted benzenes	8.16	4.82	94	153
389	1,3,5-C13 trisubstituted benzenes	7.38	4.38	128	187
390	1,3,5-C14 trisubstituted benzenes	6.76	4.02	154	222
391	1,3,5-C15 trisubstituted benzenes	6.22	3.71	177	266
392	1,3,5-C16 trisubstituted benzenes	5.75	3.44	192	303
393	5-ethyl-3,6,8-trimethyl-nonyl acetate	0.69	1.12	948	889
394	5-methyl-2-hexanone	2.26	2.62	511	440
395	5-methylhexyl acetate	0.73	1.08	934	910
396	5-methyl-heptyl acetate	0.67	1.05	959	928
397	5-methyloctyl acetate	0.62	1.01	992	949
398	5-methyl undecane	0.63	1.13	983	883
399	5-methyl dodecane	0.56	1.06	1014	921
400	6-methyl tridecane	0.53	1.02	1029	941

401	6-methyl tetradecane	0.50	0.97	1047	966
402	7-methyl pentadecane	0.45	0.91	1069	984
403	acetic acid	0.68	0.67	951	1051
404	acetal (1,1-diethoxyethane)	3.72	3.43	332	307
405	acetaldehyde	6.92	5.17	142	133
406	acetone	0.36	0.29	1091	1123
407	acetylene	0.95	0.80	845	1015
408	acrolein	7.81	6.00	111	78
409	acrylonitrile	2.27	2.04	510	550
410	acrylic acid	13.43	8.25	10	23
411	adipic acid (hexanedioic acid)	2.93	3.04	419	369
412	1,2-propadiene (allene)	8.74	9.13	80	12
413	allylbenzene	1.59	1.57	641	691
414	amyl acetate (n-pentyl acetate)	1.01	1.30	828	803
415	amyl cinnamal	3.31	2.28	368	503
416	a-methyl styrene	1.59	1.57	642	692
417	2-amino-2-methyl-1-propanol	0.22	1.83	1106	607
418	alpha-methyl tetrahydrofuran	4.12	4.45	300	186
419	anethol (p-propenyl-anisole)	0.86	1.07	885	916
420	alpha-pinene	4.61	3.34	264	321
421	Base ROG Mixture	3.71	0.95	333	971
422	Aromatic 100®	7.66	1.45	112	739
423	Regular mineral spirits	1.96	0.62	563	1059
424	Reduced Aromatics Mineral Spirits	1.23	0.48	747	1083
425	Dearomatized Alkanes, mixed, predominately C10-C12	0.88	0.42	871	1093
426	Synthetic isoparaffinic alkane mixture, predominately C10-C12	0.77	0.38	912	1099
427	a-terpineol	4.76	2.98	254	377
428	butyl benzyl phthalate	N/A	1.09	1180	906
429	C10 bicycloalkanes	1.11	1.65	787	656
430	C11 bicycloalkanes	0.90	1.46	862	734
431	C12 bicycloalkanes	0.83	1.35	892	787
432	C13 bicycloalkanes	0.73	1.25	933	827
433	C14 bicycloalkanes	0.68	1.17	956	865
434	C15 bicycloalkanes	0.64	1.11	976	899
435	C16 bicycloalkanes	0.60	1.04	998	934
436	C17 bicycloalkanes	0.56	0.98	1011	961
437	C18 bicycloalkanes	0.53	0.93	1027	982
438	C19 bicycloalkanes	0.50	0.88	1044	995
439	C20 bicycloalkanes	0.48	0.83	1057	1005
440	C21 bicycloalkanes	0.46	0.79	1065	1017

441	C22 bicycloalkanes	0.44	0.76	1077	1026
442	C8 bicycloalkanes	1.44	1.90	677	589
443	C9 bicycloalkanes	1.37	1.90	697	590
444	benzaldehyde	-0.66	0.00	1154	1179
445	benzene	0.73	0.72	928	1036
446	biacetyl	20.06	8.80	1	15
447	ß-methyl styrene	1.08	1.34	797	792
448	ß-phenethyl alcohol (2-phenyl ethyl alcohol)	4.68	3.44	259	304
449	beta-pinene	3.63	3.38	339	318
450	branched C10 alkanes	0.96	1.46	840	735
451	branched C11 alkanes	0.74	1.24	922	830
452	branched C12 alkanes	0.69	1.20	947	851
453	branched C13 alkanes	0.63	1.13	986	884
454	branched C14 alkanes	0.57	1.06	1008	922
455	branched C15 alkanes	0.52	1.00	1032	956
456	branched C16 alkanes	0.47	0.94	1061	977
457	branched C17 alkanes	0.44	0.88	1073	994
458	branched C18 alkanes	0.42	0.83	1080	1004
459	branched C19 alkanes	0.40	0.79	1084	1018
460	branched C20 alkanes	0.38	0.75	1089	1030
461	branched C21 alkanes	0.36	0.72	1093	1038
462	branched C22 alkanes	0.34	0.68	1095	1044
463	branched C5 alkanes	1.53	1.79	657	621
464	branched C6 alkanes	1.41	1.68	687	645
465	branched C7 alkanes	1.60	1.89	634	594
466	branched C8 alkanes	1.54	1.96	655	574
467	branched C9 alkanes	1.17	1.66	762	654
468	n-butyl acetate	0.89	1.08	868	911
469	n-butyl butyrate	1.17	1.43	763	753
470	butyl methacrylate	8.93	5.20	76	131
471	di-n-butyl ether	2.94	3.37	414	319
472	n-butoxy-2-propanol (propylene glycol n-butyl ether)	2.79	3.18	436	342
473	2-butoxy-ethanol	2.99	3.05	405	368
474	butyl propionate	0.90	1.11	861	900
475	butanoic acid	2.09	2.09	542	540
476	benzyl alcohol	5.28	3.89	216	241
477	hexafluoro-benzene	0.05	0.05	1126	1155
478	methoxybenzene; anisole	6.87	5.12	143	135
479	Unspeciated C10 Aromatics	7.33	1.36	134	783
480	butylbenzenes	5.98	4.23	186	201

481	C10 monosubstituted benzenes	2.42	2.42	491	473
482	C10 disubstituted benzenes	5.86	4.33	190	194
483	C10 trisubstituted benzenes	9.56	5.88	61	84
484	C10 tetrasubstituted benzenes	9.56	5.88	62	85
485	decyl cyclohexane	0.49	0.97	1051	967
486	2-decanone	0.86	1.30	878	804
487	C10 cyclic olefins or di-olefins	3.65	3.53	336	286
488	C10 alkenes	3.15	3.17	393	343
489	C10 terminal alkenes	2.30	2.56	508	453
490	C10 internal alkenes	3.60	3.48	341	294
491	C10 alkyl phenols	1.78	1.17	592	866
492	C10 styrenes	1.42	1.41	684	759
493	Unspeciated C10 Alkanes	0.92	0.42	855	1091
494	Unspeciated C11 Aromatics	7.21	1.30	136	807
495	pentyl benzenes	5.09	3.72	236	264
496	C11 monosubstituted benzenes	2.18	2.21	527	515
497	C11 disubstituted benzenes	5.08	3.81	237	252
498	C11 trisubstituted benzenes	8.40	5.21	89	127
499	C11 tetrasubstituted benzenes	8.40	5.21	90	128
500	C11 pentasubstituted benzenes	8.40	5.21	91	129
501	C11 cyclic olefins or di-olefins	3.32	3.20	367	340
502	C11 alkenes	2.64	2.71	456	426
503	C11 terminal alkenes	1.98	2.25	559	509
504	C11 internal alkenes	3.28	3.16	374	345
505	C11 alkyl phenols	1.63	1.07	625	917
506	C11 tetralins or indanes	2.79	2.52	437	460
507	Unspeciated C11 Alkanes	0.75	0.38	918	1100
508	Unspeciated C12 Aromatics	6.25	1.12	174	886
509	hexyl benzenes	4.57	3.36	266	320
510	C12 monosubstituted benzenes	1.97	2.02	560	559
511	C12 disubstituted benzenes	4.55	3.44	270	305
512	C12 trisubstituted benzenes	7.55	4.70	114	169
513	C12 tetrasubstituted benzenes	7.55	4.70	115	170
514	C12 pentasubstituted benzenes	7.55	4.70	116	171
515	C12 hexasubstituted benzenes	7.55	4.70	117	172
516	cis-1,2-dichloroethene	1.71	1.53	609	714
517	C12 monosubstituted naphthalene	2.87	2.52	426	461
518	C12 disubstituted naphthalenes	5.16	3.30	227	331
519	C12 naphthalenes	4.07	2.91	304	394
520	C12 cyclic olefins or di-olefins	3.00	2.89	403	399
521	C12 alkenes	2.37	2.45	497	469

522	C12 terminal alkenes	1.73	2.00	602	566
523	C12 internal alkenes	2.96	2.86	411	404
524	C12 alkyl phenols	1.50	0.99	662	959
525	C12 tetralins or indanes	2.54	2.30	472	500
526	Unspeciated C12 Alkanes	0.69	0.36	946	1107
527	Unspeciated C13 Aromatics	5.02	0.94	242	976
528	C13 monosubstituted benzenes	1.81	1.87	588	596
529	C13 disubstituted benzenes	4.08	3.11	302	354
530	C13 trisubstituted benzenes	6.80	4.26	152	200
531	cis-1,3-dichloropropene	3.72	3.11	331	355
532	C13 monosubstituted naphthalene	2.63	2.31	458	499
533	C13 disubstituted naphthalenes	4.73	3.03	256	372
534	C13 trisubstituted naphthalenes	4.73	3.03	257	373
535	C13 naphthalenes	3.74	2.67	329	430
536	C13 cyclic olefins or di-olefins	2.72	2.63	443	437
537	C13 alkenes	2.12	2.24	535	511
538	C13 terminal alkenes	1.55	1.81	652	616
539	C13 internal alkenes	2.69	2.60	449	444
540	cis-1,3-pentadiene	13.10	10.00	13	3
541	C13 tetralins or indanes	2.34	2.11	499	538
542	Unspeciated C13 Alkanes	0.63	0.33	985	1112
543	Unspeciated C14 Aromatics	3.97	0.77	315	1020
544	C14 monosubstituted benzenes	1.66	1.74	616	634
545	C14 disubstituted benzenes	3.69	2.84	335	406
546	C14 trisubstituted benzenes	6.21	3.91	178	239
547	C14 naphthalenes	3.45	2.47	353	466
548	C14 cyclic olefins or di-olefins	2.47	2.41	482	478
549	C14 alkenes	1.92	2.05	567	545
550	C14 terminal alkenes	1.39	1.66	689	655
551	C14 internal alkenes	2.44	2.39	488	485
552	C14 tetralins or indanes	2.17	1.96	530	575
553	Unspeciated C14 Alkanes	0.59	0.32	1004	1117
554	Unspeciated C15 Aromatics	3.34	0.67	366	1052
555	C15 monosubstituted benzenes	1.54	1.63	654	660
556	C15 disubstituted benzenes	3.36	2.61	362	441
557	C15 trisubstituted benzenes	5.69	3.60	199	275
558	C15 naphthalenes	3.21	2.29	388	501
559	C15 cyclic olefins or di-olefins	2.26	2.23	513	512
560	C15 alkenes	1.77	1.90	596	591
561	C15 terminal alkenes	1.30	1.55	719	701
562	C15 internal alkenes	2.24	2.21	516	516

563	C15 tetralins or indanes	2.01	1.82	554	609
564	Unspeciated C15 Alkanes	0.55	0.30	1020	1120
565	Unspeciated C16 Aromatics	2.92	0.59	421	1061
566	C16 monosubstituted benzenes	1.44	1.53	675	715
567	C16 disubstituted benzenes	3.08	2.41	399	479
568	C16 trisubstituted benzenes	5.25	3.34	219	322
569	C16 naphthalenes	3.00	2.14	404	527
570	C16 tetralins or indanes	1.88	1.70	576	641
571	Unspeciated C16 Alkanes	0.50	0.29	1046	1124
572	C17 monosubstituted benzenes	1.36	1.44	702	746
573	C17 disubstituted benzenes	2.89	2.26	424	505
574	C17 trisubstituted benzenes	4.93	3.14	246	350
575	C17 naphthalenes	2.81	2.01	432	563
576	C17 tetralins or indanes	1.77	1.60	597	677
577	Unspeciated C17 Alkanes	0.47	0.27	1059	1129
578	C18 monosubstituted benzenes	1.28	1.36	731	782
579	C18 disubstituted benzenes	2.73	2.13	441	530
580	C18 trisubstituted benzenes	4.65	2.96	260	382
581	C18 naphthalenes	2.65	1.89	455	595
582	C18 tetralins or indanes	1.67	1.51	615	724
583	Unspeciated C18 Alkanes	0.45	0.25	1071	1131
584	C19 monosubstituted benzenes	1.21	1.29	754	812
585	C19 disubstituted benzenes	2.58	2.02	467	560
586	C19 trisubstituted benzenes	4.40	2.80	279	414
587	C19 naphthalenes	2.50	1.79	475	622
588	C19 tetralins or indanes	1.58	1.43	644	754
589	C20 monosubstituted benzenes	1.15	1.22	770	837
590	C20 disubstituted benzenes	2.45	1.91	484	586
591	C20 trisubstituted benzenes	4.18	2.66	296	433
592	C20 naphthalenes	2.37	1.69	498	644
593	C20 tetralins or indanes	1.50	1.35	665	788
594	C21 monosubstituted benzenes	1.09	1.16	793	870
595	C21 disubstituted benzenes	2.33	1.82	501	610
596	C21 trisubstituted benzenes	3.97	2.53	314	458
597	C21 naphthalenes	2.25	1.61	514	672
598	C21 tetralins or indanes	1.42	1.29	682	813
599	C22 monosubstituted benzenes	1.04	1.11	812	901
600	C22 disubstituted benzenes	2.22	1.74	519	635
601	C22 trisubstituted benzenes	3.79	2.41	327	480
602	C22 naphthalenes	2.15	1.53	532	716
603	C22 tetralins or indanes	1.36	1.23	701	833

604	ethyl benzene	3.12	2.98	395	378
605	ethyl bromide	0.14	0.13	1111	1141
606	cis-2-butene	14.77	9.25	8	10
607	cis-2-hexene	8.66	6.76	83	50
608	cis-2-heptene	7.40	5.87	126	87
609	ethyl chloride	0.30	0.30	1099	1121
610	cis-2-pentene	10.86	8.17	34	26
611	n-propyl bromide	0.44	0.48	1074	1084
612	cis-3-hexene	8.02	6.89	101	43
613	cis-3-heptene	6.65	5.84	157	89
614	propyl cyclohexane	1.35	1.87	705	597
615	n-propyl formate	0.82	1.05	897	929
616	cis-3-methyl-2-pentene	12.82	6.58	15	57
617	cis-3-methyl-2-hexene	10.42	5.62	40	101
618	1-nitropropane	0.22	0.27	1105	1128
619	4,4-dimethyl-cis-2-pentene	6.86	5.32	145	118
620	n-butyl bromide	0.86	0.89	880	990
621	cis-4-octene	4.01	4.10	309	213
622	1-chlorobutane	1.15	1.19	769	854
623	butyl cyclohexane	1.01	1.55	825	702
624	n-butyl formate	0.88	1.09	873	907
625	cis 4-methyl-2-pentene	8.44	6.51	86	60
626	C4 alkenes	12.72	8.89	16	14
627	C4 terminal alkenes	10.10	8.52	47	19
628	C4 internal alkenes	15.23	9.33	7	8
629	C4 aldehydes	6.27	4.83	173	152
630	cis-5-decene	2.98	3.06	406	366
631	pentyl cyclohexane	0.85	1.39	887	768
632	di-n-pentyl ether	2.68	3.12	452	352
633	pentyl alcohol	2.93	3.15	417	348
634	C5 alkenes	9.23	7.36	67	34
635	C5 terminal alkenes	7.49	6.53	120	59
636	C5 internal alkenes	10.97	8.14	32	28
637	n-pentyl propionate	0.86	1.15	881	877
638	C5 aldehydes	5.32	4.15	213	211
639	hexyl acetates	0.89	1.20	865	852
640	hexyl cyclohexane	0.70	1.24	941	831
641	1,2-dihydroxyhexane	2.16	2.41	531	481
642	C6 cyclic olefins or di-olefins	9.06	6.88	73	44
643	C6 alkenes	6.87	5.83	144	91
644	C6 terminal alkenes	5.69	5.30	198	123

645	C6 internal alkenes	8.84	6.71	78	53
646	C6 aldehydes	4.56	3.56	268	282
647	Unspeciated C6 Alkanes	1.43	0.55	678	1071
648	heptyl cyclohexane	0.61	1.14	995	881
649	2-heptanone	2.45	2.82	485	409
650	C7 cyclic olefins or di-olefins	7.53	5.98	118	79
651	C7 alkenes	5.42	5.12	209	136
652	C7 terminal alkenes	4.23	4.20	289	206
653	C7 internal alkenes	6.64	5.83	159	92
654	C7 aldehydes	3.88	3.07	323	365
655	Unspeciated C7 Alkanes	1.45	0.56	674	1067
656	Unspeciated C8 Aromatics	7.91	1.55	103	695
657	isomers of ethylbenzene	6.78	5.06	153	141
658	C8 disubstituted benzenes	8.02	5.72	100	96
659	octyl cyclohexane	0.56	1.08	1013	912
660	2-octanone	1.50	1.86	663	601
661	C8 cyclic olefins or di-olefins	4.23	4.18	287	208
662	C8 alkenes	3.77	3.77	328	261
663	C8 terminal alkenes	3.40	3.48	358	295
664	C8 internal alkenes	4.15	4.10	297	214
665	C8 alkyl phenols	2.19	1.44	526	747
666	C8 aldehydes	3.31	2.68	370	428
667	Unspeciated C8 Alkanes	1.33	0.54	712	1073
668	Unspeciated C9 Aromatics	8.26	1.53	92	711
669	isomers of propyl benzene	6.47	4.54	165	183
670	C9 monosubstituted benzenes	2.09	2.05	540	546
671	C9 disubstituted benzenes	5.98	4.63	187	179
672	C9 trisubstituted benzenes	11.20	6.83	28	46
673	nonyl cyclohexane	0.52	1.02	1031	942
674	2-nonanone	1.12	1.53	784	717
675	C9 cyclic olefins or di-olefins	4.29	4.07	286	219
676	C9 alkenes	3.46	3.51	352	289
677	C9 terminal alkenes	2.70	2.95	447	387
678	C9 internal alkenes	4.22	4.00	292	227
679	C9 alkyl phenols	1.96	1.29	564	814
680	C9 styrenes	1.59	1.57	643	693
681	Unspeciated C9 Alkanes	1.10	0.47	790	1085
682	camphor	0.51	0.81	1038	1010
683	cyclobutanone	0.65	0.76	968	1027
684	cyclopentanone	1.22	1.44	748	748
685	cyclopentanol	1.80	2.03	590	551

686	cyclohexanone	1.45	1.81	672	617
687	cyclohexanol	2.49	2.91	476	395
688	benzotrifluoride	0.30	0.28	1101	1126
689	methyl chloride	0.04	0.04	1129	1158
690	nitromethane	0.07	0.07	1120	1151
691	chloroform	0.02	0.02	1131	1160
692	Cinnamic alcohol	0.95	1.18	847	860
693	cinnamic aldehyde	5.07	3.48	240	296
694	citronellol (3,7-dimethy-6-octen-1-ol)	5.93	3.41	188	313
695	p-dichlorobenzene	0.18	0.18	1109	1138
696	2-(chloro-methyl)-3-chloro-propene	7.17	5.21	138	130
697	dichloromethane	0.04	0.05	1127	1157
698	trichloroethylene	0.66	0.69	966	1042
699	perchloroethylene	0.03	0.03	1130	1159
700	chloroacetone	9.65	5.51	55	105
701	monochlorobenzene	0.32	0.32	1097	1118
702	chloroacetaldehyde	12.53	6.41	20	65
703	vinyl chloride	2.96	3.11	413	356
704	TLEV Exhaust -- CNG	0.75	0.20	920	1132
705	carbon monoxide	0.06	0.07	1124	1153
706	C7 alkyl phenols	2.47	1.62	478	663
707	crotonaldehyde	9.85	6.63	52	56
708	2-ethoxyethyl acetate	1.90	2.00	572	567
709	C10 cycloalkanes	1.09	1.63	792	661
710	C11 cycloalkanes	0.89	1.44	867	749
711	C12 cycloalkanes	0.82	1.33	895	794
712	C13 cycloalkanes	0.72	1.23	936	834
713	C14 cycloalkanes	0.67	1.16	962	871
714	C15 cycloalkanes	0.63	1.10	980	903
715	C16 cycloalkanes	0.57	1.02	1009	943
716	C17 cycloalkanes	0.54	0.96	1024	968
717	C18 cycloalkanes	0.51	0.91	1041	987
718	C19 cycloalkanes	0.48	0.86	1056	998
719	C20 cycloalkanes	0.46	0.82	1066	1009
720	C21 cycloalkanes	0.43	0.78	1078	1019
721	C22 cycloalkanes	0.41	0.75	1082	1031
722	cyclopropane	0.09	0.11	1115	1143
723	cyclobutane	1.30	1.67	717	649
724	cyclopentane	2.17	2.65	529	436
725	cyclohexane	1.59	2.03	636	552
726	C6 cycloalkanes	1.59	2.03	637	553

727	cycloheptane	1.61	2.56	629	454
728	C7 cycloalkanes	1.87	2.14	581	528
729	cyclooctane	1.55	2.00	647	568
730	C8 cycloalkanes	1.38	2.03	694	554
731	C9 cycloalkanes	1.34	1.87	706	598
732	cyclohexene	5.23	4.74	220	166
733	cyclopentadiene	7.41	5.64	125	100
734	cyclopentene	7.19	5.47	137	106
735	Exxon Exxol® D95 Fluid	0.62	0.33	991	1113
736	dimethyl sebacate	0.45	0.71	1070	1039
737	dimethyl succinate	0.24	0.27	1104	1130
738	dimethyl glutarate	0.39	0.48	1086	1081
739	dimethyl adipate	1.74	1.87	600	599
740	glycol ether DPnB (dipropylene glycol n-butyl ether) (1-[2-butoxy-1-methylethoxy]-2-propanol)	2.13	2.52	534	462
741	dibutyl phthalate	1.28	1.23	730	835
742	3-pentanone	1.28	1.42	729	757
743	dimethyl phthalate	N/A	1.70	1181	642
744	diethylenetriamine	N/A	3.93	1182	235
745	diethylene glycol	3.96	3.99	317	230
746	diethyl phthalate	1.65	1.48	619	730
747	diethylene glycol mono(2-ethylhexyl) ether	1.64	2.02	622	561
748	2-(2-butoxyethoxy)-ethanol	2.54	2.89	473	400
749	2-(2-butoxyethoxy) ethyl acetate	1.46	1.85	671	605
750	2-(2-ethoxyethoxy) ethanol	3.37	3.51	361	290
751	2-(2-ethoxyethoxy) ethyl acetate	1.68	1.99	613	570
752	2-(2-hexyloxyethoxy) ethanol	2.14	2.49	533	464
753	2-(2-propoxyethoxy) ethanol	2.94	3.27	415	333
754	diacetone alcohol	0.62	0.68	990	1045
755	di-isobutyl ketone (2,6-dimethyl-4-heptanone)	2.79	2.82	435	410
756	Dibutyl Adipate	N/A	1.23	1183	836
757	Diethylethanolamine	N/A	3.46	1184	300
758	di-isopropyl ketone	1.36	1.65	700	657
759	diisopropyl adipate	1.34	1.38	707	773
760	diisopropyl carbonate	1.02	1.07	822	918
761	Diisopropylamine	N/A	0.73	1185	1034
762	d-limonene	4.69	3.48	258	297
763	dimethylaminoethanol	5.76	5.08	191	139
764	dimethyl amine	3.30	5.14	371	134

765	dimethyl carbonate	0.06	0.07	1122	1150
766	dimethyl naphthalenes	5.16	3.30	228	332
767	dimethyl sulfoxide (DMSO)	6.83	4.28	149	199
768	dihydroxy acetone	4.07	3.22	303	338
769	dipropylene glycol ethyl ether	2.82	2.97	429	380
770	dipropylene glycol methyl ether acetate isomers	1.85	2.13	585	531
771	dipropylene glycol methyl ether acetate isomer #1	1.83	2.12	587	536
772	dipropylene glycol methyl ether acetate isomer #2	1.87	2.13	579	532
773	dipropylene glycol n-propyl ether isomer #1	2.33	2.73	500	425
774	dipropylene glycol methyl ether: 2-(2-methoxypropoxy)-1-propanol	2.94	2.98	416	379
775	dipropylene glycol isomer (1-[2-hydroxypropyl]-2-propanol)	2.81	3.10	433	358
776	dipropylene glycol methyl ether: 1-methoxy-2-(2-hydroxypropoxy)-propane	2.55	2.90	471	396
777	ethyl 3-ethoxy propionate	3.36	2.93	363	391
778	TLEV Exhaust -- E-85	2.62	1.08	460	913
779	ethylene glycol diethyl ether; 1,2-diethoxyethane	3.06	3.25	401	334
780	2-(2-ethylhexyloxy) ethanol	1.89	2.26	575	506
781	2-n-hexyloxyethanol	2.55	3.03	470	374
782	Ethylene Glycol Monohexyl Ether	N/A	2.63	1186	438
783	2-phenoxyethanol; ethylene glycol phenyl ether	4.65	3.64	261	272
784	ethyl n-butyl ether	3.59	3.83	344	251
785	ethyl acetate	0.66	0.70	964	1040
786	ethyl acrylate	8.08	5.70	98	98
787	ethyl acetylene	6.23	5.07	176	140
788	ethyl amine	6.09	7.10	182	39
789	ethyl tert-butyl ether	2.06	2.08	546	541
790	ethyl butyrate	1.24	1.30	745	805
791	ethyl cyclopentane	1.90	2.38	573	488
792	ethyl cyclohexane	1.55	2.03	648	555
793	ethyl formate	0.50	0.55	1043	1069
794	ethylene glycol diacetate	0.71	0.91	939	986
795	ethylene glycol	3.26	3.23	378	336
796	ethane	0.30	0.34	1100	1111
797	ethyl cyanoacrylate	N/A	3.57	1187	279
798	ethene	9.08	7.51	70	31

799	ethyl lactate	2.56	2.33	469	496
800	ethyl methacrylate	12.72	7.20	17	36
801	Ethyl Nonafluorobutyl Ether	N/A	0.01	1188	1166
802	nitroethane	0.07	0.08	1121	1148
803	1-ethoxy-2-propanol	3.22	3.51	386	291
804	diethyl ether	3.86	3.70	324	268
805	2-ethoxy-ethanol	3.81	3.69	326	269
806	ethanol	1.59	1.74	640	636
807	diethanol-amine	2.62	2.97	459	381
808	triethanolamine	4.29	3.33	284	324
809	ethanolamine	6.99	6.96	141	41
810	ethyl isopropyl ether	3.88	3.43	321	308
811	ethylene oxide	0.04	0.05	1128	1156
812	ethyl propionate	0.81	0.89	899	991
813	formic acid	0.07	0.08	1119	1149
814	formaldehyde	9.47	4.10	64	215
815	furan	9.53	7.09	63	40
816	gamma-butyrolactone	1.01	1.16	823	872
817	geraniol	5.29	3.33	215	325
818	glutaraldehyde	4.44	3.53	277	287
819	glycolic acid	2.82	2.38	430	489
820	glyceryl triacetate	0.57	0.75	1007	1029
821	glycerol	2.70	2.96	445	383
822	glyoxal	12.55	4.71	19	168
823	CARB Hydrocarbon Bin 1	1.52	0.57	658	1065
824	CARB Hydrocarbon Bin 2	1.39	0.52	690	1076
825	CARB Hydrocarbon Bin 3	1.78	0.65	591	1054
826	CARB Hydrocarbon Bin 4	1.57	0.57	645	1064
827	CARB Hydrocarbon Bin 5	1.66	0.58	617	1062
828	CARB Hydrocarbon Bin 6	1.19	0.50	758	1078
829	CARB Hydrocarbon Bin 7	1.07	0.46	802	1088
830	CARB Hydrocarbon Bin 8	1.47	0.57	670	1063
831	CARB Hydrocarbon Bin 9	1.52	0.56	659	1068
832	CARB Hydrocarbon Bin 10	2.07	0.67	545	1046
833	CARB Hydrocarbon Bin 11	0.72	0.36	938	1105
834	CARB Hydrocarbon Bin 12	0.64	0.34	974	1110
835	CARB Hydrocarbon Bin 13	0.87	0.41	877	1096
836	CARB Hydrocarbon Bin 14	1.02	0.42	819	1092
837	CARB Hydrocarbon Bin 15	1.64	0.53	624	1074
838	CARB Hydrocarbon Bin 16	0.53	0.30	1028	1122
839	CARB Hydrocarbon Bin 17	0.49	0.28	1053	1125

840	CARB Hydrocarbon Bin 18	0.62	0.32	988	1116
841	CARB Hydrocarbon Bin 19	0.68	0.31	952	1119
842	CARB Hydrocarbon Bin 20	0.99	0.37	832	1101
843	CARB Hydrocarbon Bin 21	7.91	1.55	104	696
844	CARB Hydrocarbon Bin 22	7.86	1.46	105	736
845	CARB Hydrocarbon Bin 23	7.13	1.29	140	817
846	CARB Hydrocarbon Bin 24	3.99	0.77	311	1021
847	1,1,1,2-tetrafluoroethane; HFC-134a	0.00	0.00	1141	1174
848	1,1-difluoroethane; HFC-152a	0.02	0.02	1133	1161
849	1,1,1,3,3-pentafluoropropane	0.00	0.00	1140	1173
850	methoxy-perfluoro-n-butane	0.00	0.00	1143	1175
851	ethoxy-perfluoro-isobutane	0.01	0.01	1135	1167
852	ethoxy-perfluoro-n-butane	0.01	0.01	1136	1169
853	hydroxy acetone	3.28	2.59	376	449
854	hydroxyl-methacrolein	6.57	4.95	162	147
855	hydroxypropyl acrylate	5.09	4.32	235	197
856	hexyl cinnamal	3.10	2.13	396	533
857	hydroxycitronella	2.73	2.26	440	507
858	cis-hydrindane; bicyclo[4.3.0]nonane	1.24	1.92	743	583
859	isoamyl acetate (3-methyl-butyl acetate)	1.17	1.40	765	766
860	isoamyl alcohol (3-methyl-1-butanol)	3.24	3.31	383	329
861	2,6,8-trimethyl-4-nonanone (isobutyl heptyl ketone)	1.78	2.02	593	562
862	di-isobutyl ether	1.25	1.61	739	673
863	isobutyl acetate	0.65	0.76	970	1023
864	isobutyl acrylate	4.91	3.86	247	243
865	isobutyl isobutyrate	0.61	0.80	994	1011
866	isobutyl methacrylate	8.83	5.12	79	137
867	isobutyric acid	1.24	1.25	744	828
868	8-methyl-1-nonanol (isodecyl alcohol)	1.13	1.41	776	760
869	isopropyl benzene (cumene)	2.58	2.49	466	465
870	isopropyl alcohol	0.64	0.66	975	1053
871	triisopropanolamine	2.73	2.67	439	431
872	isobutyl cyclohexane; (2-methylpropyl) cyclohexane	1.01	1.55	826	703
873	isobutyl alcohol	2.59	2.67	465	432
874	isoamyl isobutyrate	0.88	1.13	869	885
875	indane	3.45	3.12	354	353
876	indene	1.61	1.60	628	678
877	isopropyl acetate	1.10	1.07	791	919
878	isopropyl amine	7.46	7.45	121	33

879	isopropyl cyclopropane	1.30	1.50	723	728
880	isopropyl formate	0.39	0.46	1085	1086
881	diisopropyl ether	3.64	3.04	338	370
882	isobutene	6.46	4.08	166	218
883	isododecane	N/A	1.05	1155	930
884	isohexadecane	N/A	0.94	1156	974
885	Exxon Isopar® M Fluid	0.60	0.32	999	1115
886	isoprene (2-methyl-1,3-butadiene)	11.08	8.34	29	21
887	lumped C5+ unsaturated carbonyl species	6.69	4.60	156	180
888	isophorone (3,5,5-trimethyl-2-cyclohexenone)	4.85	3.33	252	326
889	Kerosene	1.68	0.54	614	1072
890	C10 ketones	0.86	1.30	879	806
891	C10 cyclic ketones	0.92	1.15	853	878
892	C5 ketones	2.91	2.90	422	397
893	C5 cyclic ketones	1.22	1.44	749	750
894	C6 ketones	3.26	3.43	379	309
895	C6 cyclic ketones	1.45	1.81	673	618
896	C7 ketones	2.45	2.82	486	411
897	C7 cyclic ketones	1.27	1.59	732	683
898	C8 ketones	1.50	1.86	664	602
899	C8 cyclic ketones	1.13	1.41	779	761
900	C9 ketones	1.12	1.53	785	718
901	C9 cyclic ketones	1.02	1.27	820	821
902	lauryl pyrrolidone	0.99	1.16	831	873
903	linalool	5.59	3.40	206	316
904	TLEV Exhaust -- LPG	2.10	0.55	537	1070
905	TLEV Exhaust -- M-85	1.59	0.67	638	1049
906	methyl cis-9-pentadecenoate	1.86	1.83	584	608
907	methacrylic acid	18.77	10.20	2	2
908	malic acid	8.62	5.41	84	109
909	methyl amyl acetate (4-methyl-2-pentanol acetate)	1.43	1.62	680	664
910	2-methyl-3-butene-2-ol	5.04	4.33	241	195
911	m-C10 disubstituted benzenes	7.35	4.78	130	160
912	m-C11 disubstituted benzenes	6.36	4.21	170	203
913	m-C12 disubstituted benzenes	5.69	3.80	195	257
914	m-C13 disubstituted benzenes	5.11	3.44	229	306
915	m-C14 disubstituted benzenes	4.61	3.13	263	351
916	m-C15 disubstituted benzenes	4.20	2.88	295	401
917	m-C16 disubstituted benzenes	3.84	2.66	325	434

918	1-methyl-3-n-propyl benzene	7.35	4.78	131	161
919	1-methyl-3-n-butyl benzene	6.36	4.21	171	204
920	m-cresol	2.47	1.62	479	665
921	2-methoxyethyl acetate	1.18	1.33	760	795
922	m-cymene; 1-methyl-3-(1-methylethyl) benzene	7.35	4.78	132	162
923	m-diethyl benzene	7.35	4.78	133	163
924	methylene diphenylene diisocyanate	0.91	0.77	857	1022
925	3-isopropyl cumene; 1,3-di-isopropyl benzene	5.69	3.80	196	258
926	methyl acetate	0.08	0.09	1117	1145
927	methyl acrylate	11.83	7.20	25	37
928	methyl acetylene	6.84	5.44	148	107
929	methylamine	8.06	9.54	99	6
930	methyl bromide	0.02	0.02	1132	1164
931	methyl butyrate	1.13	1.18	780	861
932	methyl decanoate	0.55	0.90	1018	988
933	methyl undecanoate	0.52	0.88	1035	996
934	methyl tridecanoate	0.45	0.82	1068	1008
935	methyl pentadecanoate	0.47	0.84	1062	1001
936	methyl pentanoate; methyl valerate	1.10	1.18	789	862
937	methyl hexanoate	1.07	1.25	798	829
938	methyl heptanoate	0.86	1.10	882	904
939	methyl octanoate	0.72	1.02	937	944
940	methyl nonanoate	0.62	0.94	993	973
941	methyl cyclopentane	2.03	2.43	551	472
942	methyl cyclohexane	1.61	2.14	630	529
943	methyl formate	0.06	0.07	1123	1152
944	Methylene Glycol	N/A	3.23	1157	337
945	methyl glyoxal	16.66	6.67	4	55
946	methyl isobutyrate	0.65	0.74	969	1033
947	methyl indanes	3.08	2.79	397	416
948	methyl ethyl ketone	1.52	1.29	660	815
949	methyl lactate	2.73	2.38	442	490
950	methyl dodecanoate (methyl laurate)	0.48	0.85	1055	999
951	Methacyrlate Monomer	N/A	8.70	1158	16
952	methyl methacrylate	15.84	8.70	5	17
953	methyl myristate (methyl tetradecanoate)	0.44	0.80	1076	1012
954	methyl naphthalenes	3.15	2.77	392	421
955	menthol	1.55	1.82	649	611
956	methoxy-acetone	2.11	1.99	536	571

957	1-methoxy-2-propanol	2.80	3.11	434	357
958	2-methoxy ethanol	3.02	2.83	402	407
959	methanol	0.68	0.63	954	1057
960	dimethyl ether	0.85	0.87	888	997
961	methoxypropanol acetate	1.92	2.25	568	510
962	methylparaben (4-Hydroxybenzoic acid, methyl ester)	1.76	1.15	598	879
963	methyl propionate	0.68	0.67	955	1047
964	methyl pivalate	0.37	0.43	1090	1090
965	methacrolein	6.25	4.67	175	175
966	methane	0.02	0.01	1134	1165
967	dimethoxy methane	1.36	1.63	699	662
968	m-ethyl toluene	7.64	5.23	113	124
969	4-methyl-2-pentanone	4.01	3.67	308	270
970	4-methyl-2-pentanol (methyl isobutyl carbinol)	2.30	2.57	505	451
971	methyl isopropyl carbonate	0.64	0.65	979	1055
972	methyl isopropyl ketone	1.72	1.68	608	646
973	methyl linoleate (methyl cis,cis-9,12-octadecadienoate)	1.91	1.86	571	603
974	methyl linolenate (methyl cis,cis,cis-9,12,15-octadecatrienoate)	2.43	2.23	490	513
975	methyl n-butyl ether	3.24	3.77	382	262
976	methyl n-butyl ketone	3.26	3.43	380	310
977	m-nitrotoluene	0.51	0.49	1039	1079
978	2-(2-methoxyethoxy) ethanol	3.26	3.47	377	299
979	2-pentanone	2.91	2.90	423	398
980	morpholine	2.06	3.16	547	346
981	composite mineral spirit (naphthas or lactol spirits) (CARB Profile ID 802)	1.96	0.64	566	1056
982	Safety-Kleen Mineral Spirits "A" (Type I-B, 91% Alkanes)	1.30	0.48	724	1080
983	Safety-Kleen Mineral Spirits "B" (Type II-C)	0.72	0.37	935	1104
984	Safety-Kleen Mineral Spirits "C" (Type II-C)	0.73	0.37	932	1103
985	thinning solvent/mineral spirits (Cal Poly SLO 1996)	1.99	0.67	557	1050
986	Safety-Kleen Mineral Spirits "D" (Type II-C)	0.73	0.37	930	1102
987	methyl tert-amyl ether (TAME)	1.77	1.92	595	584
988	methyl t-butyl ether	0.77	0.83	915	1007
989	methyl tert-butyl ketone	0.67	0.67	957	1048
990	methylvinyl ketone	10.02	7.88	50	30

991	m-xylene	10.07	6.40	49	66
992	naphthalene	3.50	2.96	350	384
993	n-butyl acrylate	5.25	4.15	218	212
994	n-decane	0.70	1.20	940	853
995	n-undecane	0.62	1.12	989	890
996	n-dodecane	0.56	1.05	1012	931
997	n-tridecane	0.54	1.01	1026	950
998	n-tetradecane	0.52	1.00	1036	955
999	n-pentadecane	0.49	0.97	1050	964
1000	n-C16	0.47	0.94	1060	975
1001	n-C17	0.44	0.89	1072	992
1002	n-C18	0.42	0.84	1079	1003
1003	n-C19	0.40	0.79	1083	1016
1004	n-C20	0.38	0.75	1088	1028
1005	n-C21	0.36	0.72	1092	1035
1006	n-C22	0.34	0.69	1094	1043
1007	n-propyl benzene	2.09	2.05	541	547
1008	n-propyl alcohol	2.60	2.83	461	408
1009	n-butane	1.21	1.39	752	769
1010	n-butyl benzene	2.42	2.42	492	474
1011	n-butyl alcohol	2.98	3.20	407	341
1012	n-pentane	1.38	1.68	693	647
1013	n-pentyl benzene	2.18	2.21	528	517
1014	n-hexane	1.31	1.70	715	643
1015	n-hexyl acetate	0.80	1.14	903	882
1016	n-heptane	1.12	1.58	786	688
1017	n-heptyl acetate	0.67	1.03	960	938
1018	n-octane	0.93	1.39	851	770
1019	n-octyl acetate	0.59	0.98	1002	962
1020	n-nonane	0.81	1.29	898	816
1021	n-nonyl acetate	0.54	0.93	1025	981
1022	n-methyl-2-pyrrolidone	2.54	2.96	474	385
1023	nitrobenzene	0.06	0.06	1125	1154
1024	m-Aminophenol	N/A	1.61	1159	674
1025	Oxo-Decyl Acetate	0.74	0.40	923	1097
1026	o-C10 disubstituted benzenes	5.66	4.37	201	188
1027	o-C11 disubstituted benzenes	4.88	3.81	248	253
1028	Oxo-Dodecyl Acetate	0.64	0.36	978	1106
1029	o-C12 disubstituted benzenes	4.37	3.43	281	311
1030	Oxo-Tridecyl Acetate	0.60	0.34	1000	1109
1031	o-C13 disubstituted benzenes	3.90	3.10	319	359

1032	o-C14 disubstituted benzenes	3.52	2.81	349	413
1033	o-C15 disubstituted benzenes	3.20	2.58	389	450
1034	o-C16 disubstituted benzenes	2.93	2.38	418	491
1035	1-methyl-2-n-propyl benzene	5.66	4.37	202	189
1036	1-butyl-2-methyl benzene	4.88	3.81	249	254
1037	Oxo-Hexyl Acetate	0.96	0.48	838	1082
1038	Oxo-Heptyl Acetate	0.91	0.46	859	1087
1039	Oxo-Octyl Acetate	0.87	0.45	875	1089
1040	Oxo-Nonyl Acetate	0.77	0.41	913	1095
1041	o-dichlorobenzene	0.18	0.18	1110	1139
1042	o-cresol	2.47	1.62	480	666
1043	o-cymene; 1-methyl-2-(1-methylethyl) benzene	5.66	4.37	203	190
1044	1,3-di-n-propyl benzene	4.37	3.43	282	312
1045	o-diethyl benzene	5.66	4.37	204	191
1046	1-ethyl-2-n-propyl benzene	4.88	3.81	250	255
1047	o-ethyl toluene	5.74	4.64	193	177
1048	Hydroxyethyl Methacrylate	N/A	1.44	1189	751
1049	o-tert-butyl toluene; 1-(1,1-dimethylethyl)-2-methyl benzene	4.88	3.81	251	256
1050	o-xylene	7.86	5.89	106	80
1051	peroxyacetic acid	0.54	0.53	1022	1075
1052	propylene carbonate	0.29	0.32	1103	1114
1053	p-C10 disubstituted benzenes	4.55	3.84	272	247
1054	p-C11 disubstituted benzenes	3.98	3.41	312	314
1055	p-C12 disubstituted benzenes	3.57	3.09	345	361
1056	p-C13 disubstituted benzenes	3.21	2.80	387	415
1057	p-C14 disubstituted benzenes	2.92	2.56	420	455
1058	p-C15 disubstituted benzenes	2.67	2.36	453	493
1059	p-C16 disubstituted benzenes	2.45	2.18	483	521
1060	1-methyl-4-n-propyl benzene	4.55	3.84	273	248
1061	p-trifluoromethyl-chloro-benzene	0.13	0.12	1112	1142
1062	p-cresol	2.47	1.62	481	667
1063	1-methyl-4-isopropyl benzene (p-cymene)	4.55	3.84	274	249
1064	p-diethyl benzene	4.55	3.84	275	250
1065	1,4 di-isopropyl benzene	3.57	3.09	346	362
1066	p-ethyl toluene	4.55	4.01	271	223
1067	1-tert-butoxy-2-propanol	1.90	2.15	574	525
1068	2-tert-butoxy-1-propanol	1.86	1.60	583	679
1069	1-methoxy-2-propyl acetate	1.78	1.84	594	606
1070	1-phenoxy-2-propanol	1.65	1.62	620	668

1071	Final LEV -- Phase 2	3.54	0.91	348	983
1072	TLEV exhaust – phase 2	4.00	1.00	310	952
1073	Phenyl Trimethicone	N/A	0.01	1190	1168
1074	phenol	2.84	1.87	427	600
1075	p-isobutyl toluene; 1-methyl-4-(2-methylpropyl) benzene	3.98	3.41	313	315
1076	pentaerythritol	2.05	2.17	548	522
1077	propyl acetate	0.83	1.01	893	951
1078	n-propyl butyrate	1.13	1.35	783	789
1079	propyl cyclopentane	1.59	2.10	639	539
1080	propylene glycol	2.40	2.56	494	456
1081	n-propoxy-propanol	3.88	3.85	320	245
1082	propionic acid	1.26	1.22	735	838
1083	propionaldehyde	7.45	5.73	122	95
1084	propane	0.52	0.60	1033	1060
1085	propene	12.14	9.04	23	13
1086	di-n-propyl ether	3.23	3.66	385	271
1087	propylene oxide	0.31	0.34	1098	1108
1088	1-propoxy-2-propanol (propylene glycol n-propyl ether)	3.07	3.53	400	288
1089	propylparaben	1.48	0.98	667	963
1090	n-propyl propionate	0.90	1.10	863	905
1091	phthalic anhydride	2.64	2.33	457	497
1092	p-toluene isocyanate	1.09	0.99	794	957
1093	p-xylene	5.99	4.89	184	150
1094	3,3-dichloro-1,1,1,2,2-pentafluoropropane;HCFC-225ca	0.00	0.00	1138	1171
1095	1,3-dichloro-1,1,2,2,3-pentafluoropropane;HCFC-225cb	0.00	0.00	1139	1172
1096	1,1,1,3,3-pentafluorobutane; HFC-365mfc	0.00	0.00	1142	1176
1097	1,1,1,2,2,3,4,5,5,5-decafluoropentane; HFC-43-10mee	0.00	0.00	1144	1177
1098	final LEV – RFA	3.64	0.94	337	978
1099	TLEV Exhaust -- RFA	4.09	1.02	301	939
1100	sabinene	4.40	4.07	278	220
1101	stillbenzene derivates	N/A	0.72	1191	1037
1102	sec-butyl acetate	1.39	1.60	692	680
1103	sec-butyl cyclohexane	1.01	1.55	827	704
1104	sec-butyl benzene	2.42	2.42	493	475
1105	sec-butyl alcohol	1.43	1.60	681	681
1106	substituted C7 ester (C12)	0.96	1.12	841	891
1107	substituted C9 ester (C12)	0.96	1.12	842	892

1108	hexamethyl-disiloxane	-0.02	0.02	1145	1163
1109	hydroxymethyl-disiloxane	-0.13	-0.06	1151	1192
1110	styrene	1.80	1.78	589	625
1111	trans-1,2-dichloroethene	1.71	1.53	610	719
1112	trans-1,3-dichloropropene	5.09	3.93	234	236
1113	trans-1,3-hexadiene	10.86	8.30	35	22
1114	trans-1,3-pentadiene	13.10	10.00	14	4
1115	trans-1,4-hexadiene	9.00	7.15	75	38
1116	trans-2,2-dimethyl 3-hexene	5.22	4.91	221	149
1117	trans-2,5-dimethyl 3-hexene	4.93	4.75	245	164
1118	trans-2-butene	15.65	9.38	6	7
1119	trans-2-hexene	9.02	6.68	74	54
1120	trans-2-heptene	7.38	5.86	129	88
1121	trans-2-octene	6.17	4.97	179	145
1122	trans-2-pentene	11.06	8.12	30	29
1123	trans-3-hexene	7.99	6.83	102	47
1124	trans-3-heptene	6.64	5.83	160	93
1125	trans-3-octene	5.10	4.74	233	167
1126	trans-3-methyl-2-pentene	13.37	6.82	11	48
1127	trans-3-methyl-2-hexene	10.42	5.62	41	102
1128	trans-4,4-dimethyl-2-pentene	6.86	5.32	146	119
1129	trans-4-decene	3.60	3.48	342	298
1130	trans-4-octene	4.15	4.10	298	216
1131	trans-4-nonene	4.22	4.00	293	228
1132	trans-4-methyl-2-pentene	8.44	6.51	87	61
1133	trans-4-methyl-2-hexene	7.43	5.88	123	86
1134	trans-5-undecene	3.28	3.16	375	347
1135	trans-5-dodecene	2.96	2.86	412	405
1136	trans-5-tridecene	2.69	2.60	450	445
1137	trans-5-tetradecene	2.44	2.39	489	486
1138	trans-5-pentadecene	2.24	2.21	517	518
1139	tert-butyl acetate	0.18	0.19	1108	1133
1140	tert-butyl amine	-0.42	1.00	1152	953
1141	1-(1,1-dimethylethyl)-3,5-dimethylbenzene	8.16	4.82	95	154
1142	tert-butyl benzene	2.00	1.82	555	612
1143	tert-butyl alcohol	0.42	0.42	1081	1094
1144	C12 tricycloalkanes	0.84	1.37	890	777
1145	C13 tricycloalkanes	0.74	1.26	925	824
1146	C14 tricycloalkanes	0.68	1.18	950	863
1147	C15 tricycloalkanes	0.65	1.12	971	893
1148	C16 tricycloalkanes	0.61	1.05	996	932

1149	C17 tricycloalkanes	0.57	0.99	1010	958
1150	C18 tricycloalkanes	0.54	0.93	1023	980
1151	C19 tricycloalkanes	0.51	0.88	1040	993
1152	C20 tricycloalkanes	0.48	0.84	1054	1002
1153	C21 tricycloalkanes	0.46	0.80	1064	1013
1154	C22 tricycloalkanes	0.44	0.76	1075	1024
1155	2,4-toluene diisocyanate	-0.07	0.19	1147	1135
1156	2,6-toluene diisocyanate	-0.07	0.19	1148	1136
1157	toluene diisocyanate (mixed isomers)	-0.07	0.19	1149	1137
1158	triethyl amine	3.95	4.01	318	224
1159	triethylene glycol	3.35	3.55	365	285
1160	terpene (monoterpenes)	4.14	3.39	299	317
1161	triethyl citrate	0.73	0.76	931	1025
1162	tetraethylene glycol	2.59	2.93	463	392
1163	triethylene diamine	3.56	3.61	347	274
1164	3,6,9,12-tetraoxa-hexadecan-1-ol	1.64	2.03	623	556
1165	2,5,8,11-tetraoxatridecan-13-ol	2.08	2.52	543	463
1166	tetralin (1,2,3,4-tetrahydronaphthalene)	3.08	2.79	398	417
1167	2,2,4-trimethyl-1,3-pentanediol monoisobutyrate and isomers (texanol®)	0.96	1.12	843	894
1168	3-hydroxy-2,2,4-trimethylpentyl-1-isobutyrate	0.98	1.15	835	880
1169	1-hydroxy-2,2,4-trimethylpentyl-3-isobutyrate	0.91	1.05	858	933
1170	2-[2-(2-butoxyethoxy) ethoxy] ethanol	2.08	2.45	544	470
1171	2-[2-(2-ethoxyethoxy) ethoxy] ethanol	2.59	2.95	464	388
1172	tripropylene glycol n-butyl ether	1.73	2.03	606	557
1173	2-[2-(2-methoxyethoxy) ethoxy] ethanol	2.69	3.04	451	371
1174	2-[2-(2-propoxyethoxy) ethoxy] ethanol	2.31	2.68	504	429
1175	tetrahydro-2-furanmethanol (tetrahydrofurfuryl alcohol)	3.39	3.15	359	349
1176	tetrahydrofuran	4.45	4.96	276	146
1177	Tetrahydrofurfuryl Methacrylate	N/A	4.06	1192	221
1178	tetrahydropyran	3.36	3.97	364	232
1179	trimethyl amine	6.52	6.75	164	51
1180	trimethyl cyclohexanol	1.73	2.06	603	542
1181	trimethylene oxide	4.74	5.39	255	114
1182	2,2,4-trimethyl-1,3-pentanediol	1.62	1.82	627	613

1183	tolualdehyde	-0.58	0.00	1153	1178
1184	toluene	4.07	3.75	305	263
1185	tripropylene glycol	2.30	2.75	506	423
1186	tripropylene glycol monomethyl ether	2.04	2.42	550	476
1187	Terpinolene	6.46	3.64	167	273
1188	trans,trans-2,4-hexadiene	9.24	6.85	66	45
1189	2,2,4-trimethyl-1,3-pentanediol diisobutyrate	0.38	0.63	1087	1058
1190	vinyl acetate	3.29	2.36	372	494
1191	1-buten-3-yne (vinyl acetylene)	10.89	9.18	33	11
1192	VMP Naphtha	1.25	0.52	737	1077

5.4   Conclusions

The updated model scenarios for the year 2010 indicate that VOCs have become 17.3% more reactive for the "regular atmospheric condition" or base case scenario in 39 cities across the United States compared to conditions in 1988. MIR values for the year 2010 are 41.1% lower than previously calculated using 1988 conditions, but this artificial metric is likely less relevant than the base case IR condition described above. The increase in reactivity can be attributed to improvements to planetary boundary layer measurements in the WRF model, improvements to biogenic emissions, VOC aloft composition profile and changes in ambient atmospheric conditions (reduction in anthropogenic emissions, seasonality of ozone events and initially present VOC/NOx concentrations).

The relative ranking of IR has not changed dramatically for the most reactive VOCs between 2010 and 1988. The calculated values suggest that the atmospheric conditions where IR is evaluated have a similar impact on all compounds.

The most reactive VOCs with the highest IRs should be revisited in locations that continue to exceed the National Ambient Air Quality Standards for ozone. Regionally stratified calculations should determine if regional IRs are warranted. The incremental reactivity calculated by the 2D box model for select compounds spanning the range of compound classes should also be compared to values calculated with a full 3D air quality model to verify the accuracy of the technique.

6   INFLUENCE OF BIOGENIC VOC REACTIONS WITH NOX ON PREDICTED CONCENTRATIONS OF SECONDARY ORGANIC AEROSOL AND NITRATE

6.1   Introduction

Organic aerosol (OA) makes up approximately 33-50% of PM2.5 mass in California's South Coast Air Basin (SoCAB) and San Joaquin Valley (SJV). These regions consistently have the some of the worst air quality in the United States, requiring additional emissions controls that should be based on the best available science describing sources and formation mechanisms for OA. Recently, organic nitrates have been recognized as a significant contributor to PM2.5 OA mass in Alabama, Colorado, and California [167, 192-194]. More than half of that organic nitrate is thought to come from NO3 radical oxidation of monoterpenes; which is also shown to be an important pathway to account for half of the monoterpene SOA in US. This finding suggests that controls on anthropogenic NOx emissions have the potential to reduce the formation of secondary organic aerosol (SOA) from biogenic sources.

The detailed chemical reactions between anthropogenic NOx and biogenic precursors must be explicitly represented in reactive chemical transport models in order to predict how NOx reductions could reduce the concentrations of particle-phase biogenic organic nitrate compounds. Pye et al. [195] formulated a coupled gas and aerosol system within the CMAQ model to describe the formation of organic nitrates from isoprene and monoterpenes and the subsequent partitioning of these compounds to the particle phase. The expanded version of the CMAQ model was applied to the continental US with 36 km resolution over the period May 21 – June 30, 2103. The new reactions improved the ability to predict PM2.5 OA and gas / particle phase organic nitrates. As much as 60% of the "less oxidized-oxygenated OA" (LOOA) was produced by the organic nitrate mediated chemistry. A 9% reduction in PM2.5 OA mass was predicted for 25% reduction in NOx emissions. The above simulations focused only on mid and eastern US and should be tested for western US including California in summer and winter conditions.

In this study, the SAPRC11 chemical mechanism is expanded to include reactions between NOx and biogenic VOCs based on the mechanism used in Pye et al. [195]. The expanded model is applied using the UCD/CIT air quality model to a winter air quality episode in the SJV (DISCOVER-AQ Jan 16 – Feb 10, 2013) and a summer air quality episode in the SoCAB (CALNEX, May 19 – June 14, 2010). All model calculations use a resolution of 4km. Concentrations of major species predicted with the original SAPRC11 and the expanded SAPRC11 mechanisms are compared to measurements to assess the impact of the expanded reactions. The potential effectiveness of NOx controls to reduce biogenic SOA formation is then evaluated.

6.2 Methods

6.2.1 Air Quality Model

The UCD/CIT air quality model is a regional chemical transport model (CTM) (Kleeman and Cass, 2001) that simulates the emissions, transport, gas-phase chemistry, aerosol physics and aerosol chemistry in the lower troposphere. The model been used to predict regional ozone and aerosol concentrations in numerous previous studies (see for example [105, 196, 197]). The UCD/CIT model uses the SAPRC gas-phase chemical mechanism (one of SAPRC90, SAPRC99, SAPRC07 and SAPRC11) for gas-phase chemical reactions and the ISORROPIA thermodynamic model to simulate aerosol surface vapor pressures. Gas-to-particle conversion is simulated dynamically for the particle size distribution represented by 15 moving sections between 10 nm-10 µm.

The UCD/CIT model was applied to the DISCOVER-AQ (Jan 16 – Feb 10, 2013) and CALNEX (May 19 – June 14, 2010) field studies with two different gas-phase mechanisms (SAPRC11 and expanded SAPRC11). Simulations were carried out for the entire state of California with a grid resolution of 24 km × 24 km followed by nested simulations over the SJV and SoCAB at a grid resolution of 4 km × 4 km. Model calculations were carried out in 16 telescoping vertical levels up to a maximum height of 5 km above ground.

6.2.2 Emissions

Anthropogenic VOC and primary particulate emissions for California are based on the emission inventory provided by California Air Resources Board (CARB) for the year 2010. The wildfire emissions are estimated using FINN (Fire Inventory for National Center for Atmospheric Research) (Wiedinmyer et al., 2011) while biogenic emissions are estimated using MEGAN (Model of Emissions of Gases and Aerosols from Nature) (Guenther et al., 2006). Numerous species were added in the expanded SAPRC11 mechanism by splitting the original SAPRC11 species ARO2, OLE1, OLE2, TERP, ALK3, ARO2 and ARO1 into more detailed species as summarized in Table 1 below.

Table 6-1: Emissions rates of added species SOAALK, NAPHTHAL, PROPENE, APIN, 13BDE, ETOH, ARO2MN, OXYL, PXYL, MXYL, B124, and TOLUENE based on standard SAPRC11 species ALK3, ALK4, ALK5, OLE1, OLE2, ARO1, ARO2, and TERP

1)	SOAALK = O.1 ALK4 + 0.7 ALK5	7)	ARO2MN = 0.96*0.366 ARO2
2)	NAPHTHAL = 0.04 ARO2	8)	OXYL = 0.96*0.171 ARO2
3)	PROPENE = 0.68 OLE1	9)	PXYL = 0.96*0.073 ARO2
4)	APIN = 0.44 TERP	10)	MXYL = 0.96*0.293 ARO2
5)	13BDE = 0.15 OLE2	11)	B124 = 0.96*0.097 ARO2
6)	ETOH = 0.654 ALK3	12)	TOLUENE = 0.804 ARO1

6.2.3 Meteorology and Initial / Boundary Conditions

The Weather Research and Forecasting (WRFv3.4) was used to generate hourly meteorological fields for the CALNEX and DISCOVER-AQ time periods. WRF was configured with the Advanced Research core (ARW) model version v3.4 with a horizontal resolution of 4 km and 31 vertical layers up to 100mb (~12km) to provide meteorological input to the UCD/CIT model. The National Center for Environmental Protection's (NCEP) North American Region Reanalysis (NARR) data were used to set the initial and boundary conditions for WRF.

The gas and particle phase initial and hourly varying boundary conditions for the UCD/CIT model were taken from the global model MOZART-4/NCEP (a model for ozone and related chemical Tracers). Additional details of MOZART simulations are provided by Emmons et al. [101].

6.2.4 Gas Phase Chemistry

Reaction rates between NO2+OH and isoprene+OH / ozone were updated in both SAPRC11 and the expanded SAPRC11 mechanisms based on the latest published values. The expanded SAPRC11 mechanism was then modified to include the explicit reactions between NOx and isoprene that are described in the mechanism of Xie et al. [7] and Pye et al. [195]. The expanded reactions were then further updated to separately track isoprene dinitrates (ISOPNN) produced from isoprene + NO3. ISOPNN is a semi-volatile organic nitrate molecule that readily partitions into the particle phase. The formation of organic nitrates from monoterpenes (analogous to PAN) was also tracked explicitly in the expanded mechanism to better represent their role as NOx reservoirs and SOA precursors. Species lumped into TERP (including β-pinene, δ-limonene, α-terpinene, γ-terpinene, camphene, Δ-3-carene, myrcene, pcymene, ocimene, β-hellandrene, sabinene etc.) are reported to form significant aerosol including organic nitrates [16, 198]. TERP chemistry was updated in the expanded SAPRC11 mechanism to represent organic nitrates formed from monoterpenes as a new species named MTNO3. The rate constants of TERP peroxy + HO2 reactions were updated based on values listed in the Master Chemical Mechanism (MCM v3.3) which increased their reaction rate by a factor of 2.7 at 298 K. Pye et al. [6] also incorporated heterogeneous conversion of NO3 to nitric acid but this pathway was not included in the present study. Sensitivity tests show that this omission has negligible effects on HNO3 / nitrate concentrations since NO3 concentrations are very low. Table 6-2 summarizes a complete list of the expanded reactions in the expanded SAPRC11 mechanism.

Table 6-2: Updated reactions and added reactions to the expanded SAPRC11 mechanism. All reaction labels listed in rate constants refer to the base SAPRC11 mechanism if not otherwise listed. See footnotes for details on rate constants. Adapted from Pye et al. [195].

Label	Reaction	k (cm^{-3} molec sec^{-1})	Notes
<25>	OH + NO2 = HNO3	k0=3.2e-30*(T/300)(-4.50), kinf=3.0e-11, F=0.41, n=1.24. See footnote 1.	updated based on IUPAC

<BR32>	RCO3 + HO2 = 0.3075*RCOOOH + 0.1025*RCOOH + 0.15*O3 + 0.44*OH + 0.44*xHO2 + 0.44*RO2C + 0.44*CO2 + 0.44*xCCHO + 0.44*yROOH	1.0*K<BR22>	revised
<BR43>	BZCO3 + HO2 = 0.3075*RCOOOH + 0.1025*RCOOH + 0.15*O3 + 0.44*OH + 0.44*BZO + 0.44*RO2C + 0.44*CO2	1.0*K<BR22>	revised
<BP32>	GLY + OH = 0.70*HO2 + 1.40*CO + 0.3*HCOCO3	3.10e-12*exp(342.2/T)	revised
<BP33>	GLY + NO3 = HNO3 + 0.70*HO2 + 1.40*CO + 0.3*HCOCO3	2.80e-12*exp(-2390/T)	revised
<BP84>	HCOCO3 + NO = HO2 + CO + CO2 + NO2	1.0*K<BR31>	new glyoxal product added
<BP85>	HCOCO3 + NO2 = HO2 + CO + CO2 + NO3	1.0*K<BR28>	new glyoxal product added
<BP86>	HCOCO3 + HO2 = 0.44*OH + 0.44*HO2 + 0.44*CO + 0.44*CO2 + 0.56*GLY + 0.15*O3	1.0*K<BR22>	new glyoxal product added
<PX161>	xMTNO3 + NO = NO + MTNO3	1.0*K<BR07>	following xRNO3
<PX162>	xMTNO3 + HO2 = HO2 + 6*XC + XN	2.65e-13*exp(1300/T)	Rate constant from MCM for 10 C
<PX163>	xMTNO3 + NO3 = NO3 + MTNO3	1.0*K<BR09>	
<PX164>	xMTNO3 + MEO2 = MEO2 + 0.5*MTNO3 + 0.5*XN + 3*XC	1.0*K<BR10>	
<PX165>	xMTNO3 + RO2C = RO2C + 0.5*MTNO3 + 0.5*XN + 3*XC	1.0*K<BR11>	
<PX166>	xMTNO3 + RO2XC = RO2XC + 0.5*MTNO3 + 0.5*XN + 3*XC	1.0*K<BR11>	
<PX167>	xMTNO3 + MECO3 = MECO3 + MTNO3	1.0*K<BR25>	
<PX168>	xMTNO3 + RCO3 = RCO3 + MTNO3	1.0*K<BR25>	
<PX169>	xMTNO3 + BZCO3 = BZCO3 + MTNO3	1.0*K<BR25>	
<PX170>	xMTNO3 + MACO3 = MACO3 + MTNO3	1.0*K<BR25>	
<PX170b>	xMTNO3 + IMACO3 = MACO3 + MTNO3	1.0*K<BR25>	
<PZ201>	zMTNO3 + NO = NO + MTNO3-1*XN	1.0*K<BR07>	following zRNO3
<PZ202>	zMTNO3 + HO2 = HO2 + 6*XC	2.65e-13*exp(1300/T)	Rate constant from MCM for 10 C
<PZ203>	zMTNO3 + NO3 = NO3 + PRD2 + HO2	1.0*K<BR09>	
<PZ204>	zMTNO3 + MEO2 = MEO2 + 0.5*PRD2 + 0.5*HO2 + 3*XC	1.0*K<BR10>	
<PZ205>	zMTNO3 + RO2C = RO2C + 0.5*PRD2 + 0.5*HO2 + 3*XC	1.0*K<BR11>	
<PZ206>	zMTNO3 + RO2XC = RO2XC + 0.5*PRD2 + 0.5*HO2 + 3*XC	1.0*K<BR11>	
<PZ207>	zMTNO3 + MECO3 = MECO3 + PRD2 + HO2	1.0*K<BR25>	
<PZ208>	zMTNO3 + RCO3 = RCO3 + PRD2 + HO2	1.0*K<BR25>	

<PZ209>	zMTNO3 + BZCO3 = BZCO3 + PRD2 + HO2	1.0*K<BR25>	
<PZ210>	zMTNO3 + MACO3 = MACO3 + PRD2 + HO2	1.0*K<BR25>	
<PZ210b>	zMTNO3 + IMACO3 = IMACO3 + PRD2 + HO2	1.0*K<BR25>	
<P211>	xHOCCHO + NO = NO + HOCCHO	1.0*K<BR07>	
<P212>	xHOCCHO + HO2 = HO2 + 2*XC	1.0*K<BR08>	
<P213>	xHOCCHO + NO3 = NO3 + HOCCHO	1.0*K<BR09>	
<P214>	xHOCCHO + MEO2 = MEO2 + 0.5*HOCCHO + XC	1.0*K<BR10>	
<P215>	xHOCCHO + RO2C = RO2C + 0.5*HOCCHO + XC	1.0*K<BR11>	
<P216>	xHOCCHO + RO2XC = RO2XC + 0.5*HOCCHO + XC	1.0*K<BR11>	
<P217>	xHOCCHO + MECO3 = MECO3 + HOCCHO	1.0*K<BR25>	
<P218>	xHOCCHO + RCO3 = RCO3 + HOCCHO	1.0*K<BR25>	
<P219>	xHOCCHO + BZCO3 = BZCO3 + HOCCHO	1.0*K<BR25>	
<P220>	xHOCCHO + MACO3 = MACO3 + HOCCHO	1.0*K<BR25>	
<P221>	xACROLEIN + NO = NO + ACROLEIN	1.0*K<BR07>	
<P222>	xACROLEIN + HO2 = HO2 + 3*XC	1.0*K<BR08>	
<P223>	xACROLEIN + NO3 = NO3 + ACROLEIN	1.0*K<BR09>	
<P224>	xACROLEIN + MEO2 = MEO2 + 0.5*ACROLEIN + 1.5*XC	1.0*K<BR10>	
<P225>	xACROLEIN + RO2C = RO2C + 0.5*ACROLEIN + 1.5*XC	1.0*K<BR11>	
<P226>	xACROLEIN + RO2XC = RO2XC + 0.5*ACROLEIN + 1.5*XC	1.0*K<BR11>	
<P227>	xACROLEIN + MECO3 = MECO3 + ACROLEIN	1.0*K<BR25>	
<P228>	xACROLEIN + RCO3 = RCO3 + ACROLEIN	1.0*K<BR25>	
<P229>	xACROLEIN + BZCO3 = BZCO3 + ACROLEIN	1.0*K<BR25>	
<P230>	xACROLEIN + MACO3 = MACO3 + ACROLEIN	1.0*K<BR25>	
<BE04>	ETHENE + NO3 = xHO2 + RO2C + xRCHO + yROOH + XN-1*XC	3.30e-12*exp(-2880/T)	corrected temperature power (set to zero)
<BT05>	BUTADIENE13 + OH = 0.951*xHO2 + 1.189*RO2C + 0.049*RO2XC + 0.049*zRNO3 + 0.708*xHCHO + 0.58*xACROLEIN + 0.471*xIPRD + yROOH-0.797*XC	1.48e-11*exp(448/T)	Acrolein yield increased from 0.48 to 0.58
<BT06>	BUTADIENE13 + O3 = 0.08*HO2 + 0.08*OH + 0.255*CO + 0.185*CO2 + 0.5*HCHO + 0.185*HCOOH + 0.5*ACROLEIN + 0.375*MVK + 0.125*PRD2-0.875*XC	1.34e-14*exp(-2283/T)	

<BT07>	BUTADIENE13 + NO3 = 0.815*xHO2 + 0.12*xNO2 + 1.055*RO2C + 0.065*RO2XC + 0.065*zRNO3 + 0.115*xHCHO + 0.46*xMVK + 0.12*xIPRD + 0.355*xRNO3 + yROOH + 0.525*XN-1.075*XC	1.00E-13	
<BT08>	BUTADIENE13 + O3P = 0.25*HO2 + 0.117*xHO2 + 0.118*xMACO3 + 0.235*RO2C + 0.015*RO2XC + 0.015*zRNO3 + 0.115*xCO + 0.115*xACROLEIN + 0.001*xAFG1 + 0.001*xAFG2 + 0.75*PRD2 + 0.25*yROOH-1.532*XC	2.26e-11*exp(-40/T)	
<BT09>	APIN + OH = 0.799*xHO2 + 0.004*xRCO3 + 1.042*RO2C + 0.197*RO2XC + 0.197*zRNO3 + 0.002*xCO + 0.022*xHCHO + 0.776*xRCHO + 0.034*xACETONE + 0.02*xMGLY + 0.023*xBACL + yR6OOH + TRPRXN + 6.2*XC	1.21e-11*exp(436/T)	
<BT10>	APIN + O3 = 0.009*HO2 + 0.102*xHO2 + 0.728*OH + 0.001*xMECO3 + 0.297*xRCO3 + 1.511*RO2C + 0.337*RO2XC + 0.337*zRNO3 + 0.029*CO + 0.051*xCO + 0.017*CO2 + 0.344*xHCHO + 0.24*xRCHO + 0.345*xACETONE + 0.008*MEK + 0.002*xGLY + 0.081*xBACL + 0.255*PRD2 + 0.737*yR6OOH + TRPRXN + 2.999*XC	5.00e-16*exp(-530/T)	
<BT11>	APIN + NO3 = 0.056*xHO2 + 0.643*xNO2 + 0.007*xRCO3 + 1.05*RO2C + 0.293*RO2XC + 0.293*zRNO3 + 0.005*xCO + 0.007*xHCHO + 0.684*xRCHO + 0.069*xACETONE + 0.002*xMGLY + 0.056*xRNO3 + yR6OOH + 0.301*XN + 5.608*XC	1.19e-12*exp(490/T)	no longer forms TRPRXN
<BT12>	APIN + O3P = PRD2 + TRPRXN + 4*XC	3.20E-11	
<BE10>	ACETYLENE + OH = 0.3*HO2 + 0.7*OH + 0.3*CO + 0.3*HCOOH + 0.7*GLY	k0=5.50e-30, kinf=8.30e-13*(T/300)(-2.00), F=0.60, n=1.0. See footnote 1.	corrected temperature dependence (infinity rate has T dependence)
<BT13>	TOLUENE + OH = 0.181*HO2 + 0.454*xHO2 + 0.312*OH + 0.454*RO2C + 0.054*RO2XC + 0.054*zRNO3 + 0.238*xGLY + 0.151*xMGLY + 0.181*CRES + 0.065*xBALD + 0.195*xAFG1 + 0.195*xAFG2 + 0.312*AFG3 + 0.073*yR6OOH + 0.435*yRAOOH + TOLRO2-0.109*XC	1.81e-12*exp(338/T)	

<BT14>	MXYL + OH = 0.159*HO2 + 0.52*xHO2 + 0.239*OH + 0.52*RO2C + 0.082*RO2XC + 0.082*zRNO3 + 0.1*xGLY + 0.38*xMGLY + 0.159*CRES + 0.041*xBALD + 0.336*xAFG1 + 0.144*xAFG2 + 0.239*AFG3 + 0.047*yR6OOH + 0.555*yRAOOH + XYLRO2 + 0.695*XC	2.31E-11	
<BT15>	OXYL + OH = 0.161*HO2 + 0.554*xHO2 + 0.198*OH + 0.554*RO2C + 0.087*RO2XC + 0.087*zRNO3 + 0.084*xGLY + 0.238*xMGLY + 0.185*xBACL + 0.161*CRES + 0.047*xBALD + 0.253*xAFG1 + 0.253*xAFG2 + 0.198*AFG3 + 0.055*yR6OOH + 0.586*yRAOOH + XYLRO2 + 0.484*XC	1.36E-11	
<BT16>	PXYL + OH = 0.159*HO2 + 0.487*xHO2 + 0.278*OH + 0.487*RO2C + 0.076*RO2XC + 0.076*zRNO3 + 0.286*xGLY + 0.112*xMGLY + 0.159*CRES + 0.088*xBALD + 0.045*xAFG1 + 0.067*xAFG2 + 0.278*AFG3 + 0.286*xAFG3 + 0.102*yR6OOH + 0.461*yRAOOH + XYLRO2 + 0.399*XC	1.43E-11	
<BT17>	TMBENZ124 + OH = 0.022*HO2 + 0.627*xHO2 + 0.23*OH + 0.627*RO2C + 0.121*RO2XC + 0.121*zRNO3 + 0.074*xGLY + 0.405*xMGLY + 0.112*xBACL + 0.022*CRES + 0.036*xBALD + 0.088*xAFG1 + 0.352*xAFG2 + 0.23*AFG3 + 0.151*xAFG3 + 0.043*yR6OOH + 0.705*yRAOOH + XYLRO2 + 1.19*XC	3.25E-11	
<BT18>	ETOH + OH = 0.95*HO2 + 0.05*xHO2 + 0.05*RO2C + 0.081*xHCHO + 0.95*CCHO + 0.01*xHOCCHO + 0.05*yROOH-0.001*XC	5.49e-13*(T/300)(2.00)*exp(530/T)	
<BL05>	ALK5 + OH = 0.647*xHO2 + 1.605*RO2C + 0.353*RO2XC + 0.353*zRNO3 + 0.04*xHCHO + 0.106*xCCHO + 0.209*xRCHO + 0.071*xACETONE + 0.086*xMEK + 0.407*xPROD2 + yR6OOH + 2.004*XC	2.70e-12*exp(374/T)	no longer forms ALKRXN/ALK5RXN
<AALK>	SOAALK + OH = OH + 0.47*ALKRXN	2.70e-12*exp(374/T)	0.47 accounts for the fact that not all SOAALK behaves like dodecane

<BL15a>	ARO2MN + OH = 0.077*HO2 + 0.617*xHO2 + 0.178*OH + 0.617*RO2C + 0.128*RO2XC + 0.128*zRNO3 + 0.088*xGLY + 0.312*xMGLY + 0.134*xBACL + 0.077*CRES + 0.026*xBALD + 0.221*xAFG1 + 0.247*xAFG2 + 0.178*AFG3 + 0.068*xAFG3 + 0.057*xPROD2 + 0.101*yR6OOH + XYLRO2 + 1.459*XC	3.09E-11	same products as ARO2
<BL15b>	NAPHTHAL + OH = 0.077*HO2 + 0.617*xHO2 + 0.178*OH + 0.617*RO2C + 0.128*RO2XC + 0.128*zRNO3 + 0.088*xGLY + 0.312*xMGLY + 0.134*xBACL + 0.077*CRES + 0.026*xBALD + 0.221*xAFG1 + 0.247*xAFG2 + 0.178*AFG3 + 0.068*xAFG3 + 0.057*xPROD2 + 0.101*yR6OOH + PAHRO2 + 1.459*XC	3.09E-11	same products as ARO2, PAHRO2 tracks SOA
<BL16>	TERP + OH = 0.734*xHO2 + 0.064*xRCO3 + 1.211*RO2C + 0.201*RO2XC + 0.201*zMTNO3 + 0.001*xCO + 0.411*xHCHO + 0.385*xRCHO + 0.037*xACETONE + 0.007*xMEK + 0.003*xMGLY + 0.009*xBACL + 0.003*xMVK + 0.002*xIPRD + 0.409*xPROD2 + yR6OOH + TRPRXN + 4.375*XC	2.27e-11*exp(435/T)	zRNO3 product replaced with zMTNO3 for SOA purposes
<BL17>	TERP + O3 = 0.078*HO2 + 0.046*xHO2 + 0.499*OH + 0.202*xMECO3 + 0.059*rRCO3 + 0.49*RO2C + 0.121*RO2XC + 0.121*zMTNO3 + 0.249*CO + 0.063*CO2 + 0.127*HCHO + 0.033*xHCHO + 0.208*xRCHO + 0.057*xACETONE + 0.002*MEK + 0.172*HCOOH + 0.068*RCOOH + 0.003*xMGLY + 0.039*xBACL + 0.002*xMACR + 0.001*xIPRD + 0.502*PRD2 + 0.428*yR6OOH + TRPRXN + 3.852*XC	8.28e-16*exp(-785/T)	zRNO3 replaced with zMTNO3 for SOA purposes
<BL18>	TERP + NO3 = TERPNRO2	1.33e-12*exp(490/T)	no longer forms TRPXN for SOA
<BL18a>	TERPNRO2 + NO = 0.827*NO2 + 0.688*MTNO3 + 0.424*RO2C + 0.227*HO2 + 0.026*RCO3 + 0.012*CO + 0.023*HCHO + 0.002*HOCCHO + 0.403*RCHO + 0.239*ACETONE + 0.005*MACR + 0.001*MVK + 0.004*IPRD + 0.485*XN + 1.035*XC	1.0*K<BR07>	
<BL18b>	TERPNRO2 + HO2 = 1.0*MTNO3	2.65e-13*exp(1300/T)	
<BL18c>	TERPNRO2 + NO3 = 1.531*NO2 + 0.422*MTNO3 + 0.786*RO2C + 0.420*HO2 + 0.048*RCO3 + 0.022*CO + 0.043*HCHO + 0.004*HOCCHO + 0.746*RCHO + 0.443*ACETONE + 0.009*MACR + 0.002*MVK +	1.0*K<BR09>	

	0.007*IPRD + 0.047*XN + 1.917*XC	
<BL18d>	TERPNRO2 + MEO2 = 0.266*NO2 + 0.711*MTNO3 + 0.393*RO2C + 0.710*HO2 + 0.024*RCO3 + 0.011*CO + 0.772*HCHO + 0.002*HOCCHO + 0.373*RCHO + 0.222*ACETONE + 0.005*MACR + 0.001*MVK + 0.004*IPRD + 0.024*XN + 0.959*XC + 0.250*MEOH	1.0*K<BR10>
<BL18e>	TERPNRO2 + RO2C = 0.266*NO2 + 0.711*MTNO3 + 0.393*RO2C + 0.210*HO2 + 0.024*RCO3 + 0.011*CO + 0.022*HCHO + 0.002*HOCCHO + 0.373*RCHO + 0.222*ACETONE + 0.005*MACR + 0.001*MVK + 0.004*IPRD + 0.024*XN + 0.959*XC	1.0*K<BR11>
<BL18f>	TERPNRO2 + RO2XC = 0.266*NO2 + 0.711*MTNO3 + 0.393*RO2C + 0.210*HO2 + 0.024*RCO3 + 0.011*CO + 0.022*HCHO + 0.002*HOCCHO + 0.373*RCHO + 0.222*ACETONE + 0.005*MACR + 0.001*MVK + 0.004*IPRD + 0.024*XN + 0.959*XC	1.0*K<BR11>
<BL18g>	TERPNRO2 + MECO3 = 0.531*NO2 + 0.422*MTNO3 + 0.786*RO2C + 0.420*HO2 + 0.048*RCO3 + 0.022*CO + 0.043*HCHO + 0.004*HOCCHO + 0.746*RCHO + 0.443*ACETONE + 0.009*MACR + 0.002*MVK + 0.007*IPRD + 0.047*XN + 1.917*XC + MEO2 + CO2	1.0*K<BR25>
<BL18h>	TERPNRO2 + RCO3 = 0.531*NO2 + 0.422*MTNO3 + 1.786*RO2C + 0.420*HO2 + 0.048*RCO3 + 0.022*CO + 0.043*HCHO + 0.004*HOCCHO + 0.746*RCHO + 0.443*ACETONE + 0.009*MACR + 0.002*MVK + 0.007*IPRD + 0.047*XN + 1.917*XC + CO2 + xHO2 + xCCHO + yROOH	1.0*K<BR25>
<BL18i>	TERPNRO2 + BZCO3 = 0.531*NO2 + 0.422*MTNO3 + 1.786*RO2C + 0.420*HO2 + 0.048*RCO3 + 0.022*CO + 0.043*HCHO + 0.004*HOCCHO + 0.746*RCHO + 0.443*ACETONE + 0.009*MACR + 0.002*MVK + 0.007*IPRD + 0.047*XN + 1.917*XC + CO2 + BZO	1.0*K<BR25>
<BL19j>	TERPNRO2 + MACO3 = 1.0*CO2 + 1.0*HCHO + 1.0*MECO3 + 0.786*RO2C + 0.420*HO2 + 0.531*NO2 + 0.048*RCO3 + 0.022*CO + 0.043*HCHO + 0.004*HOCCHO + 0.746*RCHO + 0.443*ACETONE + 0.009*MACR + 0.002*MVK + 0.007*IPRD + 0.422*MTNO3 + 0.047*XN + 1.917*XC	1.0*K<BR25>

\<BL19k\>	TERPNRO2 + IMACO3 = 1.0*CO2 + 1.0*HCHO + 1.0*MECO3 + 0.786*RO2C + 0.420*HO2 + 0.531*NO2 + 0.048*RCO3 + 0.022*CO + 0.043*HCHO + 0.004*HOCCHO + 0.746*RCHO + 0.443*ACETONE + 0.009*MACR + 0.002*MVK + 0.007*IPRD + 0.422*MTNO3 + 0.047*XN + 1.917*XC	1.0*K\<BR25\>	
\<BL19\>	TERP + O3P = 0.237*RCHO + 0.763*PRD2 + TRPRXN + 4.711*XC	4.02E-11	
\<TE02\>	BUTADIENE13 + CL = 0.39*xHO2 + 0.541*xCL + 1.884*RO2C + 0.069*RO2XC + 0.069*zRNO3 + 0.863*xHCHO + 0.457*xACROLEIN + 0.473*xIPRD + yROOH-1.013*XC	4.90E-10	
\<TE03\>	APIN + CL = 0.548*HCL + 0.252*xHO2 + 0.068*xCL + 0.034*xMECO3 + 0.05*xRCO3 + 0.016*xMACO3 + 2.258*RO2C + 0.582*RO2XC + 0.582*zRNO3 + 0.035*xCO + 0.158*xHCHO + 0.185*xRCHO + 0.274*xACETONE + 0.007*xGLY + 0.003*xBACL + 0.003*xMVK + 0.158*xIPRD + 0.006*xAFG1 + 0.006*xAFG2 + 0.001*xAFG3 + 0.109*xCLCCHO + yR6OOH + 3.543*XC	5.46E-10	
\<TE04\>	TOLUENE + CL = 0.894*xHO2 + 0.894*RO2C + 0.106*RO2XC + 0.106*zRNO3 + 0.894*xBALD + 0.106*XC	6.20E-11	
\<TE05\>	MXYL + CL = 0.864*xHO2 + 0.864*RO2C + 0.136*RO2XC + 0.136*zRNO3 + 0.864*xBALD + 1.136*XC	1.35E-10	
\<TE06\>	OXYL + CL = 0.864*xHO2 + 0.864*RO2C + 0.136*RO2XC + 0.136*zRNO3 + 0.864*xBALD + 1.136*XC	1.40E-10	
\<TE07\>	PXYL + CL = 0.864*xHO2 + 0.864*RO2C + 0.136*RO2XC + 0.136*zRNO3 + 0.864*xBALD + 1.136*XC	1.44E-10	
\<TE08\>	TMBENZ124 + CL = 0.838*xHO2 + 0.838*RO2C + 0.162*RO2XC + 0.162*zRNO3 + 0.838*xBALD + 2.162*XC	2.42E-10	
\<BC09a\>	ARO2MN + CL = 0.828*xHO2 + 0.828*RO2C + 0.172*RO2XC + 0.172*zRNO3 + 0.469*xBALD + 0.359*xPROD2 + 2.531*XC	2.66E-10	ARO2>ARO2MN
\<BC09b\>	NAPHTHAL + CL = 0.828*xHO2 + 0.828*RO2C + 0.172*RO2XC + 0.172*zRNO3 + 0.469*xBALD + 0.359*xPROD2 + 2.531*XC	2.66E-10	behaves like ARO2
\<AE57\>	PAHRO2 + NO = NO + PAHNRXN	1.0*K\<BR07\>	High-NOx SOA
\<AE58\>	PAHRO2 + HO2 = HO2 + PAHHRXN	1.0*K\<BR08\>	Low-NOx SOA

\<IS1\>	ISOPRENE + OH = ISOPO2 + ISOPRXN	2.54e-11*exp(410/T)	
\<IS2\>	ISOPO2 + NO = 0.40*MVK + 0.26*MACR + 0.883*NO2 + 0.07*ISOPND + 0.047*ISOPNB + 0.66*HCHO + 0.10*HC5 + 0.043*ARO2MN + 0.08*DIBOO + 0.803*HO2	2.60e-12*exp(380/T)	ARO2>ARO2MN
\<IS3\>	ISOPO2 + HO2 = 0.880*ISOPOOH + 0.120*OH + 0.047*MACR + 0.073*MVK + 0.120*HO2 + 0.120*HCHO	2.06e-13*exp(1300/T)	
\<IS4\>	ISOPO2 + MEO2 = 0.45*HO2 + 0.37*HCHO + 0.23*MVK + 0.15*MACR + 0.05*DIBOO + 0.06*HC5 + 0.02*ARO2MN + 0.5*PRD2 + 0.5*HCHO + 0.5*HO2 + 0.25*HCHO + 0.25*MEOH-0.62*XC	1.80E-12	ARO2>ARO2MN
\<IS5\>	ISOPO2 + RO2C = 0.45*HO2 + 0.37*HCHO + 0.23*MVK + 0.15*MACR + 0.05*DIBOO + 0.06*HC5 + 0.02*ARO2MN + 0.5*PRD2-0.62*XC	6.80E-13	ARO2>ARO2MN
\<IS6\>	ISOPO2 + ISOPO2 = 0.91*HO2 + 0.75*HCHO + 0.45*MVK + 0.29*MACR + 0.09*DIBOO + 0.11*HC5 + 0.05*ARO2MN + PRD2-1.24*XC	2.30E-12	ARO2>ARO2MN
\<IS7\>	ISOPO2 + MECO3 = MEO2 + CO2 + 0.91*HO2 + 0.75*HCHO + 0.45*MVK + 0.29*MACR + 0.09*DIBOO + 0.11*HC5 + 0.05*ARO2MN-0.16*XC	4.40e-13*exp(1070/T)	ARO2>ARO2MN
\<IS107\>	ISOPO2 = HO2 + HPALD	4.07e8*exp(-7694/T)	
\<IS137\>	HPALD = OH + HO2 + 0.5*HACET + 0.5*MGLY + 0.25*HOCCHO + 0.25*GLY + HCHO	1.0/\<HPALD\>	
\<IS138\>	HPALD + OH = OH + PRD2-XC	4.60E-11	
\<IS9\>	ISOPRENE + NO3 = NISOPO2	3.03e-12*exp(-448/T)	
\<IS10\>	NISOPO2 + NO3 = 0.70*NIT1 + 0.035*MVK + 0.035*MACR + 1.3*NO2 + 0.80*HO2 + 0.070*HCHO + 0.23*HC5	2.30E-12	
\<IS11\>	NISOPO2 + NO = 0.70*NIT1 + 0.035*MVK + 0.035*MACR + 1.3*NO2 + 0.80*HO2 + 0.070*HCHO + 0.23*HC5	2.60e-12*exp(380/T)	
\<IS12\>	NISOPO2 + HO2 = NISOPOOH	2.06e-13*exp(1300/T)	
\<IS13\>	NISOPO2 + MEO2 = 0.35*NIT1 + 0.0175*MVK + 0.0175*MACR + 0.15*NO2 + 0.40*HO2 + 0.035*HCHO + 0.115*HC5 + 0.25*NIT1 + 0.25*ISOPND + 0.5*HCHO + 0.5*HO2 + 0.25*HCHO + 0.25*MEOH	1.30E-12	
\<IS14\>	NISOPO2 + RO2C = 0.35*NIT1 + 0.0175*MVK + 0.0175*MACR + 0.15*NO2 + 0.40*HO2 + 0.035*HCHO + 0.115*HC5 + 0.25*NIT1 + 0.25*ISOPND	6.04E-13	

<IS140>	NISOPO2 + NISOPO2 = 0.70*NIT1 + 0.035*MVK + 0.035*MACR + 0.3*NO2 + 0.80*HO2 + 0.070*HCHO + 0.23*HC5 + 0.5*NIT1 + 0.5*ISOPND	1.20E-12	
<IS15>	NISOPO2 + MECO3 = MEO2 + CO2 + 0.70*NIT1 + 0.035*MVK + 0.035*MACR + 0.3*NO2 + 0.80*HO2 + 0.070*HCHO + 0.23*HC5	4.40e-13*exp(1070/T)	
<IS17>	HC5 + OH = HC5OO	1.42e-11*exp(610/T)	
<IS18>	HC5OO + NO = NO2 + 0.234*HOCCHO + 0.234*MGLY + 0.216*GLY + 0.216*HACET + 0.29*DHMOB + 0.17*RCOOH + 0.09*PRD2 + 0.09*CO + HO2 + 0.16*XC	2.60e-12*exp(380/T)	
<IS19>	HC5OO + HO2 = R6OOH-XC	2.06e-13*exp(1300/T)	
<IS20>	HC5OO + MEO2 = 0.117*HOCCHO + 0.117*MGLY + 0.108*GLY + 0.108*HACET + 0.145*DHMOB + 0.085*RCOOH + 0.045*PRD2 + 0.045*CO + 0.5*HO2 + 0.5*PRD2 + 0.25*HCHO + 0.25*MEOH + 0.5*HO2 + 0.5*HCHO-0.42*XC	2.00E-13	
<IS21>	HC5OO + RO2C = 0.117*HOCCHO + 0.117*MGLY + 0.108*GLY + 0.108*HACET + 0.145*DHMOB + 0.085*RCOOH + 0.045*PRD2 + 0.045*CO + 0.5*HO2 + 0.5*PRD2-0.42*XC	3.50E-14	
<IS22>	HC5OO + MECO3 = MEO2 + CO2 + 0.234*HOCCHO + 0.234*MGLY + 0.216*GLY + 0.216*HACET + 0.29*DHMOB + 0.17*RCOOH + 0.09*PRD2 + 0.09*CO + HO2 + 0.16*XC	4.40e-13*exp(1070/T)	
<IS24>	HC5 + O3 = 0.50*MGLY + 0.35*GLY + 0.79*OH + 0.02*HCHO + 0.35*HOCCHO + 0.59*CO + 0.15*HACET + 0.13*RCOOH + 0.08*CO2 + 0.6*HO2 + 0.35*MECO3-0.13*XC	3.94-15*exp(-1520/T)	
<IS25>	ISOPND + OH = ISOPNOOD	1.20e-11*exp(652/T)	rate constant updated
<IS26>	ISOPNOOD + NO = 0.34*PRD2 + 0.15*PROPNN + 0.44*HACET + 0.07*MVKN + 0.13*ETHLN + 0.31*HCOOH + 0.31*NO3 + 0.72*HCHO + 0.15*HOCCHO + 1.34*NO2 + 0.35*HO2-0.68*XC	2.40e-12*exp(360/T)	rate constant updated
<IS141>	ISOPNOOD + HO2 = RNO3I-XC	2.06e-13*exp(1300/T)	
<IS142>	ISOPNOOD + MEO2 = 0.17*PRD2 + 0.075*PROPNN + 0.22*HACET + 0.035*MVKN + 0.065*ETHLN + 0.155*HCOOH + 0.155*NO3 + 0.36*HCHO + 0.075*HOCCHO + 0.17*NO2 + 0.175*HO2 + 0.5*RNO3I + 0.25*HCHO + 0.25*MEOH + 0.5*HO2 +	2.00E-13	

	0.5*HCHO-0.84*XC		
<IS143>	ISOPNOOD + RO2C = 0.17*PRD2 + 0.075*PROPNN + 0.22*HACET + 0.035*MVKN + 0.065*ETHLN + 0.155*HCOOH + 0.155*NO3 + 0.36*HCHO + 0.075*HOCCHO + 0.17*NO2 + 0.175*HO2 + 0.5*RNO3I-0.84*XC	3.50E-14	
<IS144>	ISOPNOOD + MECO3 = MEO2 + CO2 + 0.34*PRD2 + 0.15*PROPNN + 0.44*HACET + 0.07*MVKN + 0.13*ETHLN + 0.31*HCOOH + 0.31*NO3 + 0.72*HCHO + 0.15*HOCCHO + 0.34*NO2 + 0.35*HO2-0.68*XC	4.40e-13*exp(1070/T)	
<IS27>	ISOPND + O3 = 0.36*ETHLN + 0.29*PROPNN + 0.70*MGLY + 0.12*RCOOH + 0.39*HO2 + 0.038*HCHO + 0.029*CO + 0.73*OH + 0.017*CO2 + 0.36*NO2 + 0.16*HACET + 0.34*HOCCHO-0.26*XC	2.90E-17	
<IS28>	ISOPNB + OH = ISOPNOOB	2.4e-12*exp(745/T)	rate constant updated
<IS29>	ISOPNOOB + NO = 0.6*HOCCHO + 0.6*HACET + 0.4*HCHO + 0.4*HO2 + 0.26*MACRN + 0.14*MVKN + 1.6*NO2	2.40e-12*exp(360/T)	rate constant updated
<IS145>	ISOPNOOB + HO2 = RNO3I-XC	2.06e-13*exp(1300/T)	
<IS146>	ISOPNOOB + MEO2 = 0.3*HOCCHO + 0.3*HACET + 0.2*HCHO + 0.2*HO2 + 0.13*MACRN + 0.07*MVKN + 0.3*NO2 + 0.5*RNO3I + 0.25*HCHO + 0.25*MEOH + 0.5*HO2 + 0.5*HCHO-0.5*XC	2.00E-13	
<IS147>	ISOPNOOB + RO2C = 0.3*HOCCHO + 0.3*HACET + 0.2*HCHO + 0.2*HO2 + 0.13*MACRN + 0.07*MVKN + 0.3*NO2 + 0.5*RNO3I-0.5*XC	3.50E-14	
<IS148>	ISOPNOOB + MECO3 = MEO2 + CO2 + 0.6*HOCCHO + 0.6*HACET + 0.4*HCHO + 0.4*HO2 + 0.26*MACRN + 0.14*MVKN + 0.6*NO2	4.40e-13*exp(1070/T)	
<IS30>	ISOPNB + O3 = 0.12*MVKN + 0.32*MACRN + 0.34*OH + 0.08*HO2 + 0.26*CO + 0.07*CO2 + 0.16*HCOOH + 0.56*HCHO + 0.28*RNO3I + 0.04*HACET + 0.28*NO2 + 0.24*BACL-0.57*XC	3.70E-19	rate constant updated
<IS31>	NIT1 + NO3 = 0.6*NIT1NO3OOA + 0.6*HNO3 + 0.4*NIT1NO3OOB	3.15e-13*exp(-448/T)	
<IS32>	NIT1NO3OOA + NO3 = NO2 + PROPNN + CO + CO2 + HO2	4.00E-12	PROPNNB>PROPNN
<IS34>	NIT1NO3OOA + NO = NO2 + PROPNN + CO + CO2 + HO2	1.0*K<BR31>	PROPNNB>PROPNN
<IS109>	NIT1NO3OOA + NO2 = MAPAN + XN + XC	1.0*K<BR28>	

\<IS36\>	NIT1NO3OOA + HO2 = 0.75*RCOOOH + 0.25*RCOOH + 0.25*O3 + XN + 2*XC	1.0*K\<BR22\>	
\<IS38\>	NIT1NO3OOA + RO2C = PROPNN + CO + CO2 + HO2	1.0*K\<BR25\>	PROPNNB>PROPNN
\<IS40\>	NIT1NO3OOA + MEO2 = PROPNN + CO + CO2 + HO2 + HCHO + HO2	1.0*K\<BR24\>	PROPNNB>PROPNN
\<IS41\>	NIT1NO3OOA + MECO3 = MEO2 + CO2 + PROPNN + CO + CO2 + HO2	1.0*K\<BR27\>	PROPNNB>PROPNN
\<IS33\>	NIT1NO3OOB + NO3 = ISOPNN + GLY + NO2	2.30E-12	PROPNN>ISOPNN
\<IS35\>	NIT1NO3OOB + NO = 0.94*ISOPNN + 0.94*GLY + 0.94*NO2 + 0.06*RNO3I-0.06*XC + 0.13*XN	2.60e-12*exp(380/T)	PROPNN>ISOPNN
\<IS37\>	NIT1NO3OOB + HO2 = RNO3I-XC + XN	2.06e-13*exp(1300/T)	
\<IS39\>	NIT1NO3OOB + RO2C = 0.7*ISOPNN + 0.7*GLY + 0.3*RNO3I-0.3*XC + 0.3*XN	3.50E-14	PROPNN>ISOPNN
\<IS43\>	NIT1NO3OOB + MEO2 = 0.7*ISOPNN + 0.7*GLY + 0.3*RNO3I + 0.25*HCHO + 0.25*MEOH + 0.5*HO2 + 0.5*HCHO-0.3*XC + 0.3*XN	2.00E-13	PROPNN>ISOPNN
\<IS44\>	NIT1NO3OOB + MECO3 = MEO2 + CO2 + ISOPNN + GLY	4.40e-13*exp(1070/T)	PROPNN>ISOPNN
\<IS46\>	NIT1 + O3 = 0.3*PROPNN + 0.45*CO + 0.15*OH + 0.45*HO2 + 0.15*CO2 + 0.7*GLY + 0.7*OH + 0.7*NO2 + 0.7*MGLY	4.15e-15*exp(-1520/T)	PROPNNB>PROPNN
\<IS47\>	NIT1 + OH = 0.345*NIT1NO3OOA + 0.655*NIT1OHOO	7.48e-12*exp(410/T)	
\<IS48\>	NIT1OHOO + NO = 0.919*PROPNN + 0.919*GLY + 0.015*CO + 0.015*RNO3I + 0.934*NO2 + 0.934*HO2 + 0.066*RNO3I-0.096*XC + 0.066*XN	2.60e-12*exp(380/T)	PROPNNB>PROPNN
\<IS50\>	NIT1OHOO + HO2 = R6OOH + XN-XC	2.06e-13*exp(1300/T)	
\<IS51\>	NIT1OHOO + RO2C = 0.689*PROPNN + 0.689*GLY + 0.011*CO + 0.011*RNO3I + 0.7*HO2 + 0.3*RNO3I-0.323*XC	3.50E-14	PROPNNB>PROPNN
\<IS52\>	NIT1OHOO + MEO2 = 0.689*PROPNN + 0.689*GLY + 0.011*CO + 0.011*RNO3I + 0.7*HO2 + 0.3*RNO3I + 0.25*HCHO + 0.25*MEOH + 0.50*HCHO + 0.50*HO2-0.323*XC	2.00E-13	PROPNNB>PROPNN
\<IS53\>	NIT1OHOO + MECO3 = MEO2 + CO2 + 0.984*PROPNN + 0.984*GLY + 0.016*CO + 0.016*RNO3I + HO2-0.033*XC	4.40e-13*exp(1070/T)	PROPNNB>PROPNN
\<IS55\>	DIBOO + NO = NO2 + HO2 + 0.52*HOCCHO + 0.52*MGLY + 0.48*GLY + 0.48*HACET	2.60e-12*exp(380/T)	
\<IS102\>	DIBOO + HO2 = R6OOH-XC	2.06e-13*exp(1300/T)	

<IS103>	DIBOO + MEO2 = 0.5*HO2 + 0.26*HOCCHO + 0.26*MGLY + 0.24*GLY + 0.24*HACET + 0.5*PRD2 + 0.25*HCHO + 0.25*MEOH + 0.5*HCHO + 0.50*HO2-0.5*XC	2.00E-13	
<IS104>	DIBOO + RO2C = 0.5*HO2 + 0.26*HOCCHO + 0.26*MGLY + 0.24*GLY + 0.24*HACET + 0.5*PRD2-0.5*XC	3.50E-14	
<IS105>	DIBOO + MECO3 = HO2 + 0.52*HOCCHO + 0.52*MGLY + 0.48*GLY + 0.48*HACET + MEO2 + CO2	4.40e-13*exp(1070/T)	
<IS56>	MVK + OH = MVKOO	2.60e-12*exp(610/T)	
<IS57>	MVKOO + NO = 0.625*HOCCHO + 0.625*MECO3 + 0.265*MGLY + 0.265*HCHO + 0.265*HO2 + 0.11*MVKN + 0.89*NO2	2.60e-12*exp(380/T)	
<IS58>	MVKOO + HO2 = ROOH + XC	1.82e-13*exp(1300/T)	
<IS59>	MVKOO + MEO2 = 0.35*HOCCHO + 0.35*MECO3 + 0.15*MGLY + 0.15*HCHO + 0.15*HO2 + 0.5*MEK + 0.25*HCHO + 0.25*MEOH + 0.5*HCHO + 0.50*HO2	2.00E-13	
<IS60>	MVKOO + RO2C = 0.35*HOCCHO + 0.35*MECO3 + 0.15*MGLY + 0.15*HCHO + 0.15*HO2 + 0.5*MEK	3.50E-14	
<IS61>	MVKOO + MECO3 = MEO2 + CO2 + 0.7*HOCCHO + 0.7*MECO3 + 0.3*MGLY + 0.3*HCHO + 0.3*HO2	4.40e-13*exp(1070/T)	
<IS63>	MACROO + NO = 0.85*NO2 + 0.85*HO2 + 0.72*HACET + 0.72*CO + 0.13*HCHO + 0.13*MGLY + 0.15*MACRN	2.60e-12*exp(380/T)	
<IS64>	MACROO + HO2 = ROOH + XC	1.82e-13*exp(1300/T)	
<IS65>	MACROO + MEO2 = 0.50*HO2 + 0.424*HACET + 0.424*CO + 0.076*HCHO + 0.076*MGLY + 0.5*PRD2 + 0.25*HCHO + 0.25*MEOH + 0.5*HCHO + 0.5*HO2-XC	2.00E-13	
<IS66>	MACROO + RO2C = 0.50*HO2 + 0.424*HACET + 0.424*CO + 0.076*HCHO + 0.076*MGLY + 0.5*PRD2-XC	3.50E-14	
<IS67>	MACROO + MECO3 = MEO2 + CO2 + HO2 + 0.15*MGLY + 0.85*HACET + 0.85*CO + 0.15*HCHO	4.40e-13*exp(1070/T)	
<IS69>	MACO3 + NO = NO2 + CO + CO2 + HCHO + MEO2	6.70e-12*exp(340/T)	
<IS70>	MACO3 + HO2 = 0.3075*RCOOOH + 0.1025*RCOOH + 0.15*O3 + 0.44*OH + 0.44*HCHO + 0.44*MECO3 + 0.44*CO2	1.0*K<BR22>	revised acyl peroxy radical with HO2 by splitting organic into two parts

<IS71>	MACO3 + NO3 = NO2 + CO + CO2 + HCHO + MEO2	4.00E-12	
<IS72>	MACO3 + MEO2 = HCHO + HO2 + CO + CO2 + HCHO + MEO2	1.0*K<BR24>	
<IS73>	MACO3 + RO2C = CO + CO2 + HCHO + MEO2	1.0*K<BR25>	
<IS74>	MACO3 + RO2XC = CO + CO2 + HCHO + MEO2	1.0*K<BR25>	
<IS75>	MACO3 + MECO3 = CO2 + MEO2 + CO + CO2 + HCHO + MEO2	1.0*K<BR27>	
<IS76>	MACO3 + RCO3 = CO + CO2 + HCHO + MEO2 + RO2C + xHO2 + yROOH + xCCHO + CO2	1.0*K<BR27>	
<IS77>	MACO3 + BZCO3 = CO + CO2 + HCHO + MEO2 + BZO + RO2C + CO2	1.0*K<BR27>	
<IS78>	MACO3 + MACO3 = 2*CO + 2*CO2 + 2*HCHO + 2*MEO2	1.0*K<BR27>	
<IS108>	MAPAN + OH = HACET + CO + NO2	2.90E-11	
<IS79>	HOCCHO + OH = 0.75*HO2 + 0.25*OH + 0.13*GLY + 0.52*CO + 0.35*CO2 + 0.16*HCOOH + 0.71*HCHO	8.00E-12	
<IS80>	HACET + OH = 0.75*MGLY + 0.825*HO2 + 0.125*HCOOH + 0.1*OH + 0.125*MEO2 + 0.20*CO2 + 0.05*CO + 0.125*CCOOH	2.15e-12*exp(305/T)	
<IS81>	HACET = HO2 + MECO3 + HCHO	1.75e-1/<MEK_06>	
<IS82>	ETHLN + OH = HCHO + CO2 + NO2	2.94e-12*exp(365/T)	
<IS111>	ETHLN = NO2 + HCHO + HO2 + CO	1.0/<NOA>	
<IS83>	PROPNN + OH = MGLY + NO2	4.00E-13	
<IS93>	ISOPNN + OH = PROPNN + NO2	4.00E-13	following PROPNN, makes a single nitrate (PROPNN) instead of glyoxal since ISOPNN is dinitrate
<IS97>	PROPNN = MECO3 + HCHO + NO2	1.0/<NOA>	
<IS98>	ISOPNN = MECO3 + HCHO + 2*NO2	1.0/<IC3ONO2>	following PROPNN but making 2 NO2 since ISOPNN is dinitrate, also uses different photolysis rate
<IS84>	MVKN + OH = 0.65*HCOOH + 0.65*MGLY + 0.35*HCHO + 0.35*PYRUACD + NO3	3.50e-12*exp(140/T)	
<IS106>	MVKN = MECO3 + NO2 + HOCCHO	1.0/<NOA>	
<IS85>	MACRN + OH = 0.08*CCOOH + 0.08*HCHO + 0.08*NO3 + 0.07*HCOOH + 0.07*NO3 + 0.07*MGLY + 0.85*HACET + 0.85*NO2 + 0.93*CO2	1.28e-11*exp(405/T)	
<IS110>	MACRN = HACET + NO2 + CO + HO2	1.0/<C2CHO>	

<IS86>	DHMOB + OH = 1.5*CO + 0.5*HO2 + 0.5*HACET + 0.5*PRD2-XC	1.00E-11	
<IS87>	PYRUACD = CCHO + CO2	1.0/<MGLY_06>	
<IS88>	ISOPOOH + OH = IEPOX + OH	1.9e-11*exp(390/T)	
<IS89>	ISOPOOH + OH = 0.387*ISOPO2 + 0.613*HC5 + 0.613*OH	4.75e-12*exp(200/T)	
<IS90>	IEPOX + OH = IEPOXOO	5.78e-11*exp(-400/T)	
<IS91>	IEPOXOO + HO2 = 0.725*HACET + 0.275*HOCCHO + 0.275*GLY + 0.275*MGLY + 1.125*OH + 0.825*HO2 + 0.200*CO2 + 0.375*HCHO + 0.074*HCOOH + 0.251*CO	2.06e-13*exp(1300/T)	
<IS96>	IEPOXOO + NO = 0.725*HACET + 0.275*HOCCHO + 0.275*GLY + 0.275*MGLY + 0.125*OH + 0.825*HO2 + 0.200*CO2 + 0.375*HCHO + 0.074*HCOOH + 0.251*CO + NO2	2.60e-12*exp(380/T)	
<IS112>	IEPOXOO + MEO2 = 0.363*HACET + 0.138*HOCCHO + 0.138*GLY + 0.138*MGLY + 0.063*OH + 0.413*HO2 + 0.100*CO2 + 0.188*HCHO + 0.037*HCOOH + 0.126*CO + 0.5*PRD2 + 0.5*HCHO + 0.5*HO2 + 0.25*HCHO + 0.25*MEOH-0.5*XC	2.00E-13	
<IS113>	IEPOXOO + RO2C = 0.363*HACET + 0.138*HOCCHO + 0.138*GLY + 0.138*MGLY + 0.063*OH + 0.413*HO2 + 0.100*CO2 + 0.188*HCHO + 0.037*HCOOH + 0.126*CO + 0.5*PRD2-0.5*XC	3.50E-14	
<IS114>	IEPOXOO + MECO3 = 0.725*HACET + 0.275*HOCCHO + 0.275*GLY + 0.275*MGLY + 0.125*OH + 0.825*HO2 + 0.200*CO2 + 0.375*HCHO + 0.074*HCOOH + 0.251*CO + MEO2 + CO2	4.40e-13*exp(1070/T)	
<IS92>	ISOPOOH = OH + 0.91*HO2 + 0.75*HCHO + 0.45*MVK + 0.29*MACR + 0.09*DIBOO + 0.11*HC5 + 0.05*ARO2MN-0.16*XC	1.0/<COOH>	ARO2>ARO2MN
<IS94>	RNO3I + OH = NO2 + HO2 + PRD2	8.00E-12	
<IS99>	NISOPOOH + OH = RNO3I + OH	5.00E-11	
<IS139>	NISOPOOH + OH = 0.3*NISOPO2 + 0.7*OH + 0.7*NIT1	0.38e-11*exp(200/T)	
<IS00>	MACR + OH = 0.53*MACROO + 0.47*IMACO3	8.00e-12*exp(380/T)	IMACO3 specifically from isoprene, yields adjusted
<BP56>	MACR + NO3 = 0.5*IMACO3 + 0.5*RO2C + 0.5*HNO3 + 0.5*xHO2 + 0.5*xCO + 0.5*yROOH + 1.5*XC + 0.5*XN	1.50e-12*exp(-1815/T)	

<BP58>	MACR = 0.33*OH + 0.67*HO2 + 0.34*MECO3 + 0.33*IMACO3 + 0.33*RO2C + 0.67*CO + 0.34*HCHO + 0.33*xMECO3 + 0.33*xHCHO + 0.33*yROOH	1.0/<MACR_06>	
<CP16>	MACR + CL = 0.25*HCL + 0.165*IMACO3 + 0.802*RO2C + 0.033*RO2XC + 0.033*zRNO3 + 0.802*xHO2 + 0.541*xCO + 0.082*xIPRD + 0.18*xCLCCHO + 0.541*xCLACET + 0.835*yROOH + 0.208*XC	3.85E-10	
<IA69>	IMACO3 + NO = NO2 + CO + CO2 + HCHO + MEO2	6.70e-12*exp(340/T)	
<IA70>	IMACO3 + HO2 = 0.75*IMPAA + 0.25*RCOOH + 0.25*O3 + XC	1.0*K<BR22>	
<IA71>	IMACO3 + NO3 = NO2 + CO + CO2 + HCHO + MEO2	4.00E-12	
<IA72>	IMACO3 + MEO2 = HCHO + HO2 + CO + CO2 + HCHO + MEO2	1.0*K<BR24>	
<IA73>	IMACO3 + RO2C = CO + CO2 + HCHO + MEO2	1.0*K<BR25>	
<IA74>	IMACO3 + RO2XC = CO + CO2 + HCHO + MEO2	1.0*K<BR25>	
<IA75>	IMACO3 + MECO3 = CO2 + MEO2 + CO + CO2 + HCHO + MEO2	1.0*K<BR27>	
<IA76>	IMACO3 + RCO3 = CO + CO2 + HCHO + MEO2 + RO2C + xHO2 + yROOH + xCCHO + CO2	1.0*K<BR27>	
<IA77>	IMACO3 + BZCO3 = CO + CO2 + HCHO + MEO2 + BZO + RO2C + CO2	1.0*K<BR27>	
<IA78>	IMACO3 + MACO3 = 2*CO + 2*CO2 + 2*HCHO + 2*MEO2	1.0*K<BR27>	
<IA79>	IMACO3 + IMACO3 = 2*CO + 2*CO2 + 2*HCHO + 2*MEO2	1.0*K<BR27>	
<IA80>	MACROO = HACET + CO + OH	2.9e7*exp(-5297/T)	isomerization of MACR_OH-H addition (MACROO) species
<IA51>	IMACO3 + NO2 = IMAPAN	1.0*K<BR28>	MPAN from isoprene tracked as IMAPAN
<IA52>	IMAPAN = IMACO3 + NO2	1.60e16*exp(-13486/T)	
<IA53>	IMAPAN = 0.6*IMACO3 + 0.6*NO2 + 0.4*CO2 + 0.4*HCHO + 0.4*MECO3 + 0.4*NO3	1.0/<PAN>	
<IC01>	xCO + IMACO3 = IMACO3 + CO	1.0*K<BR25>	
<IC02>	xTBUO + IMACO3 = IMACO3 + TBUO	1.0*K<BR25>	
<IC03>	xMACO3 + IMACO3 = IMACO3 + MACO3	1.0*K<BR25>	
<IC04>	xRCO3 + IMACO3 = IMACO3 + RCO3	1.0*K<BR25>	
<IC05>	xMECO3 + IMACO3 = IMACO3 +	1.0*K<BR25>	

	MECO3	
<IC06>	xMEO2 + IMACO3 = IMACO3 + MEO2	1.0*K<BR25>
<IC07>	xNO2 + IMACO3 = IMACO3 + NO2	1.0*K<BR25>
<IC08>	xOH + IMACO3 = IMACO3 + OH	1.0*K<BR25>
<IC09>	xHO2 + IMACO3 = IMACO3 + HO2	1.0*K<BR25>
<IC10>	xACROLEIN + IMACO3 = IMACO3 + ACROLEIN	1.0*K<BR25>
<IC11>	xHOCCHO + IMACO3 = IMACO3 + HOCCHO	1.0*K<BR25>
<IC12>	zRNO3 + IMACO3 = IMACO3 + PRD2 + HO2	1.0*K<BR25>
<IC13>	yRAOOH + IMACO3 = IMACO3	1.0*K<BR25>
<IC14>	yR6OOH + IMACO3 = IMACO3	1.0*K<BR25>
<IC15>	yROOH + IMACO3 = IMACO3	1.0*K<BR25>
<IC16>	xRNO3 + IMACO3 = IMACO3 + RNO3	1.0*K<BR25>
<IC17>	xIPRD + IMACO3 = IMACO3 + IPRD	1.0*K<BR25>
<IC18>	xMVK + IMACO3 = IMACO3 + MVK	1.0*K<BR25>
<IC19>	xMACR + IMACO3 = IMACO3 + MACR	1.0*K<BR25>
<IC20>	xAFG3 + IMACO3 = IMACO3 + AFG3	1.0*K<BR25>
<IC21>	xAFG2 + IMACO3 = IMACO3 + AFG2	1.0*K<BR25>
<IC22>	xAFG1 + IMACO3 = IMACO3 + AFG1	1.0*K<BR25>
<IC23>	xBALD + IMACO3 = IMACO3 + BALD	1.0*K<BR25>
<IC24>	xBACL + IMACO3 = IMACO3 + BACL	1.0*K<BR25>
<IC25>	xMGLY + IMACO3 = IMACO3 + MGLY	1.0*K<BR25>
<IC26>	xGLY + IMACO3 = IMACO3 + GLY	1.0*K<BR25>
<IC27>	xPROD2 + IMACO3 = IMACO3 + PRD2	1.0*K<BR25>
<IC28>	xMEK + IMACO3 = IMACO3 + MEK	1.0*K<BR25>
<IC29>	xACETONE + IMACO3 = IMACO3 + ACETONE	1.0*K<BR25>
<IC30>	xRCHO + IMACO3 = IMACO3 + RCHO	1.0*K<BR25>
<IC31>	xCCHO + IMACO3 = IMACO3 + CCHO	1.0*K<BR25>
<IC32>	xHCHO + IMACO3 = IMACO3 + HCHO	1.0*K<BR25>
<IC33>	xCL + IMACO3 = IMACO3 + CL	1.0*K<BR25>
<IC34>	xCLACET + IMACO3 = IMACO3 + CLACET	1.0*K<BR25>
<IC35>	xCLCCHO + IMACO3 = IMACO3 + CLCCHO	1.0*K<BR25>
<IA108>	IMAPAN + OH = 0.03*HACET + 0.03*CO + 0.81*NO3 + 0.21*IMAE + 0.57*IHMML + 0.19*PAN + 0.19*HCHO + 0.19*HO2	3.00E-11
<IA90>	IMAE + OH =	1.00E-12

<IA91>	IHMML + OH =	4.40E-12	
<IA92>	IMPAA + OH = 0.83*IMACO3 + 0.17*IHMML	1.66E-11	
<CP07mtp>	MTNO3 + CL = HCL + 0.038*NO2 + 0.055*HO2 + 1.282*RO2C + 0.202*RO2XC + 0.202*zMTNO3 + 0.009*RCHO + 0.018*MEK + 0.012*PRD2 + 0.055*MTNO3 + 0.159*xNO2 + 0.547*xHO2 + 0.045*xHCHO + 0.3*xCCHO + 0.02*xRCHO + 0.003*xACETONE + 0.041*xMEK + 0.046*xPROD2 + 0.547*xMTNO3 + 0.908*yR6OOH + 0.201*XN-0.149*XC	1.92E-10	
<BP70mtp>	MTNO3 + OH = 0.189*HO2 + 0.305*xHO2 + 0.019*NO2 + 0.313*xNO2 + 0.976*RO2C + 0.175*RO2XC + 0.175*zMTNO3 + 0.011*xHCHO + 0.429*xCCHO + 0.001*RCHO + 0.036*xRCHO + 0.004*xACETONE + 0.01*MEK + 0.17*xMEK + 0.008*PRD2 + 0.031*xPROD2 + 0.189*MTNO3 + 0.305*xMTNO3 + 0.157*yROOH + 0.636*yR6OOH + 0.174*XN + 0.04*XC	7.20E-12	slow
<BP71mtp>	MTNO3 = 0.344*HO2 + 0.554*xHO2 + NO2 + 0.721*RO2C + 0.102*RO2XC + 0.102*zMTNO3 + 0.074*HCHO + 0.061*xHCHO + 0.214*CCHO + 0.23*xCCHO + 0.074*RCHO + 0.063*xRCHO + 0.008*xACETONE + 0.124*MEK + 0.083*xMEK + 0.19*PRD2 + 0.261*xPROD2 + 0.066*yROOH + 0.591*yR6OOH + 0.396*XC	1.0/<IC3ONO2>	slow photolysis (timescale of day)

[1]$k = [\ k_0[M]/(1+k_0[M]/k_{inf})]FG$, where $G = 1/[1+(\log(k_0[M]/k_{inf})/n)^{-2})]$

[2]$k = A*K$<LABEL> translates to a reaction constant of A x rate constant for reaction with label="LABEL".

[3]$k = A/$<LABEL> translates to a reaction constant of A x photolysis rate for reaction with label="LABEL".

6.2.5 Organic Aerosol Treatment

The treatment of organic aerosol in the UCD/CIT model version employed in this study follows the scheme of Carlton et al. [4]. Primary organic aerosol (POA) is considered to be non-volatile while semivolatile secondary organic aerosol (SOA) forms via a 2-product parametrization from precursors such as monoterpenes, sesquiterpenes, isoprene, benzene, toluene, xylene and naphthalenes. These aerosol species then undergo oligomerization to produce non-volatile species. The expanded SAPRC11 model also includes SOA formation from IEPOX and MPAN in the form of AIETET, AIEOS, ADIM etc. Additionally, SOA from isoprene dinitrates and monoterpene nitrates (ISOPNN and MTNO3 respectively) is implemented by treating them as semivolatile species capable of partitioning to the particle phase. ISOPNN was modeled as a C5 dihydroxy dinitrate with a molecular weight of 226 g mol^{-1} and saturation pressure (C*) of 8.9

μg m^{-3} [199]. MTNO3 was modeled as a dihydroxy nitrate with a molecular weight of 231 g mol^{-1} and saturation pressure (C*) of 12.1 ug m^{-3} [198]. Temperature effects on partitioning were modeled using an enthalpy of vaporization equivalent to 40 kJ mol^{-1}. ISOPNN and MTNO3 undergo hydrolysis (more of a pseudo hydrolysis designed to maximize the amount of particulate organic nitrate) that converts them to nonvolatile SOA (Table 6-3). The sum of particle-phase monoterpene nitrates, isoprene dinitrates, and their hydrolysis products is referred to as particulate organic nitrate-derived aerosol. Finally, SOA formation from glyoxal and methyl glyoxal uptake to particles was also incorporated in the expanded model, using the uptake rates listed in Table 6-3. Previous studies have found that glyoxal and methyl glyoxal can produce ~1 μg m^{-3} of OA.

Table 6-3: Organic aerosol formation reactions and rate constants (K) added to the expanded SAPRC11 mechanism. Note that the K's not having values are calculated based on an approach described in Pye et al. [6].

Reaction	K (sec^{-1})	Reaction	K (sec^{-1})
IEPOX = IEPOXP	K_{IEPOX}	ATOL1 = 1.0000*AOLGA	9.48816e-6
IMAE = IMAEP	K_{IMAE}	ATOL2 = 1.0000*AOLGA	9.48816e-6
IHMML = IHMMLP	K_{IMAE}	ABNZ1 = 0.85714*AOLGA	9.48816e-6
IEPOXP = AIETET	K_{TETROL}	ABNZ2 = 0.85714*AOLGA	9.48816e-6
IEPOXP = AIEOS	$K_{IEPOXOS}$	ATRP1 = 1.0000*AOLGB	9.48816e-6
IEPOXP + AIETET = ADIM	$K_{TETROLDIM}$	ATRP2 = 1.0000*AOLGB	9.48816e-6
IEPOXP + AIEOS = ADIM	$K_{IEPOXOSDI}$	AISO1 = 0.50*AOLGB	9.48816e-6
IMAEP = AIMGA	K_{2MG}	AISO2 = 0.50*AOLGB	9.48816e-6
IMAEP = AIMOS	K_{IMAEOS}	ASQT = 1.50*AOLGB	9.48816e-6
IHMMLP = AIMGA	K_{2MG}	APAH1 = 1.4286*AOLGA	9.48816e-6
IHMMLP = AIMOS	K_{IMAEOS}	APAH2 = 1.4286*AOLGA	9.48816e-6
AALK1 = 1.7143*AOLGA	9.48816e-6	AMTNO3 = HNO3 + 1.00*AMTHYD	9.25900e-5
AALK2 = 1.7143*AOLGA	9.48816e-6	AISOPNN =2.0*HNO3 +0.5*AMTHYD	9.25900e-5
AXYL1 = 1.1428*AOLGA	9.48816e-6	GLY = AGLY	K_{GLY}
AXYL2 = 1.1428*AOLGA	9.48816e-6	MGLY = AGLY	K_{MGLY}

6.2.6   Discover-AQ and CALNEX Field Observations

This study focused on evaluation of the expanded SAPRC11 mechanism by comparing to measurements from two different field campaigns: DISCOVER-AQ in the SJV (Jan 16 - Feb 10, 2013) and CALNEX in the SoCAB (May 19 – June 14, 2010). Measurements were made at multiple locations during these campaigns; the current analysis is focused on the core sites of Fresno (Garland) (36.7853°N latitude, -119.7742°W longitude) for DISCOVER-AQ and Pasadena (CalTech) (34.1405°N latitude, -118.1225°W longitude) for CALNEX. Vertical profiles were measured with an aircraft-equipped with a HR-ToF-AMS, GCMS, TDILF-MS etc. above Fresno during DISCOVER-AQ to probe the details of local chemistry. These profiles enable a rigorous evaluation of model performance as a function of elevation with a vertical resolution as fine as 20 m. CALNEX focused more on the ground measurements and flights that were designed to investigate long range transport in the upper troposphere. The utility of the

CALNEX aircraft measurements is therefore more limited for the current study of local production mechanisms.

Table 6-4 summarizes all measurements used in this work. All ground level measurements and averaged diurnal profiles were compared to UCD/CIT model predictions from the first level (representing 0 to about 30 m above ground level). Vertical measurements were compared to model predictions from the 16 vertical levels reaching a maximum height of 5 km above ground level.

Table 6-4: Measurement data sources for CALNEX (http://esrl.noaa.gov/csd/projects/calnex/) and DISCOVER-AQ (http://www-air.larc.nasa.gov/missions/discover-aq/discover-aq.html) field campaigns.

Campaign	Measurement/ Species	Phase	Technique	Location
CALNEX 2010	Isoprene Benzene Methanol (MEOH) Formic Acid (HCOOH) Acetaldehyde (CCHO)	Gas	GCMS	Ground
CALNEX 2010	NO NO2 O3 CO	Gas	Nitrogen species by chemiluminescence, O3 via UV absorption, CO via IR absorption	Ground
CALNEX 2010	Inorganic Aerosol Constituents (sulfate and nitrate)	Particle	Anion-Metrohm Ion Chromatography	Ground
CALNEX 2010	Vertical species measured though an aircraft (NOx, CO, nitrate, sulfate, benzene etc.)	Particle/Gas	HR-ToF-AMS, PILS-AMS, GCMS etc.	Aloft
CALNEX 2010	NO3 (ss)	Gas	Steady state calculation of nitrate radical concentration	Ground
DISCOVER-AQ	Species measured in an aircraft flight with spirals planned at particular locations (NOx, CO, nitrate, sulfate, benzene, Methanol, Isoprene etc.)	Gas/Particle	HR-ToF-AMS, PILS-AMS, GCMS etc.	Aloft and close to the ground as well
DISCOVER-AQ	Some ground measurements (NOx, CO, PM2.5, O3 etc.)	Gas/Particle	ARB Air Quality Now database with station measurements	Ground

6.3 Results

6.3.1 DISCOVER-AQ

Figures 6-1 through 6-3 illustrate the vertical profile of measured and predicted pollutant concentrations between 0-1km above Fresno at 11am, 1pm, and 3pm, respectively. All plots represent averages from 5 days between Jan 16 – Feb 10, 2013. Solid lines represent average values while uncertainty bars represent 3 times the standard deviation.

The model predictions using the SAPRC11 and modified SAPRC11 mechanisms are (red and blue lines in Figures 6-1 through 6-3) are virtually identical for all pollutants indicating that the updated mechanism had very little impact. Isoprene concentrations were under-predicted by a factor of 10 at all elevations and at all three times suggesting that isoprene emissions and / or the predicted wind fields should be reviewed. The relatively uniform measured isoprene concentration profile in the vertical direction indicates that isoprene emissions sources are far from the measurement site (allowing time for vertical mixing) and the rate of chemical reaction with NOx is relatively slow (avoiding a decrease in ground-level concentrations).

Predicted NOx and O3 concentrations are in reasonable agreement with measured values above ground at 11am, 1pm, and 3pm but it should be noted that elevated NOx measurements are missing below 100m. In contrast, predicted concentrations of particulate nitrate and ammonium ion are a factor of 5-10 lower than measured concentrations. Approximately 4-6 ppb of additional NOx would need to be converted to particulate nitrate in order to close the gap between predicted and measured nitrate concentrations. This discrepancy is within the uncertainty range of the comparison between predicted and measured NOx / O3 concentrations.

Figure 6-1: Averaged vertical profiles of species (name written in the graphs) at Garland, Fresno at 11:00 AM. the profiles are obtained by averaging over 7 days of the DISCOVER-AQ campaign.

Figure 6-2: Averaged vertical profiles of species (name written in the graphs) at Garland, Fresno at 01:00 PM. The profiles are obtained by averaging over 5 days of the DISCOVER-AQ campaign.
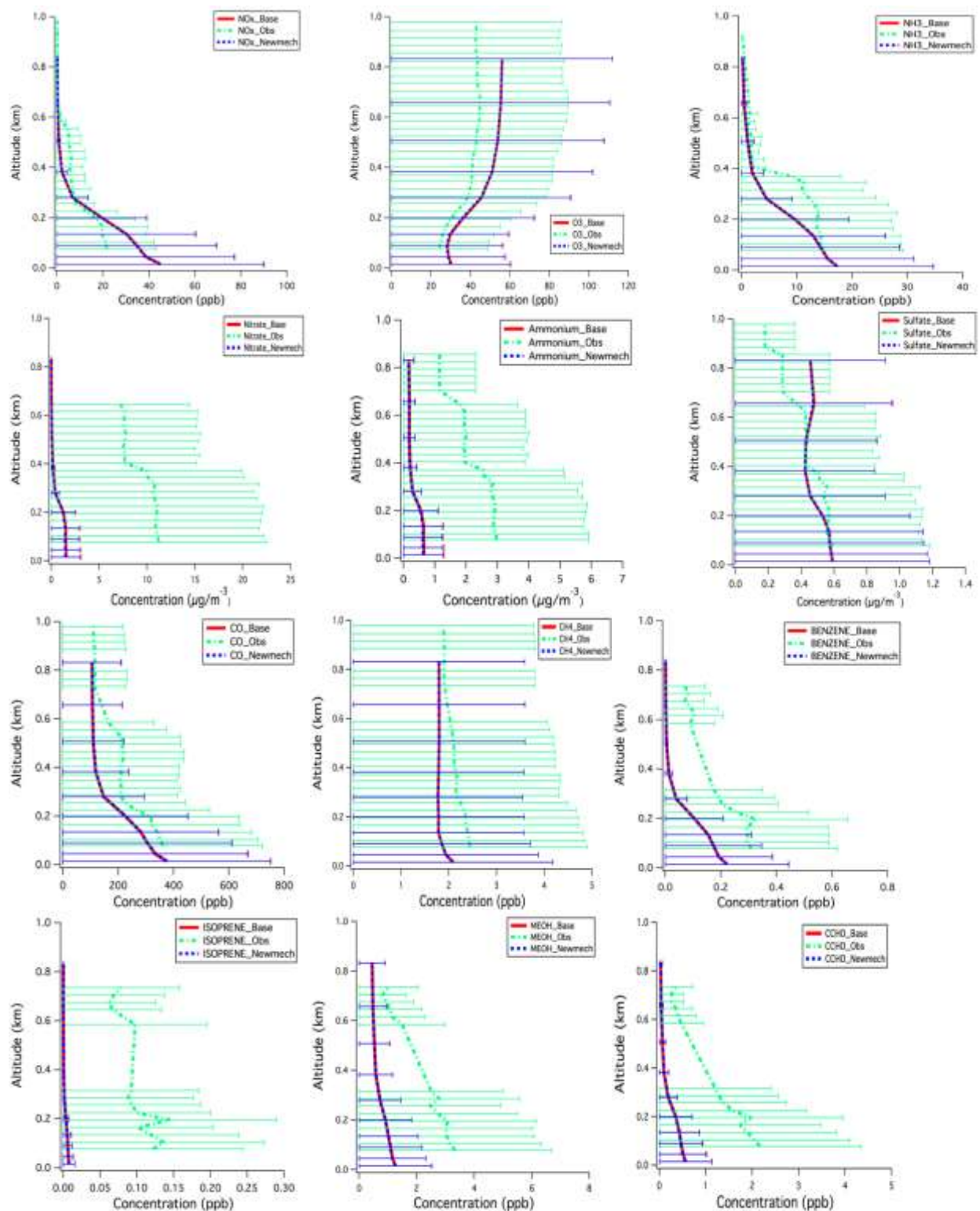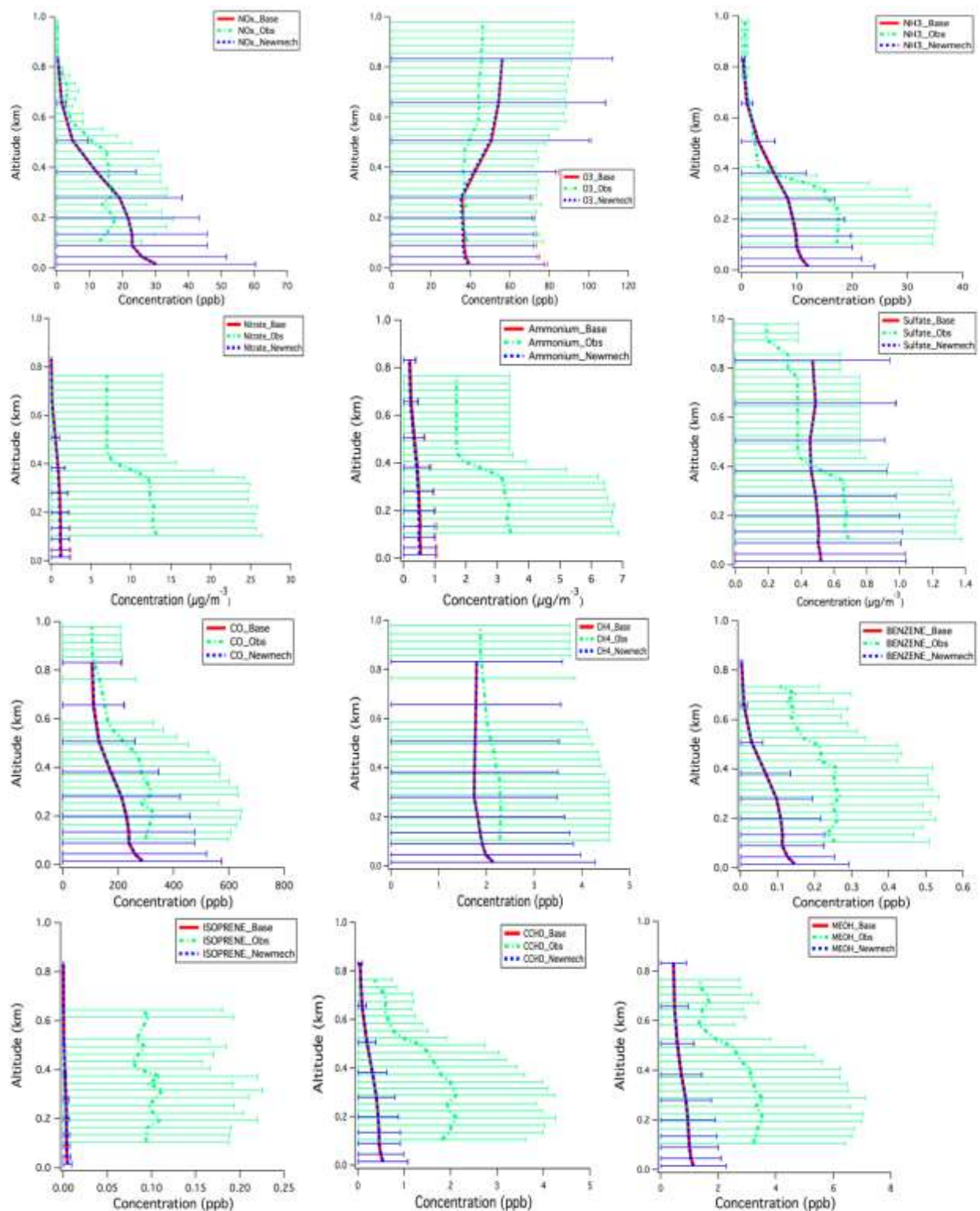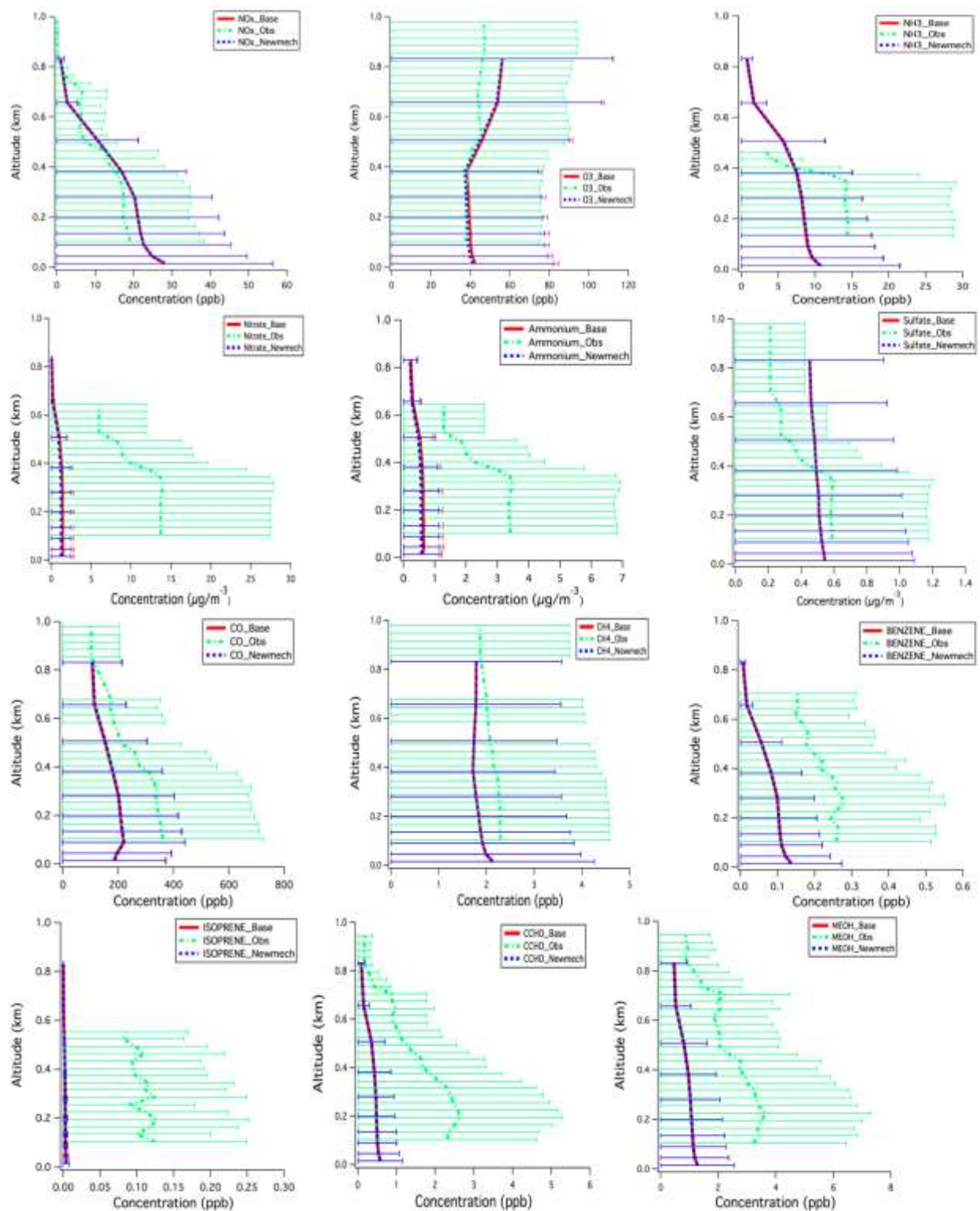
Figure 6-3: Averaged vertical profiles of species (name written in the graphs) at Garland, Fresno at 03:00 PM. The profiles are obtained by averaging over 5 days of the DISCOVER-AQ campaign.

Figure 6-4 illustrates the average diurnal profile of predicted and measured pollutant concentrations at ground level in Fresno between Jan 16-Feb 10 2013. Concentrations predicted with the original SPARC11 mechanism are shown in red while concentrations predicted with the expanded mechanism are shown in blue. Both sets of predictions are very similar suggesting that the expanded mechanism has limited impact under the conditions experienced during the simulated period.

Ground level concentrations of pollutants with major contributions from primary emissions (CO and NOx) are significantly under-predicted by model calculations in the morning suggesting that either the emissions strength is too low or (more likely) the dilution is too high. The real atmosphere is very stable during the night but the model calculations may have induced an early start to mixing that precedes the morning traffic peak. Model calculations also inherently have numerical diffusion associated with instant mixing of nighttime emissions within 4km grid cells, but this issue does not appear to bias the increase in predicted NOx concentrations during the later afternoon and early evening.

Local ozone production is weak during the simulated winter conditions represented in Figure 6-4 and so the majority of the ozone measured at the ground level site results from the competition between transport down from background concentrations and chemical reaction where ozone acts as an oxidant for reactive nitrogen species and VOCs. Nighttime ozone concentrations are over-predicted reflecting the under-prediction of NOx concentrations possibly related to artificial diffusion as discussed above. Predicted ozone concentrations begin to increase at 6am approximately 1.5 hrs before measured ozone concentrations. Sunrise during January 2013 occurred at approximately 7:30am which corresponds to the onset of increasing measured ozone concentrations. The early onset of increased ozone concentrations in model predictions reflects premature mixing that also may have prevented the accurate prediction of enhanced ground-level concentrations of CO and NOx as discussed above. Maximum predicted ozone concentrations are ~40ppb while maximum measured concentrations are ~28ppb. This offset appears to be explained by the higher starting concentrations of ozone at the beginning of the day due to the under-prediction of NOx concentrations.
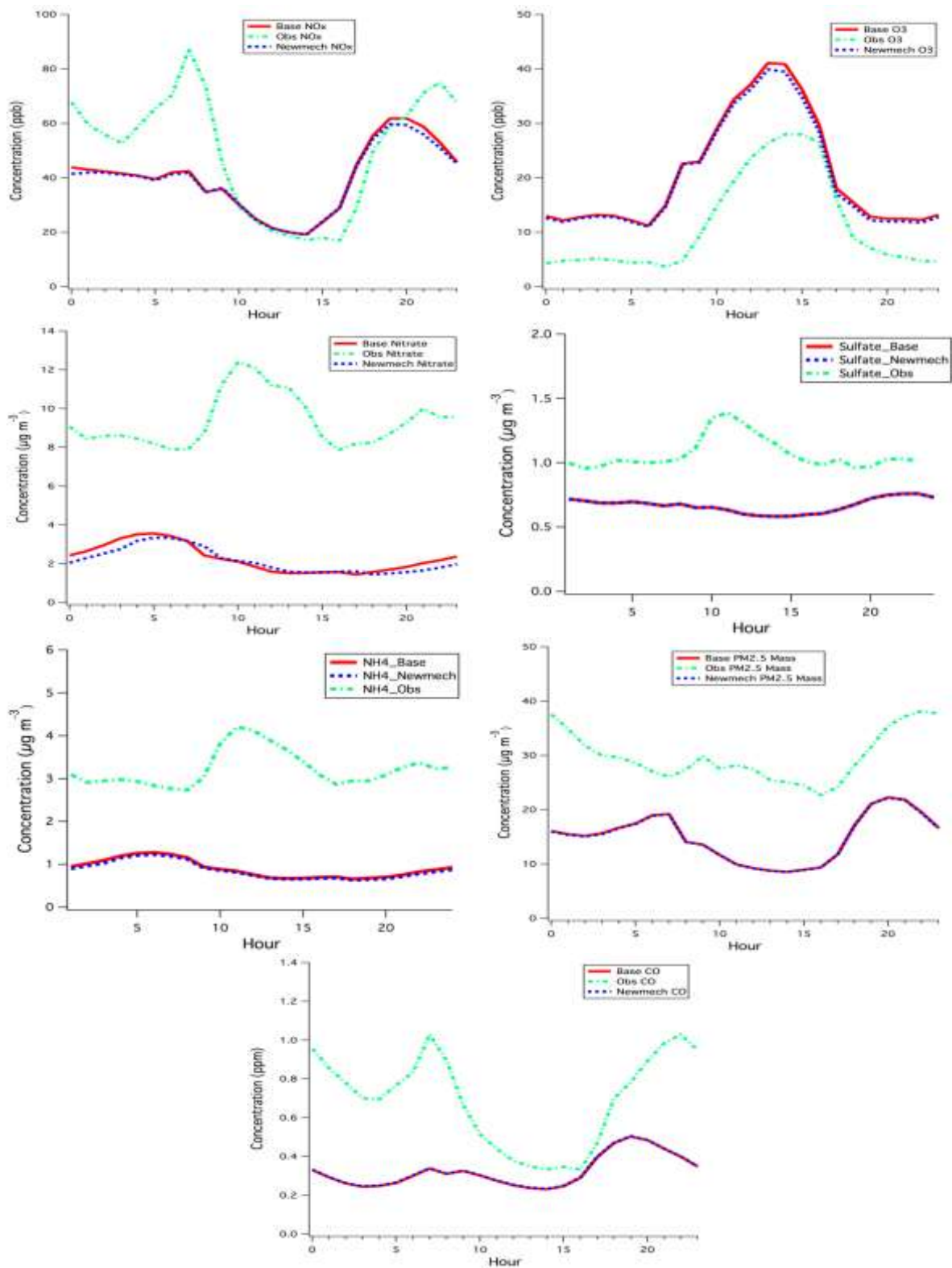
Figure 6-4: Diurnal profiles of species (name written in the graphs) at Garland, Fresno for the DISCOVER-AQ campaign. These profiles are generating by averaging available everyday data during a DISCOVER-AQ.

Figure 6-5 summarizes the time series of predicted and measured pollutant concentrations at ground level at the Fresno site between Jan 16 – Feb 10, 2013. Daytime concentrations of NOx (daily minimum) and ozone (daily maximum) show reasonable agreement with measurements on most days. Diurnal NOx patterns are less resolved after Jan 21 2013 with greater variability in daily maximum (nighttime concentrations) indicating different levels of nighttime stagnation. Daily ozone cycles are generally more repeatable since the daily maximum (daytime concentrations) reflects the relatively consistent background concentration. Variability in nighttime concentrations is observable as non-zero ozone concentrations during the evening hrs because NOx concentrations are not sufficiently high to titrate all the ozone.

Particulate nitrate and ammonium concentrations follow a diurnal pattern that peaks in the daytime as the material produced in the upper portions of the atmosphere mixes to the ground each day. Measured concentrations reach a minimum between Jan 26-31 corresponding to a time when NOx concentrations were also very low and ozone concentrations were consistently at background levels. This patterns suggests a period of extensive mixing with little nighttime stagnation. This pattern is repeated around Feb 7. Predicted particulate nitrate and ammonium concentrations were consistently below the measured values across the entire study period except during the transition between stagnation and ventilated conditions (around Jan 26 and Feb 7).
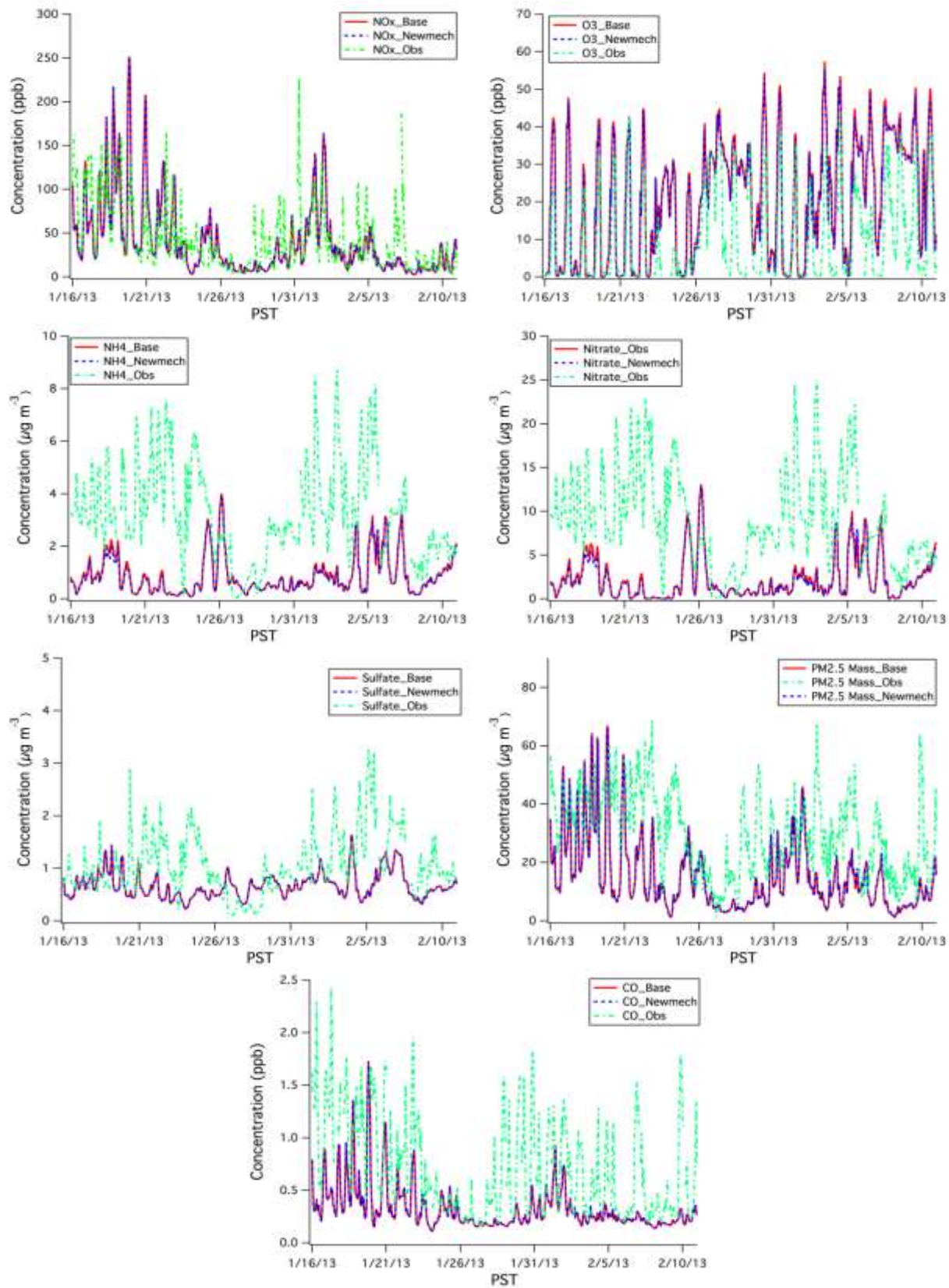
Figure 6-5: Time series of various species (name written in the plots) at Garland, Fresno during the DISCOVER-AQ campaign.

Figures 6-6 through 6-9 illustrate the predicted ground-level concentrations of PM2.5 mass and various chemical components averaged over the period January 16 – Feb 10, 2013 in central California. The left column in each Figure shows the base SAPRC11 prediction, and center column shows the expanded SAPRC11 prediction, and the right column shows the difference (base – expanded). PM2.5 mass generally decreases with the adoption of the expanded mechanism mostly due to a reduction in particulate ammonium and nitrate concentrations. Small isolated regions of increasing PM2.5 mass were predicted between San Francisco and Sacramento and between Fresno and Bakersfield due to the formation of SOA through the glyoxal pathway (see AGLY in Figure 6-10) but this enhanced formation is isolated with little regional impact.

Changes in OA concentrations associated with the expanded chemistry are generally smaller than 0.1 $\mu g\ m^{-3}$ for all species except ATRP1 + ATRP2 +ATRP3 (Figure 6-8) that decrease by 0.13 $\mu g\ m^{-3}$ due to the redirection of material into AMTNO3 (Figure 6-10) that increases by 0.32 $\mu g\ m^{-3}$ in the same area. Thus, the net effect of the expanded chemistry appears to be a 0.19 $\mu g\ m^{-3}$ increase in predicted SOA concentrations in the region between San Francisco and Sacramento, with little impact at other locations in central California during the winter conditions studied.

MASS

Nitrate
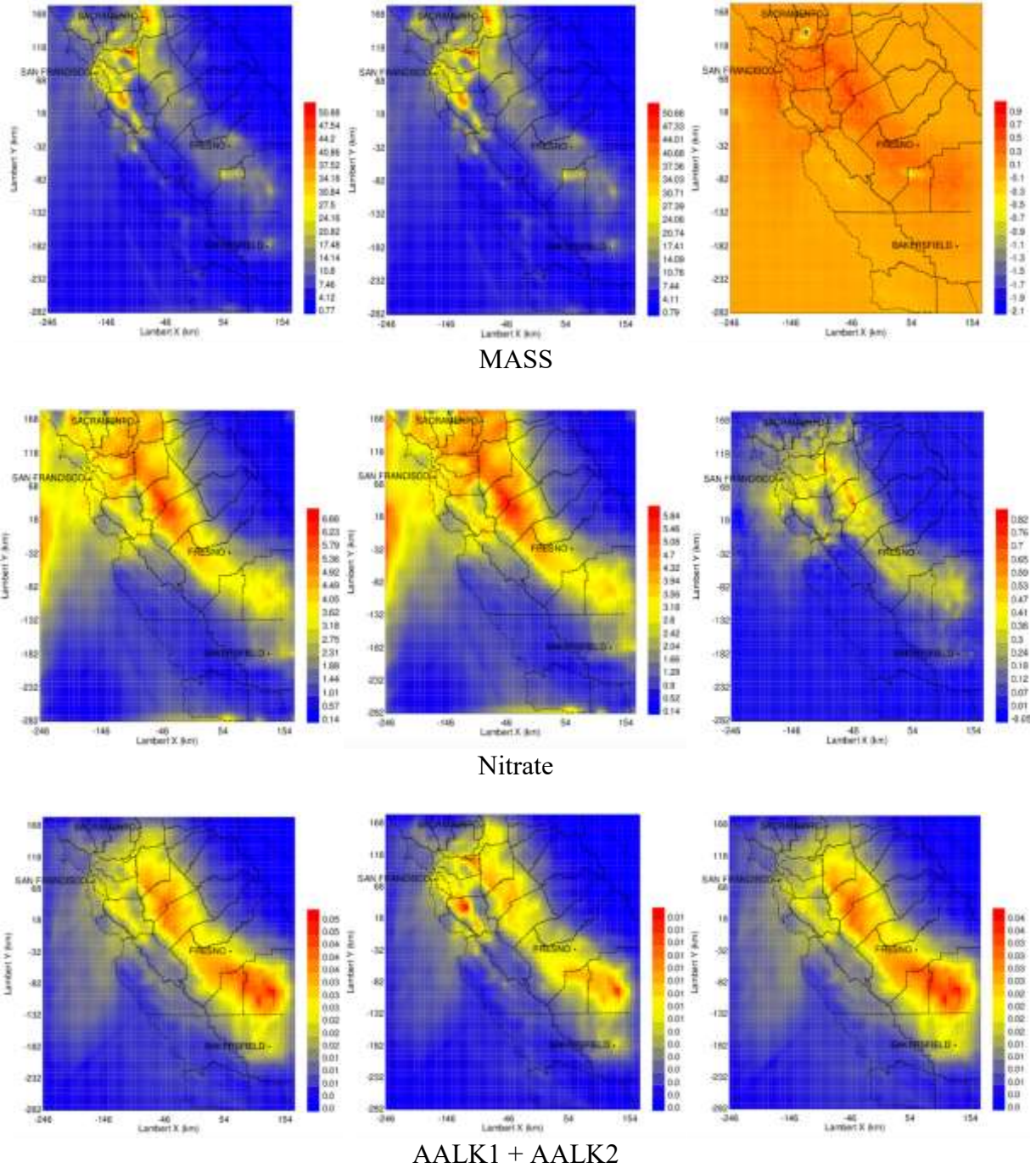
AALK1 + AALK2

Figure 6-6: Ground-level concentration predictions for PM2.5 mass, nitrate (=inorganic+organic), and AALK1+AALK2 averaged between Jan 16-Feb 10, 2013. Left column represents the base case SAPRC11 mechanism, the center column is the expanded SAPRC11 mechanism, and the right column is base case – expanded results.
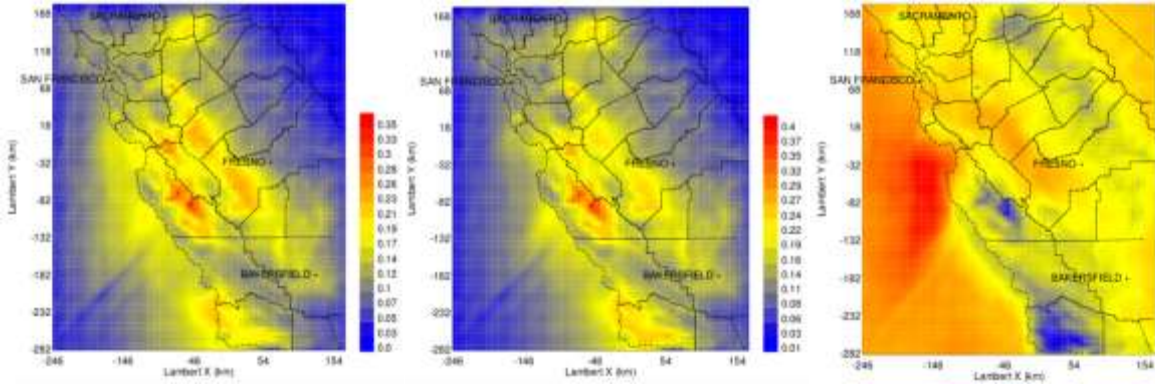
AXYL1 + AXYL2 + AXYL3
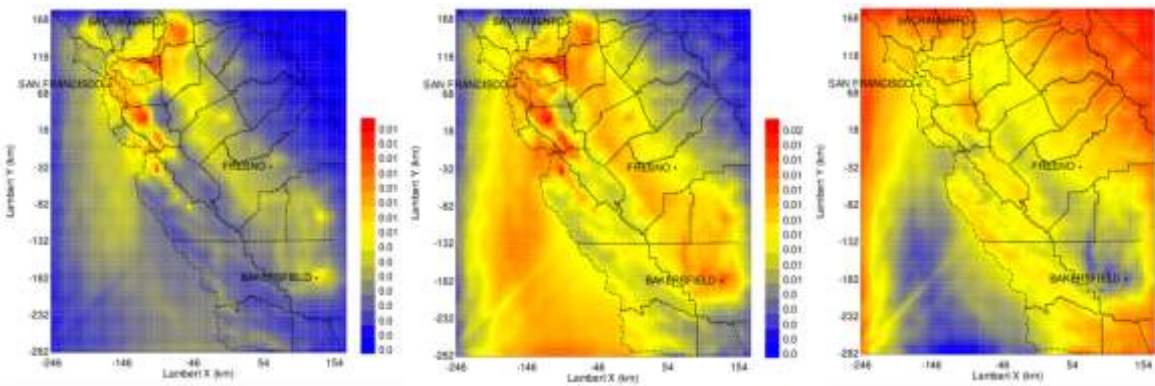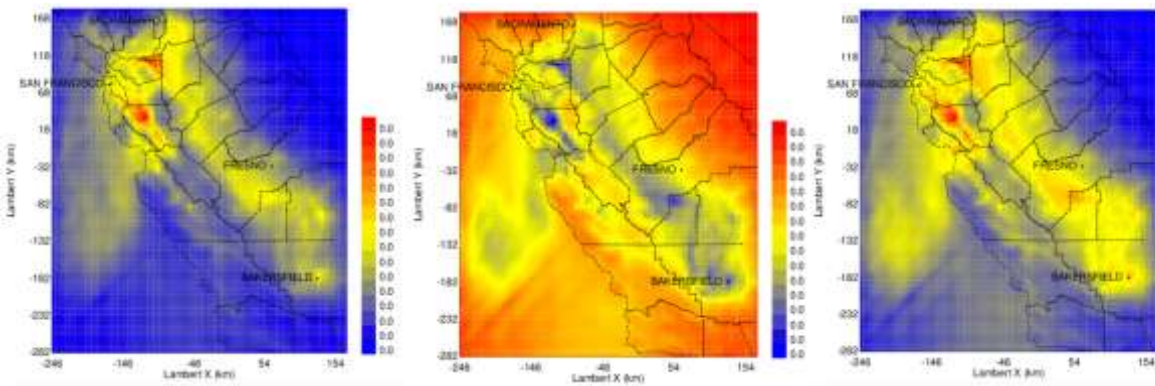
ATOL1 +ATOL2 +ATOL3

ABNZ1 + ABNZ2 + ABNZ3

Figure 6-7: Ground-level concentration predictions for PM2.5 AXYL1+AXYL2+AXYL3, ATOL1+ATOL2+ATOL3, and ABNZ1+ABZN2+ABZN3 averaged between Jan 16-Feb 10, 2013. Left column represents the base case SAPRC11 mechanism, the center column is the expanded SAPRC11 mechanism, and right column is base case – expanded results.

ATRP1 + ATRP2 +ATRP3
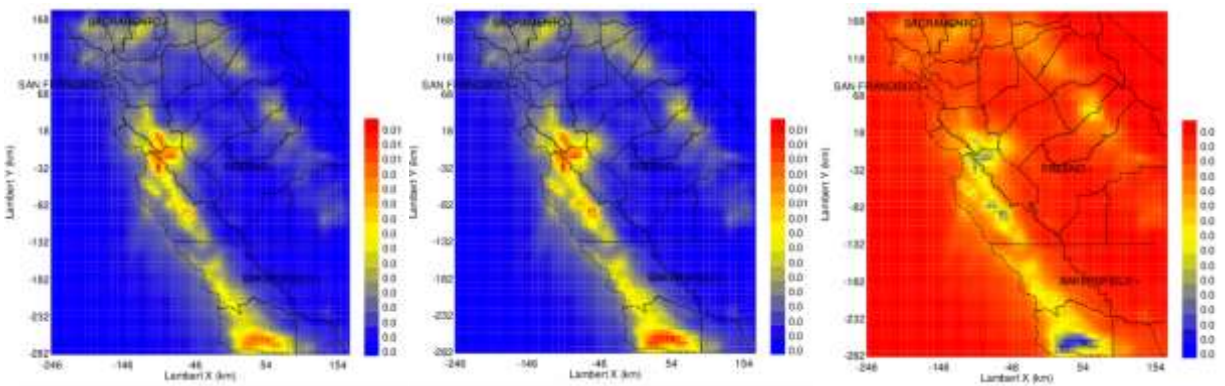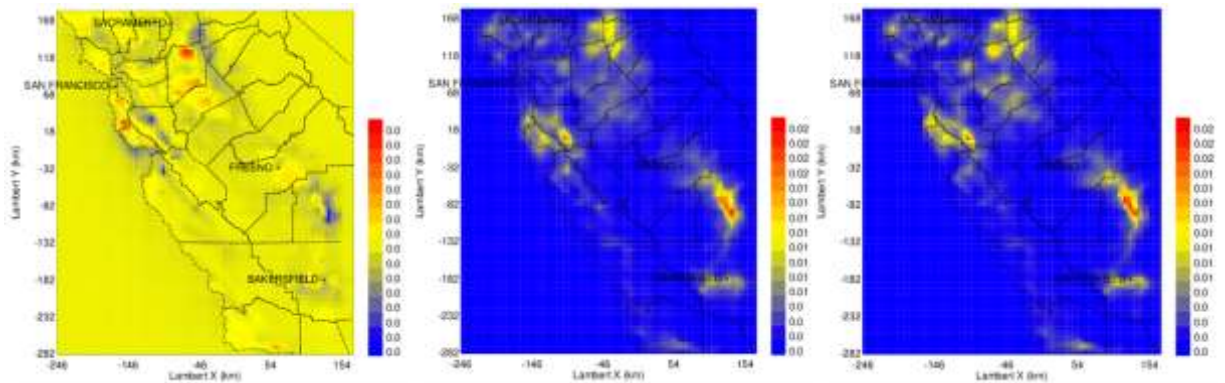
AISO1 + AISO2 +AISO3

ASQT

Figure 6-8: Ground-level concentration predictions for PM2.5 ATRP1+ATRP2+ATRP3, AISO1+AISO2+AISO3, and ASQT averaged between Jan 16-Feb 10, 2013. Left column represents the base case SAPRC11 mechanism, the center column is the expanded SAPRC11 mechanism, and the right column is base case – expanded results.
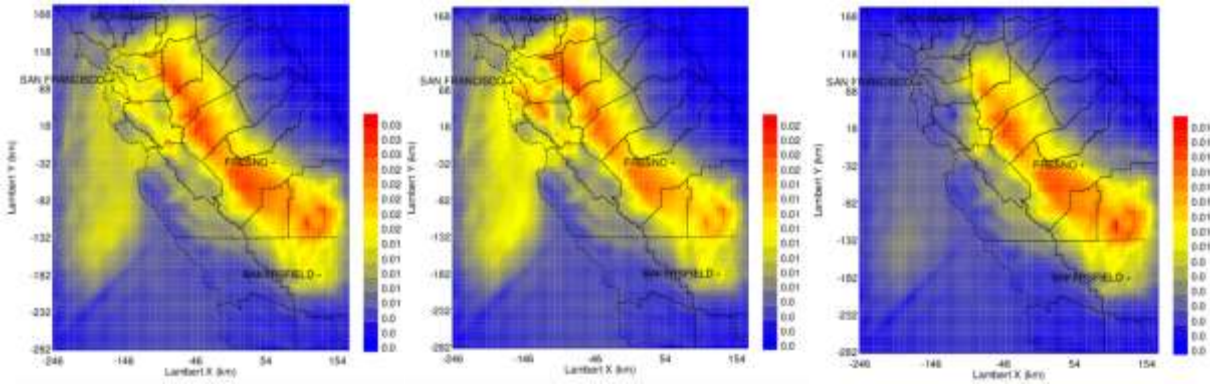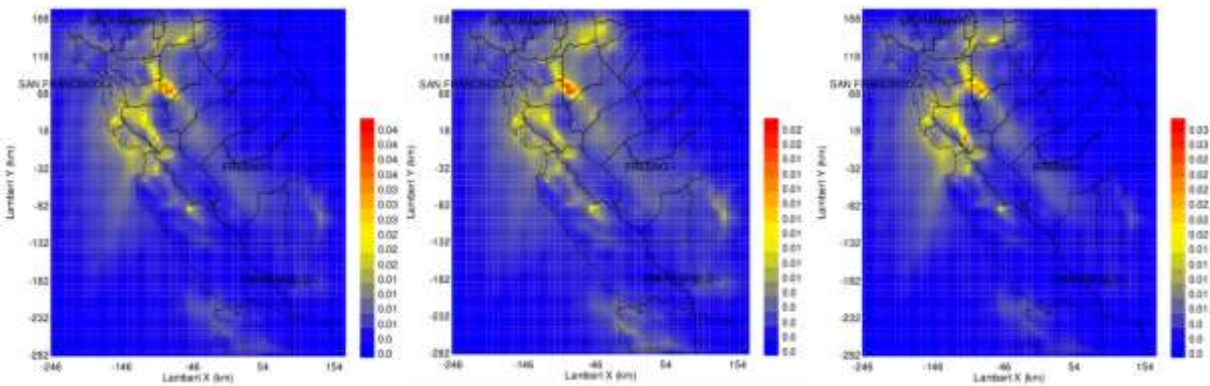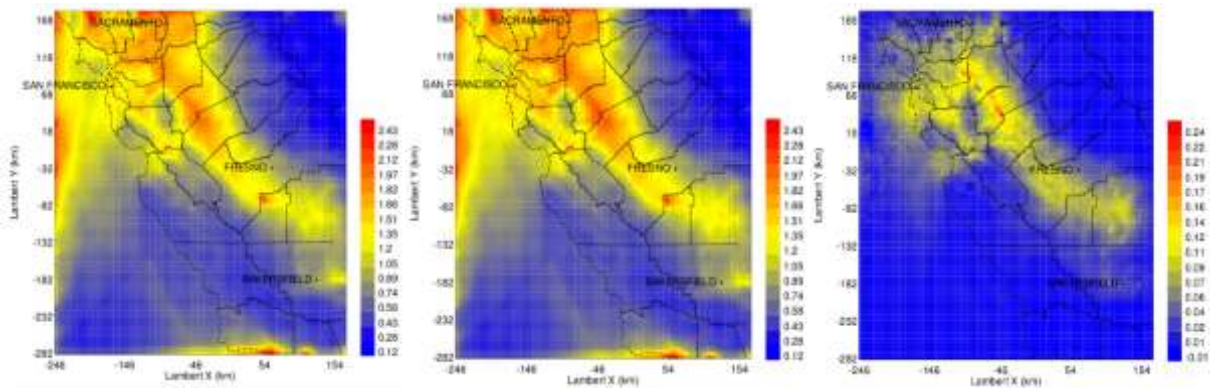
AOLGA

AOLGB

Ammonium

Figure 6-9: Ground-level concentration predictions for PM2.5 AOLGA, AOLGB, and Ammonium averaged between Jan 16-Feb 10, 2013. Left column represents the base case SAPRC11 mechanism, the center column is the expanded SAPRC11 mechanism, and the right column is base case – expanded results.

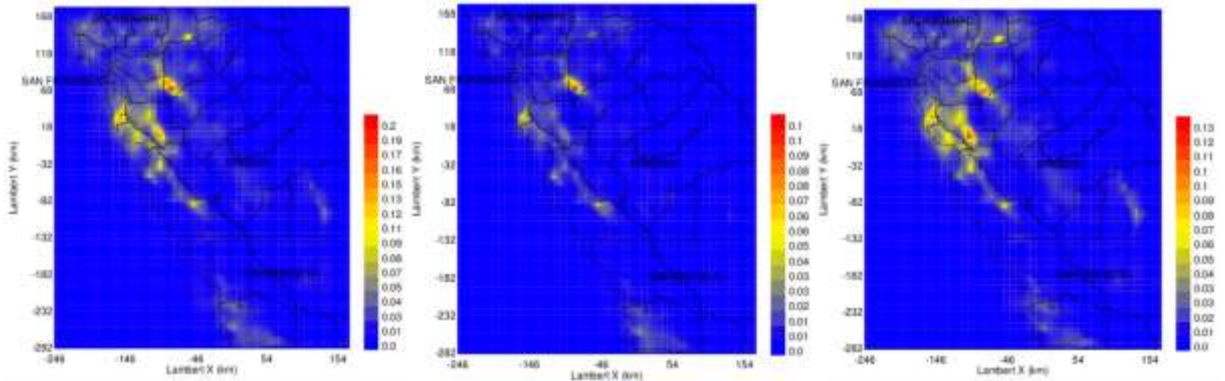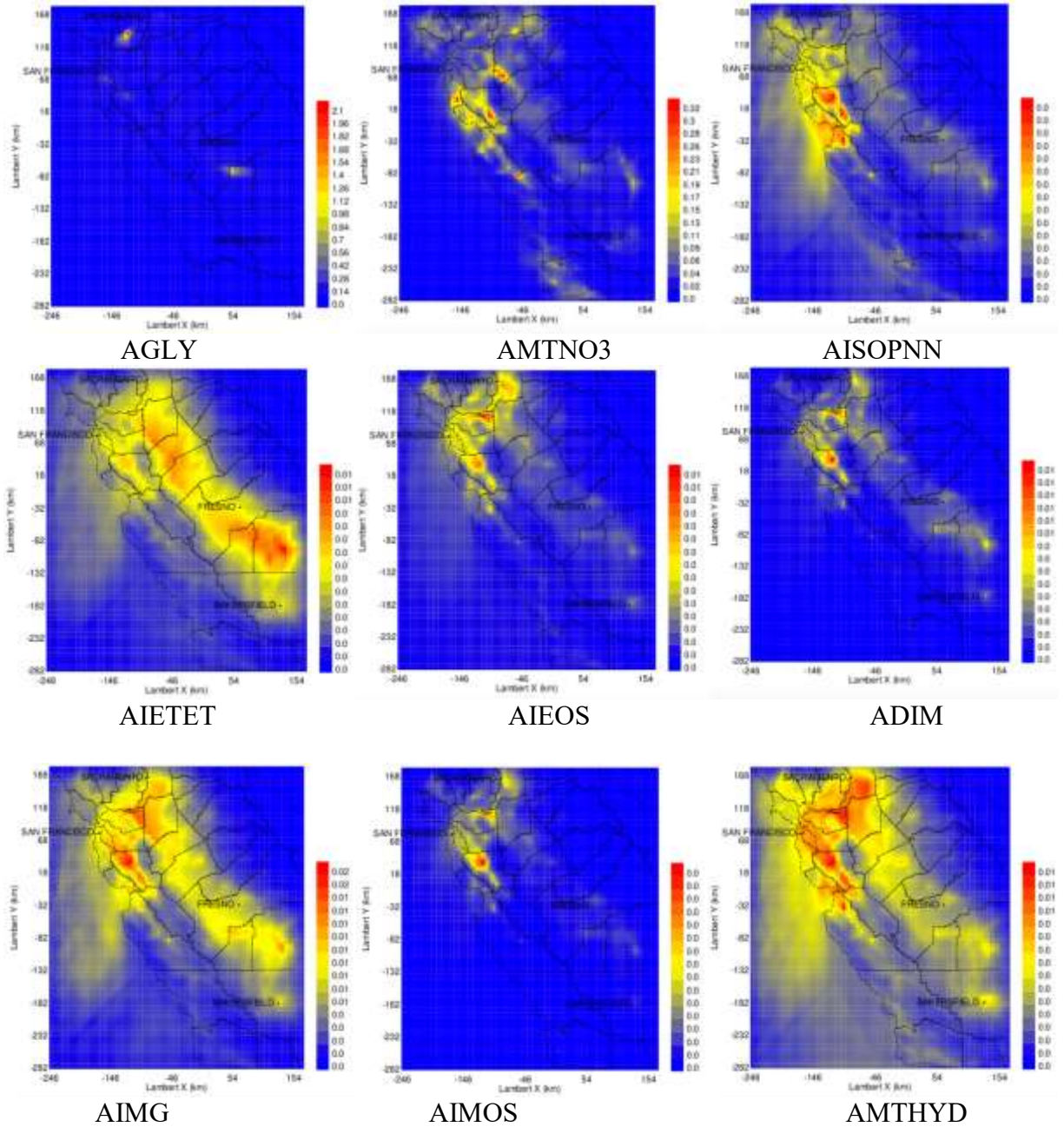Figure 6-10: Ground-level concentration predictions for PM2.5 AGLY, AMTNO3, AISOPNN, AIETET, AIEOS, ADIM, AIMG, AIMOS, and AMTHYD averaged between Jan 16-Feb 10, 2013. All predictions generated with the expanded SAPRC11 mechanism.

6.3.2   CALNEX

Figures 6-11 through 6-12 illustrate the average vertical profile of pollutants measured above Pasadena on May 30, 2010 and June 3, 2010, respectively. Solid lines represent average values while uncertainty bars represent 3 times the standard deviation.

Model predictions with the original SAPRC11 mechanism are shown as red lines while model predictions with the expanded SAPRC11 mechanism are shown as blue lines in Figures 6-11 through 6-12. Concentrations predicted by the original and expanded SAPRC11 mechanism are very similar at all times and locations for all the indicated pollutants with the exception that organic aerosol concentrations predicted by the expanded mechanism are slightly higher and isoprene concentrations predicted by the expanded mechanism are slightly lower than those predicted with the original mechanism.

The expanded chemical mechanism does not increase predicted nitrate and ammonium ion concentrations, which are significantly lower than measured values at all available elevations. The vertical concentration profile of NOx and particulate nitrate suggests the presence of an elevated plume of reactive nitrogen with a maximum at approximately 1km which likely corresponds to the penetration of this plume into the stable elevated inversion layer.

Isoprene and benzene concentrations appear to be moderately under-predicted by model calculations below the height of the mixing layer.
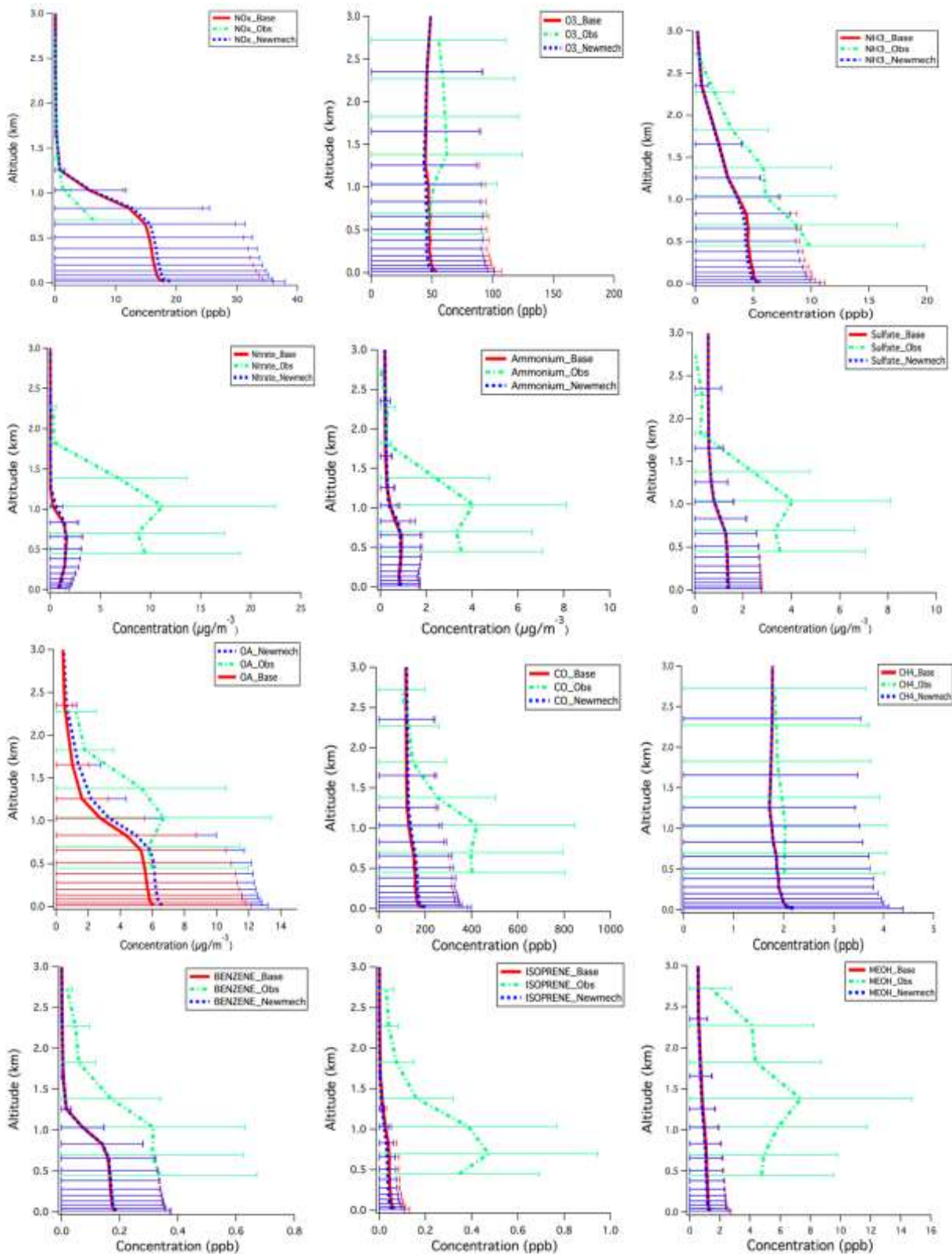
Figure 6-11: Vertical profiles above Pasadena at 03:00 PM on May 30, 2010.
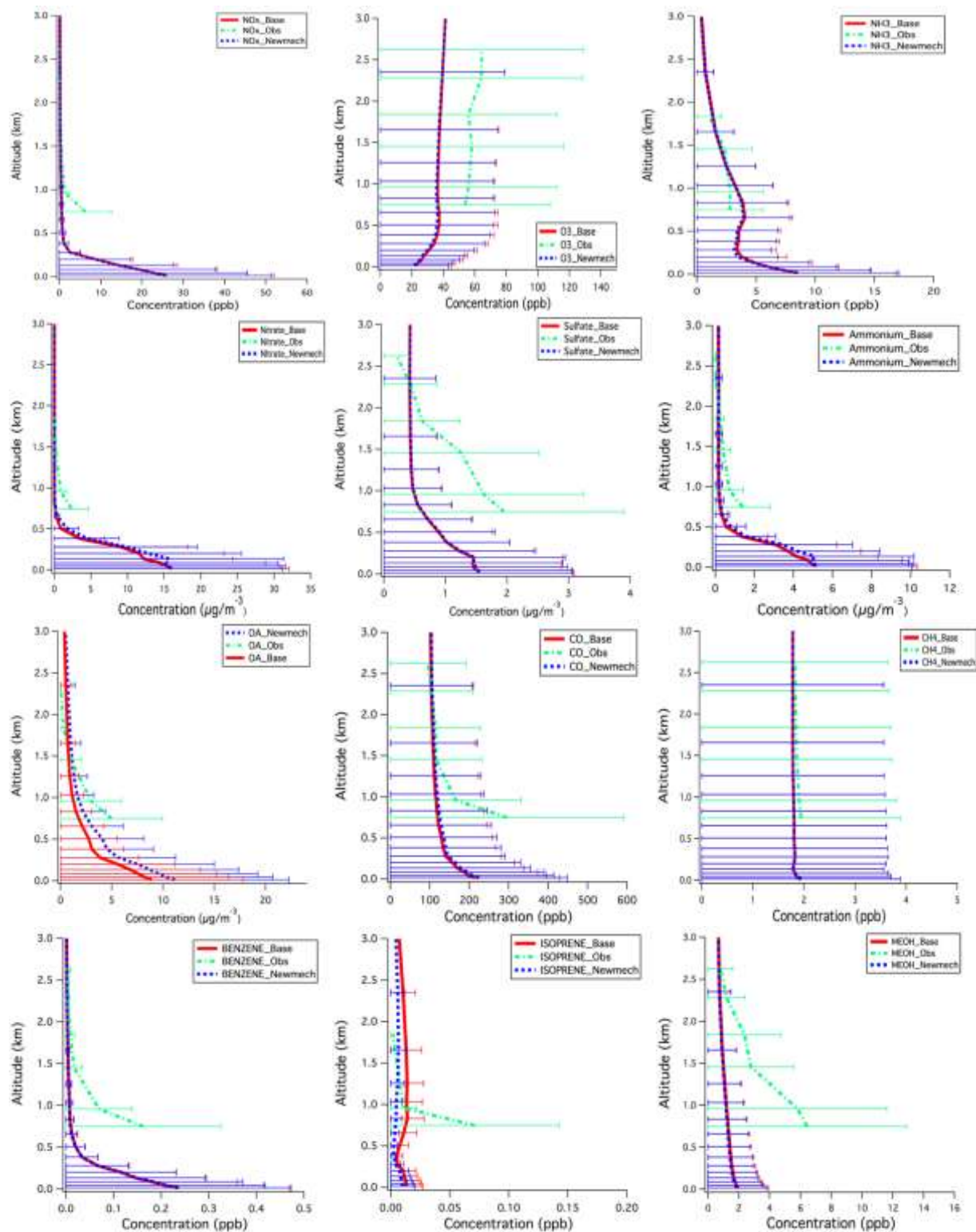
Figure 6-12: Vertical profiles above Pasadena at 06:00 AM on June 03, 2010..

Figure 6-13 summarizes the time series of predicted and measured pollutant concentrations at ground level at the Pasadena site between May 19 – June 14, 2010. The expanded SAPRC11 mechanisms and the base SAPRC11 mechanisms produce very similar concentrations for gas and particle phase species with the exception of slightly increased OA predictions from the expanded mechanism during June 2010.

Predicted and measured ozone concentrations follow the expected diurnal cycle with reasonable agreement for maximum daily concentrations except during periods with higher measured ozone concentrations. Likewise, predicted and measured NOx concentrations are in reasonable agreement but the details of the diurnal cycle are not aligned perfectly suggesting some issue with mixing as a function of time.

Nitrate concentrations are generally under predicted during May 2010 and similar to measured values during June 2010. Isoprene concentrations are consistently under predicted by model calculations, which has implications for the importance of the NOx reactions with biogenic VOCs.
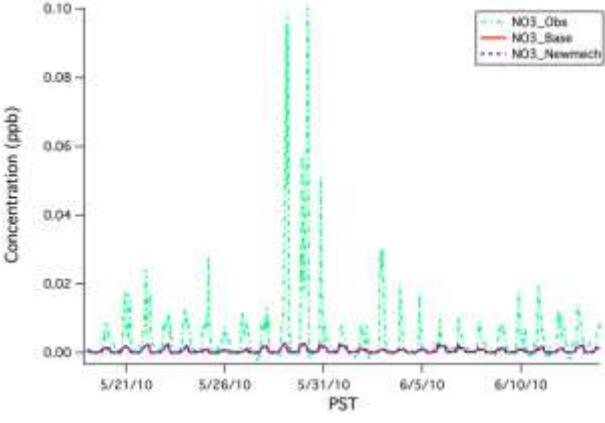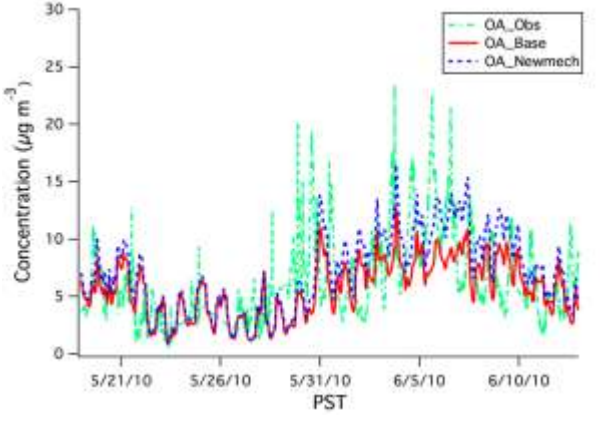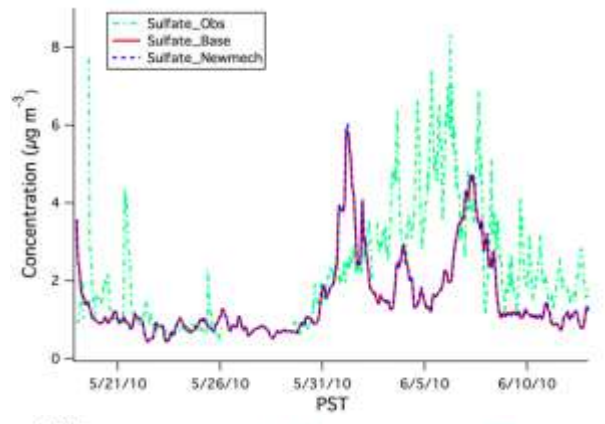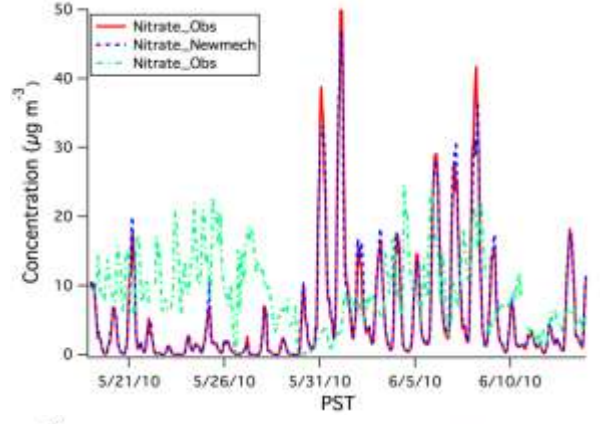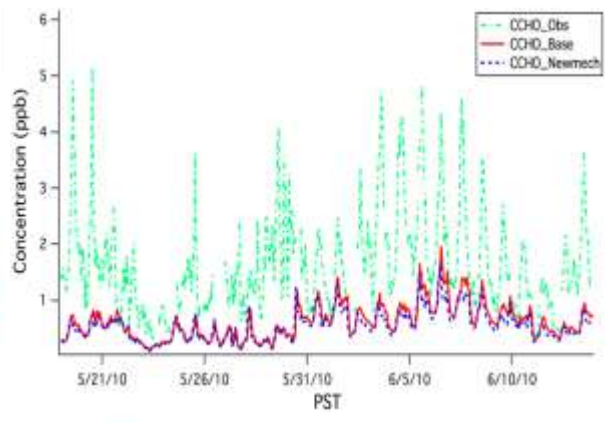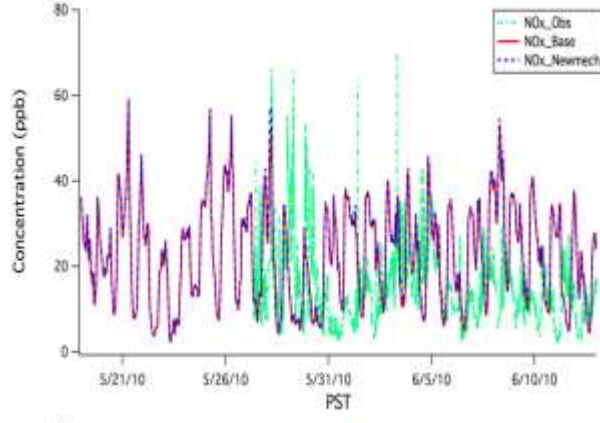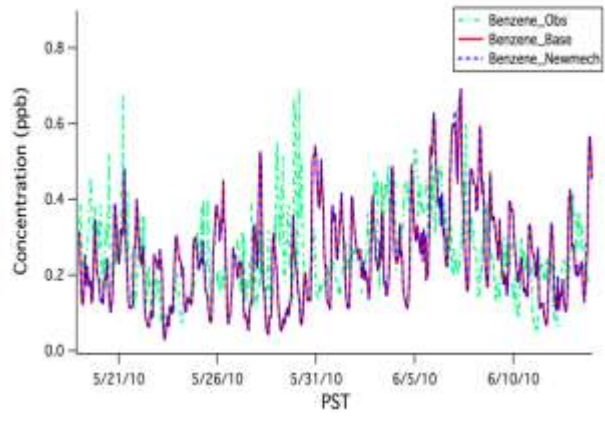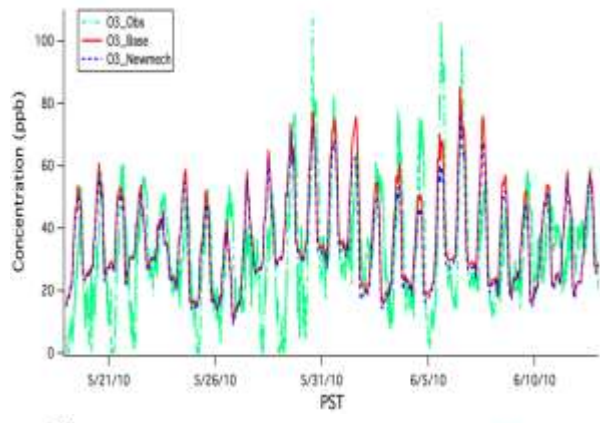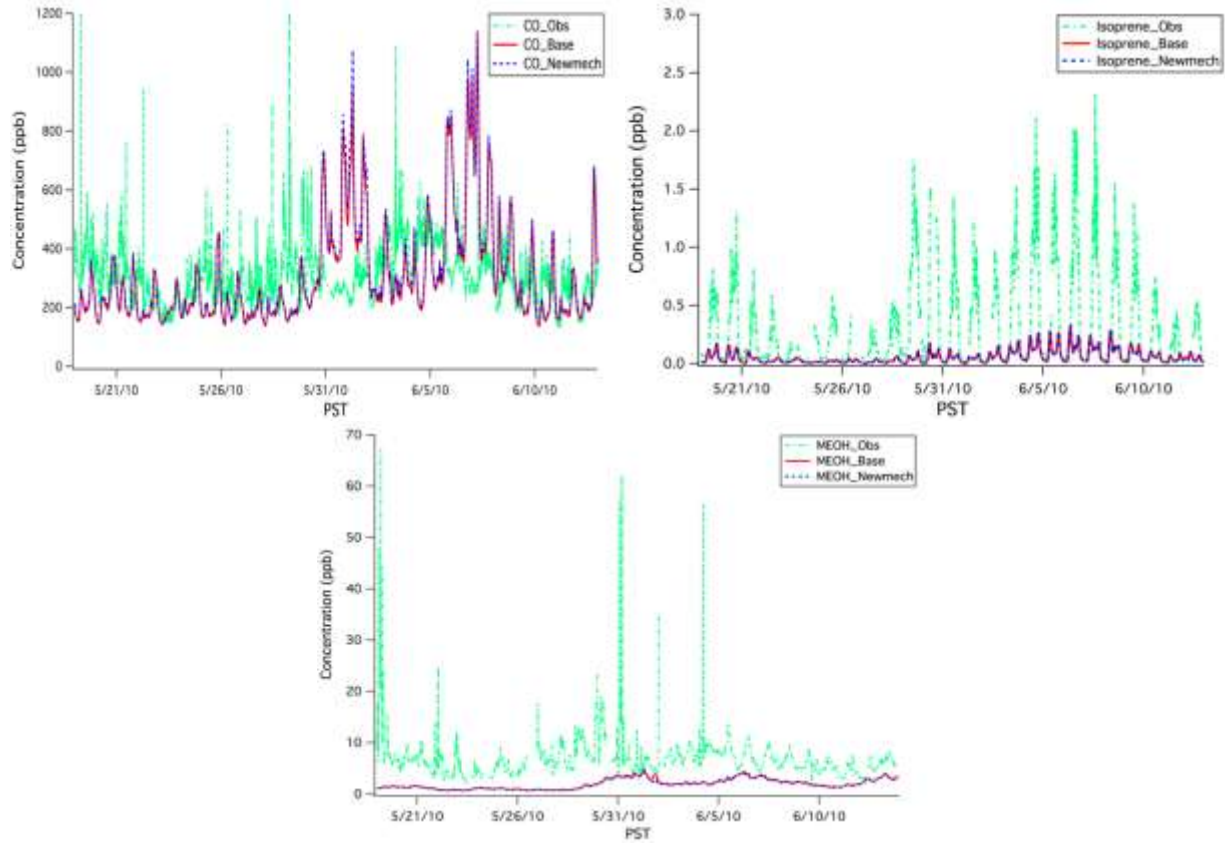
Figure 6-13: Time series of various species (name written in the plots) at Pasadena during the CALNEX campaign.

Figures 6-14 through 6-17 illustrate the predicted ground-level concentrations of PM2.5 mass and various chemical components averaged over the period May 19 – June 14, 2010 in Southern California with a resolution of 4 km. Figures 6-18 through 6-23 show the model predictions for the SJV with the same format over the same time period. The left column in each Figure shows the base SAPRC11 prediction, and center column shows the expanded SAPRC11 prediction, and the right column shows the difference (base – expanded). During the summer conditions the expanded chemistry increases predicted PM2.5 mass concentrations by ~0.8 µg m^{-3} in the SJV and ~2 µg m^{-3} in the SoCAB. Particulate nitrate and ammonium ion accounts for ~0.08 µg m^{-3} (~10%) of this increase in the SJV and ~0.53 µg m^{-3} (~27%) of the increase in the SoCAB. The remaining increase in PM2.5 mass is attributed to organic nitrate species and glyoxal. AMTNO3 concentrations increase by ~0.26 µg m^{-3} in the SJV around Bakersfiled and ~0.4 µg m^{-3} in the SoCAB. AGLY+AMGLY increases by ~0.1 µg m^{-3} in the SJV along the Sierra foothills and 0.59 µg m^{-3} in the SoCAB. Other organic nitrate species account for smaller increases in total PM2.5 OA concentrations.

MASS
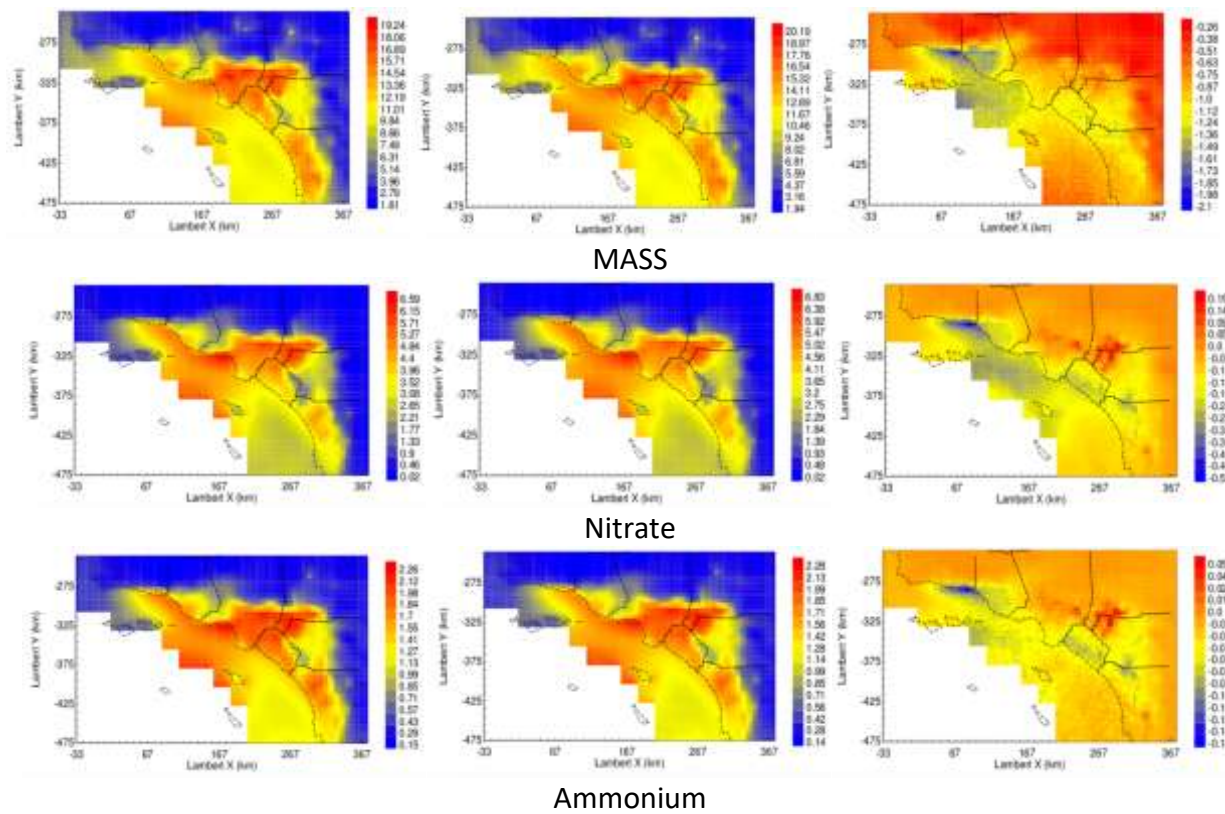
Nitrate

Ammonium

Figure 6-14: Ground-level concentration predictions for PM2.5 mass, nitrate
(=inorganic+organic), and ammonium averaged between May 19 – June 14, 2010 in the SoCAB.
Left column represents the base case SAPRC11 mechanism, the center column is the expanded
SAPRC11 mechanism, and right column is base case – expanded results.
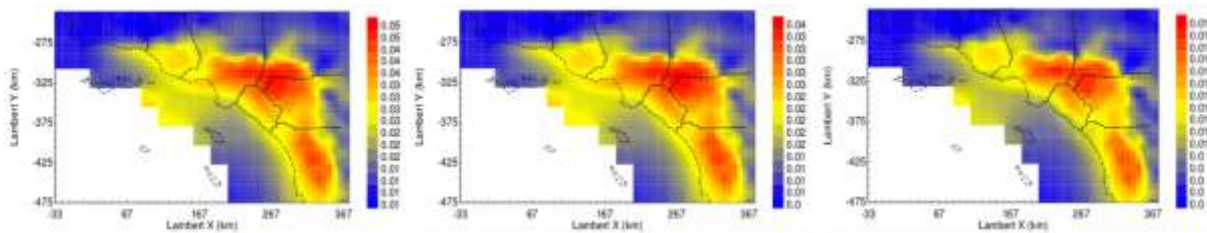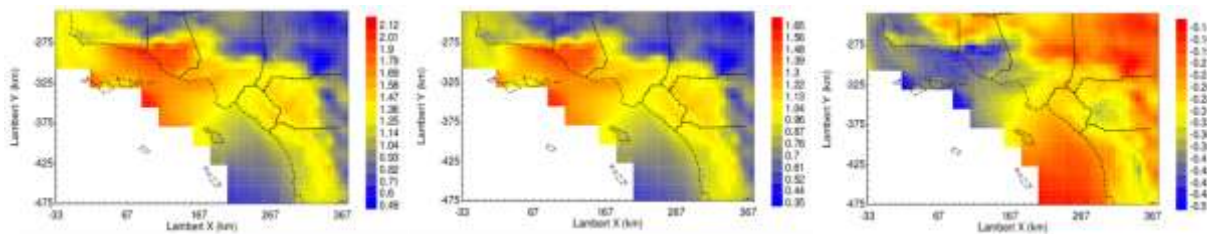
AALK1 + AALK2
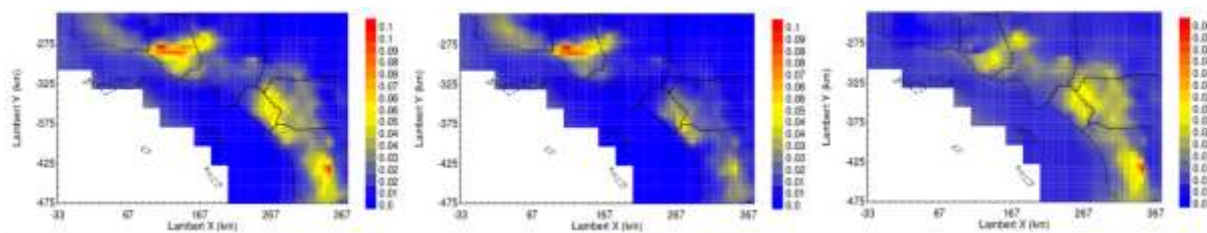
AXYL1 + AXYL2 +AXYL3

ATRP1 + ATRP2 + ATRP3

Figure 6-15: Ground-level concentration predictions for PM2.5 AALK1+AALK2, AXYL1+AXYL2+AXYL3, and ATRP1+ATRP2+ATRP3 averaged between May 19 – June 14, 2010 in the SoCAB. Left column represents the base case SAPRC11 mechanism, the center column is the expanded SAPRC11 mechanism, and right column is base case – expanded results.
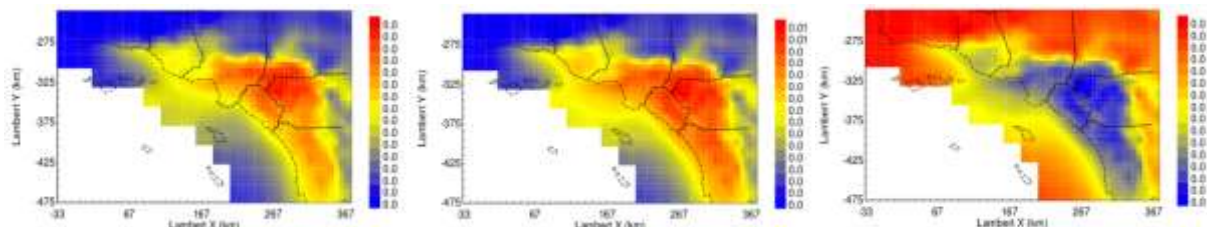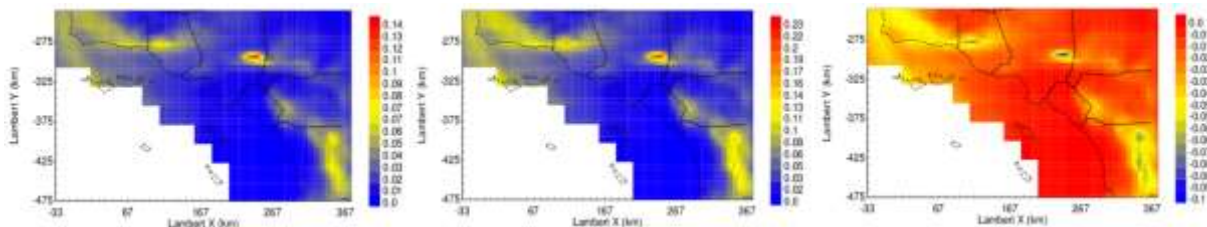
ABNZ1 + ABNZ2 + ABNZ3
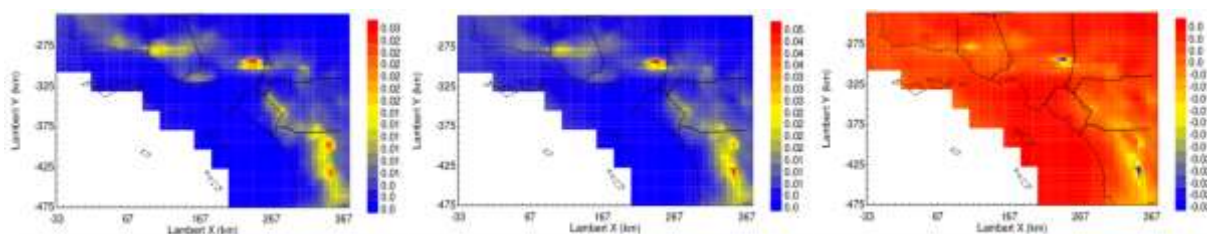
AISO1 + AISO2 + AISO3

ASQT

Figure 6-16: Ground-level concentration predictions for PM2.5 ABNZ1+ABNZ2+ABNZ3, AISO1+AISO2+AISO3, and ASQT averaged between May 19 – June 14, 2010 in the SoCAB. Left column represents the base case SAPRC11 mechanism, the center column is the expanded SAPRC11 mechanism, and right column is base case – expanded results.
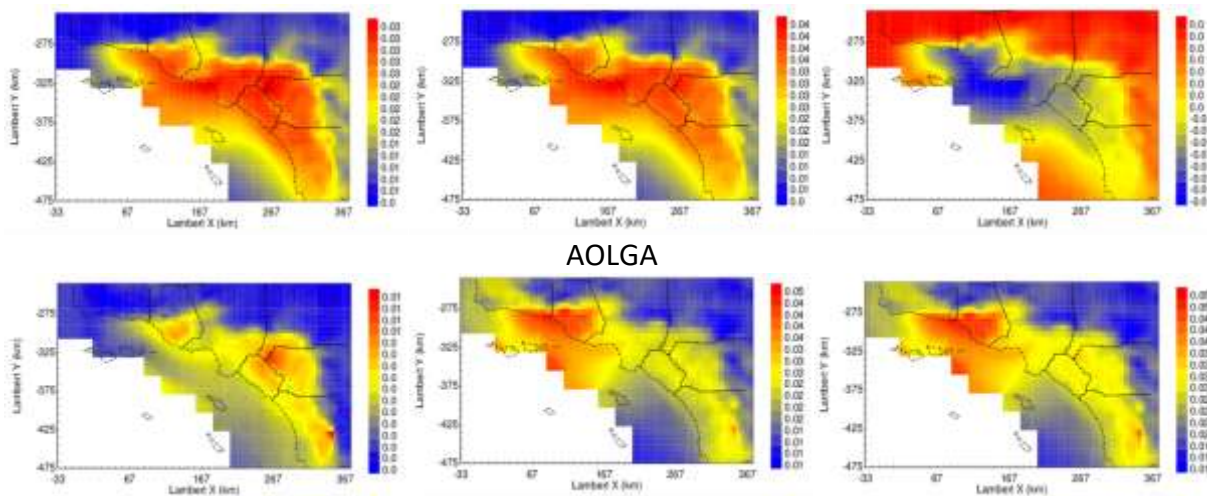
AOLGA

AOLGB

Figure 6-17: Ground-level concentration predictions for PM2.5 AOLGA and AOLGB averaged between May 19 – June 14, 2010 in the SoCAB. Left column represents the base case SAPRC11 mechanism, the center column is the expanded SAPRC11 mechanism, and right column is base case – expanded results.

AISOPNN   AMTNO3   AGLY + AMGLY

AIETET   AIEOS   ADIM
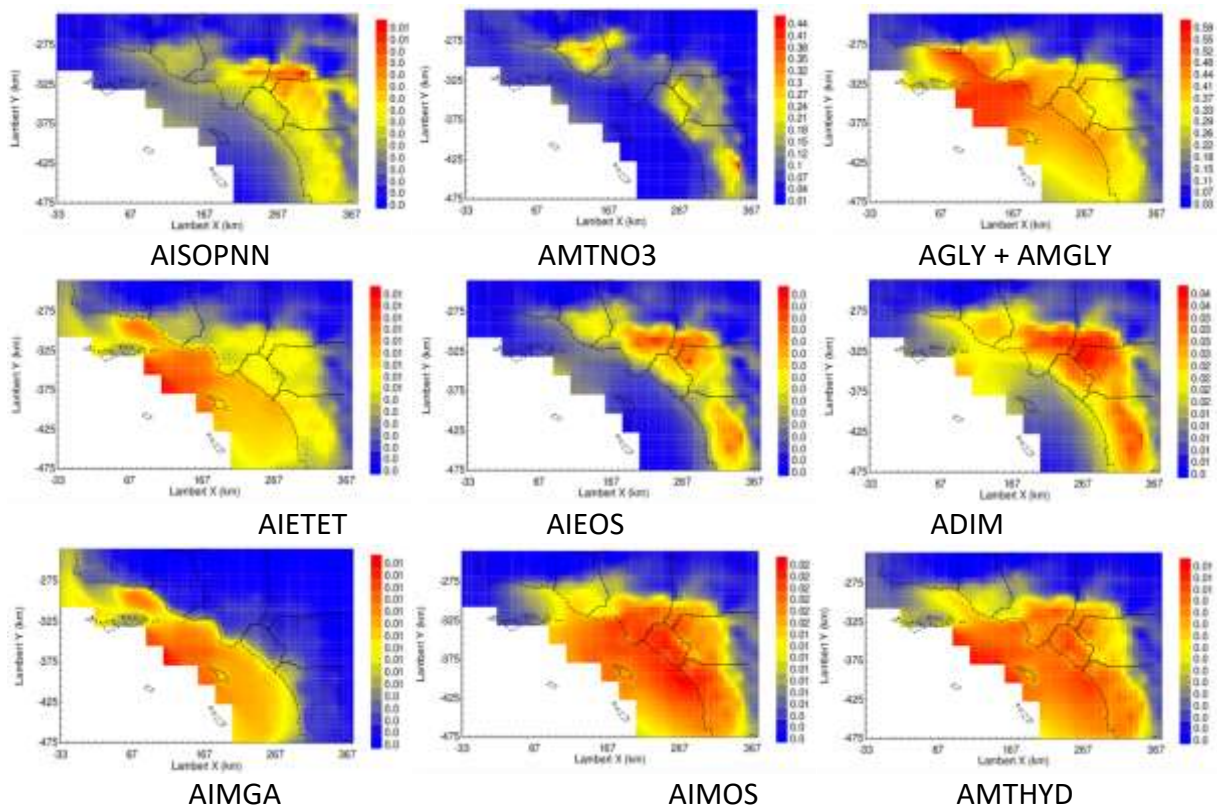
AIMGA   AIMOS   AMTHYD

Figure 6-18: Ground-level concentration predictions for PM2.5 AISOPNN, AMTNO3, AGLY+AMGLY, AIETET, AIEOS, ADIM, AIMGA, AIMOS, and AMTHYD averaged between May 19 – June 14, 2010 in the SoCAB. All predictions generated with the expanded SAPRC11 mechanism
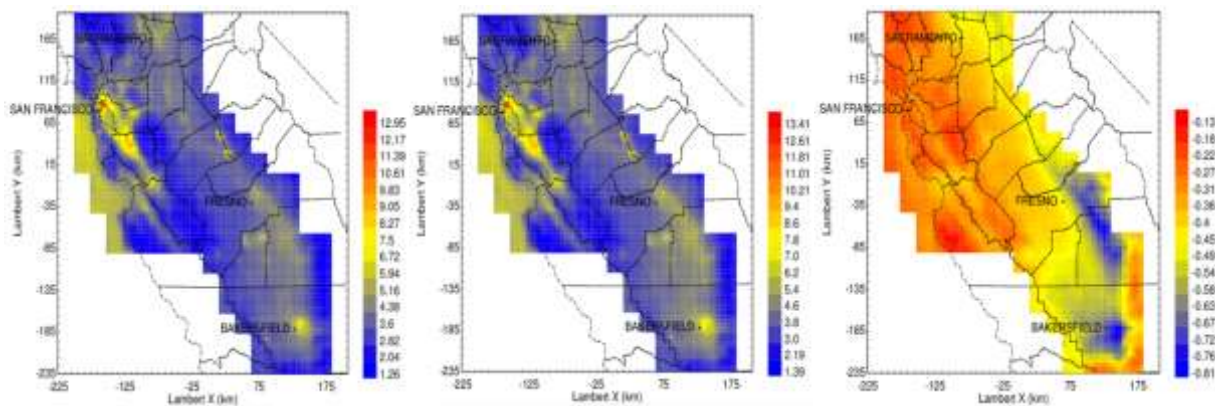
MASS
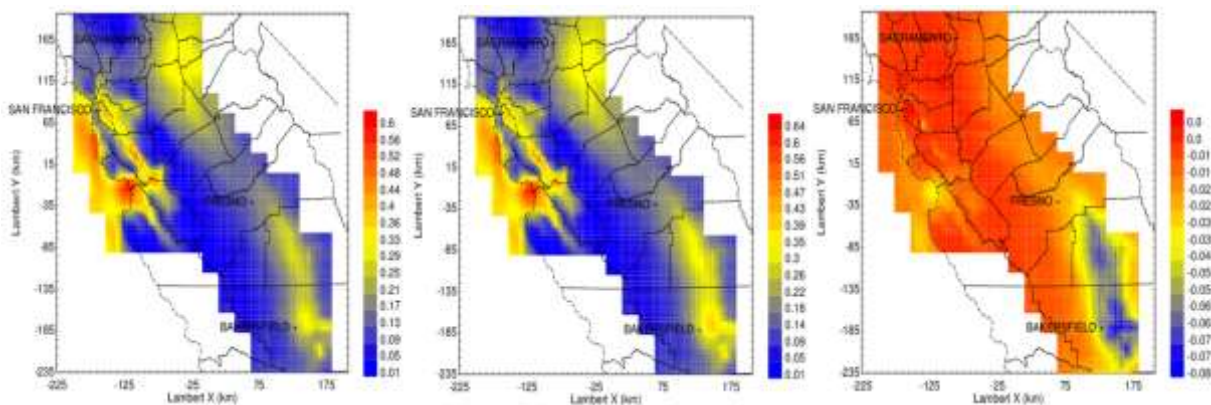
Nitrate
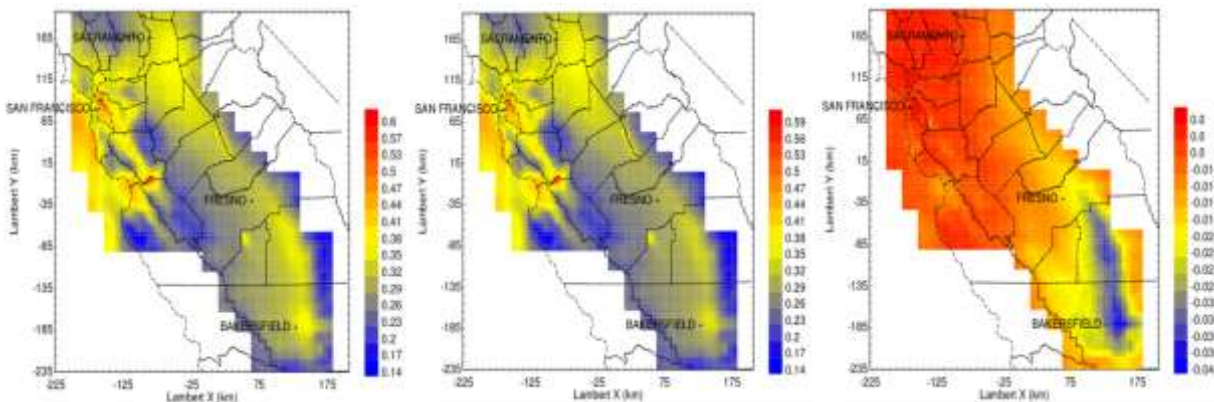
Ammonium

Figure 6-19: Ground-level concentration predictions for PM2.5 mass, nitrate (=inorganic+organic), and ammonium averaged between May 19 – June 14, 2010 in the SJV. Left column represents the base case SAPRC11 mechanism, the center column is the expanded SAPRC11 mechanism, and right column is base case – expanded results.
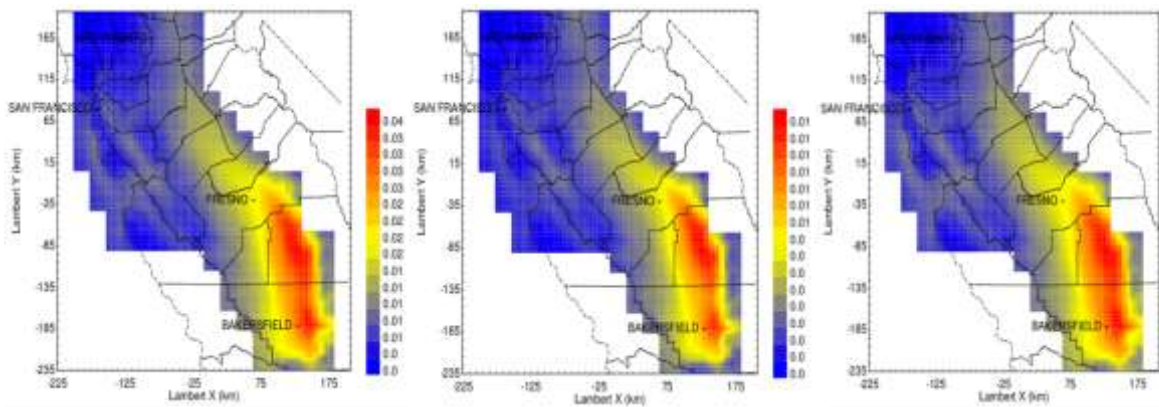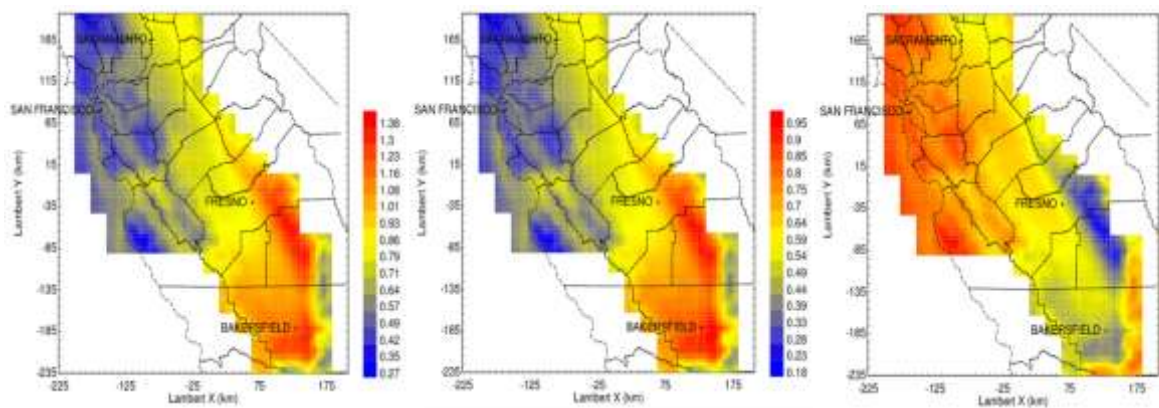
AALK1 + AALK2
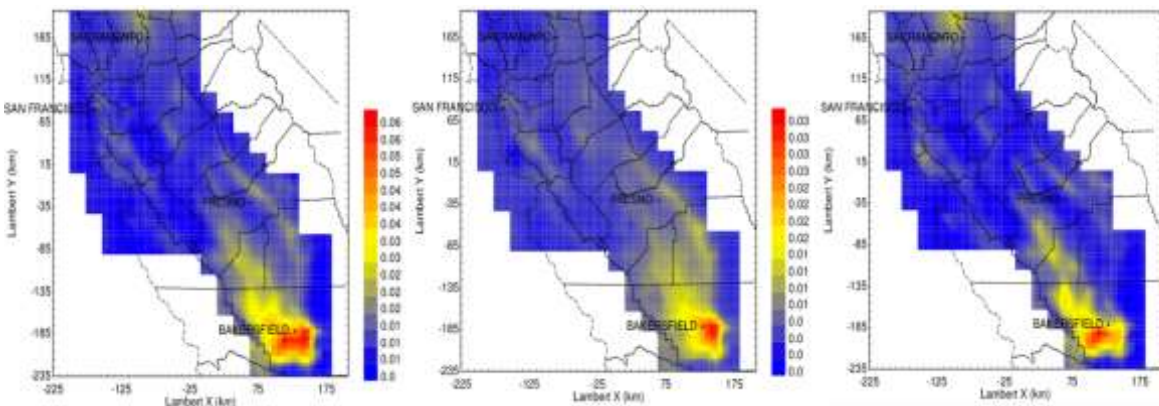
AXYL1 + AXYL2 +AXYL3

ATRP1 + ATRP2 + ATRP3

Figure 6-20: Ground-level concentration predictions for PM2.5 AALK1+AALK2, AXYL1+AXYL2+AXYL3, and ATRP1+ATRP2+ATRP3 averaged between May 19 – June 14, 2010 in the SJV. Left column represents the base case SAPRC11 mechanism, the center column is the expanded SAPRC11 mechanism, and right column is base case – expanded results.
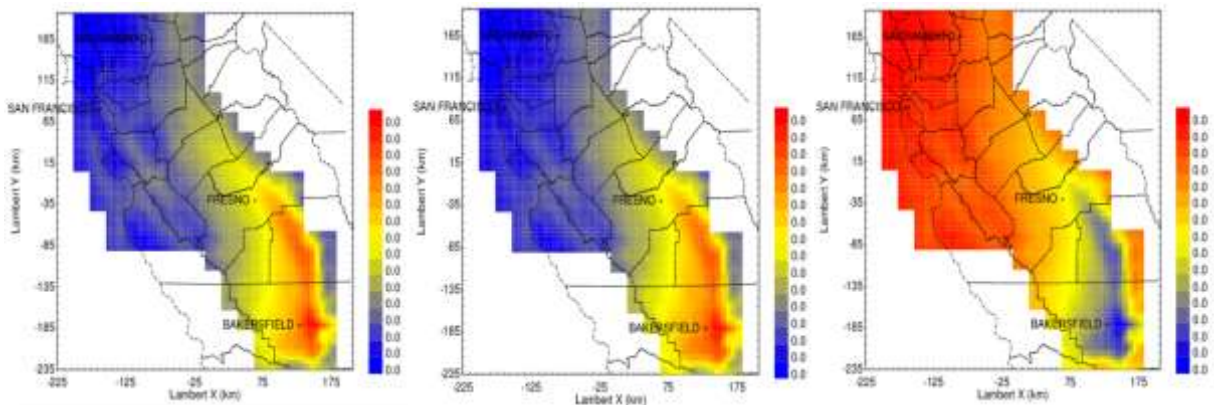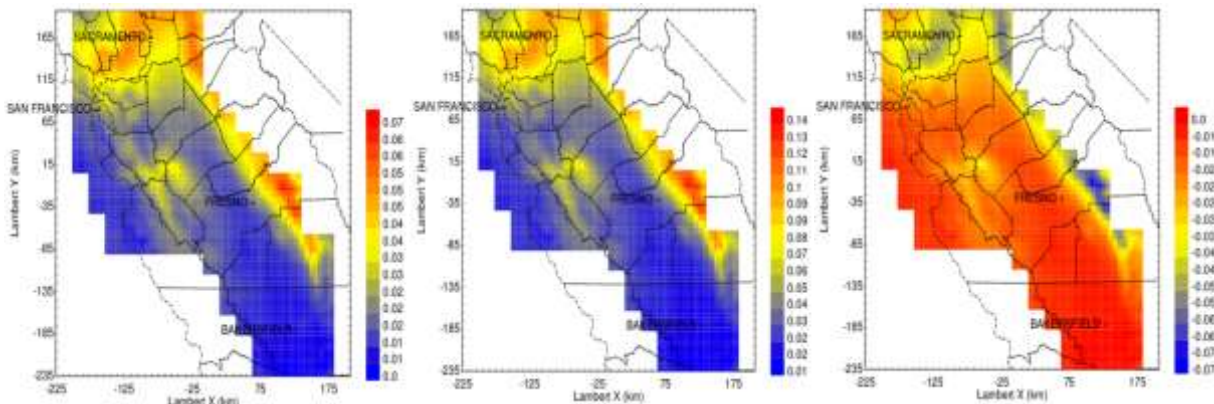
ABNZ1 + ABNZ2 + ABNZ3
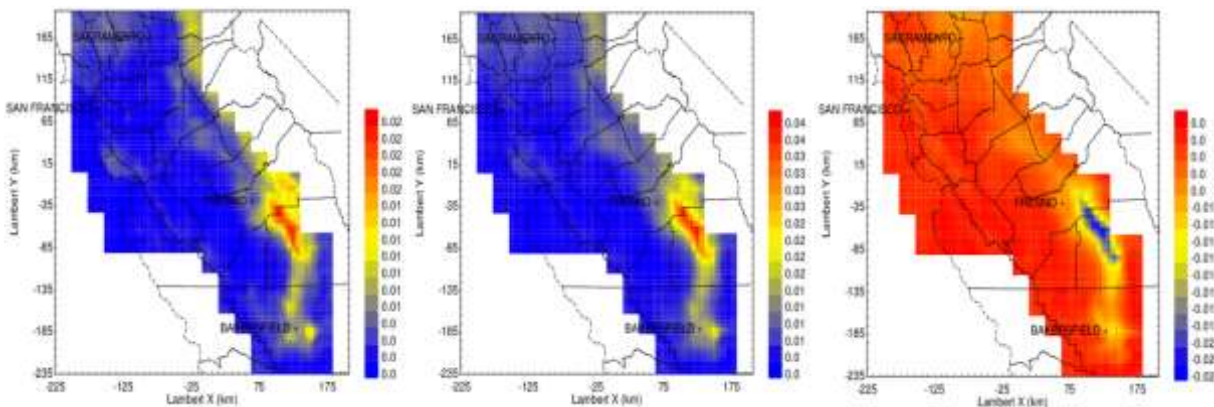
AISO1 + AISO2 + AISO3

ASQT

Figure 6-21: Ground-level concentration predictions for PM2.5 ABNZ1+ABNZ2+ABNZ3, AISO1+AISO2+AISO3, and ASQT averaged between May 19 – June 14, 2010 in the SJV. Left column represents the base case SAPRC11 mechanism, the center column is the expanded SAPRC11 mechanism, and right column is base case – expanded results.
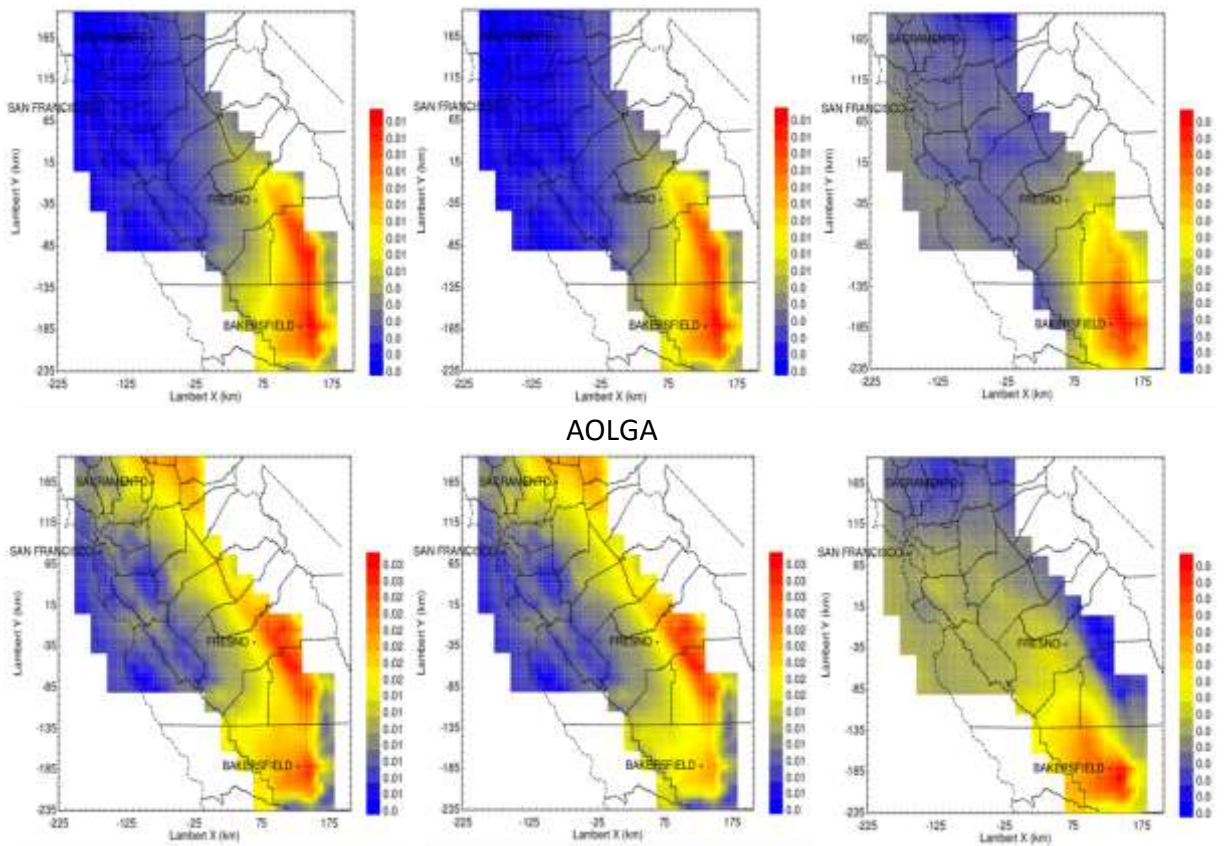
AOLGA

AOLGB

Figure 6-22: Ground-level concentration predictions for PM2.5 AOLGA and AOLGB averaged between May 19 – June 14, 2010 in the SJV. Left column represents the base case SAPRC11 mechanism, the center column is the expanded SAPRC11 mechanism, and right column is base case – expanded results.

AISOPNN   AMTNO3   AGLY + AMGLY

AIETET   AIEOS   ADIM
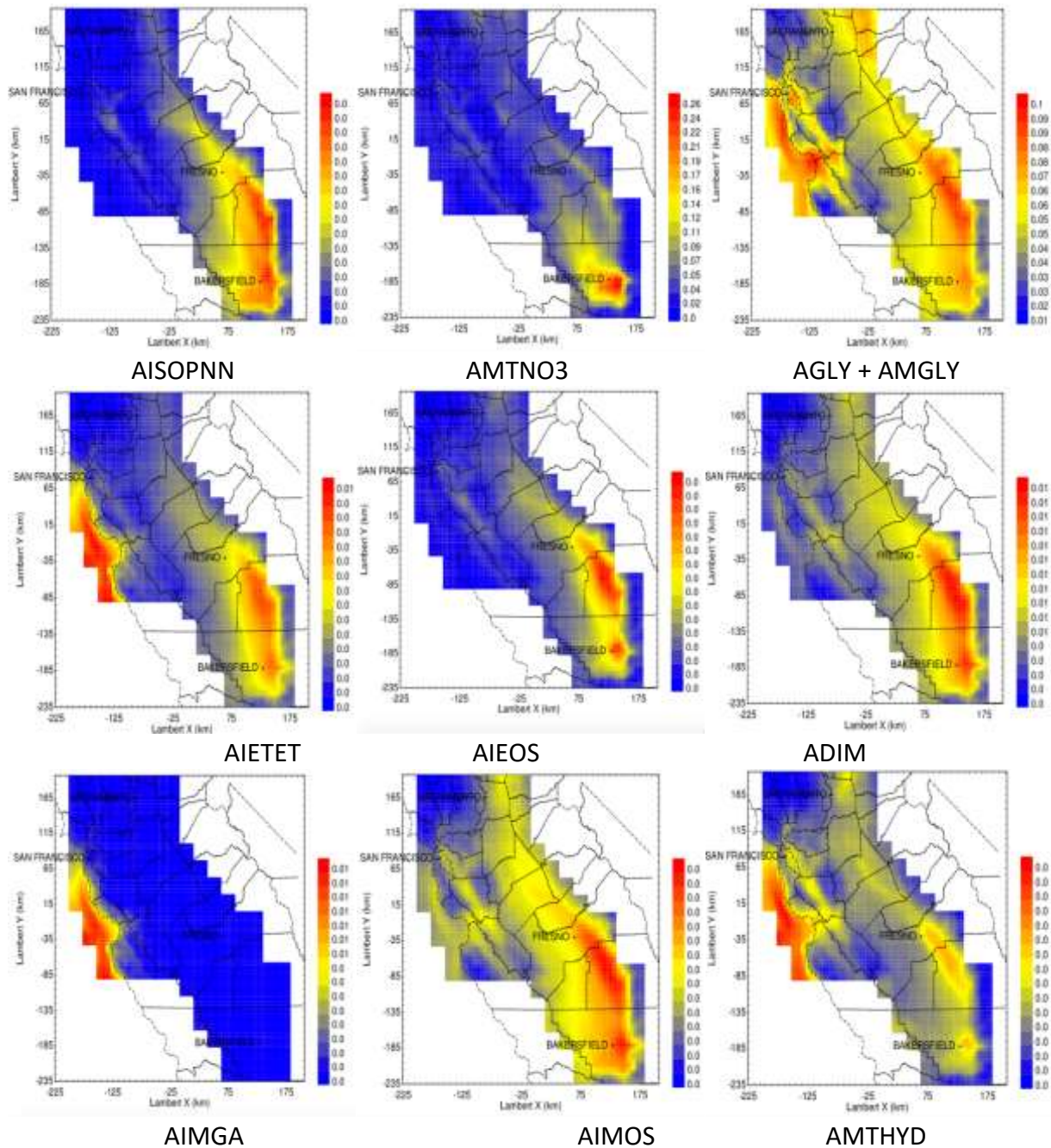
AIMGA   AIMOS   AMTHYD

Figure 6-23: Ground-level concentration predictions for PM2.5 AISOPNN, AMTNO3, AGLY+AMGLY, AIETET, AIEOS, ADIM, AIMGA, AIMOS, and AMTHYD averaged between May 19 – June 14, 2010 in the SJV. All predictions generated with the expanded SAPRC11 mechanism

6.4   Discussion

The simulations for a typical summer time period in California (May 19 – June 14, 2010) indicate that reactions between anthropogenic NOx and biogenic hydrocarbons can produce up to ~0.9-1 µg m^{-3} of PM2.5 SOA in the SoCAB that is ~33% mono terpene nitrates (terpene analogs to PAN) and ~66% glyoxal / methylglyoxal.   Typical monthly-averaged PM2.5 OA concentrations during summer are 3-4 µg m^{-3} at measurement sites in the SoCAB, and so biogenically-derived SOA represents a minor but potentially important fraction of the total OA burden.

Pye et al. [195] showed that monoterpene nitrate concentrations decrease in direct proportion with NOx emissions, while the glyoxal / methyl glyoxal reductions are more related to changes in oxidant concentrations.   Pye et al. determined that a 25% reduction in NOx emissions translated to an 8% reduction in glyoxal / methyl glyoxal particulate matter in the Southeastern United States.   Extending these findings to the current study, it is likely that a 25% NOx reduction in Southern California would reduce monoterpene nitrate concentrations by 25% (~0.08 µg m^{-3}) and glyoxal / methyl glyoxal concentrations by 8% (0.05 µg m^{-3}) yielding a total decrease of 0.13 µg m^{-3} during the summer CALNEX conditions. This level of modest decrease in PM2.5 concentrations would not seem to warrant extreme NOx reductions, but given that NOx reductions are being pursued in order to control other pollutants such as ozone and particulate nitrate, it is important to also account for the predicted reduction in biogenically-derived SOA concentrations.

The simulations for a typical winter time period in California (Jan 16-Feb 10, 2013) indicates that reactions between anthropogenic NOx and biogenic hydrocarbons produces very little PM2.5 SOA in the SJV. Isoprene concentrations were under-predicted during this episode suggesting that further work should be done to improve the basecase simulation. Despite the shortcomings in base case performance, the contrast between the summer vs. winter results suggests that NOx reactions with biogenic hydrocarbons likely have the strongest effect on PM2.5 SOA during the warmer summer months rather than the cooler winter months.

6.5   Conclusions

The SAPRC11 chemical mechanism was expanded to explicitly track reactions between NOx and biogenic hydrocarbons. Model simulations were conducted for California under typical summer (May 19-June 14, 2010) and winter (Jan 16-Feb 10, 2013) conditions. Monoterpene nitrates and glyoxal / methyl glyoxal species were consistently the biggest contributors to predicted increases in aerosol mass associated with the expanded mechanism. PM2.5 SOA concentrations of these species approached 1 µg m^{-3} during the summer conditions but were < 0.1 µg m^{-3} during winter conditions. It is expected that monoterpene nitrate concentrations will decrease in direct proportion to NOx emissions, while glyoxal / methyl glyoxal concentrations will decrease more slowly than NOx emissions in future control scenarios. Using the values predicted during the summer episode analyzed in the present study, a 25% reduction in NOx emissions could produce a 0.13 µg m^{-3} reduction in PM2.5 SOA concentrations.

7 SUMMARY AND CONCLUSIONS

A coordinated set of modeling studies was carried out to investigate new mechanisms of secondary organic aerosol (SOA) and nitrate formation in California.

7.1 Multi-Generational Oxidation Model Formulation within a 3D Air Quality Model

Multi-generational gas-phase oxidation of organic vapors can influence the abundance, composition and properties of secondary organic aerosol (SOA). Only recently have SOA models been developed that explicitly represent multi-generational SOA formation. In this work, we integrated the statistical oxidation model (SOM) into SAPRC-11 to simulate the multi-generational oxidation and gas/particle partitioning of SOA in the regional UCD/CIT air quality model. In SOM, evolution of organic vapors by reaction with the hydroxyl radical is defined by (1) the number of oxygen atoms added per reaction, (2) the decrease in volatility upon addition of an oxygen atom and (3) the probability that a given reaction leads to fragmentation of the organic molecule. These SOM parameter values were fit to laboratory "smog chamber" data for each precursor/compound class. SOM was installed in the UCD/CIT model, which simulated air quality over two-week periods in the South Coast Air Basin of California and the eastern United States. For the regions and episodes tested, the two-product SOA model and SOM produce similar SOA concentrations but a modestly different SOA chemical composition. Predictions of the oxygen-to-carbon ratio qualitatively agree with those measured globally using aerosol mass spectrometers. Overall, the implementation of the SOM in a 3D model provides a comprehensive framework to simulate the atmospheric evolution of OA.

7.2 Simulating Secondary Organic Aerosol in a Regional Air Quality Model using the Statistical Oxidation Model: Assessing the Influence of Constrained Multi-Generational Ageing

Multi-generational oxidation of volatile organic compound (VOC) oxidation products can significantly alter the mass, chemical composition and properties of secondary organic aerosol (SOA) compared to calculations that consider only the first few generations of oxidation reactions. However, the most commonly used state-of-the-science schemes in 3-D regional or global models that account for multi-generational oxidation (1) consider only functionalization reactions but do not consider fragmentation reactions; (2) have not been constrained to experimental data; and (3) are added on top of existing parameterizations. The incomplete description of multi-generational oxidation in these models has the potential to bias source apportionment and control calculations for SOA. In this work, we used the Statistical Oxidation Model (SOM) of Cappa and Wilson (2012), constrained by experimental laboratory chamber data, to evaluate the regional implications of multi-generational oxidation considering both functionalization and fragmentation reactions. SOM was implemented into the regional UCD/CIT air quality model and applied to air quality episodes in California and the eastern US. The mass, composition and properties of SOA predicted using SOM were compared to SOA predictions generated by a traditional "two-product" model to fully investigate the impact of explicit and self-consistent accounting of multi-generational oxidation.

Results show that SOA mass concentrations predicted by the UCD/CIT-SOM model are very similar to those predicted by a two-product model when both models use parameters that are

derived from the same chamber data. Since the two-product model does not explicitly resolve multi-generational oxidation reactions, this finding suggests that the chamber data used to parameterize the models captures the majority of the SOA mass formation from multi-generational oxidation under the conditions tested. Consequently, the use of low and high NOx yields perturbs SOA concentrations by a factor of two and are probably a much stronger determinant in 3-D models than multi-generational oxidation. While total predicted SOA mass is similar for the SOM and two-product models, the SOM model predicts increased SOA contributions from anthropogenic (alkane, aromatic) and sesquiterpenes and decreased SOA contributions from isoprene and monoterpene relative to the two-product model calculations. The SOA predicted by SOM has a much lower volatility than that predicted by the traditional model; resulting in better qualitative agreement with volatility measurements of ambient OA. On account of its lower-volatility, the SOA mass produced by SOM does not appear to be as strongly influenced by the inclusion of oligomerization reactions, whereas the two-product model relies heavily on oligomerization to form low volatility SOA products. Finally, an unconstrained contemporary hybrid scheme to model multi-generational oxidation within the framework of a two-product model in which "ageing" reactions are added on top of the existing two-product parameterization is considered. This hybrid scheme formed at least three times more SOA than the SOM during regional simulations as a result of excessive transformation of semi-volatile vapors into lower volatility material that strongly partitions to the particle phase. This finding suggests that these "hybrid" multi-generational schemes should be used with great caution in regional models..

7.3 Simulating Secondary Organic Aerosol in a Regional Air Quality Model with the Statistical Oxidation Model: Assessing the Influence of Vapor Wall Losses

The influence of losses of organic vapors to chamber walls during secondary organic aerosol (SOA) formation experiments has recently been established. Here, the influence of such losses on simulated ambient SOA concentrations and properties is assessed in the UCD/CIT regional air quality model using the statistical oxidation model (SOM) for SOA. The SOM was fit to laboratory chamber data both with and without accounting for vapor wall losses following the approach of Zhang et al. (2014). Two vapor wall loss scenarios are considered when fitting of SOM to chamber data to determine best-fit SOM parameters, one with "low" and one with "high" vapor wall-loss rates to approximately account for the current range of uncertainty in this process. Simulations were run using these different parameterizations (scenarios) for both the southern California/South Coast Air Basin (SoCAB) and the eastern United States (US). Accounting for vapor wall losses leads to substantial increases in the simulated SOA concentrations from VOCs in both domains, by factors of ~2-5 for the low and ~5-10 for the high scenario. The magnitude of the increase scales approximately inversely with the absolute SOA concentration of the no loss scenario. In SoCAB, the predicted SOA fraction of total OA increases from ~0.2 (no) to ~0.5 (low) and to ~0.7 (high), with the high vapor wall loss simulations providing best general agreement with observations. In the eastern US, the SOA fraction is large in all cases but increases further when vapor wall losses are accounted for. The total OA/ΔCO ratio captures the influence of dilution on SOA concentrations. The simulated OA/ΔCO in SoCAB (specifically, at Riverside, CA) is found to increase substantially during the day only for the high vapor wall loss scenario, which is consistent with observations and indicative of photochemical production of SOA. Simulated O:C atomic ratios for both SOA and

for total OA increase when vapor wall losses are accounted for, while simulated H:C atomic ratios decrease. The agreement between simulations and observations of both the absolute values and the diurnal profile of the O:C and H:C atomic ratios for total OA was greatly improved when vapor wall-losses were accounted for. These results overall demonstrate that vapor wall losses in chambers have the potential to exert a large influence on simulated ambient SOA concentrations, and further suggest that accounting for such effects in models can explain a number of different observations and model/measurement discrepancies.

7.4   Reactivity Assessment of Volatile Organic Compounds Using Modern Conditions

Updated scenarios representing the year 2010 were created for 39 cities across the US to support an evaluation of incremental reactivity (IR) (ozone formation potential) for more than 1000 VOCs. Meteorological conditions for a representative ozone episode in each city were simulated with the Weather Research and Forecast (WRF) model. Emissions inputs were predicted using the SMOKE model. Aloft VOC composition and concentrations were simulated using the UCD/CIT air quality model.

The updated model scenarios for the year 2010 indicate that VOCs have become ~17% more reactive for the "regular atmospheric condition" or base case scenario in 39 cities across the United States compared to conditions in 1988. MIR values for artificially high NOx concentration in the year 2010 are ~41% lower than previously calculated using 1988 conditions.

The relative ranking of IR has not changed dramatically for the most reactive VOCs between 2010 and 1988, suggesting that most compounds behave similarly to changes in atmospheric conditions.

The VOCs with the highest IRs should be revisited in locations that continue to exceed the National Ambient Air Quality Standards for ozone. Regionally stratified calculations should determine if regional IRs are warranted. The incremental reactivity calculated by the 2D box model for select compounds spanning the range of compound classes should also be compared to values calculated with a full 3D air quality model to verify the accuracy of the technique.

7.5   Influence of Biogenic VOC Reactions with NOx on Predicted Concentrations of Secondary Organic Aerosol and Nitrate

The SAPRC11 chemical mechanism was expanded to explicitly track reactions between NOx and biogenic hydrocarbons. Model simulations were conducted for California under typical summer (May 19-June 14, 2010) and winter (Jan 16-Feb 10, 2013) conditions. Monoterpene nitrates and glyoxal / methyl glyoxal species were consistently the biggest contributors to predicted increases in aerosol mass associated with the expanded mechanism. PM2.5 SOA concentrations of these species approached 1 μg m^{-3} during the summer conditions but were < 0.1 μg m^{-3} during winter conditions. It is expected that monoterpene nitrate concentrations will decrease in direct proportion to NOx emissions, while glyoxal / methyl glyoxal concentrations will decrease more slowly than NOx emissions in future control scenarios. Using the values predicted during the summer episode analyzed in the present study, a 25% reduction in NOx emissions could produce a 0.13 μg m^{-3} reduction in PM2.5 SOA concentrations.

7.6 Future research

The latest information about multi-generational oxidation, vapor wall losses, POA volatility, and S/IVOC emissions should be combined in a comprehensive model evaluation to determine the net effect on predicted organic aerosol concentrations in California.

The algorithms used to select between high-NOx vs. low-NOx parameterizations in regional air quality models should be reviewed given the significant impact that this choice has on predicted SOA concentrations.

SOM parameterizations should be developed that include the effects of ozone and nitrate radical in addition to the parameterizations for OH reaction developed in the current study.

The cause of significant under-predictions for isoprene concentrations in California should be identified and corrected.

Simulations should be conducted at spatial resolution finer than 4km for systems where night time formation pathways are important.

Longer simulations should be conducted with the expanded SAPRC11 chemical mechanism to determine SOA yields from NOx reactions with biogenic hydrocarbons and the potential to reduce biogenic SOA concentrations through NOx control programs.

The limits applied to emissions of individual VOCs should be reviewed in the context of updated rankings based on contemporary conditions.

8   REFERENCES

1.   Saunders, S., et al., *Protocol for the development of the Master Chemical Mechanism, MCM v3 (Part A): tropospheric degradation of non-aromatic volatile organic compounds.* Atmospheric Chemistry and Physics, 2003. **3**(1): p. 161-180.

2.   Jenkin, M.E., et al., *Protocol for the development of the Master Chemical Mechanism, MCM v3 (Part B): tropospheric degradation of aromatic volatile organic compounds.* Atmospheric Chemistry and Physics, 2003. **3**(1): p. 181-193.

3.   Robinson, A.L., et al., *Rethinking organic aerosols: Semivolatile emissions and photochemical aging.* Science, 2007. **315**(5816): p. 1259-1262.

4.   Carlton, A.G., et al., *Model Representation of Secondary Organic Aerosol in CMAQv4.7.* Environmental Science & Technology, 2010. **44**(22): p. 8553-8560.

5.   Volkamer, R., et al., *Secondary organic aerosol formation from anthropogenic air pollution: Rapid and higher than expected.* Geophysical Research Letters, 2006. **33**(doi:10.1029/2006GL026899): p. L17811.

6.   Pye, H.O.T., et al., *Epoxide Pathways Improve Model Predictions of Isoprene Markers and Reveal Key Role of Acidity in Aerosol Formation.* Environmental Science & Technology, 2013. **47**(19): p. 11056-11064.

7.   Xie, Y., et al., *Understanding the impact of recent advances in isoprene photooxidation on simulations of regional air quality.* Atmospheric Chemistry and Physics, 2013. **13**(16): p. 8439-8455.

8.   Carter, W.P.L. and G. Heo, *Development of Revised SAPRC Aromatics Mechanisms.* 2012, California Air Resources Board.

9.   Camredon, M., et al., *The SOA/VOC/NO x system: an explicit model of secondary organic aerosol formation.* Atmospheric Chemistry and Physics, 2007. **7**(21): p. 5599-5610.

10.   Lee-Taylor, J., et al., *Explicit modeling of organic chemistry and secondary organic aerosol partitioning for Mexico City and its outflow plume.* Atmospheric Chemistry and Physics, 2011. **11**(24): p. 13219-13241.

11.   Valorso, R., et al., *Explicit modelling of SOA formation from α-pinene photooxidation: sensitivity to vapour pressure estimation.* Atmospheric Chemistry and Physics, 2011. **11**(14): p. 6895-6910.

12.   Aumont, B., et al., *Modeling SOA formation from the oxidation of intermediate volatility n-alkanes.* Atmospheric Chemistry and Physics, 2012. **12**(16): p. 7577-7589.

13.   Cappa, C.D. and K.R. Wilson, *Multi-generation gas-phase oxidation, equilibrium partitioning, and the formation and evolution of secondary organic aerosol.* Atmos. Chem. Phys., 2012. **12**: p. 9505-9528.

14.   Odum, J.R., et al., *The atmospheric aerosol-forming potential of whole gasoline vapor.* Science, 1997. **276**(5309): p. 96-99.

15.   Odum, J.R., et al., *Aromatics, Reformulated Gasoline, and Atmospheric Organic Aerosol Formation.* Environ. Sci. Technol., 1997. **31**(7): p. 1890-1897.

16.   Griffin, R.J., et al., *Organic aerosol formation from the oxidation of biogenic hydrocarbons.* Journal of Geophysical Research-Atmospheres, 1999. **104**(D3): p. 3555-3567.

17.   Bahreini, R., et al., *Measurements of secondary organic aerosol from oxidation of cycloalkenes, terpenes, and m-xylene using an Aerodyne aerosol mass spectrometer.* Environmental Science & Technology, 2005. **39**(15): p. 5674-5688.

18.   Kroll, J.H., et al., *Secondary organic aerosol formation from isoprene photooxidation under high-NO$_x$ conditions.* Geophysical Research Letters, 2005. **32**: p. L18808, doi: 10.1029/2005GL023637.

19.   Kroll, J.H., et al., *Secondary organic aerosol formation from isoprene photooxidation.* Environmental Science & Technology, 2006. **40**(6): p. 1869-1877.

20.   Lee, A., et al., *Gas-phase products and secondary aerosol yields from the ozonolysis of ten different terpenes.* Journal of Geophysical Research-Atmospheres, 2006. **111**(D7): p. -.

21.   Lee, A., et al., *Gas-phase products and secondary aerosol yields from the photooxidation of 16 different terpenes.* J. Geophys. Res., 2006. **111**(D17): p. D17305.

22.   Ng, N.L., et al., *Effect of NOx level on secondary organic aerosol (SOA) formation from the photooxidation of terpenes.* Atmos. Chem. Phys., 2007. **7**(19): p. 5159-5174.

23.   Ng, N.L., et al., *Secondary organic aerosol formation from m-xylene, toluene, and benzene.* Atmos. Chem. Phys., 2007. **7**(14): p. 3909-3922.

24.   Ng, N.L., et al., *Contribution of first- versus second-generation products to secondary organic aerosols formed in the oxidation of biogenic hydrocarbons.* Environ. Sci. Technol., 2006. **40**(7): p. 2283-2297.

25.   Chhabra, P.S., R.C. Flagan, and J.H. Seinfeld, *Elemental analysis of chamber organic aerosol using an aerodyne high-resolution aerosol mass spectrometer.* Atmos. Chem. Phys., 2010. **10**(9): p. 4111-4131.

26.   Chhabra, P.S., et al., *Elemental composition and oxidation of chamber organic aerosol.* Atmospheric Chemistry and Physics, 2011. **11**(17): p. 8827-8845.

27.   Loza, C.L., et al., *Chemical aging of m-xylene secondary organic aerosol: laboratory chamber study.* Atmos. Chem. Phys., 2012. **12**(1): p. 151-167.

28.   Yee, L.D., et al., *Secondary organic aerosol formation from low-NO$_x$ photooxidation of dodecane: Evolution of multigeneration gas-phase chemistry and aerosol composition.* The Journal of Physical Chemistry A, 2012. **116**(24): p. 6211-6230.

29.   Sullivan, D., Y. Kimura, and D. Allen, *Development of an Updated Base Case Ambient VOC Mixture for Assessing Atmospheric Reactivity*. 2011, Final Report prepared for the California Air Resources Board and the California Environmental Protection Agency Contract No. 08-327: Sacramento, CA.

30.   Chang, W.L., et al., *Heterogeneous Atmospheric Chemistry, Ambient Measurements, and Model Calculations of N2O5: A Review.* Aerosol Science and Technology, 2011. **45**(6): p. 665-695.

31.   Jimenez, J., et al., *Evolution of Organic Aerosols in the Atmosphere.* Science, 2009. **326**(5959): p. 1525.

32.   Goldstein, A.H. and I.E. Galbally, *Known and unexplored organic constituents in the earth's atmosphere.* Environmental Science & Technology, 2007. **41**(5): p. 1514-1521.

33.   Odum, J.R., et al., *Gas/particle partitioning and secondary organic aerosol yields.* Environmental Science & Technology, 1996. **30**(8): p. 2580-2585.

34.   Carlton, A.G., et al., *Model representation of secondary organic aerosol in CMAQv4. 7.* Environmental Science & Technology, 2010. **44**: p. 8553-8560.

35.   Lane, T.E., N.M. Donahue, and S.N. Pandis, *Simulating secondary organic aerosol formation using the volatility basis-set approach in a chemical transport model.* Atmospheric Environment, 2008. **42**(32): p. 7439-7451.

36.   Chacon-Madrid, H.J., A.A. Presto, and N.M. Donahue, *Functionalization vs. fragmentation: n-aldehyde oxidation mechanisms and secondary organic aerosol formation.* Phys. Chem. Chem. Phys., 2010. **12**(42).

37.   Chacon-Madrid, H.J., K.M. Henry, and N.M. Donahue, *Photo-oxidation of pinonaldehyde at low NO x: from chemistry to organic aerosol formation.* Atmospheric Chemistry and Physics Discussions, 2012. **12**(3): p. 7727-7752.

38.   Yee, L.D., et al., *Secondary organic aerosol formation from biomass burning intermediates: phenol and methoxyphenols.* Atmospheric Chemistry and Physics, 2013. **13**(16): p. 8019-8043.

39.   Donahue, N.M., et al., *Aging of biogenic secondary organic aerosol via gas-phase OH radical reactions.* Proceedings of the National Academy of Sciences, 2012. **109**(34): p. 13503-13508.

40.   Pye, H. and J. Seinfeld, *A global perspective on aerosol from low-volatility organic compounds.* Atmos. Chem. Phys, 2010. **10**(9): p. 4377-4401.

41.   Baek, J., et al., *Modeling secondary organic aerosol in CMAQ using multigenerational oxidation of semi-volatile organic compounds.* Journal of Geophysical Research: Atmospheres, 2011. **116**(D22).

42.   Chacon-Madrid, H. and N. Donahue, *Fragmentation vs. functionalization: chemical aging and organic aerosol formation.* Atmos. Chem. Phys, 2011. **11**: p. 10553-10563.

43.   Aumont, B., S. Szopa, and S. Madronich, *Modelling the evolution of organic carbon during its gas-phase tropospheric oxidation: development of an explicit model based on a self generating approach.* Atmospheric Chemistry and Physics, 2005. **5**(9): p. 2497-2517.

44.   Donahue, N., et al., *A two-dimensional volatility basis set: 1. organic-aerosol mixing thermodynamics.* Atmospheric Chemistry and Physics, 2011. **11**(7): p. 3303-3318.

45.   Donahue, N.M., et al., *A two-dimensional volatility basis set–Part 2: Diagnostics of organic-aerosol evolution.* Atmospheric Chemistry and Physics, 2012. **12**(2): p. 615-634.

46.   Cappa, C. and K. Wilson, *Multi-generation gas-phase oxidation, equilibrium partitioning, and the formation and evolution of secondary organic aerosol.* Atmospheric Chemistry and Physics, 2012. **12**(20): p. 9505-9528.

47.   Cappa, C.D., et al., *Application of the Statistical Oxidation Model (SOM) to Secondary Organic Aerosol formation from photooxidation of C 12 alkanes.* Atmospheric Chemistry and Physics, 2013. **13**(3): p. 1591-1606.

48.   Zhao, B., et al., *Evaluation of one-dimensional and two-dimensional volatility basis sets in simulating the aging of secondary organic aerosol with smog-chamber experiments.* Environmental Science & Technology, 2015.

49.   Kleeman, M.J. and G.R. Cass, *A 3D Eulerian Source-Oriented Model for an Externally Mixed Aerosol.* Environmental Science & Technology, 2001. **35**(24): p. 4834-4848.

50.   Chen, J., Q. Ying, and M.J. Kleeman, *Source apportionment of wintertime secondary organic aerosol during the California regional PM10/PM2.5 air quality study.* Atmospheric Environment, 2010. **44**(10): p. 1331-1340.

51.   Kleeman, M.J., et al., *Source apportionment of secondary organic aerosol during a severe photochemical smog episode.* Atmospheric Environment, 2007. **41**(3): p. 576-591.

52.   Carter, W.P. and G. Heo, *Development of revised SAPRC aromatics mechanisms.* Atmospheric Environment, 2013. **77**: p. 404-414.

53.   Nenes, A., S.N. Pandis, and C. Pilinis, *ISORROPIA: A new thermodynamic equilibrium model for multiphase multicomponent inorganic aerosols.* Aquatic geochemistry, 1998. **4**(1): p. 123-152.

54.   Davis, J.M., P.V. Bhave, and K.M. Foley, *Parameterization of N2O5 reaction probabilities on the surface of particles containing ammonium, sulfate, and nitrate.* Atmospheric Chemistry and Physics, 2008. **8**(17): p. 5295-5311.

55.   CARB, *EMFAC (Mobile Source Emission Inventory)*, in *EMFAC (Mobile Source Emission Inventory)*. 2011, California Air Resources Board.

56.   Wiedinmyer, C., et al., *The Fire INventory from NCAR (FINN): A high resolution global model to estimate the emissions from open burning.* Geoscientific Model Development, 2011. **4**: p. 625.

57.   Guenther, A., et al., *Estimates of global terrestrial isoprene emissions using MEGAN (Model of Emissions of Gases and Aerosols from Nature).* Atmospheric Chemistry & Physics, 2006. **6**: p. 3181-3210.

58.   Jathar, S.H., et al., *Water uptake and its influence on gas/particle partitioning of secondary organic aerosol in the United States.* Atmospheric Environment, submitted.

59.   Lim, Y.B. and P.J. Ziemann, *Effects of molecular structure on aerosol yields from OH radical-initiated reactions of linear, branched, and cyclic alkanes in the presence of NO x.* Environmental Science & Technology, 2009. **43**(7): p. 2328-2334.

60.   Presto, A.A., et al., *Secondary organic aerosol formation from high-NO x photo-oxidation of low volatility precursors: n-alkanes.* Environmental Science & Technology, 2010. **44**(6): p. 2029-2034.

61.   Tkacik, D.S., et al., *Secondary organic aerosol formation from intermediate-volatility organic compounds: cyclic, linear, and branched alkanes.* Environmental Science & Technology, 2012. **46**(16): p. 8773-8781.

62.   Gentner, D.R., et al., *Elucidating secondary organic aerosol from diesel and gasoline vehicles through detailed characterization of organic carbon emissions.* Proceedings of the National Academy of Sciences, 2012. **109**(45): p. 18318-18323.

63.   Surratt, J.D., et al., *Effect of acidity on secondary organic aerosol formation from isoprene.* Environmental science & technology, 2007. **41**(15): p. 5363-5369.

64.   Kalberer, M., et al., *Identification of polymers as major components of atmospheric organic aerosols.* Science, 2004. **303**(5664): p. 1659-1662.

65.   Aw, J. and M.J. Kleeman, *Evaluating the first‐order effect of intraannual temperature variability on urban air pollution.* Journal of Geophysical Research: Atmospheres (1984–2012), 2003. **108**(D12).

66.   Epstein, S.A., I. Riipinen, and N.M. Donahue, *A Semiempirical Correlation between Enthalpy of Vaporization and Saturation Concentration for Organic Aerosol.* Environmental Science \& Technology, 2010.

67.   Zhang, X., et al., *Influence of vapor wall loss in laboratory chambers on yields of secondary organic aerosol.* Proceedings of the National Academy of Sciences, 2014. **111**(16): p. 5802-5807.

68.   Pankow, J.F., *An absorption model of gas/particle partitioning of organic compounds in the atmosphere.* Atmospheric Environment, 1994. **28**(2): p. 185-188.

69.   Yatavelli, R.L.N., et al., *A chemical ionization high-resolution time-of-flight mass spectrometer coupled to a micro orifice volatilization impactor (MOVI-HRToF-CIMS) for analysis of gas and particle-phase organic species.* Aerosol Science and Technology, 2012. **46**(12): p. 1313-1327.

70.   Shiraiwa, M., et al., *Size distribution dynamics reveal particle-phase chemistry in organic aerosol formation.* Proceedings of the National Academy of Sciences, 2013. **110**(29): p. 11746-11750.

71.   Griffin, R.J., et al., *Estimate of global atmospheric organic aerosol from oxidation of biogenic hydrocarbons.* Geophysical research letters, 1999. **26**(17): p. 2721--2724.

72.   McVay, R.C., C.D. Cappa, and J.H. Seinfeld, *Vapor–Wall Deposition in Chambers: Theoretical Considerations.* Environmental science & technology, 2014. **48**(17): p. 10251-10258.

73.   Carter, W.P.L., *Documentation of the SAPRC Chemical Mechanism Modeling System and Files Part 1. Basic System.* 2015, California Air Resources Board.

74.   Docherty, K.S., et al., *The 2005 Study of Organic Aerosols at Riverside(SOAR-1): instrumental intercomparisons and fine particle composition.* Atmospheric Chemistry and Physics, 2011. **11**(23): p. 12387-12420.

75.   Docherty, K.S., et al., *Apportionment of primary and secondary organic aerosols in Southern California during the 2005 Study of Organic Aerosols in Riverside (SOAR-1).* Environmental Science & Technology, 2008. **42**(20): p. 7655-7662.

76.   Farina, S.C., P.J. Adams, and S.N. Pandis, *Modeling global secondary organic aerosol formation and processing with the volatility basis set: Implications for anthropogenic secondary organic aerosol.* Journal of Geophysical Research, 2010. **115**(D9): p. D09202.

77.   Jathar, S.H., et al., *Unspeciated organic emissions from combustion sources and their influence on the secondary organic aerosol budget in the United States.* Proceedings of the National Academy of Sciences, 2014. **111**(29): p. 10473-10478.

78.   McNeill, V.F., *Aqueous Organic Chemistry in the Atmosphere: Sources and Chemical Processing of Organic Aerosols.* Environmental Science & Technology, 2015.

79.   Chhabra, P.S., et al., *Application of high-resolution time-of-flight chemical ionization mass spectrometry measurements to estimate volatility distributions of α-pinene and naphthalene oxidation products.* Atmospheric Measurement Techniques, 2015. **8**(1): p. 1-18.

80.   Aljawhary, D., A.K.Y. Lee, and J.P.D. Abbatt, *High-resolution chemical ionization mass spectrometry (ToF-CIMS): application to study SOA composition and processing.* Atmospheric Measurement Techniques, 2013. **6**(11): p. 3211-3224.

81.   Jimenez, J.L., et al., *Evolution of Organic Aerosols in the Atmosphere.* Science, 2009. **326**(5959): p. 1525-1529.

82.   IPCC, *Climate change 2007: The physical science basis.* Agenda, 2007. **6**: p. 07.

83.   Bernstein, J.A., et al., *Health effects of air pollution.* The Journal of Allergy and Clinical Immunology, 2004. **114**(5): p. 1116-1123.

84.   Chacon-Madrid, H.J., A.A. Presto, and N.M. Donahue, *Functionalization vs. fragmentation: n-aldehyde oxidation mechanisms and secondary organic aerosol formation.* Phys. Chem. Chem. Phys., 2010. **12**(42): p. 13975–13982.

85.   Chacon-Madrid, H.J., K.M. Henry, and N.M. Donahue, *Photo-oxidation of pinonaldehyde at low NO x: from chemistry to organic aerosol formation.* Atmospheric Chemistry and Physics, 2013. **13**(6): p. 3227-3236.

86.   Henry, K.M. and N.M. Donahue, *Photochemical aging of α-pinene secondary organic aerosol: effects of OH radical sources and photolysis.* The Journal of Physical Chemistry A, 2012. **116**(24): p. 5932-5940.

87.   Lambe, A.T., et al., *Transitions from functionalization to fragmentation reactions of laboratory secondary organic aerosol (SOA) generated from the OH oxidation of alkane precursors.* Environmental science & technology, 2012. **46**(10): p. 5430-5437.

88.   Donahue, N., et al., *Coupled partitioning, dilution, and chemical aging of semivolatile organics.* Environ. Sci. Technol, 2006. **40**(8): p. 2635-2643.

89.   Baek, J., et al., *Modeling secondary organic aerosol in CMAQ using multigenerational oxidation of semi-volatile organic compounds.* Journal of Geophysical Research: Atmospheres, 2011. **116**: p. D22204.

90.   Koo, B., E. Knipping, and G. Yarwood, *1.5-Dimensional volatility basis set approach for modeling organic aerosol in CAMx and CMAQ.* Atmospheric Environment, 2014. **95**: p. 158-164.

91.   Murphy, B. and S. Pandis, *Simulating the formation of semivolatile primary and secondary organic aerosol in a regional chemical transport model.* Environmental science & technology, 2009. **43**(13): p. 4722-4728.

92.   Tsimpidi, A., et al., *Evaluation of the volatility basis-set approach for the simulation of organic aerosol formation in the Mexico City metropolitan area.* Atmos. Chem. Phys, 2009. **10**: p. 525-546.

93.   Ahmadov, R., et al., *A volatility basis set model for summertime secondary organic aerosols over the eastern United States in 2006.* Journal Of Geophysical Research-Atmospheres, 2012. **117**: p. D06301.

94.   Johnson, D., et al., *Simulating regional scale secondary organic aerosol formation during the TORCH 2003 campaign in the southern UK.* Atmospheric Chemistry and Physics, 2006. **6**(2): p. 403-418.

95.   Chen, J., et al., *Application of the CACM and MPMPO modules using the CMAQ model for the eastern United States.* Journal of Geophysical Research: Atmospheres (1984–2012), 2006. **111**(D23).

96.   Ying, Q. and J. Li, *Implementation and initial application of the near-explicit Master Chemical Mechanism in the 3D Community Multiscale Air Quality (CMAQ) model.* Atmospheric Environment, 2011. **45**(19): p. 3244-3256.

97.   Utembe, S.R., et al., *Simulating secondary organic aerosol in a 3-D Lagrangian chemistry transport model using the reduced Common Representative Intermediates mechanism (CRI v2-R5).* Atmospheric Environment, 2011. **45**(8): p. 1604-1614.

98.   Lin, G., et al., *Global modeling of SOA formation from dicarbonyls, epoxides, organic nitrates and peroxides.* Atmospheric Chemistry and Physics, 2012. **12**(10): p. 4743-4774.

99.   Jathar, S.H., et al., *Multi-generational oxidation model to simulate secondary organic aerosol in a 3-D air quality model.* Geosci. Model Dev., 2015. **8**(8): p. 2553-2567.

100.   Jathar, S.H., et al., *Multi-generational Oxidation Model to Simulate Secondary Organic Aerosol in a 3D Air Quality Model.* Geophysical Model Development, accepted for publication.

101.   Emmons, L., et al., *Description and evaluation of the Model for Ozone and Related chemical Tracers, version 4 (MOZART-4).* Geoscientific Model Development, 2010. **3**(1): p. 43-67.

102. Henze, D., et al., *Global modeling of secondary organic aerosol formation from aromatic hydrocarbons: high- vs. low-yield pathways.* Atmospheric Chemistry and Physics, 2008. **8**(9): p. 2405--2420.

103. Loza, C.L., et al., *Secondary organic aerosol yields of 12-carbon alkanes.* Atmospheric Chemistry and Physics, 2014. **14**(3): p. 1423-1439.

104. Matsunaga, A. and P.J. Ziemann, *Gas-wall partitioning of organic compounds in a Teflon film chamber and potential effects on reaction product and aerosol yield measurements.* Aerosol Science and Technology, 2010. **44**(10): p. 881-892.

105. Cappa, C.D., et al., *Simulating secondary organic aerosol in a regional air quality model using the statistical oxidation model – Part 2: Assessing the influence of vapor wall losses.* Atmospheric Chemistry & Physics Discussions, 2015. **15**: p. 30081-30126.

106. Carlton, A.G., et al., *To what extent can biogenic SOA be controlled?* Environmental Science & Technology, 2007. **44**(9): p. 3376-3380.

107. Fast, J.D., et al., *Modeling regional aerosol and aerosol precursor variability over California and its sensitivity to emissions and long-range transport during the 2010 CalNex and CARES campaigns.* Atmospheric Chemistry and Physics, 2014. **14**: p. 10013-10060.

108. Dzepina, K., et al., *Evaluation of recently-proposed secondary organic aerosol models for a case study in Mexico City.* Atmospheric Chemistry and Physics, 2009. **9**(15): p. 5681-5709.

109. Boylan, J.W. and A.G. Russell, *PM and light extinction model performance metrics, goals, and criteria for three-dimensional air quality models.* Atmospheric Environment, 2006. **40**(26): p. 4946-4959.

110. Cappa, C.D. and J.L. Jimenez, *Quantitative estimates of the volatility of ambient organic aerosol.* Atmospheric Chemistry & Physics, 2010. **10**: p. 5401-5924.

111. Huffman, J., et al., *Chemically-resolved volatility measurements of organic aerosol fom different sources.* Environmental science & technology, 2009. **43**(14): p. 5351–5357.

112. Cappa, C.D., *A model of aerosol evaporation kinetics in a thermodenuder.* Atmospheric Measurement Techniques, 2010. **3**(3): p. 579-592.

113. Lee, B.H., et al., *Measurement of the ambient organic aerosol volatility distribution: application during the Finokalia Aerosol Measurement Experiment (FAME-2008).* Atmospheric Chemistry and Physics, 2010. **10**(24): p. 12149-12160.

114. Simon, H. and P.V. Bhave, *Simulating the degree of oxidation in atmospheric organic particles.* Environmental science & technology, 2011. **46**(1): p. 331-339.

115. Shrivastava, M.K., et al., *Effects of gas particle partitioning and aging of primary emissions on urban and regional organic aerosol concentrations.* Journal of Geophysical Research-Atmospheres, 2008. **113**(D18): p. D18301.

116. Zhao, B., et al., *Evaluation of One-Dimensional and Two-Dimensional Volatility Basis Sets in Simulating the Aging of Secondary Organic Aerosol with Smog-Chamber Experiments.* Environmental Science & Technology, 2015. **49**(4): p. 2245-2254.

117. Jathar, S., et al., *The influence of semi-volatile and reactive primary emissions on the abundance and properties of global organic aerosol.* Atmospheric Chemistry and Physics, 2011. **11**: p. 7727-7746.

118. Ervens, B., B. Turpin, and R. Weber, *Secondary organic aerosol formation in cloud droplets and aqueous particles (aqSOA): a review of laboratory, field and model studies.* Atmospheric Chemistry and Physics, 2011. **11**(21): p. 11069-11102.

119. Liggio, J., S.M. Li, and R. McLaren, *Reactive uptake of glyoxal by particulate matter.* Journal of Geophysical Research: Atmospheres (1984–2012), 2005. **110**: p. D10304.

120. Wilson, K.R., et al., *The statistical evolution of multiple generations of oxidation products in the photochemical aging of chemically reduced organic aerosol.* Physical Chemistry Chemical Physics, 2012. **14**(4): p. 1468-1479.

121. Gordon, T.D., et al., *Secondary Organic Aerosol Formed from Light Duty Gasoline Vehicle Exhaust Dominates Primary Particulate Matter Emissions.* Atmospheric Chemistry & Physics, 2014. **14**(9): p. 4461-4678.

122. Gordon, T.D., et al., *Secondary organic aerosol production from diesel vehicle exhaust: impact of aftertreatment, fuel chemistry and driving cycle.* Atmospheric Chemistry & Physics, 2014. **14**(9): p. 4643-4659.

123. Gordon, T.D., et al., *Primary Gas- and Particle-Phase Emissions and Secondary Organic Aerosol Production from Gasoline and Diesel Off-Road Engines.* Environmental Science & Technology, 2013. **47**(24): p. 14137-14146.

124. Grieshop, A., N. Donahue, and A. Robinson, *Laboratory investigation of photochemical oxidation of organic aerosol from wood fires 2: analysis of aerosol mass spectrometer data.* Atmospheric Chemistry and Physics, 2009. **9**(6): p. 2227-2240.

125. Grieshop, A.P., et al., *Laboratory investigation of photochemical oxidation of organic aerosol from wood fires 1: measurement and simulation of organic aerosol evolution.* Atmospheric Chemistry and Physics, 2009. **9**(4): p. 1263-1277.

126. Hennigan, C.J., et al., *Chemical and physical transformations of organic aerosol from the photo-oxidation of open biomass burning emissions in an environmental chamber.* Atmospheric Chemistry and Physics, 2011. **11**(15): p. 7669-7686.

127. Miracolo, M., et al., *Secondary aerosol formation from photochemical aging of aircraft exhaust in a smog chamber.* Atmos. Chem. Phys, 2011. **11**: p. 4135-4147.

128. Miracolo, M.A., et al., *Fuel composition and secondary organic aerosol formation: gas-turbine exhaust and alternative aviation fuels.* Environmental Science & Technology, 2012. **46**(15): p. 8493-8501.

129. Platt, S.M., et al., *Secondary organic aerosol formation from gasoline vehicle emissions in a new mobile environmental reaction chamber.* Atmospheric Chemistry and Physics, 2013. **13**(18): p. 9141-9158.

130. Platt, S.M., et al., *Two-stroke scooters are a dominant source of air pollution in many cities.* Nature communications, 2014. **5**.

131. Nordin, E.Z., et al., *Secondary organic aerosol formation from idling gasoline passenger vehicle emissions investigated in a smog chamber.* Atmospheric Chemistry and Physics, 2013. **13**(12): p. 6101-6116.

132. Chirico, R., et al., *Impact of aftertreatment devices on primary emissions and secondary organic aerosol formation potential from in-use diesel vehicles: results from smog chamber experiments.* Atmospheric Chemistry and Physics, 2010. **10**(23): p. 11545-11563.

133. Heringa, M., et al., *Investigations of primary and secondary particulate matter of different wood combustion appliances with a high-resolution time-of-flight aerosol mass spectrometer.* Atmospheric Chemistry and Physics, 2011. **11**(12): p. 5945-5957.

134. Tkacik, D.S., et al., *Secondary Organic Aerosol Formation from in-Use Motor Vehicle Emissions Using a Potential Aerosol Mass Reactor.* Environmental Science & Technology, 2014. **48**(19): p. 11235-11242.

135. Zhang, Q., et al., *Ubiquity and dominance of oxygenated species in organic aerosols in anthropogenically-influenced Northern Hemisphere midlatitudes.* Geophys. Res. Lett., 2007. **34**(13): p. L13801.

136. Ziemann, P.J. and R. Atkinson, *Kinetics, products, and mechanisms of secondary organic aerosol formation.* Chemical Society Reviews, 2012. **41**(19): p. 6582-6605.

137. Odum, J.R., et al., *Gas/particle partitioning and secondary organic aerosol yields.* Environ. Sci. Technol., 1996. **30**(8): p. 2580-2585.

138. Tsigaridis, K., et al., *The AeroCom evaluation and intercomparison of organic aerosol in global models.* Atmospheric Chemistry and Physics, 2014. **14**(19): p. 10845-10895.

139. Heald, C.L., et al., *A large organic aerosol source in the free troposphere missing from current models.* Geophys. Res. Lett., 2005. **32**: p. L18809.

140. Ensberg, J.J., et al., *Emission factor ratios, SOA mass yields, and the impact of vehicular emissions on SOA formation.* Atmos. Chem. Phys., 2013. **14**: p. 2383-2397.

141. Tsimpidi, A.P., et al., *Evaluation of the volatility basis-set approach for the simulation of organic aerosol formation in the Mexico City metropolitan area.* Atmospheric Chemistry and Physics, 2010. **10**: p. 525-546.

142. Dzepina, K., et al., *Modeling the Multiday Evolution and Aging of Secondary Organic Aerosol During MILAGRO 2006.* Environ. Sci. Technol., 2011. **45**(8): p. 3496-3503.

143. Lane, T.E., N.M. Donahue, and S.N. Pandis, *Simulating secondary organic aerosol formation using the volatility basis-set approach in a chemical transport model.* Atmos. Environ., 2008. **42**(32): p. 7439-7451.

144. Dzepina, K., et al., *Evaluation of recently-proposed secondary organic aerosol models for a case study in Mexico City.* Atmos. Chem. Phys., 2009. **9**(15): p. 5681-5709.

145. Ervens, B., B.J. Turpin, and R.J. Weber, *Secondary organic aerosol formation in cloud droplets and aqueous particles (aqSOA): a review of laboratory, field and model studies.* Atmospheric Chemistry and Physics, 2011. **11**(21): p. 11069-11102.

146. Matsunaga, A. and P.J. Ziemann, *Gas-Wall Partitioning of Organic Compounds in a Teflon Film Chamber and Potential Effects on Reaction Product and Aerosol Yield Measurements.* Aerosol Sci. Technol., 2010. **44**(10): p. 881-892.

147. Yeh, G.K. and P.J. Ziemann, *Gas-wall partitioning of oxygenated organic compounds: Measurements, structure-activity relationships, and correlation with gas chromatographic retention factor.* Aerosol Science and Technology, 2015. **49**(9): p. 727-738.

148. Zhang, X., et al., *Vapor wall deposition in Teflon chambers.* Atmospheric Chemistry and Physics, 2015. **15**: p. 4197-4214.

149. Krechmer, J.E., et al., *Formation of Low Volatility Organic Compounds and Secondary Organic Aerosol from Isoprene Hydroxyhydroperoxide Low-NO Oxidation.* Environmental Science & Technology, 2015. **49**(17): p. 10330-10339.

150. Kokkola, H., et al., *The role of low volatile organics on secondary organic aerosol formation.* Atmospheric Chemistry and Physics, 2014. **14**(3): p. 1689-1700.

151. Hodzic, A., et al., *Volatility dependence of Henry's law constants of condensable organics: Application to estimate depositional loss of secondary organic aerosols.* Geophysical Research Letters, 2014. **41**(13): p. 4795-4804.

152. Hayes, P.L., et al., *Modeling the formation and aging of secondary organic aerosols in Los Angeles during CalNex 2010.* Atmospheric Chemistry and Physics, 2015. **15**: p. 5773-5801.

153. Baker, K.R., et al., *Gas and aerosol carbon in California: comparison of measurements and model predictions in Pasadena and Bakersfield.* Atmospheric Chemistry and Physics, 2015. **15**: p. 5243-5258.

154. Jathar, S.H., et al., *Multi-generational Oxidation Model to Simulate Secondary Organic Aerosol in a 3D Air Quality Model.* Geoscientific Model Development, 2015. **8**: p. 2553-2567.

155. Cappa, C.D., et al., *Application of the Statistical Oxidation Model (SOM) to secondary organic aerosol formation from photooxidation of C12 Alkanes.* Atmos. Chem. Phys., 2013. **13**: p. 1591-1606.

156. Pankow, J.F., *An absorption-model of the gas aerosol partitioning involved in the formation of secondary organic aerosol.* Atmos. Environ., 1994. **28**(2): p. 189-193.

157. Jathar, S.H., et al., *Simulating secondary organic aerosol in a regional air quality model using the statistical oxidation model – Part 1: Assessing the influence of constrained multi-generational ageing.* Atmospheric Chemistry and Physics Discussions, 2015. **15**: p. 25837-25872.

158. Chhabra, P.S., et al., *Elemental composition and oxidation of chamber organic aerosol.* Atmos. Chem. Phys., 2011. **11**(17): p. 8827-8845.

159. Hodzic, A., et al., *Rethinking the global secondary organic aerosol (SOA) budget: stronger production, faster removal, shorter lifetime.* Atmospheric Chemistry and Physics Discussions, 2015. **15**: p. 32413-32468.

160. Carlton, A.G., et al., *Model Representation of Secondary Organic Aerosol in CMAQv4.7.* Environ. Sci. Technol., 2010. **44**(22): p. 8553-8560.

161. Ng, N.L., et al., *Changes in organic aerosol composition with aging inferred from aerosol mass spectra.* Atmospheric Chemistry and Physics, 2011. **11**(13): p. 6465-6474.

162. Lane, T.E., N.M. Donahue, and S.N. Pandis, *Effect of NOx on Secondary Organic Aerosol Concentrations.* Environmental Science & Technology, 2008. **42**(16): p. 6022-6027.

163. Xu, L., et al., *Effects of NOx on the Volatility of Secondary Organic Aerosol from Isoprene Photooxidation.* Environmental Science & Technology, 2014. **48**(4): p. 2253-2262.

164. Pye, H.O.T., et al., *Epoxide Pathways Improve Model Predictions of Isoprene Markers and Reveal Key Role of Acidity in Aerosol Formation.* Environmental Science & Technology, 2013. **47**(19): p. 11056-11064.

165. Docherty, K.S., et al., *The 2005 Study of Organic Aerosols at Riverside (SOAR-1): instrumental intercomparisons and fine particle composition.* Atmospheric Chemistry and Physics, 2011. **11**(23): p. 12387-12420.

166. Hayes, P.L., et al., *Organic aerosol composition and sources in Pasadena, California, during the 2010 CalNex campaign.* Journal of Geophysical Research: Atmospheres, 2013. **118**(16): p. 9233-9257.

167. Xu, L., et al., *Aerosol characterization over the southeastern United States using high-resolution aerosol mass spectrometry: spatial and seasonal variation of aerosol composition and sources with a focus on organic nitrates.* Atmospheric Chemistry and Physics, 2015. **15**(13): p. 7307-7336.

168. The Visibility Information Exchange Web System (VIEWS 2.0). *The Visibility Information Exchange Web System.* 2015   11 February 2015]; Available from: http://views.cira.colostate.edu/web/.

169. Turpin, B.J. and H.-J. Lim, *Species Contributions to PM2.5 Mass Concentrations: Revisiting Common Assumptions for Estimating Organic Mass.* Aerosol Science and Technology, 2001. **35**(1): p. 602-610.

170. Subramanian, R., et al., *Positive and Negative Artifacts in Particulate Organic Carbon Measurements with Denuded and Undenuded Sampler Configurations.* Aerosol Science and Technology, 2004. **38**(sup1): p. 27-48.

171. Kim, P.S., et al., *Sources, seasonality, and trends of southeast US aerosol: an integrated analysis of surface, aircraft, and satellite observations with the GEOS-Chem chemical transport model.* Atmospheric Chemistry and Physics, 2015. **15**(18): p. 10411-10433.

172. Docherty, K.S., et al., *Apportionment of Primary and Secondary Organic Aerosols in Southern California during the 2005 Study of Organic Aerosols in Riverside (SOAR-1).* Environmental Science & Technology, 2008. **42**(20): p. 7655-7662.

173. De Gouw, J. and J.L. Jimenez, *Organic Aerosols in the Earth's Atmosphere.* Environmental Science & Technology, 2009. **43**(20): p. 7614-7618.

174. Zhao, Y., et al., *Intermediate-Volatility Organic Compounds: A Large Source of Secondary Organic Aerosol.* Environmental Science & Technology, 2014. **48**(23): p. 13743-13750.

175. Budisulistiorini, S.H., et al., *Real-Time Continuous Characterization of Secondary Organic Aerosol Derived from Isoprene Epoxydiols in Downtown Atlanta, Georgia, Using the Aerodyne Aerosol Chemical Speciation Monitor.* Environmental Science & Technology, 2013. **47**(11): p. 5686-5694.

176. Hu, W.W., et al., *Characterization of a real-time tracer for Isoprene Epoxydiols-derived Secondary Organic Aerosol (IEPOX-SOA) from aerosol mass spectrometer measurements.* Atmospheric Chemistry and Physics, 2015. **15**: p. 11807-11833.

177. Xu, L., et al., *Effects of anthropogenic emissions on aerosol formation from isoprene and monoterpenes in the southeastern United States.* Proceedings of the National Academy of Sciences, 2015. **112**(1): p. 37-42.

178. Worton, D.R., et al., *Observational Insights into Aerosol Formation from Isoprene.* Environmental Science & Technology, 2013. **47**(20): p. 11403-11413.

179. Russell, A.R., L.C. Valin, and R.C. Cohen, *Trends in OMI NO2 observations over the United States: effects of emission control technology and the economic recession.* Atmospheric Chemistry and Physics, 2012. **12**(24): p. 12197-12209.

180. Zotter, P., et al., *Diurnal cycle of fossil and nonfossil carbon using radiocarbon analyses during CalNex.* Journal of Geophysical Research: Atmospheres, 2014. **119**(11): p. 6818-6835.

181. Murphy, B.N., et al., *Simulating the oxygen content of ambient organic aerosol with the 2D volatility basis set.* Atmospheric Chemistry and Physics, 2011. **11**(15): p. 7859-7873.

182. Canagaratna, M.R., et al., *Elemental ratio measurements of organic compounds using aerosol mass spectrometry: characterization, improved calibration, and implications.* Atmos. Chem. Phys., 2015. **15**(1): p. 253-272.

183. Chen, Q., et al., *Elemental composition of organic aerosol: the gap between ambient and laboratory measurements.* Geophysical Research Letters, 2015. **42**(10): p. 4182-4189.

184. SEAC4RS.

185. Jathar, S.H., et al., *Unspeciated organic emissions from combustion sources and their influence on the secondary organic aerosol budget in the United States.* Proceedings of the National Academy of Sciences, 2014. **111**(29): p. 10473-10478.

186.   Carter, W.P.L., *Development of Ozone Reactivity Scales for Volatile Organic Compounds.* Journal of the Air and Waste Management Association, 1994. **44**: p. 881-899.

187.   EPA, U. *Air Quality Trends*. 2014 10/8/2014 [cited 2015 03/24/15].

188.   Agency, U.S.E.P. *State Implementation Plans*. Region 5 Air and Radiation 2011 [cited 2015 03/30/2015]; Available from: http://www.epa.gov/reg5oair/sips/.

189.   Hu, J., et al., *Particulate air quality model predictions using prognostic vs. diagnostic meteorology in central California.* Atmospheric Environment, 2010. **44**(2): p. 215-226.

190.   Guenther, A.B., et al., *The Model of Emissions of Gases and Aerosols from Natureversion 2.1 (MEGAN2.1): an extended and updated framework modeling biogenic emissions.* 2012(5,1471–1492).

191.   Held, T., et al., *A comparision of the UCD/CIT air quality model and the CMB source-receptor model for primary airborne particulate matter.* Atmospheric Enviornment, 2005. **39**: p. 2281-2297.

192.   Day, D.A., et al., *Organonitrate group concentrations in submicron particles with high nitrate and organic fractions in coastal southern California.* Atmospheric Environment, 2010. **44**(16): p. 1970-1979.

193.   Rollins, A.W., et al., *Gas/particle partitioning of total alkyl nitrates observed with TD-LIF in Bakersfield.* Journal of Geophysical Research-Atmospheres, 2013. **118**(12): p. 6651-6662.

194.   Farmer, D.K., et al., *Response of an aerosol mass spectrometer to organonitrates and organosulfates and implications for atmospheric chemistry.* Proceedings of the National Academy of Sciences of the United States of America, 2010. **107**(15): p. 6670-6675.

195.   Pye, H.O.T., et al., *Modeling the Current and Future Roles of Particulate Organic Nitrates in the Southeastern United States.* Environmental Science & Technology, 2015. **49**(24): p. 14195-14203.

196.   Hu, J., et al., *Long-term particulate matter modeling for health effect studies in California - Part 1: Model performance on temporal and spatial variations.* Atmospheric Chemistry and Physics, 2015. **15**(6): p. 3445-3461.

197.   Hu, J.L., et al., *Predicting Primary PM2.5 and PM0.1 Trace Composition for Epidemiological Studies in California.* Environmental Science & Technology, 2014. **48**(9): p. 4971-4979.

198.   Fry, J.L., et al., *Organic nitrate and secondary organic aerosol yield from NO3 oxidation of beta-pinene evaluated using a gas-phase kinetics/aerosol partitioning model.* Atmospheric Chemistry and Physics, 2009. **9**(4): p. 1431-1449.

199.   Rollins, A.W., et al., *Isoprene oxidation by nitrate radical: Alkyl nitrate and secondary organic aerosol yields.* Abstracts of Papers of the American Chemical Society, 2009. **237**: p. 288-288.